

**SYNTHESIS AND REACTIVITY OF GROUP 6 AND GROUP 8  
ORGANOMETALLIC COMPLEXES WITH SULFUR-  
CONTAINING LIGANDS**

**KUAN SEAH LING**

**NATIONAL UNIVERSITY OF SINGAPORE**

**2008**

**SYNTHESIS AND REACTIVITY OF GROUP 6 AND GROUP 8  
ORGANOMETALLIC COMPLEXES WITH SULFUR-  
CONTAINING LIGANDS**

**KUAN SEAH LING**

*(B.Sc.(Hons.), NUS)*

**A THESIS SUBMITTED FOR THE DEGREE OF  
DOCTOR OF PHILOSOPHY  
DEPARTMENT OF CHEMISTRY  
NATIONAL UNIVERSITY OF SINGAPORE**

**2008**

### **Acknowledgements**

The decision to take my PhD and completing it will not be possible by my own efforts alone and I would like to take this opportunity to express my heartfelt gratitude to the following people:

My supervisors, A/P Leong Weng Kee and Dr Goh Lai Yoong: For their guidance, inspiration, support and all that they taught me in science and in life.

Mrs Hoo Boon Leng: For inspiring me to choose study Chemistry.

Dr Richard Webster from NTU: For the electrochemical studies and his invaluable assistance in the discussion of the electrochemical studies; Dr Fan: For the invaluable suggestions; Prof Peter McGill from ANU: For the computational studies; Dr Koh, Ms Tan, Yanhui, Peggy, Mdm Wong, Hui Ngee and Zing: For their technical expertise.

Sin Yee, Victor, Marlin, Huishan, Xiaofeng, and Jialin: It is my good fortune and greatest pleasure to have worked with and become good friends with them. They have been role models whom I learnt from and have contributed greatly to my growth in the past few years. Their friendship, constant aid and discussion have made the road to PhD smoother and more enjoyable.

Zhiqiang, Richard Shin, Alaric, Biqi, Chunxiang, Garvin, Kong, Chang Hong, Sridevi, Pearly, Zhijie, Xueping and Kaining: For the helpful discussions and friendship.

My mum: For her unconditional support and encouragement all this while, without which I would not have come this far.

Other members of my family and friends, including Xueli, Weihong, Jo, Kayla, Wenxin, Huaying, Elaine Chan, Guihua, Elaine Tay TT and Han Yuan: For their constant support and encouragement.

NUSNNI: For my research scholarship.

---

**Table of Contents**

<b>Summary</b> .....	<b>V</b>
<b>Chart A: Compounds encountered in this thesis</b> .....	<b>VIII</b>
<b>List of Tables</b> .....	<b>X</b>
<b>List of Figures</b> .....	<b>XI</b>
<b>List of Abbreviations</b> .....	<b>XIV</b>
<b>Chapter 1. Transition Metal Complexes with Sulfur-containing Ligands</b> .....	<b>1</b>
1.1. Scorpionate Complexes .....	2
1.1.1. Poly(methimazolyl)borates .....	4
1.1.2. Electrochemistry of scorpionate complexes .....	12
1.2. Heterocyclic Thiolate Complexes .....	14
1.2.1. Complexes of 2-mercaptobenzothiazole .....	16
1.2.2. Complexes of 2-mercaptopyridine .....	17
1.2.3. Complexes of 2-mercaptobenzoic acid .....	18
1.2.4. Complexes of 6-mercaptonicotinic acid .....	19
References .....	21
<b>Chapter 2. Syntheses of mixed-sandwich Cp*Cr complexes containing poly(methimazolyl)borates (Cp* = C<sub>5</sub>Me<sub>5</sub>)</b> .....	<b>28</b>
2.1. Reaction of [Cp*CrBr <sub>2</sub> ] <sub>2</sub> ( <b>1</b> ) with poly(methimazolyl)borate salts .....	30
2.2. Crystallographic studies .....	32

---

2.3. Electrochemistry .....	35
2.4. Conclusion .....	39
2.5. Experimental .....	40
References .....	48
 <b>Chapter 3. Syntheses of mixed-sandwich (HMB)Ru complexes containing</b>	
<b>poly(methimazolyl)borates (HMB=C<sub>6</sub>Me<sub>6</sub>) .....</b>	<b>49</b>
3.1. Reaction of [(HMB)RuCl <sub>2</sub> ] <sub>2</sub> ( <b>8</b> ) with poly(methimazolyl)borate salts ...	51
3.2. Crystallographic studies .....	54
3.3. Electrochemistry .....	56
3.4. Conclusion .....	58
3.5. Experimental .....	59
References.....	63
 <b>Chapter 4. Syntheses of mixed-sandwich Cp*Ru complexes containing</b>	
<b>poly(methimazolyl)borates (Cp* = C<sub>5</sub>Me<sub>5</sub>) .....</b>	<b>64</b>
4.1. Syntheses of [Cp*Ru] complexes containing poly(methimazolyl)borate ligands .....	67
4.2. Cyclic Voltammetry .....	74
4.3. Isomerisation .....	79
4.4. Reactivity studies of Cp*Ru[HB(mt) <sub>2</sub> (pz)] ( <b>18</b> ) towards O <sub>2</sub> and CO ....	86
4.5. Conclusion .....	91
4.6. Experimental .....	93

References.....	104
<b>Chapter 5. One-Electron Electrochemical Oxidation of Half Sandwich</b>	
<b>Ruthenium</b>	
<b>Complexes, [Cp*<sup>IV</sup>RuCl<sub>2</sub>(S<sub>2</sub>CR)] (Cp* = C<sub>5</sub>Me<sub>5</sub>, R = NMe<sub>2</sub>, NEt<sub>2</sub>, O<sup>i</sup>Pr)</b> .....	<b>106</b>
5.1. Electrochemical oxidation and spectroscopic studies of [Cp* <sup>IV/V</sup> RuCl <sub>2</sub> (S <sub>2</sub> CR)] complexes .....	108
5.2. Chemical oxidation of [Cp* <sup>IV</sup> RuCl <sub>2</sub> (S <sub>2</sub> CNMe <sub>2</sub> )] .....	116
5.3. Conclusion .....	120
5.4. Experimental .....	121
References.....	125
<b>Chapter 6. Reactivity of [Cp'Ru(CO)<sub>2</sub>]<sub>2</sub> (Cp' = C<sub>5</sub>H<sub>5</sub> or C<sub>5</sub>Me<sub>5</sub>) towards disulfide ligands</b> .....	
6.1. Reaction of [Cp'Ru(CO) <sub>2</sub> ] <sub>2</sub> (Cp' = C <sub>5</sub> H <sub>5</sub> or C <sub>5</sub> Me <sub>5</sub> ) with heterocyclic disulfides .....	133
6.1.1. Electrochemical studies .....	138
6.1.2. Screening against cell lines .....	140
6.2. S-S bond cleavage reaction of [Cp'Ru(CO) <sub>2</sub> ] <sub>2</sub> (Cp' = C <sub>5</sub> H <sub>5</sub> or C <sub>5</sub> Me <sub>5</sub> ) with lysozyme.....	142
6.3. Conclusion .....	146
6.4. Experimental .....	147
References.....	154

<b>Concluding Remarks .....</b>	<b>156</b>
<b>Publications and manuscripts in preparation .....</b>	<b>158</b>
<b>Appendices.....</b>	<b>159</b>

## Summary

This thesis deals with the synthesis and reactivity of some Group 6 and 8 organometallic complexes with sulfur-containing compounds, namely the poly(methimazolyl)borate scorpionate ligands and the heterocyclic disulfides. After an introduction given in Chapter 1, the results of the investigation are described in five chapters.

Chapter 2 describes the reactions of  $[\text{Cp}^*\text{CrBr}_2]_2$  (**1**) with (i)  $\text{K}[\text{HB}(\text{mt})_3]$ , (ii)  $\text{Na}[\text{H}_2\text{B}(\text{mt})_2]$  and (iii)  $\text{Li}[\text{HB}(\text{mt})_2(\text{pz})]$ . The 15-electron Cr(III) complexes,  $[\text{Cp}^*\text{Cr}(\kappa^3\text{-S,S',S''})\text{-}\{\text{HB}(\text{mt})_3\}]\text{Br}$  (**2**),  $[\text{Cp}^*\text{Cr}(\kappa^2\text{-S,S'})\text{-}\{\text{H}_2\text{B}(\text{mt})_2\}]\text{Br}$  (**3**) and  $[\text{Cp}^*\text{Cr}(\kappa^2\text{-S,S'})\text{-}\{\text{HB}(\text{mt})_2(\text{pz})\}]\text{Br}$  (**4**) were obtained in moderate to high yield. Tridentate coordination of the  $[\text{H}_2\text{B}(\text{mt})_2]^-$  and  $[\text{HB}(\text{mt})_2(\text{pz})]^-$  can be effected by reacting **3** and **4** with a silver salt to give  $[\text{Cp}^*\text{Cr}(\kappa^2\text{-S,S'})\text{-}\{\text{H}_2\text{B}(\text{mt})_2\}(\text{NCMe})]\text{PF}_6$  (**5**) and  $[\text{Cp}^*\text{Cr}(\kappa^3\text{-H,S,S'})\text{-}\{\text{H}_2\text{B}(\text{mt})_2\}]\text{PF}_6$  (**6**), in the absence of acetonitrile. Likewise, the reaction of **4** with  $\text{AgPF}_6$  afforded  $[\text{Cp}^*\text{Cr}(\kappa^3\text{-N,S,S'})\text{-}\{\text{HB}(\text{mt})_2(\text{pz})\}]\text{Br} \text{PF}_6$  (**7**). The electrochemical behaviour of these complexes had also been studied.

The reactions of the 18-electron species,  $[(\text{HMB})\text{Ru}^{\text{II}}\text{Cl}_2]_2$  with the same scorpionate salts are described in Chapter 3. Monocationic  $(\text{HMB})\text{Ru}(\text{II})$  complexes,  $[(\text{HMB})\text{Ru}^{\text{II}}(\kappa^3\text{-S,S',S''})\text{-}\{\text{HB}(\text{mt})_3\}]\text{Cl}$  (**9**),  $[(\text{HMB})\text{Ru}^{\text{II}}(\kappa^2\text{-H,S,S'})\text{-}\{\text{H}_2\text{B}(\text{mt})_2\}]\text{Cl}$  (**10**) and  $[(\text{HMB})\text{Ru}^{\text{II}}(\kappa^2\text{-H,S,S'})\text{-}\{\text{HB}(\text{mt})_2(\text{pz})\}]\text{PF}_6$  (**11B**) were obtained from these reactions. An isomerisation process was observed for complex **11B** in solution and this process was investigated using  $^1\text{H}$  NMR. The electrochemical behaviour of complexes **9** and **10** were also investigated.

Chapter 4 describes the syntheses of mixed-sandwich  $\text{Cp}^*\text{Ru}^{\text{II/III}}$  complexes with poly(methimazolyl)borates.  $[\text{Cp}^*\text{Ru}^{\text{III}}(\kappa^3\text{-S,S',S''})\text{-}\{\text{HB}(\text{mt})_3\}](\mathbf{14A})\text{X}$  ( $\text{X} = \text{Cl}$ ,



PF<sub>6</sub>) and [Cp\*<sup>II</sup>Ru( $\kappa^3$ -S,S',S'')-{HB(mt)<sub>3</sub>}] (**16A**) were synthesized by the reactions of K[HB(mt)<sub>3</sub>] with the 17-electron precursor, [Cp\*<sup>III</sup>RuCl<sub>2</sub>]<sub>2</sub> (**12**), and the 16-electron precursor, [Cp\*<sup>II</sup>Ru(OMe)<sub>2</sub>] (**13**), respectively. [Cp\*<sup>II</sup>Ru( $\kappa^3$ -H,S,S')-{H<sub>2</sub>B(mt)<sub>2</sub>}] (**17**) and [Cp\*<sup>II</sup>Ru( $\kappa^2$ -H,S,S')-{HB(mt)<sub>2</sub>(pz)}] (**18**) were similarly synthesized from the reaction of **13** with Na[H<sub>2</sub>B(mt)<sub>2</sub>] and Li[HB(mt)<sub>2</sub>(pz)]. The electrochemistry of complexes **14A**, **16-18** was investigated. Both **14A** and **16A** were found to undergo an isomerization reaction in solution where the sulfur on one mt group is displaced in favor of coordination to the hydrogen bonded to the boron (an agostic B–H–Ru interaction) resulting in  $\kappa^3$ -H,S,S' coordination about the Ru centre. The rate and equilibrium constants associated with the isomerisation process have been determined by theoretical digital simulation comparisons of experimental <sup>1</sup>H NMR spectroscopic and cyclic voltammetric data over a range of temperatures. Oxidation of Cp\*<sup>II</sup>Ru{HB(mt)<sub>2</sub>(pz)} (**18**) with O<sub>2</sub> and reaction with CO gave the peroxo- and CO-adducts, Cp\*<sup>II</sup>Ru( $\kappa^2$ -S,S')-{HB(mt)<sub>2</sub>(pz)}(O<sub>2</sub>) (**19**) and Cp\*<sup>II</sup>Ru( $\kappa^2$ -S,S')-{HB(mt)<sub>2</sub>(pz)}(CO) (**20**). The convertibility of **18**, **19** and **20** were investigated and it was found that the reactivity of **18** towards O<sub>2</sub> and CO is similar to that of haemoglobin.

Chapter 5 describes the one-electron electrochemical oxidation of [Cp\*<sup>IV</sup>RuCl<sub>2</sub>(S<sub>2</sub>CR)] (**21-22**) to give the first examples of organometallic complexes of Ru(V). However, an attempt to synthesise the Ru(V) species via chemical oxidation of [Cp\*<sup>IV</sup>RuCl<sub>2</sub>(S<sub>2</sub>CNMe<sub>2</sub>)] (**21a**) resulted in the isolation of two Cp\*<sup>IV</sup>Ru species, **23** and **24** as a result of oxidation of the chloride co-ligands in **21a**.

The reactions of [Cp'<sup>II</sup>Ru(CO)<sub>2</sub>] (Cp'=C<sub>5</sub>H<sub>5</sub>, **25a**; Cp'=C<sub>5</sub>Me<sub>5</sub>, **25b**) with heterocyclic disulfides give complexes of the type [Cp'<sup>II</sup>Ru(CO)<sub>2</sub>( $\kappa^J$ -SR)] (**26-29**) are described in Chapter 6. The antiproliferative activity of these complexes against

MDA-MB231 and MCF-7 breast cancer cell lines were investigated. In addition, the reactivity of **25** towards *hen's egg white lysozyme* (HEWL) was investigated.

Chart A: Compounds encountered in this thesis

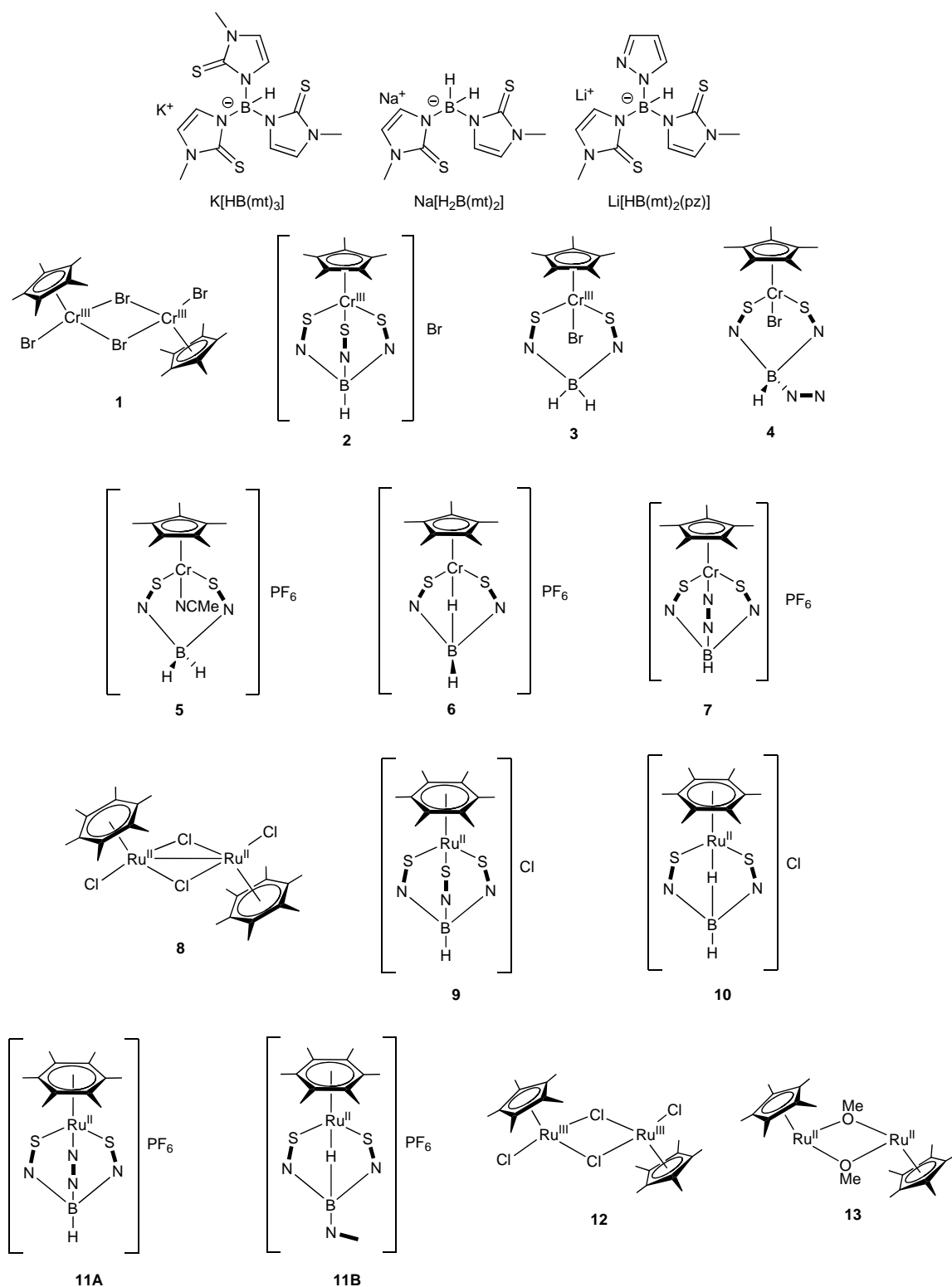
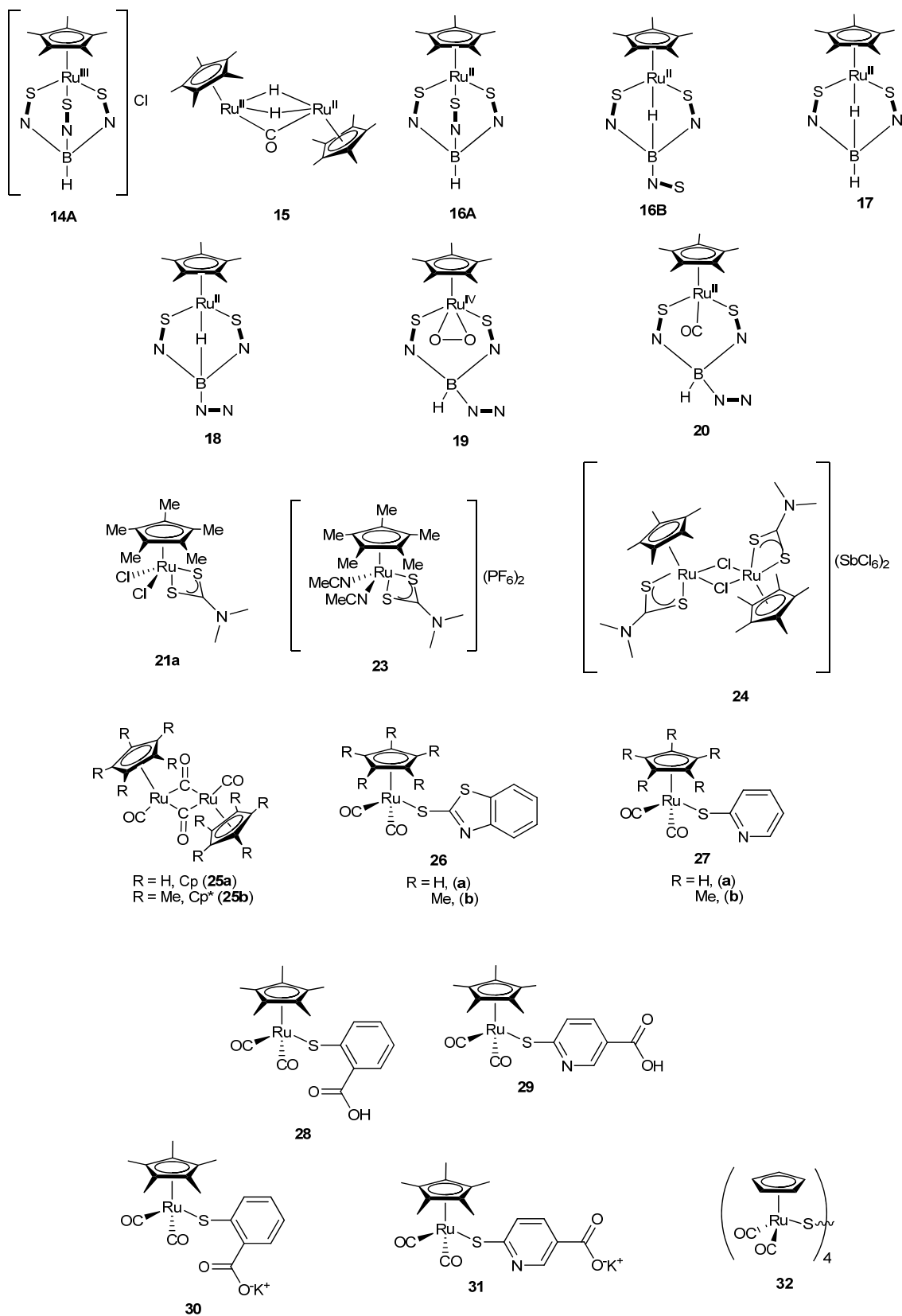


Chart A (continued)



---

**List of Tables**

Table 2.1.	Selected bond parameters of complexes <b>2-7</b> .....	34
Table 3.1.	Equilibrium constants in $d_3$ -acetonitrile for Equilibrium I.....	54
Table 3.2.	Bond parameters for complexes <b>9</b> and <b>10</b> .....	55
Table 4.1.	Variation of <b>16A: 16B</b> with solvent composition.....	70
Table 4.2.	Selected bond lengths (Å) and bond angles (°) for <b>14A, 16-18</b> .....	73
Table 4.3.	Oxidation potential of complexes <b>16-18</b> in $\text{CH}_2\text{Cl}_2$ vs. $\text{Fc}/\text{Fc}^+$ .....	75
Table 4.4.	Kinetic data and equilibrium constants in $d_8$ -toluene for Equilibrium II. .....	82
Table 4.5.	Thermodynamic parameters obtained from Eyring plots for Equilibrium II.....	82
Table 4.6.	Equilibrium, rate constants and electrochemical parameters obtained in $\text{CH}_2\text{Cl}_2$ (with 0.5 M $\text{Bu}_4\text{NPF}_6$ ).....	84
Table 4.7.	Selected bond lengths (Å) and bond angles (°) for <b>19</b> and <b>20</b> .....	89
Table 5.1.	Selected calculated atomic charges, spin densities, and spin densities at the nuclei in the neutral and oxidized forms of $[\text{Cp}^*\text{RuCl}_2(\text{S}_2\text{CNMe}_2)]$ ( <b>21a</b> ).....	115
Table 5.2.	Selected bond parameters of <b>23</b> and <b>24</b> .....	119
Table 6.1.	$\nu_{\text{C}\equiv\text{O}}$ for complexes <b>26</b> and <b>27</b> .....	135
Table 6.2.	Selected bond lengths (Å) and bond angles (°) for <b>26-29</b> .....	137

## List of Figures

Figure 2.1.	X-band EPR spectrum of <b>3</b> in CH <sub>3</sub> CN recorded at 10 K .....	31
Figure 2.2.	ORTEP plots for the molecular structures of <b>2-7</b> .....	33
Figure 2.3.	Cyclic voltammograms of 1.0 mM solutions of <b>2, 4</b> and <b>7</b> .....	37
Figure 2.4.	Cyclic voltammograms of 1.0 mM solutions of <b>3, 5</b> and <b>6</b> .....	38
Figure 3.1.	VT <sup>1</sup> H NMR of <b>11</b> from 300-345K .....	54
Figure 3.2.	ORTEP plots of <b>9, 10, 11B</b> and <b>11'</b> .....	55
Figure 3.3.	Cyclic voltammograms performed at a 1 mm diameter planar GC electrode in CH <sub>2</sub> Cl <sub>2</sub> (0.25 M Bu <sub>4</sub> NPF <sub>6</sub> ) at 233K or 293K and a scan rate of 100 mV s <sup>-1</sup> for 0.5 mM of <b>8</b> and <b>9</b> .....	57
Figure 4.1.	Continuous wave X-band EPR spectra for <b>14A</b> .....	68
Figure 4.2.	2D <sup>1</sup> H NMR EXSY spectrum for complex <b>16A/16B</b> in C <sub>6</sub> D <sub>6</sub> .....	71
Figure 4.3.	ORTEP plots for the molecular structures of <b>14A, 16A, 17</b> and <b>18</b> ...	72
Figure 4.4.	Cyclic voltammograms recorded at a scan rate of 100 mV s <sup>-1</sup> at a 1 mm GC electrode (a) 2.36 mM <b>14A.Cl</b> in CH <sub>2</sub> Cl <sub>2</sub> with 0.5 M <i>n</i> -Bu <sub>4</sub> NPF <sub>6</sub> ; 2.61 mM <b>16A/16B</b> in CH <sub>2</sub> Cl <sub>2</sub> with 0.5 M <i>n</i> -Bu <sub>4</sub> NPF <sub>6</sub> (b) 0.5 mM <b>17</b> in CH <sub>2</sub> Cl <sub>2</sub> with 0.25 M <i>n</i> -Bu <sub>4</sub> NPF <sub>6</sub> ; 1.0 mM <b>18</b> in CH <sub>2</sub> Cl <sub>2</sub> with 0.2 M <i>n</i> -Bu <sub>4</sub> NPF <sub>6</sub> .....	74
Figure 4.5.	Continuous wave X-band EPR spectra for <b>14B</b> .....	78

---

Figure 4.6.	VT 300 MHz $^1\text{H}$ NMR spectra of <b>16A/16B</b> in $d_8$ -toluene .....	80
Figure 4.7.	Experimental (solid line) and simulated (dashed line) VT 300 MHz $^1\text{H}$ NMR spectra of <b>16A/16B</b> in $d_8$ -toluene .....	81
Figure 4.8.	ORTEP plots for the molecular structures of <b>19</b> and <b>20</b> .....	89
Figure 4.9.	Cyclic voltammograms recorded at a scan rate of $100\text{ mV s}^{-1}$ at a 1 mm planar GC electrode in $\text{CH}_2\text{Cl}_2$ solutions containing 0.2 M $\text{Bu}_4\text{NPF}_6$ and 1 mM <b>19</b> and <b>20</b> .....	90
Figure 5.1.	Cyclic voltammograms recorded in $\text{CH}_2\text{Cl}_2$ with 0.5 M $\text{Bu}_4\text{NPF}_6$ at a Pt electrode of 1.0 mM solutions of <b>21</b> and <b>22</b> .....	109
Figure 5.2.	First derivative continuous wave X-band EPR spectra recorded in $\text{CH}_2\text{Cl}_2$ with 0.5 M $\text{Bu}_4\text{NPF}_6$ of (a) <b>21a</b> <sup>+</sup> at 293 K. (b) <b>21a</b> between 273 - 6 K. (c) <b>22b</b> <sup>+</sup> and <b>22</b> <sup>+</sup> at 233 K. ....	111
Figure 5.3.	UV-vis-NIR spectra obtained during the one-electron <i>in situ</i> electrochemical oxidation of 1.0 mM <b>21a</b> in $\text{CH}_2\text{Cl}_2$ with 0.5 M $\text{Bu}_4\text{NPF}_6$ in an OTTLE cell.....	113
Figure 5.4.	ORTEP plot for the molecular structure of (a) <b>21a</b> (b) <b>23</b> and (c) <b>24</b> .....	119
Figure 6.1.	(a) ORTEP plot of <b>26b</b> and (b) General numbering scheme for $\text{Cp}'\text{Ru}(\text{CO})_2(\text{SR})$ complexes.....	137
Figure 6.2.	Cyclic voltammograms of 1.0 mM of (a) <b>26a</b> . (b) <b>26b</b> . (c) <b>27b</b> and (d) <b>26c</b> recorded at a scan rate of $100\text{ mV s}^{-1}$ in $\text{CH}_2\text{Cl}_2$ solutions	

---

	containing 0.25 M Bu <sub>4</sub> NPF <sub>6</sub> at a 1 mm diameter planar Pt electrode..	
	.....	138
Figure 6.3.	MTT assay for (a) <b>26-27</b> against MDA-MB231 and (b) <b>26-27</b> against MCF10A. ....	141
Figure 6.4.	UV/Vis spectra of (a) HEWL (5 μM, -) and [CpRu(CO) <sub>2</sub> ] <sub>4</sub> -HEWL (5 μM, -) in water .....	144
Figure 6.5.	IR spectrum of <b>32</b> .....	145
Figure 6.6.	MALDI-ToF spectrum of (a) complex <b>32</b> and (b) HEWL .....	145

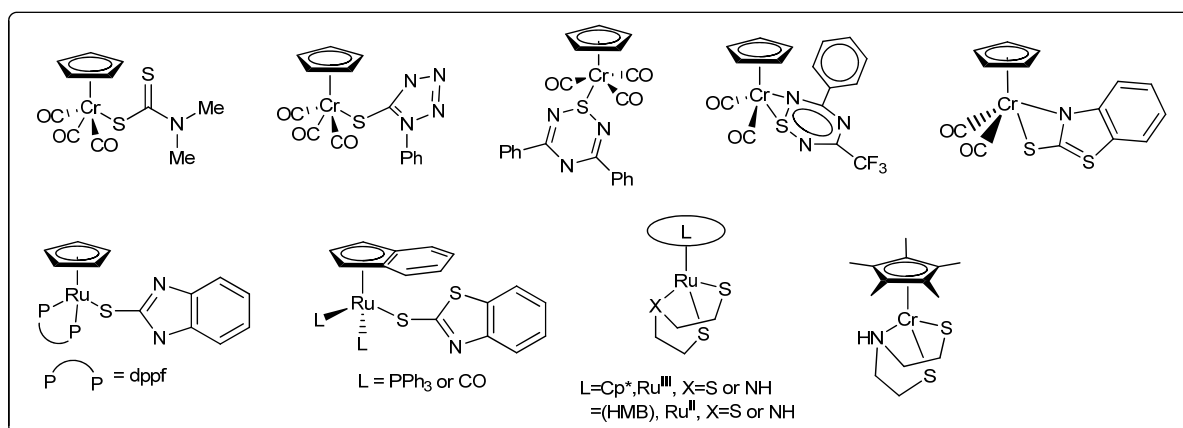


$\Delta G^\theta$	Gibbs free energy	Ind	Indenyl
$\Delta G^\ddagger$	activation energy	J	coupling constant
$\Delta H^\theta$	enthalpy	iPr	isopropyl
$\Delta H^\ddagger$	activation enthalpy	KBr	potassium bromide
$\Delta S^\theta$	entropy	$K_{eq}$	equilibrium constant
$\Delta S^\ddagger$	activation entropy	$k_f$	rate for forward reaction
br	Broad	$k_b$	rate for backward reaction
<i>ca</i>	about (Latin <i>circa</i> )	m	multiplet (NMR) / medium intensity (IR)
calc.	calculated	M+	parent ion peak (mass spectrometry)
COSY	Correlation Spectroscopy	MALDI-ToF	Matrix Assisted Laser Desorption-Time of Flight
Cp	$\eta^5$ -cyclopentadienyl	Me	methyl
Cp*	$\eta^5$ -pentamethylcyclopentadienyl	MeCN	acetonitrile
CPE	constant phase elements	MeOH	methanol
CV	Cyclic voltammetry or Cyclic voltammogram	min	minute
d	doublet (NMR)	$m/z$	mass to charge ratio
dd	doublet of doublet (NMR)	NMR	nuclear magnetic resonance
$\delta$	NMR chemical shift in ppm	NOESY	Nuclear Overhauser Enhancement Spectroscopy
e	Electron	q	quartet (NMR)
$E_{1/2}$	electrode potential	RT	room temperature
Et	ethyl	s	singlet (NMR) / strong intensity (IR)
EPR	Electron Paramagnetic Resonance	sh	shoulder (IR)
equiv.	equivalent(s)	t	triplet (NMR)
<i>et al.</i>	and other (Latin <i>et alii</i> )	t	tertiary
ESI	Electrospray Ionisation	T	temperature
FAB-MS	Fast Atom Bombardment Mass Spectrometry	THF	tetrahydrofuran
FTIR or IR	Fourier Transform Infra Red	upe	unnatural parity exchange
GC	Glassy carbon	UV-VIS	Ultraviolet-Visible
h	Hour	VT	variable temperature
HMB	$\eta^6$ -hexamethylbenzene	vs	very strong intensity (IR)
<i>i.e.</i>	this is (Latin <i>id est</i> )	vw	very weak intensity (IR)
		w	weak intensity (IR)

## Chapter 1. Transition Metal Complexes with Sulfur-containing Ligands

There are numerous reports of half-sandwich complexes of transition metals in the literature as they are good precursors for entry into a variety of organotransition metal complexes.<sup>1-16</sup> In particular, our group has been interested in the synthesis and reactivity of half-sandwich complexes of chromium and ruthenium,<sup>17-23</sup> for instance, the synthesis and reactivity of half sandwich complexes with thiolate ligands (Chart 1.1), giving complexes exhibiting unusual reactivity and coordination modes.<sup>22, 24, 25</sup> More recently, the synthesis and reactivity of a series of half-sandwich chromium and ruthenium complexes with sulfur-containing tripodal ligands was reported by our group and it was found that they can act as metalloligands to give rise to a wide variety of heterobimetallic complexes.<sup>26-28</sup>

**Chart 1.1.** Half sandwich chromium and ruthenium complexes with S-containing ligands.



Transition metal sulfur complexes and their chemistry are extensively exploited in both industry and biology.<sup>29</sup> In industry, metal sulfides play important roles in catalysis, lubrication and antioxidation processes. Many of the biologically essential transition metals made use of sulfur coordination in one way or another in their biological manifestations. Due to the importance of transition metal sulfur complexes, there is continuing research in the synthesis, reactivity and applications of

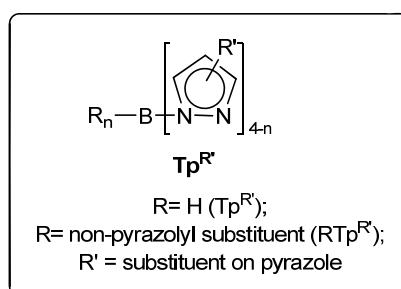
new transition metal sulfur complexes. One such class of complexes is the half-sandwich metal complexes with sulfur containing ligands.

In an extension of our interest in the reactivity of half-sandwich chromium and ruthenium complexes towards sulfur containing ligand, the synthesis and reactivity of some half-sandwich chromium and ruthenium complexes with two classes of sulfur containing ligands, namely the soft scorpionates-poly(methimzoly)borates and heterocyclic thiolates, will be investigated.

### 1.1. Scorpionate Complexes

Scorpionate ligands are a class of tetrasubstituted boron anions, with the donor atoms of two or more pyrazol-2-yl substituents (pz) attached to the boron (Chart 1.2). The first scorpionate ligand, the tris(pyrazolyl)borate (abbreviated as Tp or  $[\text{HB}(\text{pz})_3]$ ) anion, was synthesized by S. Trofimenko in 1966 via the solid state reaction of an alkali metal borohydride with pyrazole.<sup>30</sup>

**Chart 1.2.** Structural motifs for scorpionate ligands.

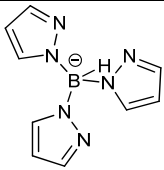
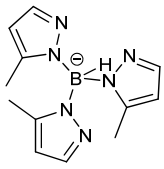
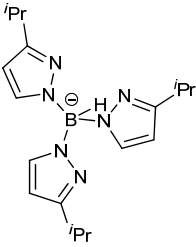


Interest in the scorpionate ligands stems from their structural analogy to the cyclopentadienyl (Cp) and pentamethylcyclopentadienyl (Cp\*) ligands, a cornerstone of organometallic chemistry. Like the Cp ligand, the scorpionate ligands are uninegative, six-electron donor and usually occupy three coordination sites. However, a wider structural variety of the polypyrazolylborate ligands, in comparison to the Cp

and Cp\* ligands, can be made available with specific steric and electronic features to fine tune and control the coordination chemistry of such ligands.

Some reported metal complexes containing the scorpionate ligands and their applications are depicted in Chart 1.3. Homoscorpionate ligands, having the structure  $[\text{HB}(\text{Rpz})_3]^-$ , have been used to stabilize the dihydrogen complexes of ruthenium,  $\text{TpRu}(\text{PR}_3)(\text{H}_2)\text{H}_2$  and  $\text{TpRu}(\text{PR}_3)(\text{H}_2)\text{H}$ .<sup>31,32</sup>

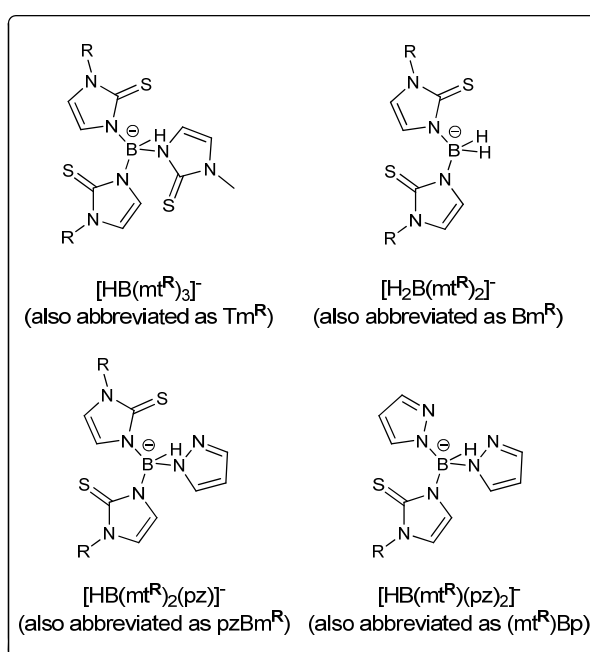
**Chart 1.3.** Metal complexes of scorpionate ligands.

Ligand	Complex	Applications
 <p>Tp</p>	<ul style="list-style-type: none"> <li>• <math>\text{TpRu}(\text{PR}_3)(\text{H}_2)(\text{H})_2</math></li> <li>• <math>\text{TpRu}(\text{PR}_3)(\text{H}_2)\text{H}</math></li> <li>• <math>\text{TpRuCl}(\text{PPh}_3)_2</math></li> </ul>	<ul style="list-style-type: none"> <li>• Stabilised dihydrogen complexes</li> <li>• Catalysts</li> </ul>
 <p>Tp*</p>	<ul style="list-style-type: none"> <li>• <math>\text{Tp}^*\text{Rh}(\text{CO})_2</math></li> </ul>	<ul style="list-style-type: none"> <li>• Activation of C-H bonds</li> </ul>
 <p>Tp<sup>iPr</sup></p>	<ul style="list-style-type: none"> <li>• <math>\text{Tp}^{\text{iPr}2}\text{Fe}(\text{OOCPh})(\text{MeCN})</math></li> </ul>	<ul style="list-style-type: none"> <li>• Synthetic model for dioxygen binding sites of non-heme iron proteins</li> </ul>

Scorpionate complexes have been used in catalytic studies and enzyme modeling. Neutral complexes of  $\text{Ru}^{\text{II}}$ , such as  $\text{TpRuCl}(\text{PPh}_3)_2$ , were found to catalyse the dimerisation of terminal alkynes;<sup>33</sup> the  $\text{Tp}_2\text{Fe}$  complex demonstrated catalytic activity in the oxidation of methyl linolate;<sup>34</sup> rhodium<sup>35-37</sup> and iridium<sup>38-41</sup> complexes such as  $\text{Tp}^*\text{Rh}(\text{CO})_2$  ( $\text{Tp}^* = \{\text{HB}(\text{pz}^{\text{Me}})_3\}^-$ ) have been studied in the activation of aliphatic and aromatic C-H. The scorpionate ligands based on the tris(pyrazolyl)borate had been used to model bioinorganic systems in which the metal is coordinated to three

imidazolyl N atoms from three histidine (His).  $\text{Tp}^{i\text{Pr}2}\text{Fe}(\text{OOCPh})(\text{MeCN})$  was synthesized and found to be a synthetic model for dioxygen binding sites of non-heme iron proteins.<sup>42</sup> Various zinc-based scorpionate complexes, e.g.,  $\text{Tp}^{\text{R}}\text{ZnOH}$  complexes, have been synthesized for modeling of carbonic anhydrase<sup>43-45</sup> and liver alcohol dehydrogenase (LAD).<sup>46</sup> Scorpionates combining two nitrogens and one sulfur have also been employed to model biologically active metal ions which are coordinated by two histidines and one methionine (met)/cysteine (cys) ligands. Soft scorpionates such as the poly(methimazolyl)borate ligands (Chart 1.4), the  $\text{S}_2$ ,  $\text{S}_3$ ,  $\text{S}_2\text{N}$  and  $\text{SN}_2$  analogues of the  $\text{N}_3$ -Tp ligand, have also been synthesized<sup>47-50</sup> and some of our work with some of these ligands will be discussed in Chapters 2-4.

**Chart 1.4.** Poly(methimazolyl)borate anions



### 1.1.1. Poly(methimazolyl)borates

In the past decade, new scorpionate ligands such as tris(methimazolyl)borate,  $[\text{HB}(\text{mt})_3]^-$  (also abbreviated as  $\text{Tm}^{\text{R}}$ ), the allied compounds, bis(methimazolyl)borate,  $[\text{H}_2\text{B}(\text{mt})_2]^-$  (also abbreviated as  $\text{Bm}^{\text{R}}$ )<sup>51</sup> and the hybrid  $\text{mt}_2\text{pz}$ ,

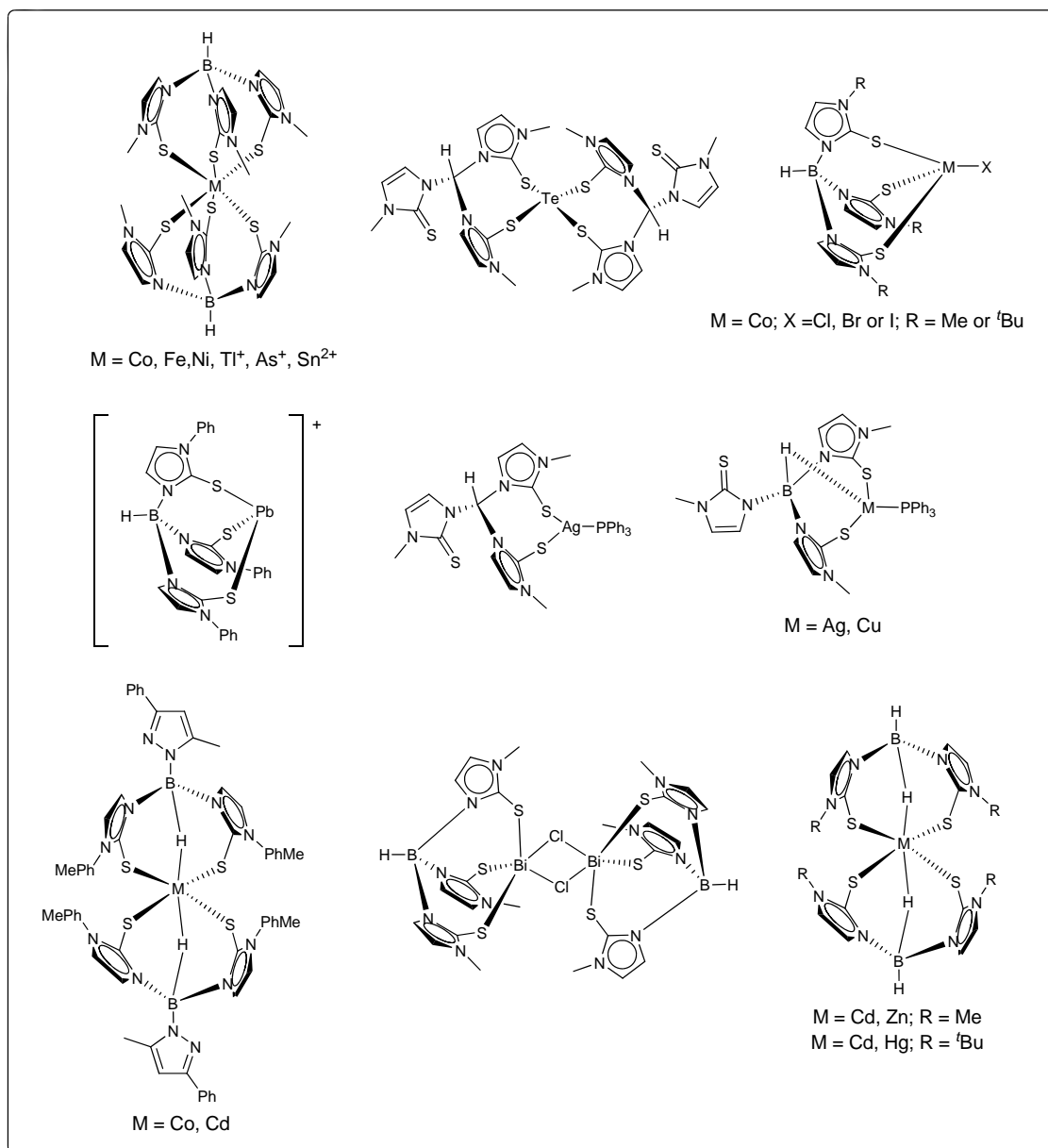
bis(methimazolyl)(pyrazolyl)borate,  $[\text{HB}(\text{mt})_2(\text{pz})]^-$  (also abbreviated as  $\text{pzBm}^{\text{R}}$ ) have been intensely studied by the groups of Reglinski, Spicer, Parkin, Hill and others. According to Hill, studies for this class of ligands can be classified under three broad areas,<sup>52</sup> namely (a) coordination/organometallic chemistry, (b) bioinorganic chemistry (biomimetic model) and (c) metallaborane chemistry.

### (a) Coordination/organometallic chemistry

The poly(methimazolyl)borates are soft analogues of Trofimenko's nitrogen donor poly(pyrazolyl)borates.<sup>53</sup> Both have been extensively developed as co-ligands in coordination and organometallic chemistry.<sup>52, 54-59</sup> To date, complexes of types  $\text{M}(\text{Tm}^{\text{R}})_2$  and  $\text{M}(\text{Bm}^{\text{R}})_2$  are known for the first row transition metals of groups 8-11, the group 12 metals and the main group elements Sn and Pb, As and Bi and Te.<sup>51, 60-68</sup> For the  $[\text{pz}^{\text{R}}\text{Bm}^{\text{R}'}]$ , the sandwich complexes,  $\text{M}(\text{pz}^{\text{R}}\text{Bm}^{\text{R}'})_2$  for Co and Cd have also been reported.<sup>69</sup> Also well characterized are compounds of type  $\text{M}(\text{Tm}^{\text{R}})$  [ $\text{M} = \text{Ag}(\text{I}), \text{Tl}(\text{I}), \text{Pb}(\text{II})$ ]<sup>70-72</sup> of type  $[\text{M}(\text{Tm}^{\text{R}})\text{X}]$  [ $\text{X} = \text{Cl}, \text{Br}, \text{I}$ , and  $\text{M} = \text{Zn}, \text{Cd}$  and  $\text{Hg}$ ]<sup>73-75</sup> and  $\text{Co}(\text{II})$ <sup>76</sup> and of type  $\text{Tm}^{\text{R}}\text{M}(\text{PR}_3)$  [ $\text{M} = \text{Cu}, \text{Ag}$  and  $\text{Au}$ ] (see Chart 1.5).<sup>56,77-79</sup> Notably, the successful isolation of the unusual  $\text{Bi}(\text{III})$   $[\text{Bi}(\text{Tm}^{\text{R}})_2]^+$  cation demonstrated that  $\text{Tm}^{\text{R}}$  is the softest in the series of  $6e^-$  donor ligands, indicating a softness order of  $\text{Tm}^{\text{R}} > \text{Cp} > \text{Tp}^{\text{R}}$  for the face-capping ligands.<sup>51</sup>

An interesting aspect of the coordination chemistry of the poly(methimazolyl)borate ligands is the wide range of coordination modes adopted by the ligands, varying from the expected  $\kappa^3\text{-S,S',H}$  for  $\text{Bm}^{\text{R}}$ ;  $\kappa^3\text{-S,S',S''}$  for  $\text{Tm}^{\text{R}}$  and  $\kappa^3\text{-S,S',N}$  for  $\text{pzBm}^{\text{R}}$  to more unusual coordination mode such as  $\mu\text{-}\kappa^1\text{-S}$ :  $\kappa^1\text{-S}$  in  $[\text{TmAu}]_2$  (see Chart 1.6).<sup>77</sup>

**Chart 1.5.** Examples of coordination complexes containing poly(methimazolyl)borate ligands.



The *organometallic* chemistry of the poly(methimazolyl)borate ligands, in particular that of the [HB(mt)<sub>2</sub>(pz)] anion, is less developed than its coordination chemistry. To date, there has been only one example of an organometallic complex with the [HB(mt)<sub>2</sub>(pz)] ligand, [(pzBm<sup>Me</sup>)Mn(CO)<sub>3</sub>] in which the ligand adopts a  $\kappa^3$ -S,S',N coordination (Chart 1.6 III).<sup>80</sup>

Chart 1.6. Different coordination modes of the poly(methimazolyl)borate anions.

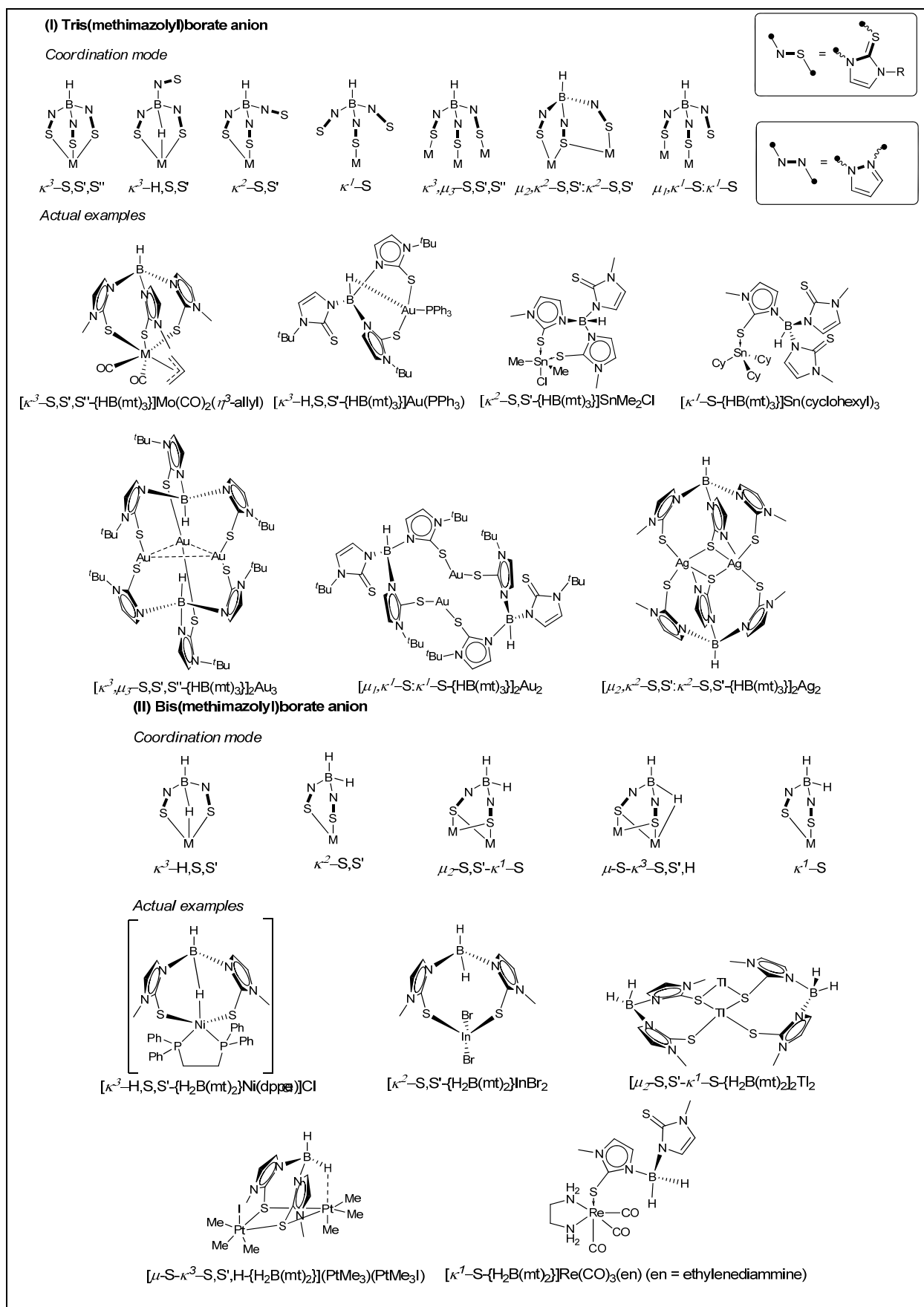
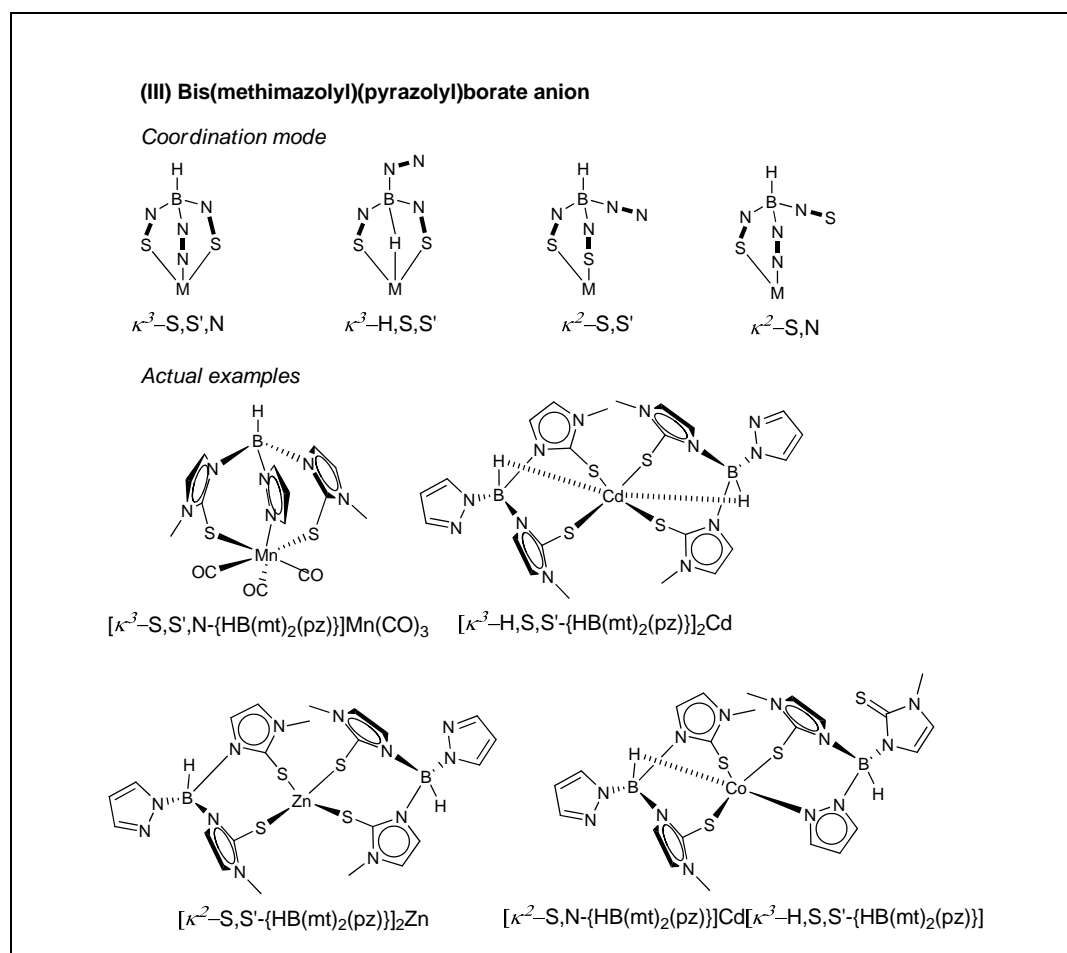




Chart 1.6. (continued)



For the  $[\text{HB(mt)}_3]^-$  and  $[\text{H}_2\text{B(mt)}_2]^-$  ligands, the organometallic carbonyl complexes of Mo<sup>81-83</sup>, W<sup>84, 85</sup>, Re, Tc<sup>48, 86, 87</sup> and Mn<sup>80</sup> have been reported (Chart 1.6 I and II). The Re(I) and Tc(I) compounds containing *fac*-M(CO)<sub>3</sub> fragments coordinated to Tm<sup>R</sup> or Bm<sup>R</sup> are of relevance to the development of new radiopharmaceuticals.<sup>48, 86-91</sup> In all instances, the Tm<sup>R</sup> and Bm<sup>R</sup> ligands occupy three coordination sites and act as six electrons donor via either a  $\kappa^3\text{-S,S',S''}$  or  $\kappa^3\text{-S,S',H}$  coordination mode to the metal centre. Also noteworthy is that the poly(methimazolyl)borate ligands behave similarly to the poly(pyrazolyl)borate ligands in this manner for the early organotransition metal complexes. Contrary to expectation imposed from the HSAB concept, Hill and coworkers have synthesized and isolated niobium and tantalum complexes,  $[\text{M}(=\text{NC}_6\text{H}_3^i\text{Pr}_2\text{-2,6})\text{Cl}_2\{\text{HB(mt)}_3\}]$  (M

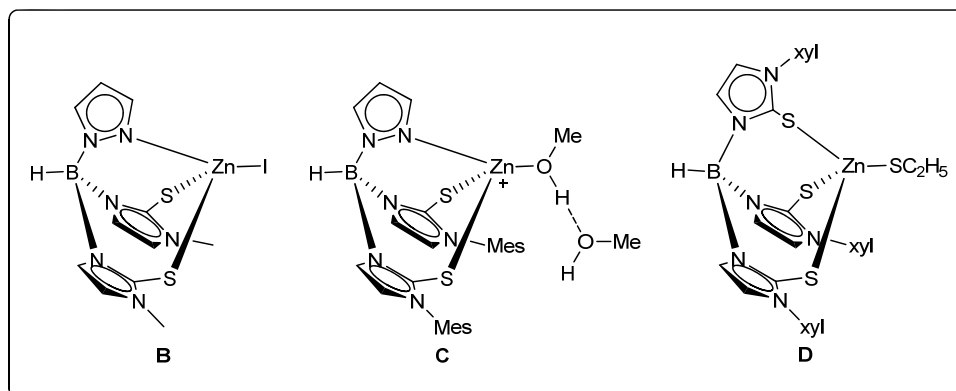
= Nb, Ta) and  $[\{\text{HB}(\text{mt})_3\}]\text{Ta}(\eta^2\text{-RC}\equiv\text{CR})\text{Cl}_2$  by using appropriate co-ligands to tune the electrophilic nature of the  $\text{Nb}^{\text{V}}$  and  $\text{Ta}^{\text{V}}$  centres to prevent decomposition of the poly(methimazolyl)borate ligands.<sup>55</sup> Other organometallic compounds include the Ru(II) compounds  $[(\text{Tm}^{\text{R}})\text{Ru}(p\text{-cymene})]\text{Cl}$  and  $[(\text{Tm}^{\text{R}})\text{RuCp}]$ ,<sup>92</sup> the tin(IV) complexes  $[(\text{Tm}^{\text{R}})\text{R}_x\text{SnCl}_y]$  ( $x = 1\text{-}3$ ;  $y = 3\text{-}x$ ).<sup>59</sup>

### (b) Biomimetic Models

From a *bioinorganic perspective*, several groups have capitalized on the tripodal "tetrahedral enforcing" nature of these  $\text{S}_3$ -ligands to generate coordination compounds of Group 12 metals suitable for use as biomimetic models of the zinc enzyme liver alcohol dehydrogenase (LADH).<sup>68, 93-95</sup> In a search for the closest coordination model of Zn in LADH (which involves one histidine and two cysteine residues), Vahrenkamp and Parkin trialed compounds containing a  $\text{S}_2\text{N}$  environment provided by  $(\text{pzBm}^{\text{R}})\text{hydroborate}$  ligands<sup>67, 76, 96, 97</sup> or  $\text{Bm}^{\text{R}}$  with a N-coligand<sup>49</sup>.

Parkin had reported the synthesis of a  $[\text{bis}(\text{thioimidazolyl})(\text{pyrazolyl})\text{hydroborato}]\text{zinc}$  complex,  $[\text{HB}(\text{mt})_2(\text{pz})]\text{ZnI}$  (**B**), which is a synthetic model of LAD; a monomeric tetrahedral zinc-methanol complex was also synthesized and isolated which is similar to the proposed alcohol intermediate in the LADH catalytic cycle (**C**)<sup>98</sup>, Vahrenkamp reported the synthesis of

**Chart 1.7.** Models of zinc enzymes based on poly(methimazolyl)borate anions.<sup>99</sup>

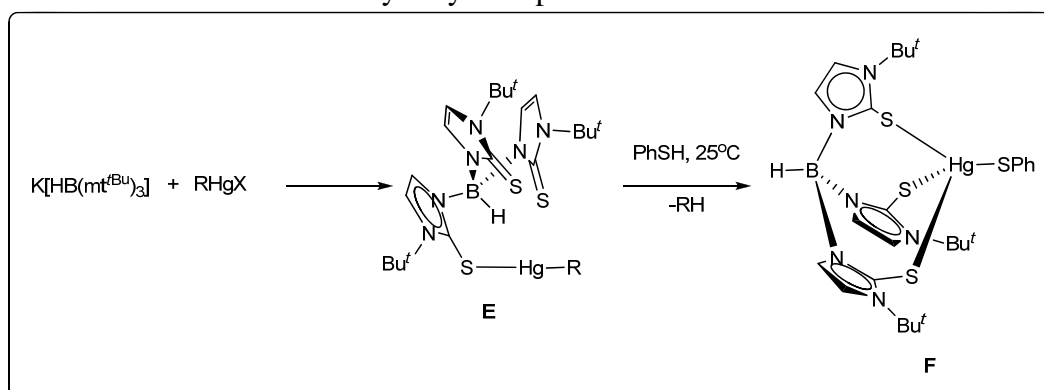


tris(thioimidazolyl)borate zinc thiolate complexes,  $\text{Tm}^{\text{R}}\text{Zn-SR}'$  (such as **D**) as biological mimics of the Ada DNA repair protein for modeling biological thiolate alkylations (Chart 1.7).

In addition, Parkin had also reported recently the  $\text{Tm}^{\text{tBu}}\text{HgR}$  alkyl compounds ( $\text{R} = \text{Me}$  or  $\text{Et}$ ) that are both synthetic and functional models of the organomercurial enzyme, *MerB*, which is made possible by the ability of the  $\text{Tm}^{\text{tBu}}$  ligand to adopt the  $\kappa^2$  (**E**) and  $\kappa^3$  (**F**) coordination modes in solution (Scheme 1.1).<sup>99</sup>

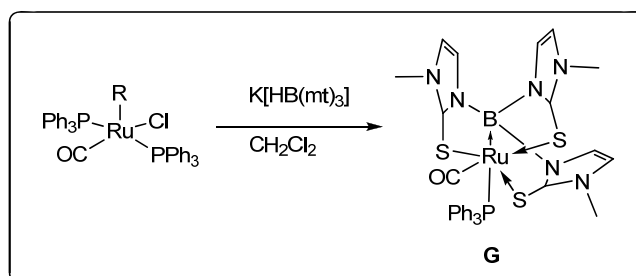
More recently, Carrano and coworkers have synthesized a series of monooxo-Mo(IV,V) and dioxo-Mo(VI) complexes containing the  $\text{Tm}^{\text{Me}}$  ligand and investigated the oxygen atom transfer kinetics, in an attempt to use them as models for the oxygen atom transfer sulfite oxidase structurally and functionally.<sup>100</sup>

**Scheme 1.1.** Protolytic cleavage by a thiol of the Hg-C bond in mercury-alkyl compounds.

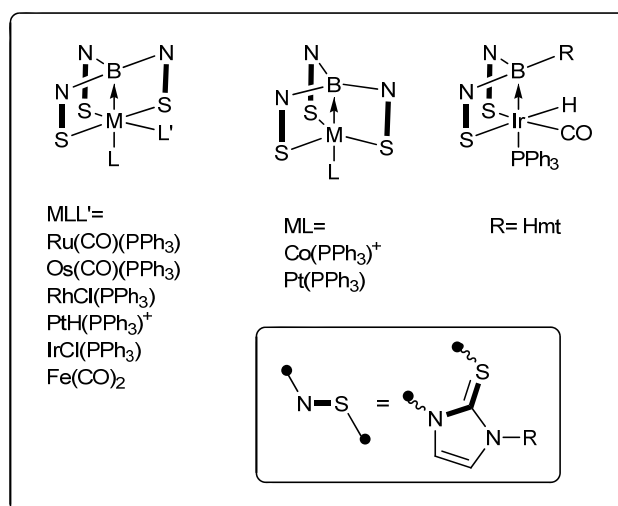


### (c) Metallaboranes

In an attempt to synthesise  $[\text{Ru}(\text{R})(\text{CO})(\text{PPh}_3)\{\text{HB}(\text{mt}_3)\}]$ , for which the Tp analogue is known,<sup>101, 102</sup> Hill and co-workers isolated the first structurally characterized metallaborane,  $[\text{Ru}\{\text{B}(\text{mt}_3)\}(\text{CO})(\text{PPh}_3)]$  (**G**, Scheme 1.2), which exhibits a  $\kappa^4\text{-B,S,S',S''}$  coordination, from the reaction of the complex  $[\text{Ru}(\text{CH}=\text{CHCPh}_2\text{OH})\text{Cl}(\text{CO})(\text{PPh}_3)_2]$  with  $\text{Na}[\text{HB}(\text{mt}_3)_3]$ .<sup>103</sup>

**Scheme 1.2.** Synthesis of ruthenaborane **G**

Since then, Hill's group has further synthesised various metallaboranes for Os,<sup>104</sup> Pt(0) Pt(II) and Pt(IV)<sup>105, 106</sup>, Ir(I)<sup>107</sup> and Rh(I),<sup>108-112</sup> whilst Parkin's group have reported metallaboranes of Ir and Rh,<sup>113</sup> Fe<sup>114</sup> and Pd<sup>115</sup> and Reglinski, the cobaltaborane (Chart 1.8).<sup>66</sup> This phenomenon of B-H bond activation is only apparent in the Tm<sup>R</sup> ligands and thus far, there have been no report of the B-H bond activation in the metal complexes of Bm<sup>R</sup> ligands while for the pzBm<sup>R</sup> and mtBp ligands, the lack of such observation is more likely due to sparse research in the organometallic chemistry.

**Chart 1.8.** Metallaboranes based on the Tm<sup>R</sup> ligands.

Hill had proposed that the B-H activation can be ascribed to a few factors: (i) the larger eight-membered chelate rings adopted in the metal complexes of the Tm<sup>R</sup> ligands, compared to the six-membered chelate rings in Tp<sup>R</sup> ligands and (ii) the

variable hybridization at sulfur in  $\text{Tm}^{\text{R}}$  compared with trigonal nitrogen donors on the pyrazolyl rings in  $\text{Tp}^{\text{R}}$ .<sup>104, 112, 116</sup> These factors confer greater flexibility to the coordinated  $\text{Tm}^{\text{R}}$  ligands, giving rise to unusual bonding scenarios, one of which is the  $\kappa^3\text{-H,S,S'}$  coordination via a three-centre two-electrons, agostic-like B-H...M bond that has a propensity to undergo B-H activation, typically in transition metals with a  $d^n$  configuration where  $n = 8$  or more.

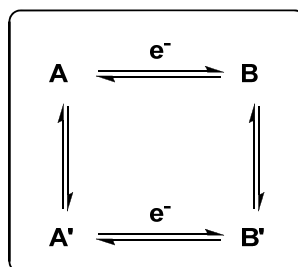
### 1.1.2. Electrochemistry of scorpionate complexes

We noted that there is only one report on the electrochemistry of poly(methimazolyl)borate complexes, Reglinski and coworkers synthesized the cobalt mixed-sandwich complexes,  $[\text{Co}(\text{Tm}^{\text{Me}})(\text{Cp}^{\text{Me}})]\text{I}$  and studied their electrochemical behavior to compare with other cobalt sandwich complexes.<sup>61</sup> They found that  $\text{Tm}^{\text{Me}}$  in  $[\text{Co}(\text{Tm}^{\text{Me}})(\text{Cp}^{\text{Me}})]^+$  is more electron-donating than Tp and Cp. This is consistent with their previous findings on the donor ability of Cp, Tp and  $\text{Tm}^{\text{Me}}$  by comparison of the carbonyl stretching frequencies in  $[\text{W}(\text{L})(\text{CO})_3\text{I}]$  and in  $[\text{Mo}(\text{L})(\text{CO})_2(\eta^3\text{-C}_3\text{H}_5)]$  ( $\text{L}=\text{Cp}, \text{Tp}, \text{Tm}^{\text{Me}}$ ).<sup>81</sup>

Conversely, there are a number of electrochemical studies reported in the literature for the complexes of poly(pyrazolyl)borates. Mann and coworkers had carried out electrochemical studies on a series of mixed-sandwich complexes with  $[\text{HB}(\text{pz})_3]$ ,  $[\text{CpRuHB}(\text{pz})_3]$ ,  $[\text{CpRuHB}(3,5\text{-Me}_2\text{pz})_3]$ , and  $[\text{CpRuB}(\text{pz})_4]$ , and found that the mixed sandwich complexes exhibit different electrochemical behaviour from ruthenocene and more nearly resemble the behaviour of ferrocene.<sup>117</sup> Geiger and coworkers reported the electrochemistry of  $[\text{LL}'\text{Rh}^{\text{III}}(\text{Tp}^{\text{Me}_2})]$  complexes, where  $\text{L} = \text{CO}$  or  $\text{PPh}_3$  and  $\text{L}' = \text{P}(\text{OPh})_3$ ,  $\text{PPh}_3$  or  $\text{PCy}_3$ .<sup>118</sup> The Rh(II) compounds were known to favor  $\kappa^3$ -bonding in  $\text{Tp}^{\text{Me}_2}$  (through 3 nitrogen atoms) resulting in five-coordinate

complexes, whereas the Rh(I) complexes favored  $\kappa^2$ -bonding in  $\text{Tp}^{\text{Me}_2}$  (or an equilibrium between  $\kappa^2$ - and weak  $\kappa^3$ - $\text{Tp}^{\text{Me}_2}$  coordination) producing four-coordinate complexes. The observed cyclic voltammetric responses were interpreted based on the rates of heterogeneous electron transfer. The compounds that displayed slow (irreversible) heterogeneous charge transfer processes were modeled according to the square scheme (Scheme 1.3), involving intramolecular associative and dissociative formation/cleavage of the Rh-N bond.

**Scheme 1.3.** Electrochemical consecutive square scheme.



Compounds that underwent fast (reversible) heterogeneous electron transfer were consistent with either a concerted (single step) mechanism or with the chemical steps in Scheme 1.3 proceeding so quickly that they were indistinguishable from the charge transfer step.

It occurred to us that such electrochemical investigations can be applied to the examination of any fluxionality between the  $\kappa^3$ -S,S',H and  $\kappa^3$ -S,S',L (L=S or N) coordination modes exhibited by the  $[\text{HB}(\text{mt})_3]^-$  and  $[\text{HB}(\text{mt})_2(\text{pz})]$  ligands, as reported in the literature.

In chapter 2-4, the syntheses of mixed sandwich complexes of chromium and ruthenium, comprising the poly(methimazolyl)borate ligands, (i)  $[\text{HB}(\text{mt})_3]^-$ , (ii)  $[\text{H}_2\text{B}(\text{mt})_2]^-$  and (iii)  $[\text{HB}(\text{mt})_2(\text{pz})]^-$  are presented (Chart 1.4.), together with the study of their solution phase chemistry using a combination of spectroscopic (NMR) and dynamic electrochemical (cyclic voltammetry) techniques, where possible.

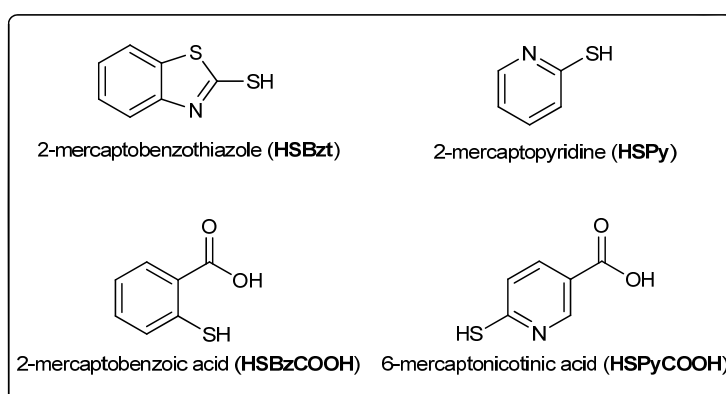
## 1.2. Heterocyclic thiolate complexes

The research interest in these heterocyclic thiolates stems from their biological activity, numerous practical applications and structural diversity.<sup>119, 120</sup> For instance, the thiazole moiety can be found in many biomolecules such as the penicillins and penems, as well as in natural products like thiamin.<sup>121</sup> In addition, heterocyclic thiolates are often used in a wide range of industrial applications such as metal-chelating agents, lubricant additives such as inhibitors and vulcanization of rubber, to name a few.<sup>122</sup>

As a follow up of previous studies by our group,<sup>22, 123, 124</sup> we focus here on four heterocyclic thiolates, namely 2-mercaptobenzothiazole (HSBzt), 2-mercaptopyridine (HSPy), 2-mercaptobenzoic acid (HSBzCOOH) and 6-mercaptonicotinic acid (HSPyCOOH) (Chart 1.9). These thiolates contain a combination of donor-atoms (N, O, S) and offers diverse coordination potential.

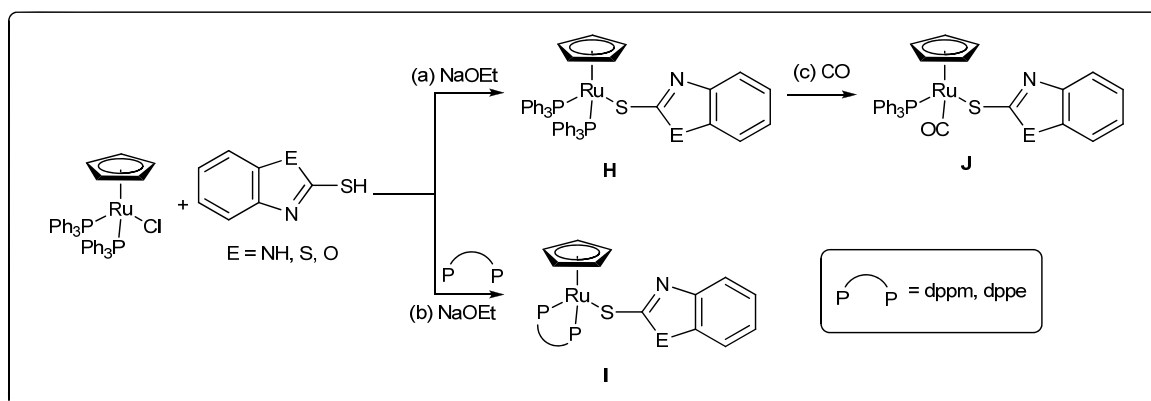
Although the chemistry of Cp'Ru-thiolate complexes is well developed, half-sandwich Ru complexes with heterocyclic ligands are rare and there have been only a few examples reported. [CpRu(PPh<sub>3</sub>)<sub>2</sub>Cl] reacted with thiolate of 2-mercaptobenzimidazolyl, 2-mercaptobenzothiazolyl and 2-mercaptobenzoxazolyl to give the corresponding thiolate complexes (**H** and **I**, Scheme 1.4(a)).

**Chart 1.9.** Heterocyclic thiolates investigated in this project.



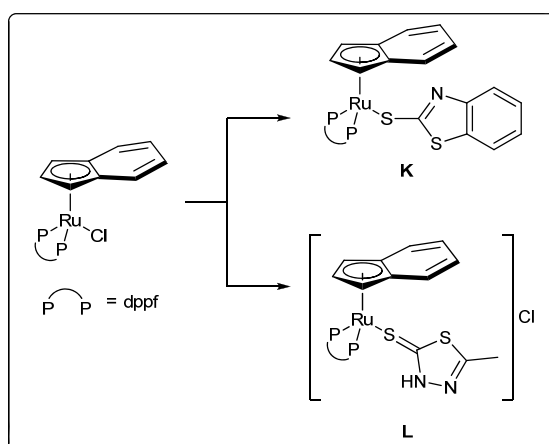
In the presence of diphosphine ligands, the corresponding diphosphine Ru complexes can be isolated (Scheme 1.4(b)). The coordinated  $\text{PPh}_3$  ligand in  $\text{CpRu}(\text{PPh}_3)_2(\text{thiolate})$  can be displaced by CO to give  $[\text{CpRu}(\text{PPh}_3)(\text{CO})(\text{thiolate})]$  (**J**) as shown in Scheme 1.4(c).<sup>125</sup>

**Scheme 1.4.** Synthesis of CpRu complexes with heterocyclic thiolates.



Recently, our group has also reported the synthesis of a series of  $[(\text{Ind})\text{RuL}_2(\text{SR})]$  complexes (**K-L**) (Ind = indenyl; R = 2-mercaptopyrimidine (HSPym) or 2-mercaptobenzothiazole (HSBzt)) from the reaction of  $[(\text{Ind})\text{Ru}(\text{dppf})\text{Cl}]$  with the respective thiolate salts (Scheme 1.5).<sup>17</sup>

**Scheme 1.5.** Synthesis of  $[(\text{Ind})\text{Ru}(\text{dppf})(\text{SR})]$  complexes



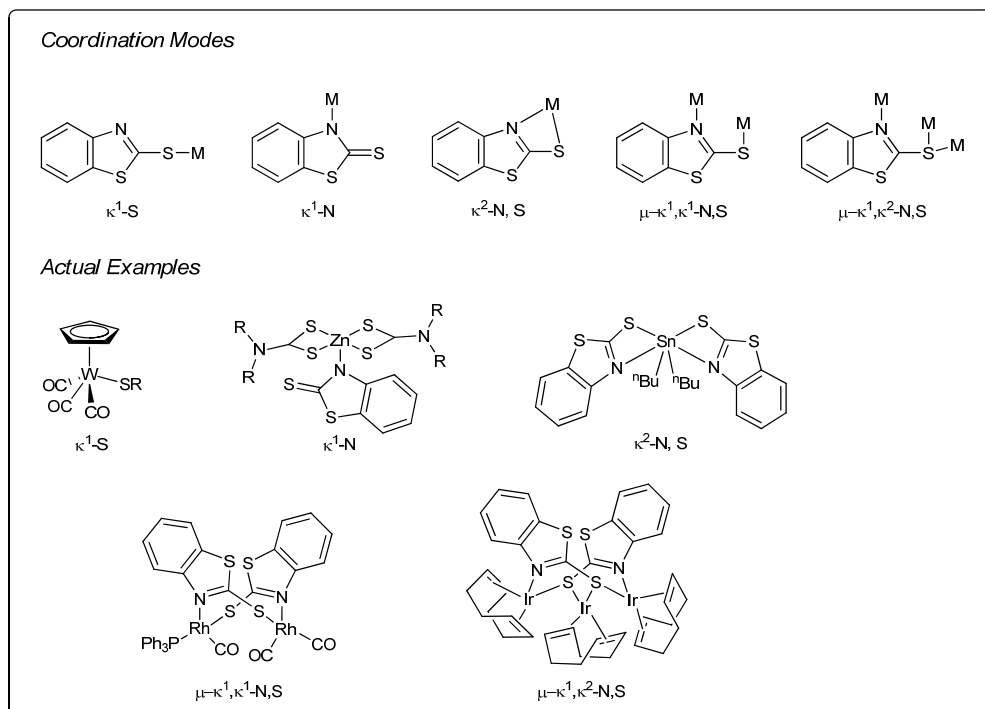


### 1.2.1. Complexes of 2-mercaptobenzothiazole

The coordination chemistry of 2-mercaptobenzothiazole (HSBzt) metal complexes has been much studied owing to interest in their biological activity, practical applications and structural diversity.<sup>119, 120, 126</sup> The structural diversity in the complexes of HSBzt results from the availability of the exocyclic S and the thioamido N atoms which give rise to a variety of coordination and bonding modes to generate compounds of different nuclearity, as illustrated in Chart 1.10.

Compared to coordination compounds of the HSBzt ligand, organometallic complexes are scarce; there only exists a limited number of bridged bi- or multi-nuclear complexes of Re, Rh, Ir, Pd, Pt, Ru and Group 11 metals, all containing CO and/or cyclooctadiene as coligands.<sup>127-135</sup>

**Chart 1.10.** Different coordination modes exhibited by HSBzt in metal complexes.



Both the coordination and organometallic complexes of SBzt have found applications as accelerators in the vulcanization of natural rubber,<sup>119, 120, 126</sup> corrosion

inhibitors,<sup>131, 133</sup> and lately also in environmental control of toxic metals like mercury.<sup>48c</sup> Other aspects of their reactivities have been rarely studied.

### 1.2.2. Complexes of 2-mercaptopyridine

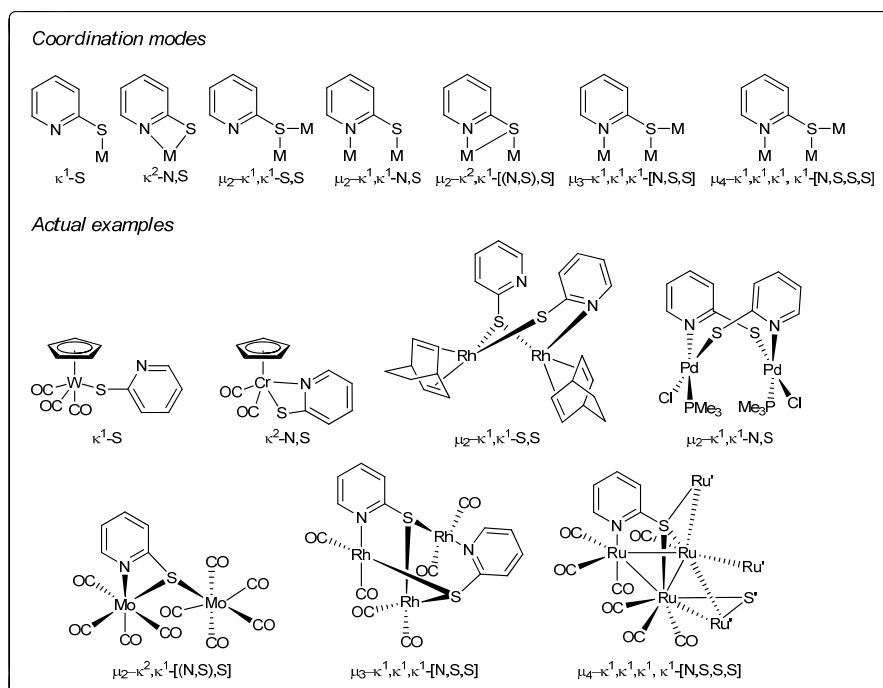
Compounds of 2-mercaptopyridine (HSPy), with transition and other main group metals received intense research interest because of their biological activity and many practical applications. In the field of bioorganic and bioinorganic studies, the use of 2-mercaptopyridine and its derivatives is prevalent. High resolution mapping of nucleoprotein complexes by site-specific protein-DNA can be achieved with the aid of this class of ligand. It can be used as a non-acidic matrix for the matrix-assisted laser desorption in the analysis of bio-macromolecules and it is also commonly used as a thio-substituted pyrimidine bases for RNA-catalysed nucleotide synthesis.<sup>136</sup> A recent study showed that women with atherosclerotic CVD and are allergic or show contraindications when using aspirin can use other antiplatelet agents, such as newer thiopyridine derivatives, to prevent vascular events.<sup>137</sup>

Recent examples of Sn-S bonded compounds such as those with 2-mercaptopyridine show fungicidal activities against a range of test samples.<sup>138</sup> A series of work on the electronic and magnetic properties of some Fe(II)-Fe(III) complexes through a 2-mercaptopyridine bridge were also investigated by Moreno and coworkers.<sup>139</sup> Besides the various application studies on 2-mercaptopyridine and its metal complexes, the free ligand has also been characterized by the thiol-thione tautomerism.<sup>140</sup>

The coordination and structural diversity of metal complexes with 2-mercaptopyridine is also an established field of study. Similar to HSBzt, the availability of the soft thiolate sulfur and the hard thioamide nitrogen atoms as coordination sites render the ligand extremely versatile, capable of coordinating to a

great variety of main-group and transition metal complexes. This is shown in the wide array of metal complexes possessing different bonding modes illustrated in Chart 1.11.<sup>123, 128, 130, 141-145</sup>

**Chart 1.11.** Different coordination modes of HSPy in metal complexes

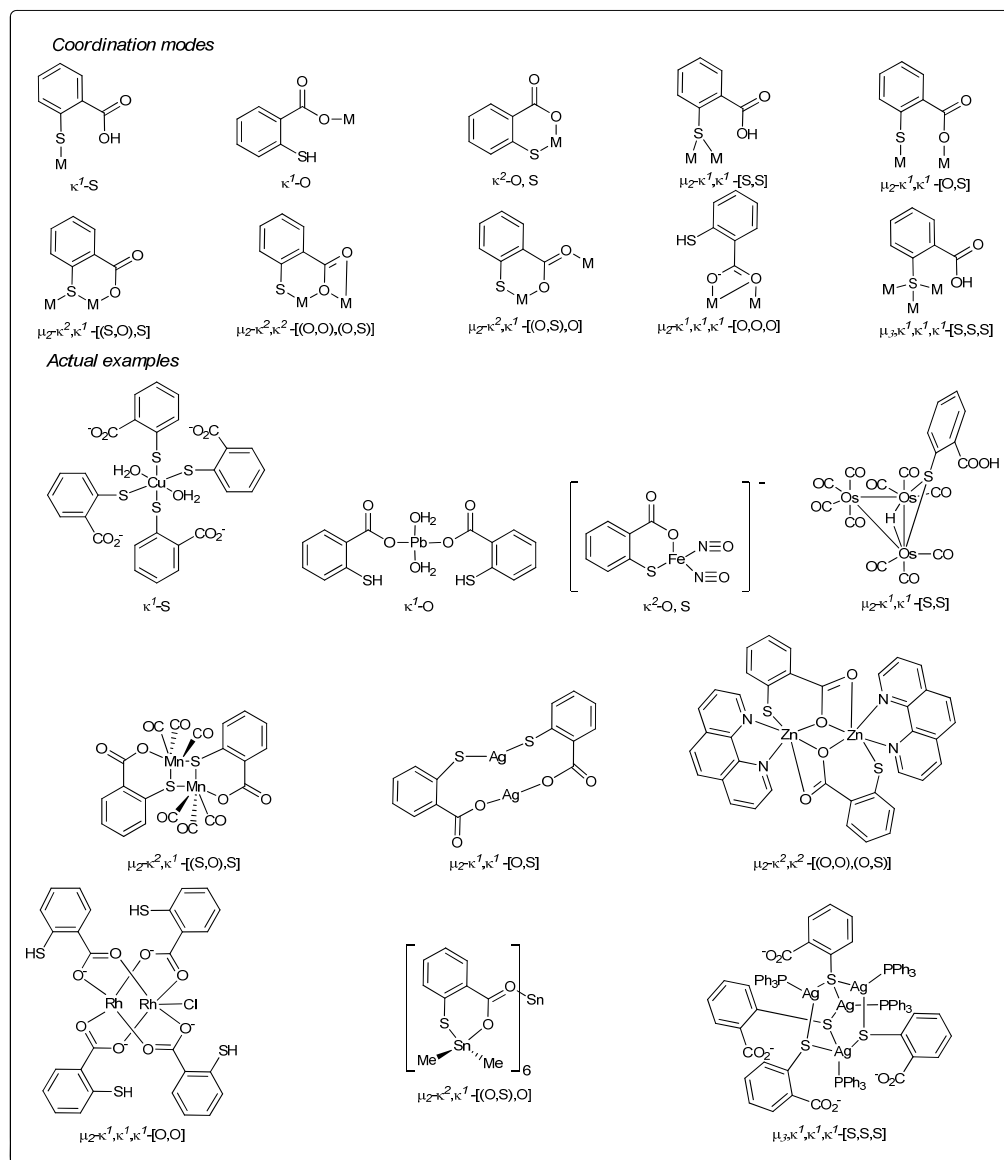


### 1.2.3. Complexes of 2-mercaptobenzoic acid

There are numerous reports in the literature on the synthesis of the coordination complexes of 2-mercaptobenzoic acid (HSBzCOOH). The research interests in these complexes stems from their biological activity, for instance antimicrobial<sup>146-149</sup>, anticancer<sup>150-152</sup> and anti-arthritic activities.<sup>153, 154</sup> The exocyclic S and the carboxylic group in HSBzCOOH gave rise to structural diversity in its complexes leading to a variety of coordination and bonding modes, as illustrated in Chart 1.12.<sup>155-159</sup>

Of particular interest to us is that the carboxylic group can possibly be converted to the corresponding carboxylate salts using an inorganic base to give water-soluble organometallic complexes.

**Chart 1.12.** Different coordination modes of HSBzCOOH in metal complexes. <sup>155-159</sup>

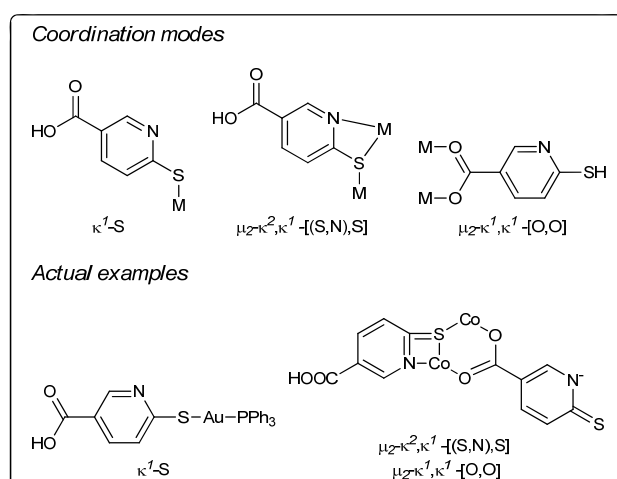


#### 1.2.4. Complexes of 6-mercaptonicotinic acid

Unlike the previous three heterocyclic thiolates, HSBzt, HSPy and HSBzCOOH, the coordination chemistry of 6-mercaptonicotinic acid (HSPyCOOH) is less developed. In fact, there are sparse reports on the metal complexes of

HSPyCOOH,<sup>160-162</sup> compared to that of its isomer, 2-mercaptonicotinic acid. Wood and coworkers have isolated magnetic clusters of Co(II) and Ni(II) within 3-dimensional organic frameworks of SPyCOOH and found the porous cobalt(II)-organic frameworks with corrugated walls to be structurally robust gas-sorption materials.<sup>161, 162</sup> Kato and coworkers have reported the synthesis of two-coordinate gold(I)-PPh<sub>3</sub> complexes with SPyCOOH and found the Au complex to exhibit selective and effective antimicrobial activities against Gram-positive bacteria (*B. subtilis* and/or *S. aureus*).<sup>147, 163</sup> Some of coordination modes exhibited by SPyCOOH in the few known metal complexes are shown in Chart 1.13.

**Chart 1.13.** Coordination modes exhibited by HSPyCOOH in metal complexes.



Even though there are reports of only three coordination modes in the literature for SPyCOOH, the presence of the exocyclic S, the carboxylic acid and the thioamido N atom offers much more possibility for coordination and this can be inferred from the coordination chemistry of its isomer, 2-mercaptonicotinic acid.<sup>164-167</sup> Moreover, like SBzCOOH, 6-mercaptonicotinic acid has a carboxylic functional group which can be readily converted to a salt to give its complexes higher solubility in aqueous media.

## References

1. Liu, S. A.; Han, Y. F.; Jin, G. X., *Chem. Soc. Rev.* **2007**, 36 (10), 1543-1560.
2. Kumar, K. N.; Venkatachalam, G.; Ramesh, R.; Liu, Y., *Polyhedron* **2008**, 27 (1), 157-166.
3. Xiao, X. Q.; Jin, G. X., *J. Organomet. Chem.* **2008**, 693 (2), 316-320.
4. Coto, A.; Tenorio, M. J.; Puerta, M. C.; Valerga, P., *Organometallics* **1998**, 17 (20), 4392-4399.
5. Werner, H., *Organometallics* **2005**, 24 (6), 1036-1049.
6. Haas, K.; Beck, W., *Z. Anorg. Allg. Chem.* **2002**, 628 (4), 788-796.
7. Coville, N. J.; Duplooy, K. E.; Pickl, W., *Coord. Chem. Rev.* **1992**, 116, 1-267.
8. Venkatesan, K.; Blacque, O.; Fox, T.; Alfonso, M.; Schmale, H. W.; Kheradmandan, S.; Berke, H., *Organometallics* **2005**, 24 (5), 920-932.
9. Esteruelas, M. A.; Lopez, A. M.; Mateo, A. C.; Onate, E., *Organometallics* **2006**, 25 (6), 1448-1460.
10. Buil, M. L.; Esteruelas, M. A.; Lopez, A. M.; Mateo, A. C., *Organometallics* **2006**, 25 (17), 4079-4089.
11. Esteruelas, M. A.; Gonzalez, A. I.; Lopez, A. M.; Oliván, M.; Onate, E., *Organometallics* **2006**, 25 (3), 693-705.
12. Jimenez-Tenorio, M.; Puerta, M. C.; Valerga, P., *Eur. J. Inorg. Chem.* **2004**, (1), 17-32.
13. Osipov, A. L.; Gerdov, S. M.; Kuzmina, L. G.; Howard, J. A. K.; Nikonov, G. I., *Organometallics* **2005**, 24 (4), 587-602.
14. Liu, S.; Wang, H.; Zhang, P. C.; Weng, L. H.; Hou, X. F., *Organometallics* **2008**, 27 (4), 713-717.
15. Han, Y. F.; Huang, Y. B.; Lin, Y. H.; Jin, G. X., *Organometallics* **2008**, 27 (5), 961-966.
16. Cheung, W.-M.; Zhang, Q.-F.; Williams, I. D.; Leung, W.-H., *Inorg. Chim. Acta* **2006**, 359 (3), 782-788.
17. Ng, S. Y.; Leong, W. K.; Goh, L. Y.; Webster, R. D., *Eur. J. Inorg. Chem.* **2007**, (3), 463-471.
18. Lu, X. L.; Vittal, J. J.; Tiekink, E. R. T.; Goh, L. Y.; Hor, T. S. A., *J. Organomet. Chem.* **2004**, 689 (9), 1444-1451.
19. Lau, H. F.; Ang, P. C. Y.; Ng, V. W. L.; Kuan, S. L.; Goh, L. Y.; Borisov, A. S.; Hazendonk, P.; Roemmele, T. L.; Boere, R. T.; Webster, R. D., *Inorg. Chem.* **2008**, 47 (2), 632-644.
20. Lau, H. F.; Ng, V. W. L.; Koh, L. L.; Tan, G. K.; Goh, L. Y.; Roemmele, T. L.; Seagrave, S. D.; Boere, R. T., *Angew. Chem. Int. Ed.* **2006**, 45 (27), 4498-4501.
21. Ang, C. Y.; Boere, R. T.; Goh, L. Y.; Koh, L. L.; Kuan, S. L.; Tan, G. K.; Yu, X., *Chem. Commun.* **2006**, (45), 4735-4737.
22. Weng, Z.; Goh, L. Y., *Acc. Chem. Res.* **2004**, 37 (3), 187-199.
23. Shin, R. Y. C.; Goh, L. Y., *Acc. Chem. Res.* **2006**, 39 (5), 301-313.
24. Ng, V. W. L.; Kuan, S. L.; Leong, W. K.; Koh, L. L.; Tan, G. K.; Goh, L. Y.; Webster, R. D., *Inorg. Chem.* **2005**, 44 (15), 5229-5240.
25. Kuan, S. L.; Leong, W. K.; Goh, L. Y.; Webster, R. D., *J. Organomet. Chem.* **2006**, 691 (5), 907-915.
26. Shin, R. Y. C.; Ng, V. W. L.; Koh, L. L.; Tan, G. K.; Goh, L. Y.; Webster, R. D., *Organometallics* **2007**, 26 (18), 4555-4561.

27. Shin, R. Y. C.; Tan, G. K.; Koh, L. L.; Vittal, J. J.; Goh, L. Y.; Webster, R. D., *Organometallics* **2005**, *24* (4), 539-551.
28. Tay, E. P. L.; Kuan, S. L.; Leong, W. K.; Goh, L. Y., *Inorg. Chem.* **2007**, *46* (4), 1440-1450.
29. Stiefel, E. I.; Matsumoto, K.; Editors, *Transition Metal Sulfur Chemistry: Biological and Industrial Significance*. **1996**.
30. Trofimenko, S., *J. Am. Chem. Soc.* **1966**, *88* (8), 1842-1844.
31. Halcrow, M. A.; Chaudret, B.; Trofimenko, S., *J. Chem. Soc., Chem. Commun.* **1993**, (5), 465-467.
32. Moreno, B.; Sabo-Etienne, S.; Chaudret, B.; Rodriguez-Fernandez, A.; Jalon, F.; Trofimenko, S., *J. Am. Chem. Soc.* **1994**, *116* (6), 2635-2636.
33. Slugovc, C.; Mereiter, K.; Zobetz, E.; Schmid, R.; Kirchner, K., *Organometallics* **1996**, *15* (25), 5275-5277.
34. Tachibana, M.; Sasaki, K.; Ueda, A.; Sakai, M.; Sakakibara, Y.; Ohno, A.; Okamoto, T., *Chem. Lett.* **1991**, (6), 993-996.
35. Purwoko, A. A.; Lees, A. J., *Inorg. Chem.* **1995**, *34* (2), 424-425.
36. Purwoko, A. A.; Drolet, D. P.; Lees, A. J., *J. Organomet. Chem.* **1995**, *504* (1-2), 107-113.
37. Shaw, M. J.; Hyde, J.; White, C.; Geiger, W. E., *Organometallics* **2004**, *23* (9), 2205-2208.
38. Boutry, O.; Gutierrez, E.; Monge, A.; Nicasio, M. C.; Perez, P. J.; Carmona, E., *J. Am. Chem. Soc.* **1992**, *114* (18), 7288-7290.
39. Perez, P. J.; Poveda, M. L.; Carmona, E., *J. Chem. Soc., Chem. Commun.* **1992**, (1), 8-9.
40. Tellers, D. M.; Yung, C. M.; Arndtsen, B. A.; Adamson, D. R.; Bergman, R. G., *J. Am. Chem. Soc.* **2002**, *124* (7), 1400-1410.
41. Tanke, R. S.; Crabtree, R. H., *Inorg. Chem.* **1989**, *28* (18), 3444-3447.
42. Kitajima, N.; Fukui, H.; Morooka, Y., *J. Chem. Soc., Chem. Commun.* **1988**, (7), 485-486.
43. Alsfasser, R.; Ruf, M.; Trofimenko, S.; Vahrenkamp, H., *Chemische Berichte* **1993**, *126* (3), 703-710.
44. Hammes, B. S.; Carrano, C. J., *Dalton Trans.* **2000**, (19), 3304-3309.
45. Looney, A.; Han, R.; McNeill, K.; Parkin, G., *J. Am. Chem. Soc.* **1993**, *115* (11), 4690-4697.
46. Bergquist, C.; Parkin, G., *Inorg. Chem.* **1999**, *38* (3), 422-423.
47. Garner, M.; Reglinski, J.; Cassidy, I.; Spicer, M. D.; Kennedy, A. R., *Chem. Commun.* **1996**, (16), 1975-1976.
48. Garcia, R.; Paulo, A.; Domingos, A.; Santos, I.; Ortner, K.; Alberto, R., *J. Am. Chem. Soc.* **2000**, *122* (45), 11240-11241.
49. Kimblin, C.; Hascall, T.; Parkin, G., *Inorg. Chem.* **1997**, *36* (25), 5680-5681.
50. Benkmil, B.; Ji, M.; Vahrenkamp, H., *Inorg. Chem.* **2004**, *43* (26), 8212-8214.
51. Reglinski, J.; Spicer, M. D.; Garner, M.; Kennedy, A. R., *J. Am. Chem. Soc.* **1999**, *121* (10), 2317-2318.
52. Hill, A. F.; Smith, M. K., *Organometallics* **2007**, *26* (16), 3900-3903.
53. Trofimenko, S., *Scorpionates: The Coordination Chemistry of Polypyrazolyborate Ligands*. 1st ed.; Imperial College Press: London, 1999.
54. Crossley, I. R.; Hill, A. F.; Willis, A. C., *Organometallics* **2007**, *26* (16), 3891-3895.
55. Hill, A. F.; Smith, M. K., *Organometallics* **2007**, *26* (18), 4688-4691.

56. Dodds, C. A.; Garner, M.; Reglinski, J.; Spicer, M. D., *Inorg. Chem.* **2006**, *45* (6), 2733-2741.
57. Biernat, A.; Schwalbe, M.; Wallace, D.; Reglinski, J.; Spicer, M. D., *Dalton Trans.* **2007**, (22), 2242-2244.
58. Wallace, D.; Gibson, L. T.; Reglinski, J.; Spicer, M. D., *Inorg. Chem.* **2007**, *46* (10), 3804-3806.
59. Santini, C.; Pellei, M.; Gioia Lobbia, G.; Pettinari, C.; Drozdov, A.; Troyanov, S., *Inorg. Chim. Acta* **2001**, *325* (1,2), 20-28.
60. Garner, M.; Lewinski, K.; Pattek-Janczyk, A.; Reglinski, J.; Sieklucka, B.; Spicer, M. D.; Szaleniec, M., *Dalton Trans.* **2003**, (6), 1181-1185.
61. Dodds, C. A.; Lehmann, M.-A.; Ojo, J. F.; Reglinski, J.; Spicer, M. D., *Inorg. Chem.* **2004**, *43* (16), 4927-4934.
62. Slavin, P. A.; Reglinski, J.; Spicer, M. D.; Kennedy, A. R., *Dalton Trans.* **2000**, (3), 239-240.
63. Dodds, C. A.; Kennedy, A. R.; Reglinski, J.; Spicer, M. D., *Inorg. Chem.* **2004**, *43* (2), 394-395.
64. Dodds, C. A.; Jagoda, M.; Reglinski, J.; Spicer, M. D., *Polyhedron* **2004**, *23* (2-3), 445-450.
65. Alvarez, H. M.; Tran, T. B.; Richter, M. A.; Alyounes, D. M.; Rabinovich, D.; Tanski, J. M.; Krawiec, M., *Inorg. Chem.* **2003**, *42* (6), 2149-2156.
66. Mihalcik, D. J.; White, J. L.; Tanski, J. M.; Zakharov, L. N.; Yap, G. P. A.; Incarvito, C. D.; Rheingold, A. L.; Rabinovich, D., *Dalton Trans.* **2004**, (10), 1626-1634.
67. Kimblin, C.; Bridgewater, B. M.; Hascall, T.; Parkin, G., *Dalton Trans.* **2000**, (8), 1267-1274.
68. Parkin, G., *Chem. Commun.* **2000**, (20), 1971-1985.
69. Shu, M.-H.; Tu, C.-L.; Cui, J.; Sun, J., *Wuji Huaxue Xuebao* **2006**, *22* (8), 1507-1510.
70. Santini, C.; Lobbia, G. G.; Pettinari, C.; Pellei, M.; Valle, G.; Calogero, S., *Inorg. Chem.* **1998**, *37* (5), 890-900.
71. Ojo, J. F.; Slavin, P. A.; Reglinski, J.; Garner, M.; Spicer, M. D.; Kennedy, A. R.; Teat, S. J., *Inorg. Chim. Acta* **2001**, *313* (1-2), 15-20.
72. Bridgewater, B. M.; Parkin, G., *J. Am. Chem. Soc.* **2000**, *122* (29), 7140-7141.
73. Cassidy, I.; Garner, M.; Kennedy, A. R.; Potts, G. B. S.; Reglinski, J.; Slavin, P. A.; Spicer, M. D., *Eur. J. Inorg. Chem.* **2002**, (5), 1235-1239.
74. Bakbak, S.; Bhatia, V. K.; Incarvito, C. D.; Rheingold, A. L.; Rabinovich, D., *Polyhedron* **2001**, *20* (28), 3343-3348.
75. White, J. L.; Tanski, J. M.; Rabinovich, D., *J. Chem. Soc., Dalton Trans.* **2002**, (15), 2987-2991.
76. Kimblin, C.; Bridgewater, B. M.; Churchill, D. G.; Hascall, T.; Parkin, G., *Inorg. Chem.* **2000**, *39* (19), 4240-4243.
77. Patel, D. V.; Mihalcik, D. J.; Kreisel, K. A.; Yap, G. P. A.; Zakharov, L. N.; Kassel, W. S.; Rheingold, A. L.; Rabinovich, D., *Dalton Trans.* **2005**, (14), 2410-2416.
78. Santini, C.; Pettinari, C.; Gioia Lobbia, G.; Spagna, R.; Pellei, M.; Vallorani, F., *Inorg. Chim. Acta* **1999**, *285* (1), 81-88.
79. Gioia Lobbia, G.; Pettinari, C.; Santini, C.; Somers, N.; Skelton, B. W.; White, A. H., *Inorg. Chim. Acta* **2001**, *319* (1,2), 15-22.



80. Graham, L. A.; Fout, A. R.; Kuehne, K. R.; White, J. L.; Mookherji, B.; Marks, F. M.; Yap, G. P. A.; Zakharov, L. N.; Rheingold, A. L.; Rabinovich, D., *Dalton Trans.* **2005**, (1), 171-180.
81. Garner, M.; Lehmann, M.-A.; Reglinski, J.; Spicer, M. D., *Organometallics* **2001**, 20 (24), 5233-5236.
82. Foreman, M. R. S. J.; Hill, A. F.; Tshabang, N.; White, A. J. P.; Williams, D. J., *Organometallics* **2003**, 22 (26), 5593-5596.
83. Foreman, M. R. S. J.; Hill, A. F.; Smith, M. K.; Tshabang, N., *Organometallics* **2005**, 24 (22), 5224-5226.
84. Foreman, M. R. S. J.; Hill, A. F.; White, A. J. P.; Williams, D. J., *Organometallics* **2003**, 22 (19), 3831-3840.
85. Abernethy, R. J.; Hill, A. F.; Neumann, H.; Willis, A. C., *Inorg. Chim. Acta* **2005**, 358 (5), 1605-1613.
86. Garcia, R.; Paulo, A.; Domingos, A.; Santos, I., *J. Organomet. Chem.* **2001**, 632 (1-2), 41-48.
87. Garcia, R.; Paulo, A.; Domingos, A.; Santos, I., *Dalton Trans.* **2003**, (13), 2757-2760.
88. Garcia, R.; Domingos, A.; Paulo, A.; Santos, I.; Alberto, R., *Inorg. Chem.* **2002**, 41 (9), 2422-2428.
89. Garcia, R.; Xing, Y.-H.; Paulo, A.; Domingos, A.; Santos, I., *J. Chem. Soc., Dalton Trans.* **2002**, (22), 4236-4241.
90. Garcia, R.; Paulo, A.; Domingos, A.; Santos, I.; Pietzsch, H. J., *Synth. React. in Inorg. Me.* **2005**, 35 (1), 35-42.
91. Garcia, R.; Gano, L.; Maria, L.; Paulo, A.; Santos, I.; Spies, H., *J. Biol. Inorg. Chem.* **2006**, 11 (6), 769-782.
92. Bailey, P. J.; Lorono-Gonzales, D. J.; McCormack, C.; Parsons, S.; Price, M., *Inorg. Chim. Acta* **2003**, 354, 61-67.
93. Vahrenkamp, H., *Acc. Chem. Res.* **1999**, 32 (7), 589-596.
94. Tesmer, M.; Shu, M.; Vahrenkamp, H., *Inorg. Chem.* **2001**, 40 (16), 4022-4029.
95. Kimblin, C.; Churchill, D. G.; Bridgewater, B. M.; Girard, J. N.; Quarless, D. A.; Parkin, G., *Polyhedron* **2001**, 20 (15-16), 1891-1896.
96. Seebacher, J.; Shu, M.; Vahrenkamp, H., *Chem. Commun* **2001**, (11), 1026-1027.
97. Shu, M.; Walz, R.; Wu, B.; Seebacher, J.; Vahrenkamp, H., *Eur. J. Inorg. Chem.* **2003**, (13), 2502-2511.
98. Kimblin, C.; Bridgewater, B. M.; Churchill, D. G.; Parkin, G., *Chem. Commun.* **1999**, (22), 2301-2302.
99. Melnick, J. G.; Parkin, G., *Science* **2007**, 317 (5835), 225-227.
100. Tran, B. L.; Carrano, C. J., *Inorg. Chem.* **2007**, 46 (13), 5429-5438.
101. Hill, A. F., *J. Organomet. Chem.* **1990**, 395 (2), C35-C38.
102. Alcock, N. W.; Hill, A. F.; Melling, R. P., *Organometallics* **1991**, 10 (11), 3898-3903.
103. Hill, A. F.; Owen, G. R.; White, A. J. P.; Williams, D. J., *Angew. Chem. Int. Ed.*, **1999**, 38 (18), 2759-2761.
104. Foreman, M. R. S. J.; Hill, A. F.; White, A. J. P.; Williams, D. J., *Organometallics* **2004**, 23 (4), 913-916.
105. Crossley, I. R.; Hill, A. F., *Organometallics* **2004**, 23 (24), 5656-5658.
106. Crossley, I. R.; Hill, A. F.; Willis, A. C., *Organometallics* **2005**, 24 (21), 4889-4892.

107. Crossley, I. R.; Hill, A. F.; Willis, A. C., *Organometallics* **2005**, *24* (6), 1062-1064.
108. Crossley, I. R.; Foreman, M. R. S. J.; Hill, A. F.; White, A. J. P.; Williams, D. J., *Chem. Commun.* **2005**, (2), 221-223.
109. Crossley, I. R.; Hill, A. F.; Humphrey, E. R.; Willis, A. C., *Organometallics* **2005**, *24* (16), 4083-4086.
110. Crossley, I. R.; Hill, A. F.; Humphrey, E. R.; Smith, M. K., *Organometallics* **2006**, *25* (16), 4038.
111. Crossley, I. R.; Hill, A. F.; Humphrey, E. R.; Smith, M. K., *Organometallics* **2006**, *25* (9), 2242-2247.
112. Crossley, I. R.; Hill, A. F.; Willis, A. C., *Organometallics* **2006**, *25* (1), 289-299.
113. Landry, V. K.; Melnick, J. G.; Buccella, D.; Pang, K.; Ulichny, J. C.; Parkin, G., *Inorg. Chem.* **2006**, *45* (6), 2588-2597.
114. Figueroa, J. S.; Melnick, J. G.; Parkin, G., *Inorg. Chem.* **2006**, *45* (18), 7056-7058.
115. Pang, K.; Quan, S. M.; Parkin, G., *Chem. Commun.* **2006**, (48), 5015-5017.
116. Foreman, M. R. S. J.; Hill, A. F.; Owen, G. R.; White, A. J. P.; Williams, D. J., *Organometallics* **2003**, *22* (22), 4446-4450.
117. McNair, A. N.; Boyd, D. C.; Mann, K. R., *Organometallics* **1986**, *5* (2), 303-310.
118. Geiger, W. E.; Ohrenberg, N. C.; Yeomans, B.; Connelly, N. G.; Emslie, D. J. H., *J. Am. Chem. Soc.* **2003**, *125* (28), 8680-8688.
119. Raper, E. S., *Coord. Chem. Rev.* **1985**, *61*, 115-84.
120. Raper, E. S., *Coord. Chem. Rev.* **1997**, *165*, 475-567.
121. Thomas, M.; Guillaume, D.; Fourrey, J.-L.; Clivio, P., *J. Am. Chem. Soc.* **2002**, *124* (11), 2400-2401.
122. Kornis, G. I., *Comprehensive Heterocyclic Chemistry II* **1996**, *4*, 379-408, 905-1006.
123. Ng, V. W. L.; Leong, W. K.; Koh, L. L.; Tan, G. K.; Goh, L. Y., *J. Organomet. Chem.* **2004**, *689* (20), 3210-3217.
124. Ng, S. Y.; Leong, W. K.; Goh, L. Y.; Webster, R. D., *Eur. J. Inorg. Chem.* **2008**, (1), 144-151.
125. El-khateeb, M., *Transit. Metal Chem.* **2001**, *26*, 267.
126. Raper, E. S., *Coord. Chem. Rev.* **1996**, *153*, 199-255.
127. Ciriano, M. A.; Perez-Torrente, J. J.; Lahoz, F. J.; Oro, L. A., *J. Organomet. Chem.* **1993**, *455* (1-2), 225-33.
128. Ciriano, M. A.; Viguri, F.; Perez-Torrente, J. J.; Lahoz, F. J.; Oro, L. A.; Tiripicchio, A.; Tiripicchio-Camellini, M., *J. Chem. Soc., Dalton Trans.* **1989**, (1), 25-32.
129. Tejel, C.; Villarroya, B. E.; Ciriano, M. A.; Oro, L. A.; Lanfranchi, M.; Tiripicchio, A.; Tiripicchio-Camellini, M., *Inorg. Chem.* **1996**, *35* (15), 4360-4368.
130. Ciriano, M. A.; Oro, L. A.; Perez-Torrente, J. J.; Tiripicchio, A.; Tiripicchio-Camellini, M., *J. Chem. Soc., Chem. Commun.* **1986**, (23), 1737-8.
131. Jeannin, S.; Jeannin, Y.; Lavigne, G., *Proc. Int. Conf. Coord. Chem., 16th* **1974**, R20, 3 pp.
132. Jeannin, S.; Jeannin, Y.; Lavigne, G., *J. Cryst. Mol. Struc.* **1978**, *7* (5), 241-249.
133. Jeannin, S.; Jeannin, Y.; Lavigne, G., *Inorg. Chem.* **1978**, *17* (8), 2103-2110.

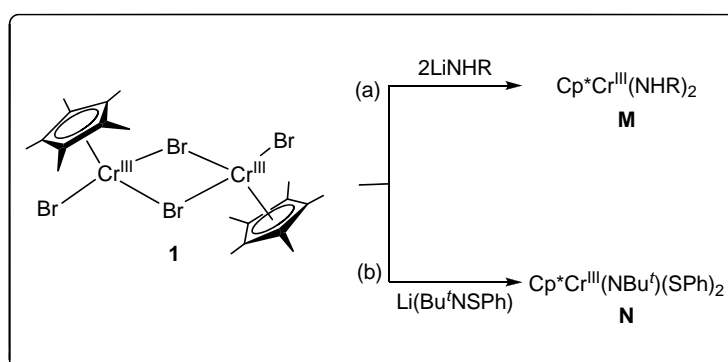
134. Sielisch, T.; Cowie, M., *Organometallics* **1988**, 7 (3), 707-14.
135. Cowie, M.; Sielisch, T., *J. Organomet. Chem.* **1988**, 348 (2), 241-254.
136. Ohba, Y.; Koto, N.; Hamase, K.; Zaitso, K., *Anal. Sci.* **2000**, 16 (6), 659-661.
137. Mosca, L.; Grundy, S. M.; Judelson, D.; King, K.; Limacher, M.; Oparil, S.; Pasternak, R.; Pearson, T. A.; Redberg, R. F.; Smith, S. C.; Winston, M.; Zinberg, S., *J. Am. Coll. Cardiol.* **1999**, 33 (6), 1751-1755.
138. James, B. D.; Magee, R. J.; Patalinghug, W. C.; Skelton, B. W.; White, A. H., *J. Organomet. Chem.* **1994**, 467 (1), 51-55.
139. Diaz, C.; Spodine, E.; Moreno, Y.; Arancibia, A., *Bol. Soc. Chil. Quim.* **2000**, 45 (2), 317-322.
140. Moran, D.; Sukcharoenphon, K.; Puchta, R.; Schaefer, H. F.; Schleyer, P. V.; Hoff, C. D., *J. Org. Chem.* **2002**, 67 (25), 9061-9069.
141. Brandenburg, K. L.; Heeg, M. J.; Abrahamson, H. B., *Inorg. Chem.* **1987**, 26 (7), 1064-1069.
142. Casado, M. A.; Perez-Torrente, J. J.; Ciriano, M. A.; Lahoz, F. J.; Oro, L. A., *Inorg. Chem.* **2004**, 43 (4), 1558-1567.
143. Deeming, A. J.; Meah, M. N. N.; Dawes, H. M.; Hursthouse, M. B., *J. Organomet. Chem.* **1986**, 299 (2), C25-C28.
144. Deeming, A. J.; Karim, M., *Polyhedron* **1991**, 10 (8), 837-840.
145. Ciriano, M. A.; Perez-Torrente, J. J.; Viguri, F.; Lahoz, F. J.; Oro, L. A.; Tiripicchio, A.; Tiripicchiocamellini, M., *J. Chem. Soc.-Dalton Trans.* **1990**, (4), 1493-1502.
146. Anjaneyulu, Y.; Rao, R. P., *P. Indian. Acad. Sci. A* **1989**, 55 (3), 563-569.
147. Nomiya, K.; Yamamoto, S.; Noguchi, R.; Yokoyama, H.; Kasuga, N. C.; Ohyama, K.; Kato, C., *J. Inorg. Biochem.* **2003**, 95 (2-3), 208-220.
148. Anjaneyulu, Y.; Rao, R. P., *Syn. React. Inorg. Met* **1986**, 16 (2), 257-272.
149. Gupta, S. K.; Sharma, R. C.; Gupta, A. K., *Asian Journal of Chemistry* **1992**, 4 (2), 234-238.
150. De Vos, D.; Clements, P.; Pyke, S. M.; Smyth, D. R.; Tiekink, E. R. T., *Metal-Based Drugs* **1999**, 6 (1), 31-40.
151. De Vos, D.; Smyth, D. R.; Tiekink, E. R. T., *Metal-Based Drugs* **2001**, 8 (6), 303-306.
152. Tiekink, E. R. T.; Cookson, P. D.; Linahan, B. M.; Webster, L. K., *Metal-Based Drugs* **1994**, 1 (4), 299-304.
153. Whitehouse, M. W.; Cookson, P. D.; Siasios, G.; Tiekink, E. R. T., *Metal-Based Drugs* **1998**, 5 (4), 245-249.
154. Dinger, M. B.; Henderson, W., *J. Organomet. Chem.* **1998**, 560 (1-2), 233-243.
155. Ainscough, E. W.; Brodie, A. M.; Coll, R. K.; Mair, A. J. A.; Waters, J. M., *J. Organomet. Chem.* **1996**, 509 (2), 259-264.
156. Depree, C. V.; Main, L.; Nicholson, B. K.; Roberts, K., *J. Organomet. Chem.* **1996**, 517 (1-2), 201-207.
157. Al-Daher, I. M.; Al-Saadi, B. M., *Journal of the Iraqi Chemical Society* **1985**, 10 (1), 84-90.
158. Henderson, W.; Nicholson, B. K.; Oliver, A. G.; Rickard, C. E. F., *J. Organomet. Chem.* **2001**, 625 (1), 40-46.
159. Lee, S.-M.; Cheung, K. K.; Wong, W.-T., *J. Cluster Science* **1996**, 7 (3), 435-453.
160. Sanchez, A.; Toma, M.; Casas, J. S.; Castellano, E. E.; Garcia-Tasende, M. S.; Ellena, J.; Santos, S., Jr.; Sordo, J., *Chemistry (Rajkot, India)* **2006**, 3 (2), 69-71.

161. Humphrey, S. M.; Mole, R. A.; McPartlin, M.; McInnes, E. J. L.; Wood, P. T., *Inorg. Chem.* **2005**, *44* (17), 5981-5983.
162. Humphrey, S. M.; Chang, J.-S.; Jhung, S. H.; Yoon, J. W.; Wood, P. T., *Angew. Chem. Int. Ed.* **2007**, *46* (1-2), 272-275.
163. Nomiya, K.; Noguchi, R.; Shigeta, T.; Kondoh, Y.; Tsuda, K.; Ohsawa, K.; Chikaraishi-Kasuga, N.; Oda, M., *B. Chem. Soc. Jpn.* **2000**, *73* (5), 1143-1152.
164. Humphrey, S. M.; Mole, R. A.; Rawson, J. M.; Wood, P. T., *Dalton Trans.* **2004**, (11), 1670-1678.
165. Quintal, S. M. O.; Nogueira, H. I. S.; Felix, V.; Drew, M. G. B., *J. Chem. Soc.-Dalton Trans.* **2002**, (23), 4479-4487.
166. Ma, C. L.; Jiang, Q.; Zhang, R. F., *J. Organomet. Chem.* **2003**, *678* (1-2), 148-155.
167. Zhang, L.; Zhang, H. X.; Chen, C. L.; Deng, L. R.; Kang, B. S., *Inorg. Chim. Acta* **2003**, *355*, 49-56.

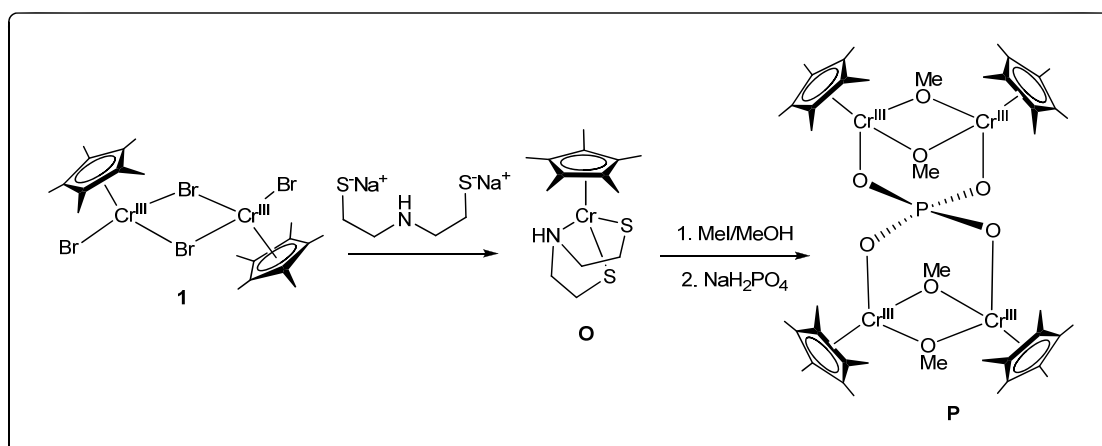
## Chapter 2. Syntheses of mixed-sandwich Cp\*Cr complexes containing poly(methimazoly)borates (Cp\* = C<sub>5</sub>Me<sub>5</sub>)

The synthesis of [Cp\*CrBr<sub>2</sub>]<sub>2</sub> (**1**) was first reported in 1988 by Rauchfuss and coworkers,<sup>1</sup> but the intervening two decades have only seen limited reports on its reactivity. The interaction of **1** with alkyl- and aryl-Li amido compounds LiNHR led to the isolation of a variety of Cp\*Cr- imido complexes (**M**, Scheme 2.1a).<sup>2</sup> An S-N cleavage of a sulfenamido species leading to the formation Cp\*Cr(NBu<sup>t</sup>)(SPh)<sub>2</sub> in the reaction with Li(Bu<sup>t</sup>NSPh) has also been reported (**N**, Scheme 2.1b).<sup>3</sup>

**Scheme 2.1.** Reaction of **1** with LiNHR and Li(Bu<sup>t</sup>NSPh)

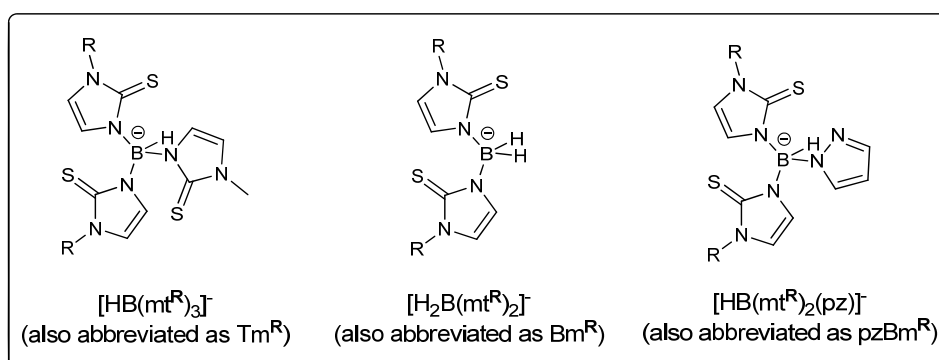


More recently, our group has reported the synthesis of [Cp\*Cr{HN(CH<sub>2</sub>CH<sub>2</sub>S)<sub>2</sub>}] (**O**) from the reaction of **1** with HN(CH<sub>2</sub>CH<sub>2</sub>SNa)<sub>2</sub> (Scheme 2.2).<sup>4</sup> The methylation of complex **O** leads to the unexpected isolation of an organometallic tetranuclear complex, [{(Cp\*Cr)<sub>2</sub>(μ-OMe)<sub>2</sub>}<sub>2</sub>(μ<sub>4</sub>-PO<sub>4</sub>)]X (X = I, PF<sub>6</sub>) (**P**) (Scheme 2.2). To the best of our knowledge, this is the only example of the reaction of **1** with a tripodal sulfur containing ligand. The successful synthesis of complex **O** prompted us to explore the feasibility of reacting **1** with the respective poly(methimazoly)borate salts as a direct entry to mixed sandwich complexes of Cp\*Cr complexes.

Scheme 2.2. Reaction of **1** with  $\text{HN}(\text{CH}_2\text{CH}_2\text{SNa})_2$ 

In this chapter we describe the investigation of the reactivity of **1** towards the poly(methimazolyl)borate ligands shown in Chart 2.1. Since  $\text{Cr}^{\text{III}}$  complexes are paramagnetic and their solution phase chemistry cannot be studied using NMR spectroscopy, the electrochemistry of the synthesized complexes will be investigated to determine if this method can be employed to detect the presence of the equilibrium processes between the coordination modes adopted by the respective poly(methimazolyl) and model such equilibrium processes, where possible.

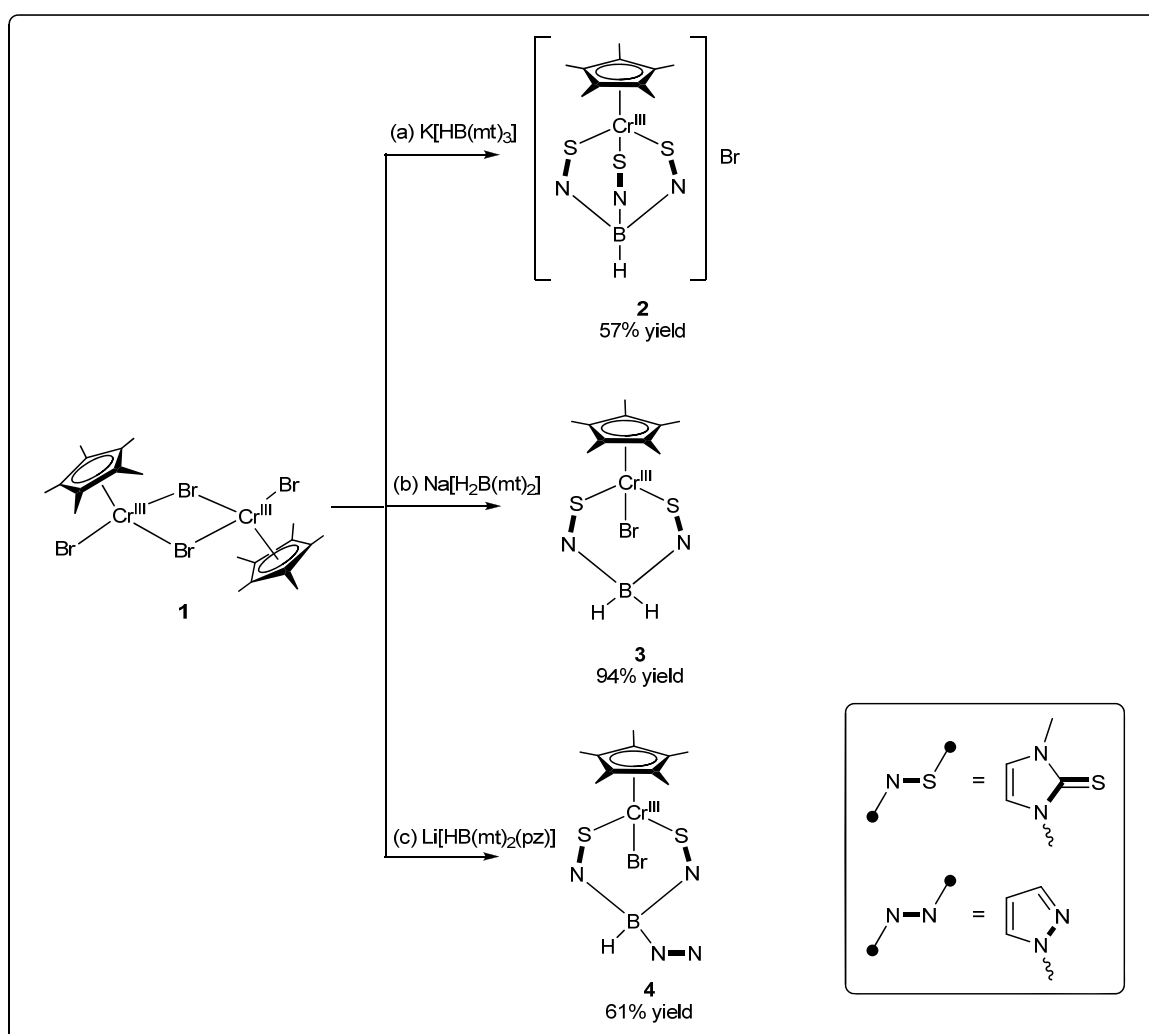
Chart 2.1. Poly(methimazolyl)borate ligands used in this study



## 2.1. Reaction of $[\text{Cp}^*\text{CrBr}_2]_2$ (**1**) with poly(methimazolyl)borate salts

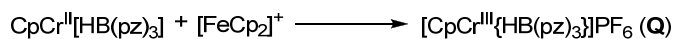
The reaction of  $[\text{Cp}^*\text{CrBr}_2]_2$  (**1**) with (i)  $\text{K}[\text{HB}(\text{mt})_3]$ , (ii)  $\text{Na}[\text{H}_2\text{B}(\text{mt})_2]$  and (iii)  $\text{Li}[\text{HB}(\text{mt})_2(\text{pz})]$  gave the 15-electron  $\text{Cr}(\text{III})$  complexes,  $[\text{Cp}^*\text{Cr}\{\text{HB}(\text{mt})_3\}]\text{Br}$  (**2**),  $[\text{Cp}^*\text{Cr}\{\text{H}_2\text{B}(\text{mt})_2\}]\text{Br}$  (**3**) and  $[\text{Cp}^*\text{Cr}\{\text{HB}(\text{mt})_2(\text{pz})\}]\text{Br}$  (**4**) as blue solids in moderate to high yields (Scheme 2.3). These are the first examples of  $\text{Cr}^{\text{III}}[\text{poly}(\text{methimazolyl})\text{borate}]$  species.

**Scheme 2.3.** Reaction of **1** with (a)  $\text{K}[\text{HB}(\text{mt})_3]$ , (b)  $\text{Na}[\text{H}_2\text{B}(\text{mt})_2]$  and (c)  $\text{Li}[\text{HB}(\text{mt})_2(\text{pz})]$ .



In context, O'Hare and coworkers had earlier synthesised the  $\text{Cr}^{\text{III}}$  complex,  $[\text{CpCr}^{\text{III}}\{\text{HB}(\text{pz})_3\}]\text{PF}_6$  (**Q**) from the oxidation of  $\text{CpCr}^{\text{II}}[\text{HB}(\text{pz})_3]$  (Scheme 2.4).<sup>5</sup>

**Scheme 2.4.** Oxidation of  $\text{CpCr}^{\text{II}}[\text{HB}(\text{pz})_3]$ .



The presence of a paramagnetic  $d^3$ -Cr(III) centre is substantiated by both the low temperature EPR spectrum of **3** which displays a broad linewidth axial shaped EPR spectrum (Figure 2.1) and the  $^1\text{H}$  NMR spectra of **2-4** in  $\text{CD}_3\text{CN}$  with broad signals for the  $\text{Cp}^*$  signal in the  $\delta$  -50 to -80 region.

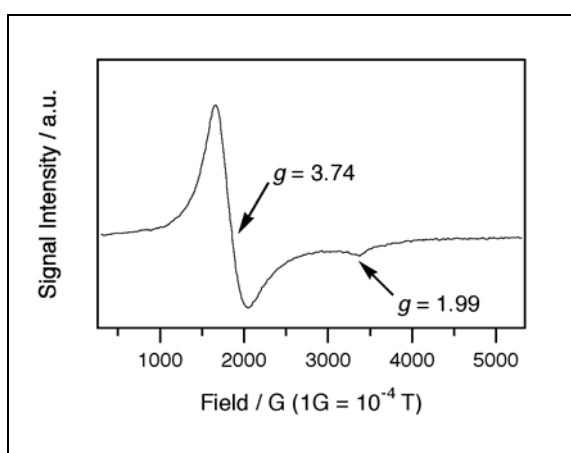


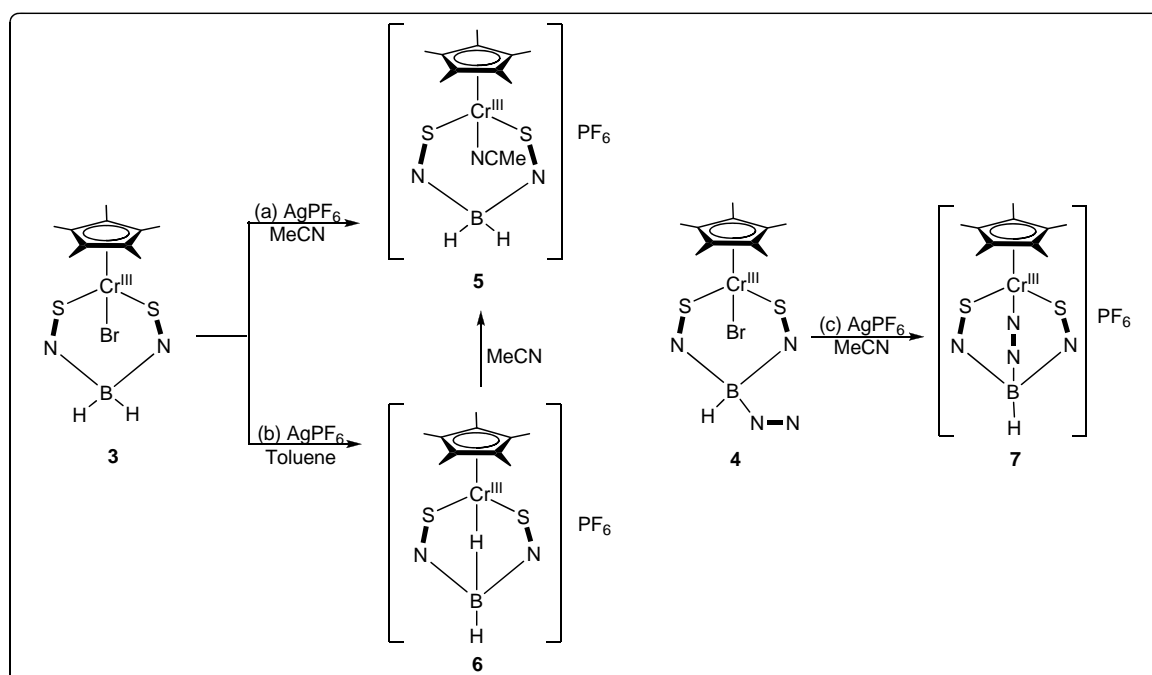
**Figure 2.1.** X-band EPR spectrum of **3** in  $\text{CH}_3\text{CN}$  recorded at 10 K.

Crystallographic studies (see below) show that the  $[\text{HB}(\text{mt})_3]$  ligand binds to the  $\text{Cp}^*\text{Cr}^{\text{III}}$  moiety in **2** in  $\kappa^3$ - $S,S',S''$  tridentate mode, similar to that found in the (*p*-cymene) $\text{Ru}^{\text{II}}$  complex,  $[(p\text{-cymene})\text{Ru}\{\text{HB}(\text{mt})_3\}]\text{Cl}$ .<sup>6</sup> In contrast, the  $[\text{H}_2\text{B}(\text{mt})_2]$  ligand coordinates in a bidentate  $\kappa^2$ - $S,S'$  mode in **3** and **4**, with a Br co-ligand. In the case of **4**, it is surprising that the pz ligand could not displace Br in the coordination sphere of Cr(III). An attempt was therefore made to remove the Br ligands by reactions of both **3** and **4** with  $\text{AgPF}_6$  (Scheme 2.5). The reaction of **3** with  $\text{AgPF}_6$  in MeCN afforded the acetonitrile adduct, **5**, as a royal blue solid, consistent with the observation of a weak  $\text{C}\equiv\text{N}$  stretch at  $2249\text{ cm}^{-1}$  in its IR spectrum. The complex **6**, where the  $[\text{H}_2\text{B}(\text{mt})_2]$  binds to the  $\text{Cr}^{\text{III}}$  centre via a  $\kappa^3$ - $H,S,S'$  coordination, was



isolated as grayish green solid when the reaction was carried out in an acetonitrile-free environment. Complex **6** can be readily converted to **5** by dissolving it in acetonitrile, upon which a royal blue solid is obtained after removal of the solvent. In the reaction of **4** with  $\text{AgPF}_6$  in acetonitrile and only the  $\kappa^3\text{-N,S,S'}$  coordinated complex, **7**, was isolated.

**Scheme 2.5.** Reaction of (a) **3** with  $\text{AgPF}_6$  in MeCN; (b) **3** with  $\text{AgPF}_6$  in toluene and (c) **4** with  $\text{AgPF}_6$  in MeCN.



## 2.2. Crystallographic studies

The molecular structures of the Cr(III) complexes **2-7** are markedly similar and are depicted in Figures 2.2a-f, respectively.

Each of the complexes contains a Cr(III) centre, sandwiched between a Cp\* ring and a poly(methimazolyl)borate ligand. With the exception of **2**, the molecular structures possess crystallographic mirror planes that cut through the Cp\* ring and Cr centre. The bond parameters of **2-7** are given in Table 2.1. The molecular structure of

**2** shows that the [HB(mt)<sub>3</sub>] ligand coordinates to the Cr<sup>III</sup> via a tridentate coordination, consistent with the observed C-S distances (1.714(7)-1.731(7) Å) which are intermediate between values of a single bond (*ca.* 1.81 Å) and a double bond (*ca.* 1.56 Å).<sup>7</sup>

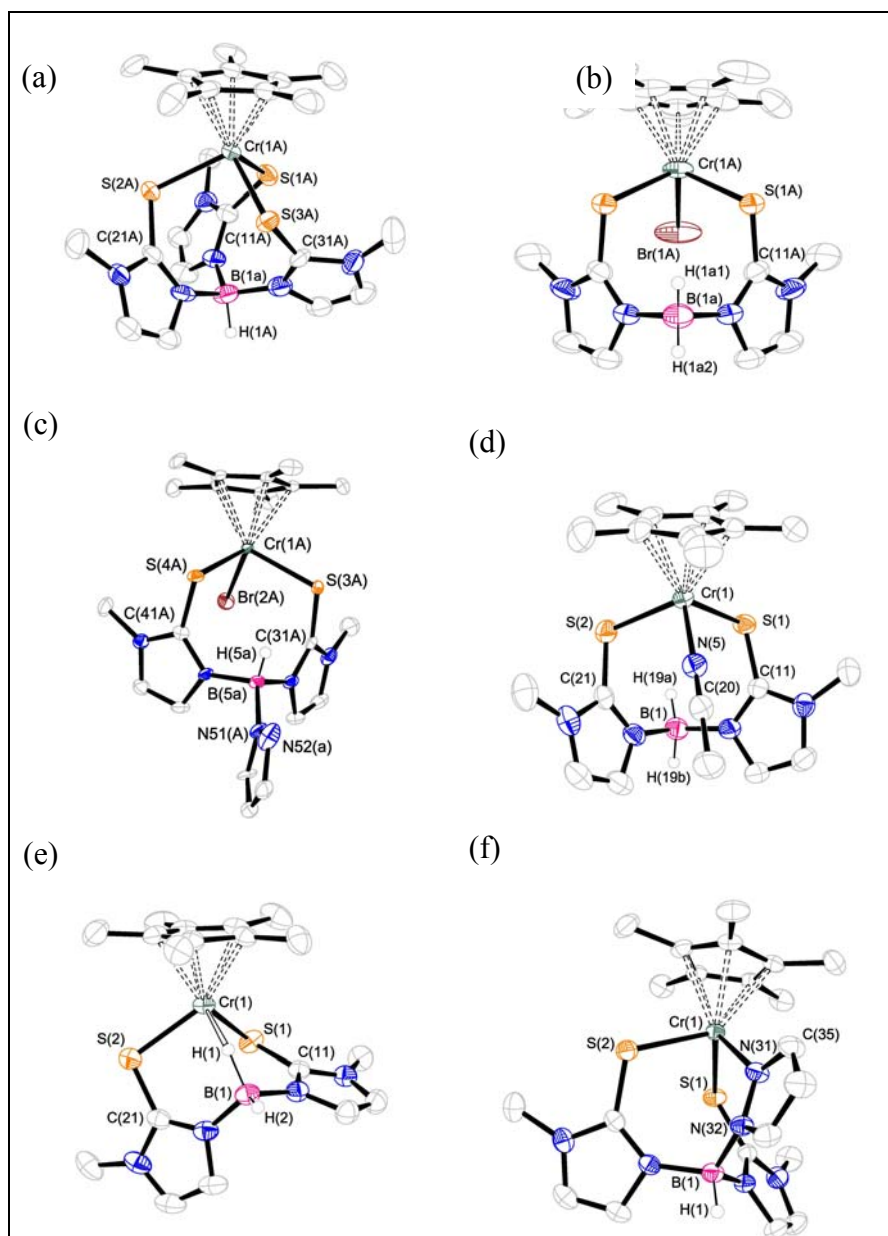


**Figure 2.2.** ORTEP plots for the molecular structures of (a) **2** monocation, (b) **3**, (c) **4** (d) **5** monocation, (e) **6** monocation and (f) **7** monocation. Thermal ellipsoids are drawn at the 50% probability level and all hydrogen atoms except those on the boron are omitted for clarity.

The molecular structures of **3** and **4** show that the  $[\text{H}_2\text{B}(\text{mt})_2]$  and  $[\text{HB}(\text{mt})_2(\text{pz})]$  ligands bind to the Cr metal centre in a bidentate fashion with the Br still coordinated to the Cr metal. Similarly, in the acetonitrile adduct, **5**, the  $[\text{H}_2\text{B}(\text{mt})_2]$  ligand binds to the Cr metal centre in a bidentate manner. The C-N bond in **5** is 1.139(3) Å, which is intermediate between values of a double bond (1.262 Å) and a triple bond (1.150 Å), consistent with the observation of the  $\text{C}\equiv\text{N}$  stretch in the IR spectrum of **5**. On the other hand, the molecular structure of **6** shows that the  $[\text{H}_2\text{B}(\text{mt})_2]$  ligand binds to the Cr metal centre in a  $\kappa^3\text{-H,S,S'}$  manner, with a Cr...H-B bond distance of 1.885(10) Å, which is much shorter than the Cr...H-B non-bonding distances found in **3-5** (3.77-3.97 Å).

**Table 2.1.** Selected bond lengths (Å) and bond angles ( $^\circ$ ).

Complex	2	3	4	5	6	7
Bond Distances (Å)						
Cr(1)-S(1)	2.366(2)	2.385(2)	2.401(2)	2.3900(7)	2.3617(10)	2.3694(5)
	2.399(2)	2.365(6)	2.388(2)			
Cr(1)-S(2)	2.363(2)	-	2.403(2)	2.3716(6)	2.3803(9)	2.3687(6)
	2.355(2)		2.401(2)			
Cr(1)-L(1)	2.378(2)	2.4544(17)	2.4591(12)	2.041(2)	-	2.0566(16)
	2.375(2)		2.4428(14)			
	(L(1)=S(3))	(L(1)=Br(1))	(L(1)=Br(1))	(L(1)=N(2))		
C(1)-S(1)	1.721(8)	1.722(7)	1.722(7)	1.722(7)	1.722(3)	1.717(2)
	1.725(8)	1.69(2)	1.721(7)	1.721(7)		
C(2)-S(2)	1.731 (7)	1.675(14)	1.718(8)	1.728(2)	1.718(3)	1.720(2)
	1.727(7)		1.716(7)			
C(3)-S(3)	1.714(7)	-	-	-	-	-
	1.717(8)					
B(1)-H(1)	1.177(10)	0.980(10)	0.979(10)	1.091 (10)	1.211(10)	1.052(10)
B(1)-H(2)	-	0.980(10)	-	1.129 (10)	1.082(10)	-
Cr(1)-H(1)	-	3.971	3.765	3.842	1.885(10)	-
Bond Angles ( $^\circ$ )						
S(1)-Cr(1)-S(2)	95.97(7)	98.62(10)	97.19(8)	100.33(20)	99.45(4)	100.79(5)
	97.70(8)	98.86(10)	95.65(8)			
S(2)-Cr(1)-S(3)	92.98(3)	-	-	-	-	-
	96.16(7)					
H(1)-B(1)-H(2)	-	108.54(10)	-	113.36(10)	99.84(10)	-

The [HB(mt)<sub>2</sub>(pz)] ligand coordinated to the Cp\*Cr<sup>III</sup> in a  $\kappa^3$ -N,S,S' manner and the Cr-N bond distance in **7** (2.0566(16) Å) was found to be shorter compared to that for Cp\*Cr<sup>II</sup>[HB(pz)<sub>3</sub>] (2.092(2)-2.439(2) Å), presumably due to stronger interaction of Cr<sup>III</sup> with the hard N donor.

### 2.3. Electrochemistry

The cyclic voltammetric responses observed at a scan rate ( $\nu$ ) of 100 mV s<sup>-1</sup> for CH<sub>3</sub>CN solutions containing **2**, **4** and **7** at two temperatures are shown in Figure 2.3. Each compound underwent an oxidation process at positive potentials and a reduction process at negative potentials, with the potential separation between the two processes between 2 – 3 V. The chemical reversibility of the oxidation and reduction processes can be estimated from the ratio of the anodic ( $i_p^{\text{ox}}$ ) to cathodic ( $i_p^{\text{red}}$ ) peak currents ( $i_p^{\text{ox}}/i_p^{\text{red}}$ ) for each process. For a fully chemically reversible process, the  $i_p^{\text{ox}}/i_p^{\text{red}}$ -ratio approach unity. Interestingly, in several instances the chemical reversibility of the oxidation and reduction processes appeared to decrease as the temperature was lowered, seen by how the  $i_p^{\text{ox}}/i_p^{\text{red}}$ -ratio shifted away from unity at low temperature (Figure 2.3). A decrease in apparent chemical reversibility at low temperature is unusual, since lowering the temperature normally increases the stability of the oxidised or reduced states. Therefore, it is more likely that when this effect is observed, it involves a follow-up homogeneous chemical reaction such as an equilibrium processes, so that varying the temperature changes the equilibrium constants and thereby makes the processes *appear* less chemically reversible.

A coordination exchange following reduction or oxidation of the Cr containing complex is possible. However, the electrochemical data is not clear to confirm this hypothesis for **2**. In CH<sub>2</sub>Cl<sub>2</sub>, the oxidation and reduction processes for **2** appear less

chemically reversible at high and low temperatures compared to the voltammetric data in CH<sub>3</sub>CN. The chemical irreversibility of the voltammetric data in CH<sub>2</sub>Cl<sub>2</sub> is likely to be caused by lower chemical stability of the Cr complex in the chlorinated solvent.

In contrast to the reduction process, the oxidation process of **4** appeared to become more chemically reversible as the temperature was lowered (Figure 2.3b), suggesting that lowering the temperature helped to stabilise the oxidised state. Also, at lower temperatures, the peak shape for the oxidation of **4** appeared similar to what is expected for a one-electron process. At higher temperatures the oxidative peak shape was broadened, possibly due to multiple electron transfer steps.

At low temperatures (< 243 K), **3** can be oxidized in a one-electron chemically reversible process at  $E_{1/2}^r = +0.245$  V vs. Fc/Fc<sup>+</sup> ( $E_{1/2}^r = (E_p^{ox} + E_p^{red})/2$ ). As the temperature was increased progressively up to 293 K, the chemical reversibility of the oxidation process diminished due to instability of **3**<sup>+</sup> at higher temperatures (Figure 2.4a).

By increasing the voltammetric scan rate for the experiments performed on **3** at  $T \geq 253$  K, it was possible to outrun the chemical step and obtain  $i_p^{ox}/i_p^{red}$ -ratios approaching 1. At 293 K, a scan rate of approximately 10 V s<sup>-1</sup> was needed in order to have  $i_p^{ox}/i_p^{red} = 1$ , indicating that **3**<sup>+</sup> has a half-life  $\approx 0.1$  s at room temperature (assuming a first order decomposition/reaction of **3**<sup>+</sup>).

The electrochemical behaviour of **3** is typical of compounds that undergo an EC mechanism (electron transfer followed by a chemical step), where the oxidised compound quickly reacts/decomposes. The oxidation product formed by reaction/decomposition of **3**<sup>+</sup> is evident in the cyclic voltammograms of solutions of **3** at 293 K (Figure 2.4a, dashed line) at potentials approximately 0.4 V more positive

than the first oxidation process. At lower temperatures ( $< 243$  K) or faster scan rates ( $> 10$  V s<sup>-1</sup>), the second oxidation process is not voltammetrically detectable, due to increased stability of  $3^+$  at low temperatures and because the chemical step is outrun at faster scan rates.

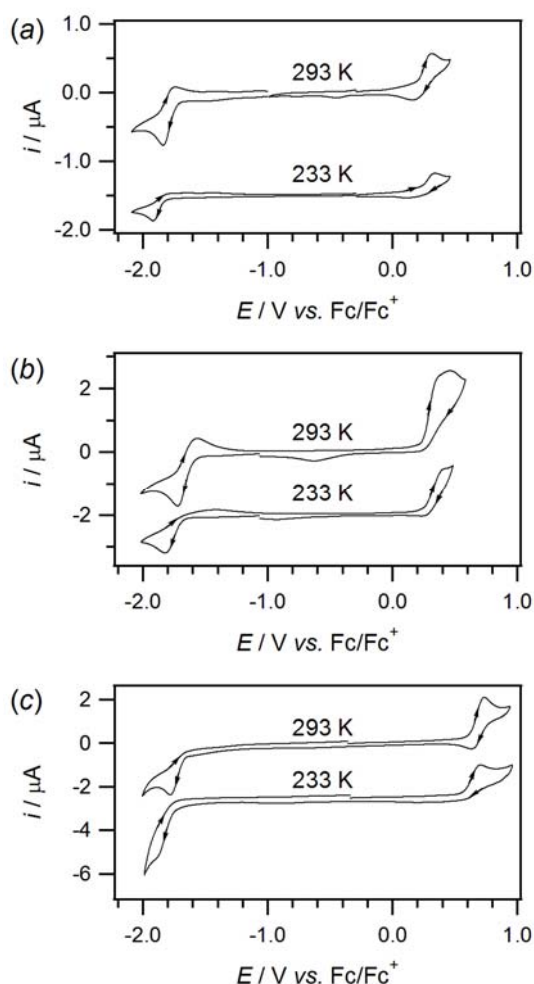


**Figure 2.3.** Cyclic voltammograms of 1.0 mM solutions of (a) **2**, (b) **4**, and (c) **7**. CVs at 233 K are offset by (a)  $-1.5$   $\mu$ A, (b)  $-2$   $\mu$ A, and (c)  $-2.5$   $\mu$ A.

The reaction of **3** with  $\text{AgPF}_6$  in  $\text{CH}_3\text{CN}$  leads to the formation of **5** in moderate yield. Cyclic voltammograms of **5** in  $\text{CH}_3\text{CN}$  at two different temperatures at a Pt electrode are displayed in Figure 2.4b. **5** undergoes chemically irreversible oxidation and reduction processes at high and low temperatures, indicating that the reduced and oxidized states are very unstable or reactive (Figure 2.4b). The anodic

peak current ( $i_p^{\text{ox}}$ ) for the oxidation process is greater than the cathodic peak current ( $i_p^{\text{red}}$ ) for the reduction process, indicating more electrons are transferred during the oxidation process. The oxidation process detected in cyclic voltammograms of **5** occurs at a very similar potential to the second oxidation process detected in cyclic voltammograms of **3** at 293 K (compare Figures 2.4a and 2.4b). Therefore, it can be concluded that the most positive oxidation process in Figure 2.3a at 293 K (dashed line) is associated with the oxidation of **5** that is formed from the rapid reaction of **3**<sup>+</sup> with CH<sub>3</sub>CN. The CVs obtained for **6** were very complicated (Figure 2.4c), indicating that the reduced and oxidized states were likely be very reactive at high and low temperatures.

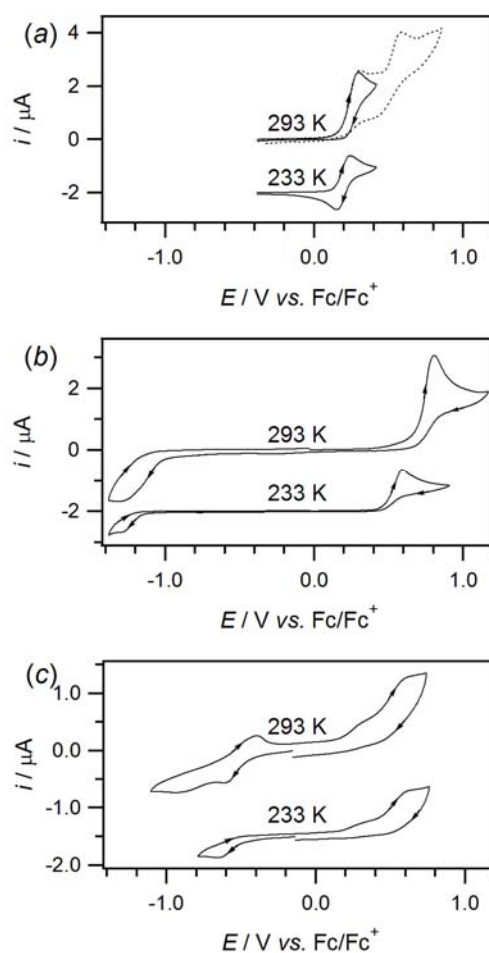


**Figure 2.4.** Cyclic voltammograms of 1.0 mM solutions of (a) **3**, (b) **5** and (c) **6**. CVs at 233 K are offset by (a) -2  $\mu\text{A}$ , (b) -2  $\mu\text{A}$ , and (c) -1.5  $\mu\text{A}$ .

## 2.4. Conclusion

A new class of mixed sandwich Cr<sup>III</sup> complexes containing the Cp\* and poly(methimazolyl)borate ligands have been synthesized from the reaction of [Cp\*Cr<sup>III</sup>Br<sub>2</sub>]<sub>2</sub> (**1**) with the corresponding poly(methimazolyl)borate salts. Our results represent a direct synthetic route to such mixed-sandwich complexes with Cp\* and poly(methimazolyl)borate ligands. In the case of [Cp\*Cr{HB(mt)<sub>3</sub>}]Br (**2**), the [HB(mt)<sub>3</sub>]<sup>-</sup> ligand adopted a  $\kappa^3$ -S,S',S'' coordination. On the other hand, in complexes **3** and **4**, the poly(methimazolyl)borates adopted a  $\kappa^2$ -S,S' coordination and the other coordination site is occupied by a Br<sup>-</sup> coligand. The tridentate coordination of the [H<sub>2</sub>B(mt)<sub>2</sub>]<sup>-</sup> in **3** and [HB(mt)<sub>2</sub>(pz)]<sup>-</sup> in **4** can be effected by using a silver salt. However, when the reaction was carried out in the presence of acetonitrile, the third coordination site in **5** was occupied by the acetonitrile, in agreement with the preference of the electron-poor Cr<sup>III</sup> centre for more electron rich ligands. Cyclic voltammetry studies of complexes **2-7** did not provide evidence for isomerisation between the various coordination modes that can be adopted by the poly(methimazolyl)borates. Nevertheless, the electrochemical studies of complexes **2**, **4** and **7** have shown that the chemical reversibility of the oxidation and reduction processes appeared to decrease as the temperature was lowered in several instances, which could possibly involve a follow-up homogeneous chemical reaction such as an equilibrium processes. In contrast, the reduced and oxidized states of complexes **3**, **5** and **6** were found to very unstable or reactive.



## 2.5. Experimental

**General Procedures.** All reactions were carried out using conventional Schlenk techniques under an inert atmosphere of nitrogen or under argon in an M. Braun Labmaster 130 Inert Gas System. NMR spectra were measured on a Bruker ACF 300 and AMX 500 spectrometers and the shifts were referenced to residual solvent shifts in the respective deuterio solvents. The spectral window for all  $^1\text{H}$  NMR spectra of the Cr(III) complexes were screened from  $\delta$  30 to -60. IR spectra in KBr discs were measured in the range of 4000-600  $\text{cm}^{-1}$  by means of a BioRad FTS-165 FTIR instrument. Mass spectra were acquired on a Finnigan Mat 95XL-T or a Finnigan Mat LCQ spectrometer. Elemental analyses were carried out by the in-house microanalytical laboratory.  $[\text{Cp}^*\text{CrBr}_2]_2$  was synthesized as reported in the literature.<sup>1</sup> Methimazole and pyrazole were purchased from Sigma Aldrich and used without further purification. Solvents were dried over sodium benzophenone ketyl or calcium hydride and distilled under argon before use. Celite (Fluka AG) and silica gel (Merck Kieselgel 60, 230-400 mesh) were dried at 140 °C overnight before use.

**Cyclic voltammetry studies.** Voltammetric experiments were conducted with a computer controlled Eco Chemie  $\mu$ Autolab III potentiostat using planar 1 mm diameter Pt and glassy carbon (GC) working electrodes in conjunction with a Pt auxiliary electrode and an Ag wire reference electrode connected to the test solution *via* a salt bridge containing 0.5 M  $\text{Bu}_4\text{NPF}_6$  in  $\text{CH}_3\text{CN}$ . Accurate potentials were obtained using ferrocene as an internal standard. The electrochemical cell was thermostated at 233 and 293 K using an Eylea PSL-1000 variable temperature cooling bath. EPR spectra were recorded on a Bruker ESP 300e spectrometer with liquid He cooling. Cyclic voltammograms were recorded at a scan rate of 100  $\text{mV s}^{-1}$  at a 1 mm planar Pt electrode with 0.25 M  $\text{Bu}_4\text{NPF}_6$  of solutions containing **2-7**. The  $E_{1/2}^{\text{f}}$ -value

[that approximates the formal potential ( $E^0$ )] was calculated from CV data under conditions where the ratio of the oxidative ( $i_p^{\text{ox}}$ ) to reductive ( $i_p^{\text{red}}$ ) peak currents were equal to unity and using the relationship

$$E_{1/2}^r = (E_p^{\text{ox}} + E_p^{\text{red}})/2 \quad (\text{i})$$

where  $E_p^{\text{ox}}$  and  $E_p^{\text{red}}$  are the anodic and cathodic peak potentials respectively.<sup>34</sup>

**X-Ray structure determination.** The crystals were mounted on glass fibers. X-ray data were collected on a Bruker APEX AXS diffractometer, equipped with a CCD detector, using MoK $\alpha$  radiation ( $\lambda$ 0.71073 Å). The program SMART was used for collecting frames of data, indexing reflection and determination of lattice parameter,<sup>8</sup> SAINT for integration of the intensity of reflections, scaling, and for correction of Lorentz and polarization effects,<sup>8</sup> SADABS for absorption correction,<sup>9</sup> and SHELXTL for space group and structure determination, and least-squares refinements on  $F^2$ .<sup>10</sup> The structures were solved by direct methods to locate the heavy atoms, followed by difference maps for the light non-hydrogen atoms. The crystal data collection and processing parameters are given in Table A1 (Appendix).

**Synthesis of potassium hydrotris(methimazoly)borate.** K[HB(mt)<sub>3</sub>] was prepared according to literature procedure:<sup>11</sup> A mixture of methimazole (2.70 g, 23.64 mmol) and KBH<sub>4</sub> (0.32 g, 5.53 mmol) was placed together with a magnetic stirring bar into a 100 mL pear-shaped flask. The flask was connected to an air condenser and placed into an oil bath. The condenser is connected to a volumetric device that measures the volume of H<sub>2</sub> evolved through displacement of water. The mixture was heated gently, with stirring and H<sub>2</sub> evolution started at ~100°C. The temperature of the oil bath was allowed to rise to 140°C and maintained at that temperature, with continuous stirring until ~400 mL of water (17.85 mmol of H<sub>2</sub>) was displaced. The melt was cooled down to RT and 40 mL of THF was added and the mixture stirred for 3 mins to wash off

unreacted starting material. Upon standing, a white solid settled at the bottom of the flask, giving a light blue solution. The mixture was filtered through a glass sinter (No. 3 porosity) in the open and the white solid thus obtained was washed with THF (3 x 40 mL). The washed white solid was dried under vacuum, yielding  $\text{K}[\text{HB}(\text{mt})_3]$  (1.50 g, 65 % yield).

Data for  $\text{K}[\text{HB}(\text{mt})_3]$ :  $^1\text{H}$  NMR ( $\text{D}_2\text{O}$ ):  $\delta$  6.94 (d,  $^3J = 2.1$ , 1H), 6.22 (d,  $^3J = 2.1$ , 1H), 3.52 (s, 3H). [Lit values:  $\delta$  6.89 (d,  $^3J = 1.8$ , 1H), 6.14 (d, 1H), 3.46 (s, 3H)]

**Synthesis of sodium hydrotris(methimazolyl)borate.**  $\text{Na}[\text{H}_2\text{B}(\text{mt})_2]$  was prepared according to literature procedure:<sup>12</sup> A stirred suspension of  $\text{NaBH}_4$  (0.500 g, 13.217 mmol) and methimazole (3.018 g, 26.434 mmol) in THF (40 mL) was refluxed for 18 h under an atmosphere of argon. The resulting slightly cloudy solution was allowed to cool to room temperature and filtered, and the clear filtrate was concentrated under reduced pressure to ca. 5 mL, leading to the formation of a white precipitate. After addition of pentane (40 mL), the product was isolated by filtration, washed with hexane (2 x 30 mL), and dried in vacuo for 5 h (3.350 g, 97 % yield)

Data for  $\text{Na}[\text{H}_2\text{B}(\text{mt})_2]$ :  $^1\text{H}$  NMR ( $d_6$ -DMSO):  $\delta$  6.96 (d,  $^3J = 1.8$ , 2 H, imidazole *H*), 6.70 (d,  $^3J = 1.8$ , 2 H, 3.34 (s, 6 H,  $\text{CH}_3$ ), imidazole *H*). [Lit values =  $\delta$  6.97 (d,  $^3J = 1.8$ , 2 H, imidazole *H*), 6.71 (d,  $^3J = 1.8$ , 2 H, 3.33 (s, 6 H,  $\text{CH}_3$ ), imidazole *H*)]

**Synthesis of lithium hydrobis(methimazolyl)(pyrazolyl)borate.** The synthesis is modified from the literature:<sup>13</sup> A mixture of 2-mercapto-1-methylimidazole (505 mg, 4.43 mmol) and  $\text{LiBH}_4$  (39 mg, 1.77 mmol) in toluene:THF (20 mL, 4:1) was heated at 60°C overnight. After which, the solvents were removed *in vacuo* giving a white solid which was washed with  $\text{Et}_2\text{O}$  (5 x 3 mL), followed by DCM:hex (1:2, 3 x 6 mL) to remove excess 2-mercapto-1-methylimidazole. The resultant white solid,

Li[H<sub>2</sub>B(mt)<sub>2</sub>] (310 mg, 1.26 mmol) and pyrazole (100 mg, 1.47 mmol) in toluene (20 mL) were heated at 105°C for 48 h. After cooling to RT, the white precipitate was isolated by filtration and washed with toluene (5 x 4 mL), followed by Et<sub>2</sub>O (3 x 2 mL), THF:Et<sub>2</sub>O (1:5, 3 x 2 mL) and DCM (5 x 2 mL). The residue was washed with THF:Et<sub>2</sub>O (4:1, 2 x 10 mL) and the colourless extract was evacuated to dryness to give a white solid, Li[HB(mt)<sub>2</sub>(pz)] (330 mg, 1.06 mmol, 60 % overall yield).

Data for Li[HB(mt)<sub>2</sub>(pz)]: <sup>1</sup>H NMR (*d*<sub>6</sub>-DMSO): δ 7.46 (d, 1H, J=2.1Hz), 7.33 (d, 1H, J=0.9Hz), 6.78 (d, 1H, J=2.1Hz), 6.20 (d, 1H, J=2.2Hz), 6.00 (t, 1H, J=1.7Hz), 3.74 (s, 6H). [Lit. values<sup>13</sup>: δ 7.44 (d, 1H, J=2Hz), 7.34 (d, 1H, J=2 Hz), 6.78 (d, 2H, J=2 Hz), 6.18 (d, 2H, J=2 Hz), 6.00 (t, 1H, J=2 Hz), 3.74 (s, 6H)]

### Reactions of [Cp\*CrBr<sub>2</sub>]<sub>2</sub> (**1**)

(a) **with K[HB(mt)<sub>3</sub>]**. To the blue-green solution of **1** (70 mg, 0.10 mmol) in THF:MeOH (4:1, 10 mL) was added K[HB(mt)<sub>3</sub>] (80 mg, 0.20 mmol). The mixture was stirred for 18 h, resulting in a suspension of a white precipitate of KCl in a deep blue supernatant. The suspension was filtered through celite and washed with Et<sub>2</sub>O (5 x 2 mL). The blue filtrate was evacuated to dryness and recrystallised from MeOH/ether at -30 °C. Multiple recrystallisations gave a blue solid, [Cp\*Cr{HB(mt)<sub>3</sub>}]Br (**2**) (70 mg, 0.11 mmol, 57 % yield). Diffraction-quality single crystals were obtained at -30 as blue plates by slow diffusion of ether into a acetonitrile solution after 1 week.

Data for **2**. Anal. Found: C, 42.3; H, 4.9; N, 13.4; S, 15.4 %. Calc. for C<sub>22</sub>H<sub>31</sub>BBrCrN<sub>6</sub>S<sub>3</sub>: C, 42.7; H, 5.1; N, 13.6; S, 15.6 %. IR (KBr, cm<sup>-1</sup>): 2443wbr (ν<sub>B-H</sub>), 3111w, 3067w, 2974w, 2911w, 2859w, 1557w, 1466m, 1375m, 1209s, 1155w, 1088w, 1018w, 748mbr, 687w, 523w. FAB<sup>+</sup>-MS: *m/z* 538 [M<sup>+</sup>]; 300 [M<sup>+</sup>-

(C<sub>4</sub>H<sub>5</sub>N<sub>2</sub>S)<sub>2</sub>H]; FAB<sup>-</sup>-MS: *m/z* 81 [Br<sup>-</sup>]. <sup>1</sup>H NMR (δ, CD<sub>3</sub>CN): -16.4 (s, br, *ν*<sub>1/2</sub> ca. 1000 Hz)

**(b) with Na[H<sub>2</sub>B(mt)<sub>2</sub>].** To a blue-green solution of **1** (69 mg, 0.10 mmol) in THF (10 mL) was added Na[H<sub>2</sub>B(mt)<sub>2</sub>] (54 mg, 0.20 mmol). The mixture was stirred for 18 h, resulting in a suspension of a white precipitate of NaBr in a bright blue supernatant. The suspension was evacuated to dryness and the resultant mixture was extracted with toluene (5 x 3 mL). The blue extract was filtered through a thin disc of celite, and the blue filtrate was evaporated to dryness to give a blue microcrystalline solid of Cp\*Cr[H<sub>2</sub>B(mt)<sub>2</sub>]Br (**3**) (95 mg, 0.19 mmol, 94 % yield). Diffraction-quality single crystals were obtained at -30 °C as blue blocks by slow diffusion of ether into a acetonitrile solution after 1.

Data for **3**. Anal. Found: C, 42.8; H, 5.5; N, 11.1; S, 12.2 %. Calc. for C<sub>18</sub>H<sub>27</sub>B<sub>1</sub>Br<sub>1</sub>Cr<sub>1</sub>N<sub>4</sub>S<sub>2</sub>: C, 42.7; H, 5.4; N, 11.1; S, 12.7 %. IR (KBr, cm<sup>-1</sup>): 2486w (*ν*<sub>B-H</sub>); 3121w, 3073w, 2914w, 2860w, 1693mbr, 1516mbr, 1188w, 1125w, 1020mbr, 808m, 729m, 684m, 569w. ESI<sup>+</sup>-MS: *m/z* 426 [M<sup>+</sup>-Br, M<sup>+</sup> = C<sub>5</sub>Me<sub>5</sub>Cr(Br){(C<sub>4</sub>H<sub>5</sub>N<sub>2</sub>S)<sub>2</sub>BH<sub>2</sub>}]. FAB<sup>+</sup>-MS: *m/z* 505 [M<sup>+</sup>], 426 [M<sup>+</sup> - Br], 300.1 [M<sup>+</sup> - Br - HB(mt)<sub>2</sub>]. <sup>1</sup>H NMR (δ, CD<sub>3</sub>CN): -58.0 (s, br, *ν*<sub>1/2</sub> ca. 830 Hz)

**(c) with Li[HB(mt)<sub>2</sub>(pz)].** To blue-green solution of **1** (69 mg, 0.10 mmol) in THF (10 mL) was added Li[HB(mt)<sub>2</sub>(pz)] (62 mg, 0.20 mmol). The mixture was stirred for 18 h, resulting in a suspension of a white precipitate of LiBr in a bright blue supernatant. The suspension was evacuated to dryness and extracted with DCM (5 x 2 mL). The blue extract was evacuated to dryness and recrystallised in THF/ether at -30 °C. Multiple recrystallisations gave blue solid of Cp\*Cr[HB(mt)<sub>2</sub>(pz)]Br (**4**) (70 mg,

0.12 mmol, 61 % yield). Diffraction-quality single crystals were obtained at -30 as blue plates by slow diffusion of ether into a acetonitrile solution after 1 week.

Data for **4**. Anal. Found: C, 43.7; H, 5.1; N, 14.0; S, 11.1 %. Calc. for  $C_{21}H_{29}B_1Br_1Cr_1N_6S_2$ : C, 44.1; H, 5.1; N, 13.4; S, 11.2 %. IR (KBr,  $cm^{-1}$ ):  $\nu(B-H)$  2542w, 2506w;  $\nu_{others}$  3122m, 3090w, 2974wsh, 2949w, 2910m, 2856w, 1693mbr, 1552m, 1466s, 1414m, 1377s, 1329m, 1296s, 1196vs, 1117s, 1090s, 1036m, 956w, 768s, 735m, 621w. ESI<sup>+</sup>-MS:  $m/z$  574 [ $M^+$ ,  $C_5Me_5CrBr\{(C_4H_5N_2S)_2(C_3H_3N_2)BH\}$ ]; 492 [ $M^+-Br$ ]. <sup>1</sup>H NMR ( $\delta$ ,  $CD_3CN$ ): No signal observed in the spectral window.

### Reactions of $Cp^*Cr[H_2B(mt)_2]Br$ (**3**) with $AgPF_6$ .

(a) **In MeCN:** To a blue solution of **3** (52 mg, 0.10 mmol) in MeCN (10 mL) was added  $AgPF_6$  (30 mg, 0.12 mmol). The mixture was stirred at RT for 6 h in the dark to give a dark blue suspension. The resultant suspension was filtered through a thin disc of celite on a glass frit to remove white solid of AgBr and the dark blue filtrate was evacuated to dryness. Multiple recrystallisation in MeCN/Et<sub>2</sub>O at -30 °C yielded more AgBr, which was removed by filtration. The purplish blue mother liquor was concentrated and dark blue needles of  $[Cp^*Cr\{H_2B(mt)_2\}(NCMe)]PF_6$  (**5**) (39 mg, 0.06 mmol, 64 % yield) was obtained after recrystallisation from MeCN/Et<sub>2</sub>O at -30°C. Diffraction-quality single crystals were obtained at -30 °C as dark blocks by slow diffusion of ether into a acetonitrile solution after 1 week.

Data for **5**. Anal. Found: C, 39.1; H, 5.0; N, 11.3; S, 10.9 %. Calc. for  $C_{20}H_{30}B_1Cr_1F_6N_5P_1S_2$ : C, 39.2; H, 4.9; N, 11.4; S, 10.5 %. IR (KBr,  $cm^{-1}$ ):  $\nu(B-H)$  2491m, 2397m, 2360m, 2341m, 2294w;  $\nu(C\equiv N)$  2249w;  $\nu(P-F)$  845. ESI<sup>+</sup>-MS:  $m/z$  467 [ $M^+$ ,  $C_5Me_5Cr(NCMe)\{(C_4H_5N_2S)_2BH_2\}$ ]; 426 [ $M^+-MeCN$ ]; ESI-MS:  $m/z$  145

[PF<sub>6</sub><sup>-</sup>]. <sup>1</sup>H NMR (δ, CD<sub>3</sub>CN): -58.8 (s, br,  $\nu_{1/2}$  ca. 1060 Hz), -75.1 (s, br,  $\nu_{1/2}$  ca. 1000 Hz)

**(b) In toluene:** To a blue solution of **3** (38 mg, 0.08 mmol) in toluene (15 mL) was added AgPF<sub>6</sub> (25 mg, 0.10 mmol). The mixture was stirred at RT for 4 h in the dark to give a greenish blue suspension. The resultant suspension was filtered to give a blue filtrate, **3** and dark green solid. The dark green solid was further purified by extraction with DCM (3 x 2 mL) to remove the AgBr byproduct. Green solid of [Cp\*Cr{H<sub>2</sub>B(mt)<sub>2</sub>}]PF<sub>6</sub> (**6**) (25 mg, 0.04 mmol, 55 % yield) was obtained after recrystallisation in DCM/Et<sub>2</sub>O at -30 °C. Diffraction-quality single crystals were obtained at -30 °C as green blocks by slow diffusion of ether into a dichloroethane solution after 1 week.

Data for **6**. IR (KBr, cm<sup>-1</sup>):  $\nu$ (B-H) 2491m, 2397m, 2360m, 2341m, 2294w, 2249w;  $\nu$ (P-F) 845. ESI<sup>+</sup>-MS:  $m/z$  426 [M<sup>+</sup>, C<sub>5</sub>Me<sub>5</sub>Cr{(C<sub>4</sub>H<sub>5</sub>N<sub>2</sub>S)<sub>2</sub>BH<sub>2</sub>}]; ESI<sup>-</sup>-MS:  $m/z$  145 [PF<sub>6</sub><sup>-</sup>]. HR ESI<sup>+</sup>-MS:  $m/z$  426.1182 (found); 426.1170 (calc.). <sup>1</sup>H NMR (δ, CD<sub>2</sub>Cl<sub>2</sub>): No signal observed in the spectral window.

#### Reactions of Cp\*Cr[HB(mt)<sub>2</sub>(pz)]Br (**4**) with AgPF<sub>6</sub>.

**(a) In MeCN:** To a blue solution of **4** (58 mg, 0.04 mmol) in MeCN (ca. 10 mL) was added AgPF<sub>6</sub> (14 mg, 0.06 mmol). The mixture was stirred at RT for 6 h in the dark to give a purplish blue suspension. The resultant suspension was evacuated to dryness and the resulting solid was extracted with CH<sub>2</sub>Cl<sub>2</sub> (4 x 2 mL). The purplish blue extract was evacuated to dryness and recrystallisation in MeCN/Et<sub>2</sub>O at -30 °C yielded white solid of AgBr, which was removed by filtration. The purplish blue mother liquor was concentrated and dark blue needles of [Cp\*Cr(HB(mt)<sub>2</sub>(pz))]PF<sub>6</sub> (**7**) (18 mg, 0.03 mmol, 71 % yield) was obtained after recrystallisation from MeCN/Et<sub>2</sub>O

at -30°C. Diffraction-quality single crystals were obtained at -30 °C as blue blocks by slow diffusion of ether into a acetonitrile solution after 1 week.

Data for **7**. Anal. Found: C, 39.6; H, 4.8; N, 14.1; S, 9.7 %. Calc. for  $C_{21}H_{29}BCrF_6N_6PS_2 \cdot 0.4 CH_3CN$ ; C, 40.1; H, 4.7; N, 13.7; S, 9.8 %. IR (KBr,  $cm^{-1}$ ):  $\nu(B-H)$  2486wm, 2374m, 2255w;  $\nu(P-F)$  845. ESI<sup>+</sup>-MS:  $m/z$  467 [ $M^+$ ,  $C_5Me_5Cr(NCMe)\{(C_4H_5N_2S)_3BH\}$ ]; 426 [ $M^+-MeCN$ ]; ESI<sup>-</sup>-MS:  $m/z$  145 [ $PF_6^-$ ]. <sup>1</sup>H NMR ( $\delta$ ,  $CD_3CN$ ): -30.7 (s, br,  $\nu_{1/2}$  ca. 600 Hz), -64.5 (s, br,  $\nu_{1/2}$  ca. 980 Hz).



---

**References**

1. Morse, D. B.; Rauchfuss, T. B.; Wilson, S. R., *J. Am. Chem. Soc.* **1988**, *110* (24), 8234-8235.
2. Danopoulos, A. A.; Wilkinson, G.; Sweet, T. K. N.; Hursthouse, M. B., *J. Chem. Soc., Dalton Trans.* **1996**, (3), 271-281.
3. Hankin, D. M.; Danopoulos, A. A.; Wilkinson, G.; Sweet, T. K. N.; Hursthouse, M. B., *J. Chem. Soc., Dalton Trans.* **1996**, (21), 4063-4069.
4. Shin, R. Y. C.; Tan, G. K.; Koh, L. L.; Goh, L. Y.; Webster, R. D., *Organometallics* **2005**, *24* (7), 1401-1403.
5. Brunker, T. J.; Cowley, A. R.; O'Hare, D., *Organometallics* **2002**, *21* (15), 3123-3138.
6. Bailey, P. J.; Lorono-Gonzales, D. J.; McCormack, C.; Parsons, S.; Price, M., *Inorg. Chim. Acta* **2003**, *354*, 61-67.
7. Pauling, L. in *The Nature Of The Chemical Bond*. 3rd ed.; Cornell University Press: Oxford, 1960.
8. *SMART & SAINT Software Reference Manuals*, version 6.22, Bruker AXS Inc.: Madison, WI, **2000**.
9. Sheldrick, G. M. *SADABS software for empirical absorption correction*; University of Göttingen: Germany, **2000**.
10. *SHELXTL Reference Manual*, version 5.1; Bruker AXS Inc.: Madison, WI, **1997**.
11. Soares, L. F.; Silva, R. M.; Smee, J.; Darensbourg, M., *Inorg. Synth.* **2002**, *33*, 199-202.
12. Alvarez, H. M.; Tran, T. B.; Richter, M. A.; Alyounes, D. M.; Rabinovich, D.; Tanski, J. M.; Krawiec, M., *Inorg. Chem.* **2003**, *42* (6), 2149-2156.
13. Kimblin, C.; Hascall, T.; Parkin, G., *Inorg. Chem.* **1997**, *36* (25), 5680-5681.

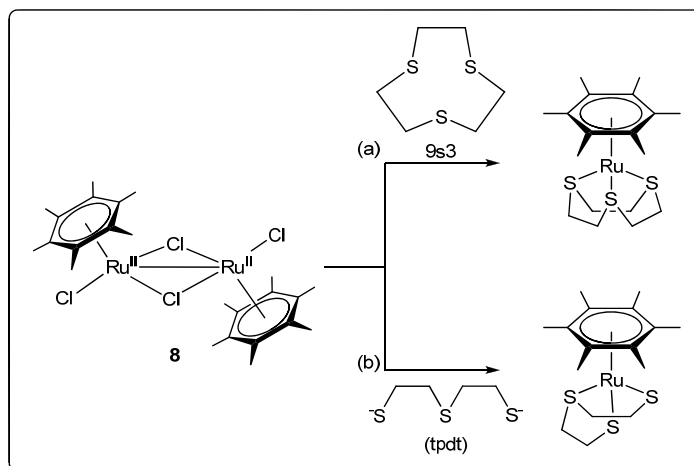
### Chapter 3. Syntheses of mixed-sandwich (HMB)Ru complexes containing poly(methimazoly)borates (HMB=C<sub>6</sub>Me<sub>6</sub>)

The study in Chapter 2 has shown that of the three poly(methimazoly)borate complexes, only that with the [H<sub>2</sub>B(mt)<sub>2</sub>] ligand can have 3c-2e M...H-B interactions with the Cr<sup>III</sup> center in the absence of a coordinating solvent. This is in agreement with the preference of the electron-poor Cr<sup>III</sup> centre for more electron rich ligands, e.g. N and S donors versus an M...H-B interactions. Thus as a comparative study, we investigate the bonding modes exhibited by the poly(methimazoly)borates in (HMB)Ru<sup>II</sup> complexes.

We noted that the chemistry of organoruthenium compounds bearing sulfur-based ligands are of special interest, because of their relevance to biological and industrial processes.<sup>1, 2</sup> While (arene)Ru(II) complexes containing mono- and bidentate thiolate ligands are well-established, those of monodentate thioethers, e.g., dimethyl sulfide and tetrahydrothiophene (R<sub>2</sub>S) such as [( $\eta^6$ -arene)RuCl<sub>2</sub>(SR<sub>2</sub>)] and [( $\eta^6$ -arene)RuCl(SR<sub>2</sub>)<sub>2</sub>]<sup>+</sup> (arene = *p*-cymene, 1,3,5-C<sub>6</sub>H<sub>3</sub>Me<sub>3</sub>, or C<sub>6</sub>Me<sub>6</sub>),<sup>3</sup> are uncommon and generally unstable. Bennett and Goh had successfully isolated a stable complex of (HMB)Ru(II) containing a tridentate macrocyclic trithioether (1,4,7-trithiacyclononane, 9S3) (Scheme 3.1a).<sup>4-6</sup> Since then, Goh and coworkers have also prepared the complexes containing the  $\eta^3$ -tpdt {3-thiapentane-1,5-dithiolate, S(CH<sub>2</sub>CH<sub>2</sub>S<sup>-</sup>)<sub>2</sub>} and  $\eta^3$ -apdt {3-azapentane-1,5-dithiolate, HN(CH<sub>2</sub>CH<sub>2</sub>S<sup>-</sup>)<sub>2</sub>} ligands in moderate to high yields from the reaction of the [(HMB)RuCl<sub>2</sub>]<sub>2</sub> (**8**) with the sodium salts of the dithiolates (Scheme 3.1b).<sup>5</sup>

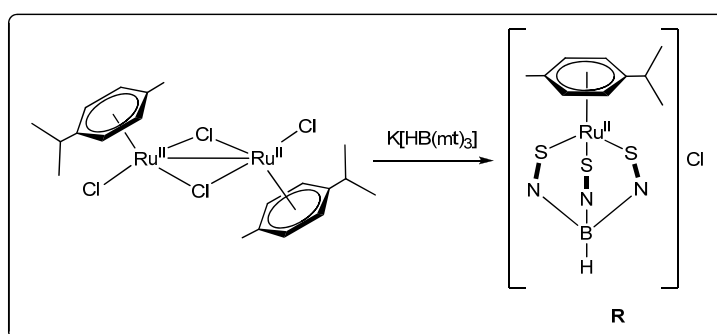
Bailey and coworkers had reported the synthesis of the mixed-sandwich complex,  $[(p\text{-cymene})\text{Ru}^{\text{II}}\{\text{HB}(\text{mt})_3\}]\text{Cl}$  (**R**), from the reaction of  $[(p\text{-cymene})\text{Ru}^{\text{II}}\text{Cl}_2]_2$  with  $\text{Na}[\text{HB}(\text{mt})_3]$  (Scheme 3.2).<sup>7</sup>

**Scheme 3.1.** Reaction of  $[(\text{HMB})\text{RuCl}_2]_2$  with (a)9s3 and (b)tpdt.



This, together with the synthesis of  $(\text{HMB})\text{Ru}^{\text{II}}(9\text{S}3)$  and  $(\text{HMB})\text{Ru}^{\text{II}}(\text{tpdt})$  suggested that it is possible to use  $[(\text{HMB})\text{RuCl}_2]_2$  as a precursor to mixed sandwich  $(\text{HMB})\text{Ru}^{\text{II}}$  complexes with poly(methimazolyl)borate.

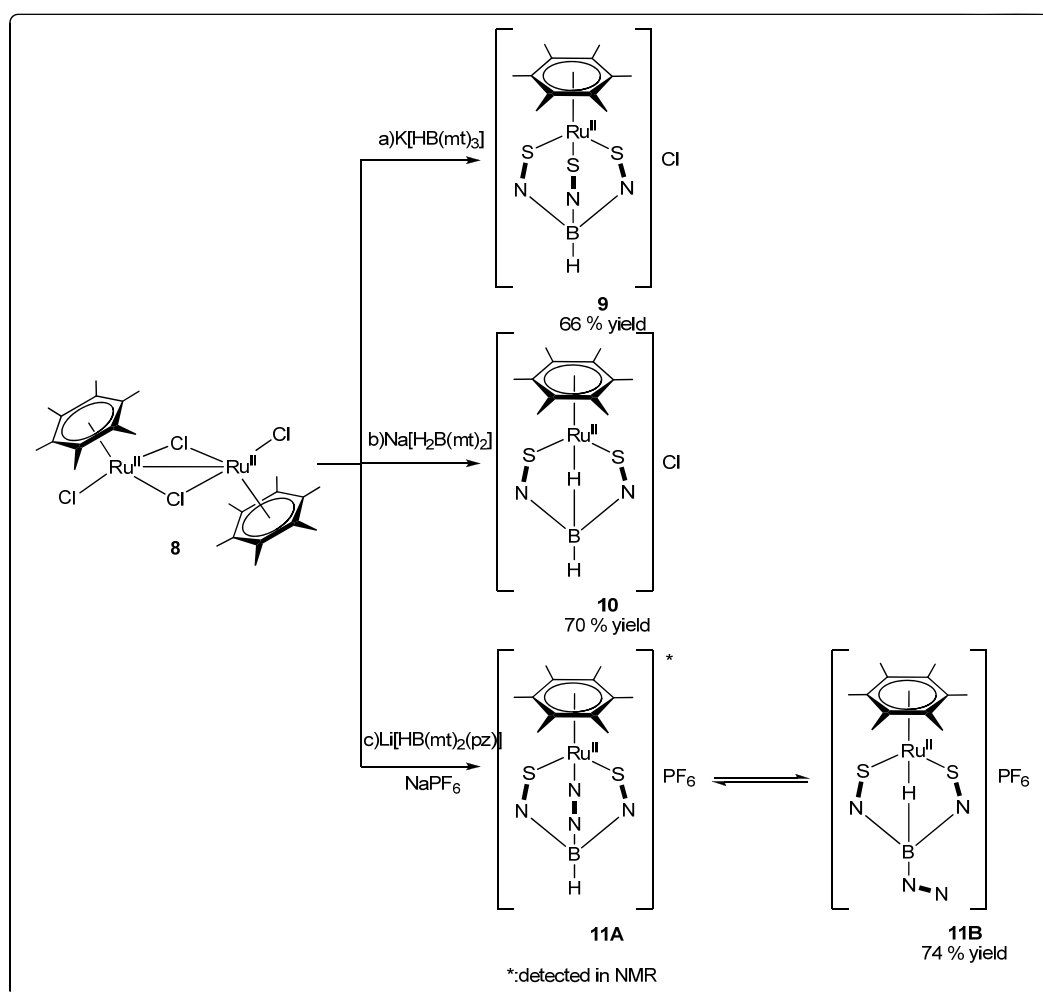
**Scheme 3.2.** Reaction of  $[(p\text{-cymene})\text{Ru}^{\text{II}}\{\text{HB}(\text{mt})_3\}]\text{Cl}$  with  $\text{K}[\text{HB}(\text{mt})_3]$



### 3.1. Reaction of $[(\text{HMB})\text{RuCl}_2]_2$ with poly(methimazolyl)borate salts

Complexes  $[(\text{HMB})\text{Ru}^{\text{II}}\{\text{HB}(\text{mt})_3\}]\text{Cl}$  (**9**),  $[(\text{HMB})\text{Ru}^{\text{II}}\{\text{H}_2\text{B}(\text{mt})_2\}]\text{Cl}$  (**10**) and  $[(\text{HMB})\text{Ru}^{\text{II}}\{\text{HB}(\text{mt})_2(\text{pz})\}]\text{PF}_6$  (**11**) were obtained as air stable, red solids from the reaction of  $[(\text{HMB})\text{RuCl}_2]_2$  with the corresponding poly(methimazolyl)borate salts at RT in moderate yields (Scheme 3.3).

**Scheme 3.3.** Reaction of  $[(\text{HMB})\text{RuCl}_2]_2$  with poly(methimazolyl)borate salts.



The  $^1\text{H}$  NMR spectrum of **9** is consistent with tridentate  $\kappa^3\text{-S,S',S''}$  coordination of the Tm ligand. For **10**, the  $^1\text{H}$  NMR spectrum (in  $\text{CD}_3\text{CN}$ ) shows a pair of doublets for the CH's of the methimazolyl rings in the  $\delta$  5.75 – 6.96 region, and two very broad, overlapping 'humps' due to unresolved boron quadrupolar coupling, centered at  $\delta$  -

10.84 for the agostic-like H's. This is consistent with  $\kappa^3\text{-H,S,S'}$  coordination of the Bm ligand. In  $\text{CD}_2\text{Cl}_2$  solution at 300 K, the  $\mu\text{-HB}$  resonances are observed as two very broad overlapping 'humps' ( $\nu_{1/2}$  ca. 100 Hz), the resolution of which decreases further with lowering of the temperature until at 183 K, the 'humps' merged to give a broad signal ( $\nu_{1/2}$  ca. 36 Hz).

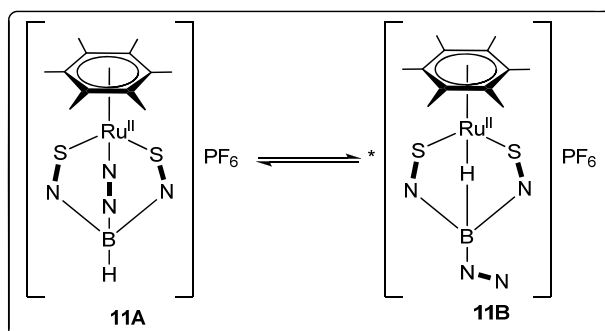
The synthesis of  $[(\text{HMB})\text{Ru}\{\text{HB}(\text{mt})_2(\text{pz})\}]\text{PF}_6$  (**11**) differs slightly from that of **9** and **10**. Complex **11** was isolated as orange red solid in 70 % yield from the 18 h reaction of  $[(\text{HMB})\text{RuCl}_2]_2$  with  $\text{Li}[\text{HB}(\text{mt})_2(\text{pz})]$  in the presence of  $\text{NaPF}_6$  (Scheme 3.3c). In the absence of  $\text{NaPF}_6$ , the complex  $[(\text{HMB})\text{Ru}(\kappa^2\text{-S,S}'\text{-}\{\text{HB}(\text{mt})_2(\text{pz})\})\text{(Cl)}]$  (**11'**) was isolated as a side product in which only one chloride was abstracted, together with  $[(\text{HMB})\text{Ru}(\kappa^3\text{-S,S}',\text{S}''\text{-}\{\text{HB}(\text{mt})_2(\text{pz})\})\text{(Cl)}]$ . Tocher and coworkers have previously reported that the reaction of a series of  $[(\eta^6\text{-arene})\text{RuCl}_2]_2$  with  $[\text{HB}(\text{pz})_3]^-$  gave a mixture of  $[(\eta^6\text{-arene})\text{Ru}(\kappa^2\text{-N,N}'\text{-}\{\text{HB}(\text{pz})_3\})\text{(Cl)}]$  and  $[(\eta^6\text{-arene})\text{Ru}(\kappa^3\text{-N,N}',\text{N}''\text{-}\{\text{HB}(\text{pz})_3\})\text{(Cl)}]$ . They have also found that the change of coordination mode of the ligand from  $\kappa^2$  to  $\kappa^3$  can be effected by treatment with  $[\text{NH}_4][\text{PF}_6]$ .<sup>8</sup>

The  $^1\text{H}$  NMR spectrum of **11** shows eight sets of doublets and two sets of triplets from  $\delta$  7.95-6.44, corresponding to the methimazolyl and pyrazolyl rings and two singlets at  $\delta$  3.65 and 3.58, corresponding to the NMe group on the methimazole. In addition, the presence of a quartet of equal intensity at  $\delta$  -10.6 ( $J = 60$  Hz), which corresponds to the agostic-like B-H interaction with the metal centre, suggesting that **11** may exhibit isomerisation between the  $\kappa^3\text{-S,S}',\text{S}''$  and  $\kappa^3\text{-H,S,S'}$  forms in solution (Scheme 3.4).

A VT NMR spectral study of **11A/11B** was conducted in  $\text{CD}_3\text{CN}$  in the temperature range 245 – 345 K (Figure 3.1). However, we did not observe any coalescence from the VT NMR experiment conducted from a temperature range of

245-345K. This may be due to the isomerisation process being too slow for the fast exchange limit to be observed on the NMR timescale. We have assigned the 2 sets of doublets at  $\delta$  7.77 and 7.45 and the triplet at  $\delta$  6.44 to **11A**, while the 2 sets of doublets at  $\delta$  7.95 and 7.75 and the triplet at  $\delta$  6.74 are assigned to **11B**, corresponding to an uncoordinated pyrazolyl ring. Both the  $\kappa^3$ -*H,S,S'* and the  $\kappa^3$ -*N,S,S'* forms were observed in solution of **11**, even when **11** is dissolved in coordinating solvent like acetonitrile. This is in contrast to our findings reported in Chapter 2 where the Cp\*Cr<sup>III</sup> analogue, [Cp\*CrHB(mt)<sub>2</sub>(pz)]PF<sub>6</sub>, adopts the  $\kappa^3$ -*N,S,S'* instead of the  $\kappa^3$ -*H,S,S'* coordination. This is in agreement with the [Cp\*Cr<sup>III</sup>]<sup>+</sup> cation being more electron-deficient than [(HMB)Ru<sup>II</sup>]<sup>+</sup>.

**Scheme 3.4.** Isomerisation of **11** in solution.



Integrals of the NMe peaks of **11A** and **11B** gave relative concentration of each species in solution at each temperature. Hence the relative concentrations of species at these temperatures were obtained by extrapolation of the linear ( $R_2 = ca.$  0.8) conc. vs. temp. plot in the range 245-345 K. The  $K_{eq}$  values listed in Table 3.1 were calculated from the [**11B**]/[**11A**] integral ratios. The thermodynamic parameters  $\Delta H^\circ$  [-5.42(84) kJ mol<sup>-1</sup>] and  $\Delta S^\circ$  [-26.6(29) J mol<sup>-1</sup> K<sup>-1</sup>] were obtained from a plot of  $\ln K_{eq}$  vs.  $(1/T)$  [ $\ln K_{eq} = -(\Delta H^\circ / RT) + (\Delta S^\circ / R)$ ] and the  $\Delta G^\circ$  value [2.6(17) kJ mol<sup>-1</sup> at 300 K] was calculated from the equation  $\Delta G^\circ = \Delta H^\circ - T\Delta S^\circ$ . The positive  $\Delta G^\circ$

value calculated for this equilibrium indicates that the forward reaction is a non-spontaneous process.

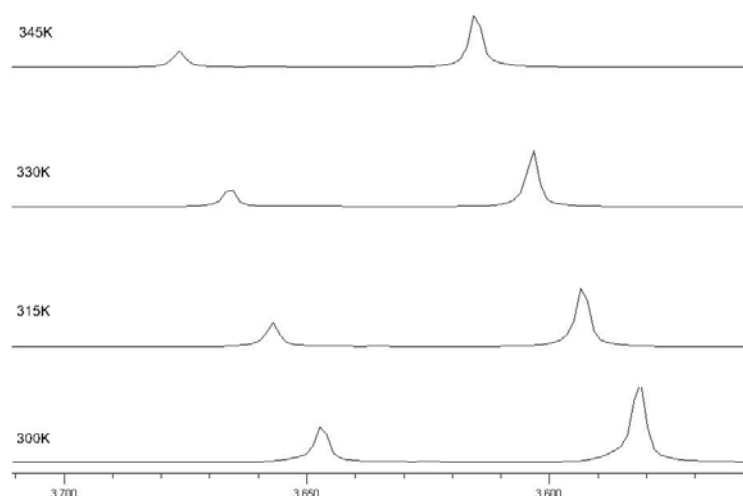


**Figure 3.1.** VT  $^1\text{H}$  NMR of **11** from 300-345K.

**Table 3.1.** Equilibrium constants in  $d_3$ -acetonitrile for Equilibrium I (Scheme 3.3).

<b>11A</b> $\rightleftharpoons$ <b>11B</b>											
T/K	345	335	325	315	305	295	285	275	265	255	245
$K_{\text{eq}}^a$	0.24(1)	0.28(1)	0.27(1)	0.34(1)	0.36(1)	0.45(1)	0.43(1)	0.49(1)	0.52(1)	0.48(1)	0.43(1)

<sup>a</sup>Obtained from integration ratios of the NMe resonance in the  $^1\text{H}$  NMR spectrum.

### 3.2. Crystallographic studies

The molecular structures of **9-11** and **11'** have been determined by single crystal X-ray diffraction analyses and their ORTEP plots are shown in Figure 3.2 and the bond parameters are given in Table 3.2. The structure of the cation in **9** possesses a three-fold axis of symmetry, and there is also disorder of the Tm ligand about this axis. In the structure of the  $[\text{H}_2\text{B}(\text{mt})_2]^-$ -containing complex **10**, a plane of symmetry cuts through the arene ring, Ru(1), B(1) and both H atoms. The  $\kappa^3\text{-H,S,S'}$  coordination mode in **10** is a recurrent feature in many Bm complexes, e. g.  $[\text{BmLi}]_2$ ,  $[\text{BmTl}]_x$  and  $\text{BmZnX}$  ( $X = \text{I}, \text{Me}$  and  $\text{NO}_3$ )<sup>9</sup>,  $(\text{Bm}^{\text{R}})_2\text{M}$  ( $\text{M} = \text{Zn}, \text{Cd}$  and  $\text{Hg}$ <sup>10</sup> and  $\text{U}$ <sup>11</sup>,  $(\text{Bm}^{\text{R}})\text{M}(\text{CO})_3$  ( $\text{M} = \text{Tc}$ <sup>12</sup> and  $\text{Re}$ <sup>12-14</sup> and  $\text{Mn}$ <sup>15</sup>) and  $[(\text{Bm})\text{Ni}(\text{dppe})]\text{Cl}$ .<sup>16</sup> The

[HB(mt)<sub>2</sub>(pz)]<sup>-</sup> ligand adopted  $\kappa^2$ -S,S' and  $\kappa^3$ -H,S,S' coordination modes in complexes **11'** and **11**, respectively.

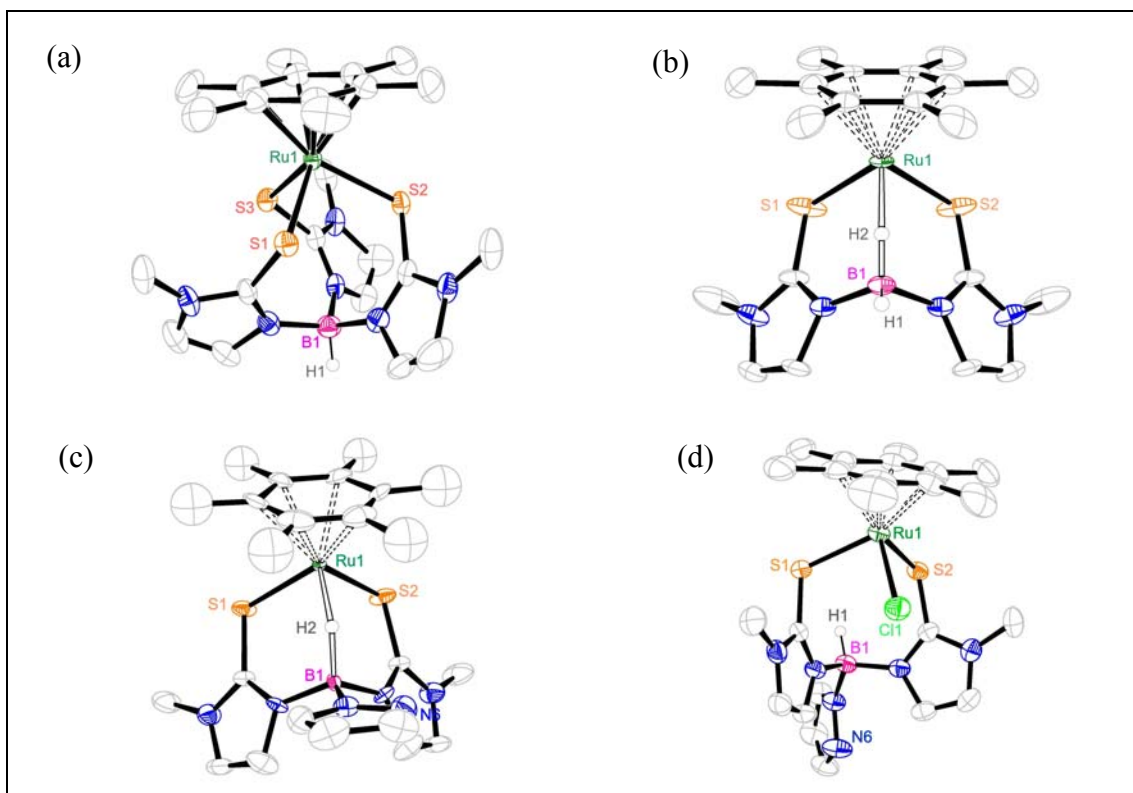


**Figure 3.2.** Ortep plots of the monocation of (a) **9**, (b) **10**, (c) **11B** and (d) **11'**. The disordered parts in the [HB(mt)<sub>3</sub>] ligand in **9** have been omitted. All H atoms, except those bonded to the boron have been omitted for clarity. Thermal ellipsoids are drawn at the 50% probability level.

**Table 3.2.** Bond parameters for complexes **9** and **10**

	<b>9</b> *	<b>10</b>	<b>11</b>	<b>11'</b>
Bond Distances (Å)				
Ru(1)-S(1)	2.4024(15)	2.376(3)	2.39(1)	2.4274(14) 2.4260(14)
	1.772(13)			
C(1)-S(1)	1.786(12)	1.703(8)	1.73(1)	1.722(5) 1.728(6)
	1.786(12)			
B(1)-H(1)	1.01(2)	0.96(2)	-	1.059(10)
B(1)-H(2)	-	1.08(2)	1.33(1)	-
Ru(1)...H(2)	5.21(1)	1.81(2)	1.82(1)	4.13(1)
Bond Angles (°)				
S(1)-Ru(1)-S(2)	91.06(5)	90.09(16)	92.1(2)	88.48(5)
H(1)-B(1)-H(2)	-	112(1)	-	-
Ru(1)...H(2)-B(1)	-	151(1)	127.9(1)	-

\*refer to disorder modelling described in the experimental



The B – H<sub>agostic</sub> bond distance in **10** (1.08(2) Å) is much shorter than that in [RuH(CO)(PPh<sub>3</sub>)(κ<sup>3</sup>-H,S',S'(Tm))] (1.29(5) Å) although the Ru – H<sub>agostic</sub> – B angles in **10** (151(1) and 140(1)°) and [RuH(CO)(PPh<sub>3</sub>)(κ<sup>3</sup>-H,S',S'(Tm))] (137(4)°) are comparable.<sup>17</sup> The B(1)-H(2) bond distance is longer than the terminal B(1)-H(1) bond distance of 0.96(2) Å, presumably due to the 3c-2e interaction. The Ru(1)···H(2) bond was found to be 1.81(2) Å in **10** and 1.82(1) Å in **11**, which are longer than that found for [RuH(CO)(PPh<sub>3</sub>)(κ<sup>3</sup>-H,S',S'(Tm))] (1.75(4) Å).<sup>17</sup> The Ru – S distances in all four molecules fall within the range found in [(*p*-cymene)Ru<sup>II</sup>{HB(mt)<sub>3</sub>}]Cl (range 2.3931(7) - 2.4274(147) Å).<sup>7</sup> The C – S bonds of the molecules fall in the range of 1.698(9) - 1.786(12) Å, intermediate between values of a single bond (*ca.* 1.81 Å) and a double bond (*ca.* 1.56 Å),<sup>18</sup> as commonly found in metal complexes of Tm<sup>R</sup>.<sup>7, 16, 17, 19, 20</sup> The S-Ru-S angles in **9-11'** are close to similar bite angles in [(*p*-cymene)Ru<sup>II</sup>{HB(mt)<sub>3</sub>}]Cl<sup>7</sup> and ruthenaboratrane.<sup>21</sup> They are generally larger than those that found for 9S3 complexes of (HMB)Ru(II) and Cp\*Ru(III) (range 85.18(4) - 92.18(4)°).<sup>5, 22</sup> This difference can be attributed to the steric bulk of the methimazolyl rings in [HB(mt)<sub>3</sub>]<sup>-</sup>, [HB(mt)<sub>2</sub>(pz)]<sup>-</sup> and [H<sub>2</sub>B(mt)<sub>2</sub>]<sup>-</sup> ligands and/or higher flexibility of these ligands, compared with that of the ethylene bridges in 9S3.

### 3.3. Electrochemistry

Electrochemical studies were performed on complexes **9** and **10** to study their electrochemical behavior and at the same time, determine if there is any isomerisation process in **9**. The cyclic voltammograms obtained at a glassy carbon electrode of 0.5 mM CH<sub>2</sub>Cl<sub>2</sub> solutions of **9** and **10** at 233 K and 293 K are shown in Figure 3.3. The  $E_{1/2}^r$ -value [that approximates the formal potential ( $E^0$ )] was calculated from CV data

under conditions where the ratio of the oxidative ( $i_p^{\text{ox}}$ ) to reductive ( $i_p^{\text{red}}$ ) peak currents were equal to unity and using the relationship

$$E_{1/2}^r = (E_p^{\text{ox}} + E_p^{\text{red}})/2 \quad (\text{i})$$

where  $E_p^{\text{ox}}$  and  $E_p^{\text{red}}$  are the anodic and cathodic peak potentials respectively.

The  $E_{1/2}^r$  values for **9** and **10** obtained from square wave voltammetry, were +0.42 V and +0.56 V vs. the Fc/Fc<sup>+</sup> couple. For both **9** and **10**, the anodic to cathodic ratios ( $i_p^{\text{ox}}/i_p^{\text{red}}$ ) were significantly < 1 over all measured temperatures, indicating that the oxidized Ru<sup>III</sup> compounds were relatively unstable, especially at higher temperatures. It is apparent from the cyclic voltammograms in that the  $E_{1/2}^r$ -values are not so sensitive to the difference in the [H<sub>2</sub>B(mt)<sub>2</sub>] and [HB(mt)<sub>3</sub>] ligands (Figure 3.3). There was no supporting evidence for the occurrence of an isomerization reaction involving  $\kappa^3$ -H,S,S'- and  $\kappa^3$ -S,S',S''-coordination of the [HB(mt)<sub>3</sub>] ligand in HMB coordinated complexes and this may be due to the inherent instability of [(arene)Ru<sup>III</sup>] complexes,<sup>23</sup> which could result in the oxidized compound (**9**<sup>2+</sup>) simply decomposing at a rate faster than the rate of rearrangement of the [HB(mt)<sub>3</sub>] ligand.

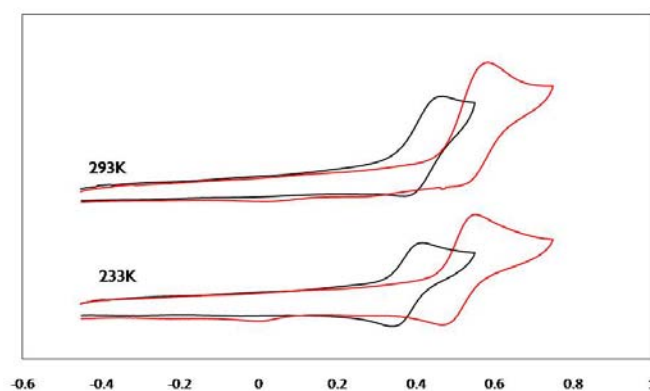


**Figure 3.3.** Cyclic voltammograms performed at a 1 mm diameter planar GC electrode in CH<sub>2</sub>Cl<sub>2</sub> (0.25 M Bu<sub>4</sub>NPF<sub>6</sub>) at 233K or 293K and a scan rate of 100 mV s<sup>-1</sup> for 0.5 mM of **9** (—) and **10** (—)

### 3.4. Conclusion

Monocationic (HMB)Ru(II) complexes of  $[\text{HB}(\text{mt})_3]^-$ ,  $[\text{H}_2\text{B}(\text{mt})_2]^-$  and  $[\text{HB}(\text{mt})_2(\text{pz})]^-$  have been synthesised from the reactions of  $[(\text{HMB})\text{RuCl}_2]_2$  (**8**) with  $\text{K}[\text{HB}(\text{mt})_3]$ ,  $\text{Na}[\text{H}_2\text{B}(\text{mt})_2]$  and  $\text{Li}[\text{HB}(\text{mt})_2(\text{pz})]$ , respectively. Single crystal X-ray analysis shows tripodal coordination of both  $[\text{HB}(\text{mt})_3]^-$  ( $\kappa^3\text{-S,S',S''}$ ) and  $[\text{H}_2\text{B}(\text{mt})_2]^-$  ( $\kappa^3\text{-H,S,S'}$ ) in the solid state complexes. No evidence (electrochemical or NMR spectroscopic) was found for the existence of a  $\kappa^3\text{-S,S',S''}$  and  $\kappa^3\text{-H,S,S'}$  equilibrium in the  $[(\text{HMB})\text{Ru}^{\text{II/III}}(\text{Tm})]$  complex **9**. However, an isomerisation process was observed for the  $[(\text{HMB})\text{Ru}^{\text{II}}\{\text{HB}(\text{mt})_3(\text{pz})\}]\text{PF}_6$  (**11**) complex and it was found that the forward process is not spontaneous.

### 3.5. Experimental

General procedures and cyclic voltammetry studies are as described in Chapter 2. [(HMB)RuCl<sub>2</sub>]<sub>2</sub> was synthesized as reported in the literature.<sup>4</sup> RuCl<sub>3</sub>.xH<sub>2</sub>O was purchased from Oxkem Limited and used without further purification.

X-ray structure determinations are as described in Chapter 2. There was disorder of the scorpionate ligand in **9**. This was modeled with two alternative positions of equal occupancies for the imidazole rings in which the C=C portions were coincident. The hydrogen atoms were placed and refined in a riding model. There was also disorder in the Cl<sup>-</sup> counterion, which was modeled with two alternative sites and the occupancies summed to unity. The crystal data collection and processing parameters are given in Table A2 (Appendix).

#### Reactions of [(HMB)RuCl<sub>2</sub>]<sub>2</sub> (**8**) with

(a) **K[HB(mt)<sub>3</sub>]**. To an orange-red suspension of **8** (33 mg, 0.05 mmol) in CH<sub>2</sub>Cl<sub>2</sub> was added K[HB(mt)<sub>3</sub>] (39 mg, 0.10 mmol). The mixture was stirred for 10 h, resulting in a suspension of a white precipitate of KCl in a deep red supernatant. The suspension was filtered and the red filtrate was evacuated to dryness and recrystallised in MeOH/ether at -30 °C. An air stable, bright red crystalline solid of [(HMB)Ru{HB(mt)<sub>3</sub>}]Cl (**9**) (43 mg, 0.07 mmol, 66 % yield) was obtained after a day. Diffraction-quality single crystals were obtained at -30 °C as red blocks by slow diffusion of ether into a methanol solution after 1 week.

Data for **9**. Anal. Found: C, 43.2; H, 5.4; N, 12.9; S, 14.7 %. Calc. for C<sub>24</sub>H<sub>34</sub>BClN<sub>6</sub>RuS<sub>3</sub>.0.7H<sub>2</sub>O: C, 43.5; H, 5.4; N, 12.7; S, 14.5 %. IR (CH<sub>2</sub>Cl<sub>2</sub>, cm<sup>-1</sup>): ν(B-H) 2440w. FAB<sup>+</sup>-MS: *m/z* 615 [M<sup>+</sup>, C<sub>6</sub>Me<sub>6</sub>Ru(C<sub>4</sub>H<sub>5</sub>N<sub>2</sub>S)<sub>3</sub>BH]; 501 [M<sup>+</sup>-(C<sub>4</sub>H<sub>5</sub>N<sub>2</sub>S)H]; 452 [M<sup>+</sup>-(C<sub>6</sub>Me<sub>6</sub>H)]; 377 [M<sup>+</sup>-(C<sub>4</sub>H<sub>5</sub>N<sub>2</sub>S)<sub>2</sub>BH]; 339 [M<sup>+</sup>-(C<sub>6</sub>

Me<sub>6</sub>(C<sub>4</sub>H<sub>5</sub>N<sub>2</sub>S)H]. HR-FAB<sup>+</sup>-MS: *m/z* for [M<sup>+</sup>] 615.1164 (found), 615.1137 (calcd). <sup>1</sup>H NMR (δ, CD<sub>3</sub>CN): 7.03 (d, 3 x 1H, <sup>3</sup>J = 1.7 Hz, CH imidazole), 6.86 (d, 3 x 1H, <sup>3</sup>J = 1.7 Hz, CH imidazole), 3.63 (s, 3 x 3H, N-CH<sub>3</sub>), 2.15 (s, H<sub>2</sub>O, relative proportion of H<sub>2</sub>O:1 = *ca.* 0.5, from peak integrals), 2.05 (s, 18H, C<sub>6</sub>(CH<sub>3</sub>)<sub>6</sub>). <sup>13</sup>C NMR (δ, CD<sub>3</sub>CN): 157.8 (s, SCN<sub>2</sub>HC=CH), 124.7 (s, C imidazole), 121.8 (s, C imidazole), 95.5 (s, C<sub>6</sub>(CH<sub>3</sub>)<sub>6</sub>), 35.7 (s, N-CH<sub>3</sub>) 15.5 (s, C<sub>5</sub>(CH<sub>3</sub>)<sub>5</sub>).

**(b) Na[H<sub>2</sub>B(mt)<sub>2</sub>].** To orange-red solution of **8** (67 mg, 0.10 mmol) in THF was added Na[H<sub>2</sub>B(mt)<sub>2</sub>] (54 mg, 0.20 mmol) and the mixture was stirred for 8 h, giving a red suspension. The suspension was filtered to give a red residue and a light red solution, from which *ca.* 5 mg of unreacted [(HMB)RuCl<sub>2</sub>]<sub>2</sub> was recovered. The red solid was extracted with CH<sub>2</sub>Cl<sub>2</sub> (5 x 2 mL). The red extract was concentrated to *ca.* 3 mL and *ca.* 2 mL of hexane added. Deep red, air stable crystals of [(HMB)Ru{H<sub>2</sub>B(mt)<sub>2</sub>}]Cl (**10**) (75 mg, 0.14 mmol, 70 % yield) were obtained after 2 days at -30°C. Diffraction-quality single crystals were obtained at -30 °C as red needles by slow diffusion of ether into a dichloromethane solution after 5 days.

Data for **10**. Anal. Found: C, 44.2; H, 5.5; N, 10.3; S, 12.0 %. Calc. for C<sub>20</sub>H<sub>30</sub>BClN<sub>4</sub>RuS<sub>2</sub>: C, 44.7; H, 5.6; N, 10.4; S, 11.9 %. IR (KBr, cm<sup>-1</sup>): ν(B-H) 2438w; ν(μ-B-H) 2162w, 2047w. FAB<sup>+</sup>-MS: *m/z* 503 [M<sup>+</sup>, C<sub>6</sub>Me<sub>6</sub>Ru(C<sub>4</sub>H<sub>5</sub>N<sub>2</sub>S)<sub>2</sub>BH<sub>2</sub>]; 377 [M<sup>+</sup>-(C<sub>4</sub>H<sub>5</sub>N<sub>2</sub>S)BH<sub>2</sub>], 339 [M<sup>+</sup>-(C<sub>6</sub>Me<sub>6</sub>)H<sub>2</sub>]. <sup>1</sup>H NMR (δ, CD<sub>3</sub>CN): 6.96 (d, 2 x 1H, <sup>3</sup>J = 2.5 Hz, CH imidazole), 6.78 (d, 2 x 1H, <sup>3</sup>J = 2.5 Hz, CH imidazole), 3.53 (s, 2 x 3H, N-CH<sub>3</sub>), 2.14 (s, 18H, C<sub>6</sub>(CH<sub>3</sub>)<sub>6</sub>), -10.84 (center of two overlapping 'humps' at δ -10.70 (ν<sub>1/2</sub> *ca.* 90 Hz) and δ -10.97 (ν<sub>1/2</sub> *ca.* 110 Hz), 1H, μ-HB). <sup>13</sup>C NMR (δ, CD<sub>3</sub>CN): 163.1 (s, SCN<sub>2</sub>HC=CH), 124.3 (s, C imidazole), 121.6 (s, C imidazole), 97.2 (s, C<sub>6</sub>(CH<sub>3</sub>)<sub>6</sub>), 34.9 (s, N-CH<sub>3</sub>) 16.2 (s,

$C_5(CH_3)_5$ .  $^1H$  NMR ( $\delta$ ,  $CD_2Cl_2$ ,  $\mu$ -HB): 300 K: -10.94 (center of two overlapping 'humps' at  $\delta$  -10.83 ( $v_{1/2}$  ca. 97 Hz) and  $\delta$  -11.05 ( $v_{1/2}$  ca. 102 Hz); 183 K: -10.93 ( $v_{1/2}$  ca. 36 Hz)

(c) **Li[HB(mt)<sub>2</sub>(pz)] in the absence of NaPF<sub>6</sub>**. A trial reaction of **8** (4 mg, 0.01 mmol) with Li[HB(mt)<sub>2</sub>(pz)] (6 mg, 0.02 mmol) in  $CH_2Cl_2$  was carried out as above in the absence of NaPF<sub>6</sub> to give a mixture of **11A**, **11B** and **11'** with relative amounts 1:3:2.3, as indicated by their NMe resonance in the  $^1H$  NMR spectrum. Diffraction-quality single crystals of **11'** were obtained at -30 °C as red needles by slow diffusion of ether into a  $CH_2Cl_2$  solution after 4 days.

(d) **Li[HB(mt)<sub>2</sub>(pz)]**. To an orange-red suspension of **8** (37 mg, 0.10 mmol) in  $CH_2Cl_2$  was added Li[HB(mt)<sub>2</sub>(pz)] (62 mg, 0.20 mmol) and NaPF<sub>6</sub> (84 mg, 0.50 mmol). The mixture was stirred for 18 h, resulting in a suspension of a white precipitate in a bright red supernatant. The suspension was filtered and the red filtrate was evacuated to dryness and recrystallised in MeCN/ether at -30 °C. Multiple recrystallisations from MeCN/Et<sub>2</sub>O yielded red fine powder of [(HMB)Ru{HB(mt)<sub>2</sub>(pz)}]PF<sub>6</sub> (**11B**) (105 mg, 0.15 mmol, 74 % yield). Diffraction-quality single crystals were obtained at -30 °C as red needles by slow diffusion of ether into a acetonitrile solution after 2 weeks.

In the absence of NaPF<sub>6</sub>, diffraction-quality single crystals of **11'** were obtained at -30 °C as red needles by slow diffusion of ether into a  $CH_2Cl_2$  solution after 4 days.

Data for **11**. Anal. Found: C, 39.0; H, 4.6; N, 11.4; S, 9.0 %. Calc. for  $C_{23}H_{32}B_1F_6N_6P_1Ru_1S_2$ : C, 38.7; H, 4.5; N, 11.8; S, 9.0 %. IR (KBr,  $cm^{-1}$ ):  $\nu$ (B-H) 2459w;  $\nu$ ( $\mu$ -B-H) 2272w, 2185w. ESI<sup>+</sup>-MS (m/z): 569 [ $M^+$  =  $[C_6Me_6Ru(C_4H_5N_2S)_2(C_3H_3N_2)BH]^+$ ]; ESI<sup>-</sup>-MS (m/z): 145 [ $M^-$  =  $PF_6^-$ ].  $^1H$  NMR

(CD<sub>3</sub>CN): *isomer 11A*:  $\delta$  7.77 (d, 1H,  $^3J = 1.4$  Hz, HC=CHNNCH), 7.45 (d, 1H,  $^3J = 2.3$  Hz, HC=CHNNCH), 7.02 (d, 2 x 1H,  $^3J = 2.2$  Hz, SCN<sub>2</sub>HC=CH), 6.83 (d, 2 x 1H,  $^3J = 2.0$  Hz, SCN<sub>2</sub>HC=CH), 6.44 (t, 1H,  $^3J = ca. 1.8$  Hz, HC=CHNNCH), 3.58 (s, 2 x 3H, NCH<sub>3</sub>), 1.97 (s, 18H, C<sub>6</sub>(CH<sub>3</sub>)<sub>6</sub>); *isomer 11B*:  $\delta$  7.95 (d, 1H,  $^3J = 2.2$  Hz, HC=CHNNCH), 7.75 (d, 1H,  $^3J = 0.6$  Hz, HC=CHNNCH), 6.95 (d, 2 x 1H,  $^3J = 2.1$  Hz, SCN<sub>2</sub>HC=CH), 6.74 (d, 2 x 1H,  $^3J = 2.1$  Hz, SCN<sub>2</sub>HC=CH), 6.32 (t, 1H,  $^3J = ca. 2.3$  Hz, HC=CHNNCH), 3.65 (s, 2 x 3H, NCH<sub>3</sub>), 2.09 (s, 18H, C<sub>6</sub>(CH<sub>3</sub>)<sub>6</sub>), -10.6 (q of equal intensity, 1H,  $J = 60$  Hz,  $\mu$ -HB); approx. relative ratio of **11A:11B** = 2.4:1 from signal integrals.

## References

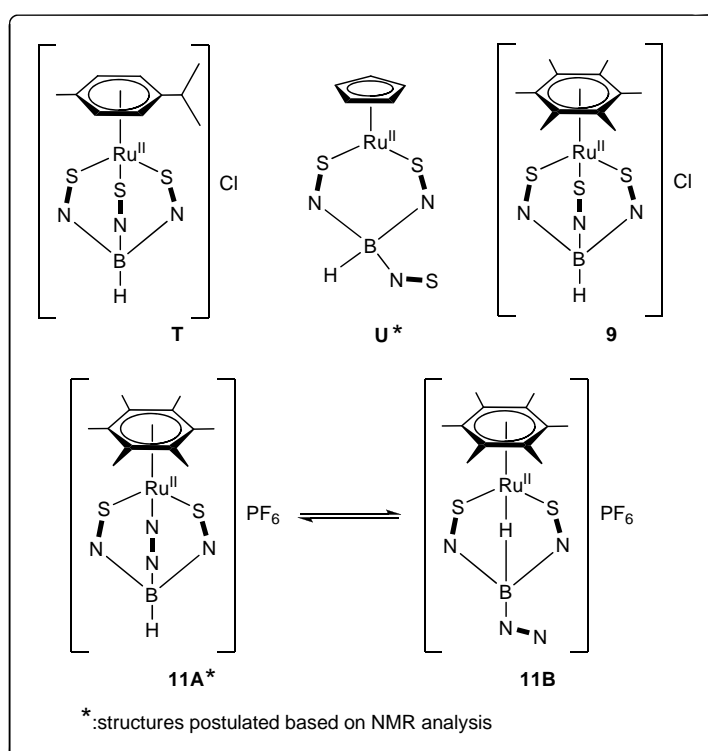
1. Rauchfuss, T. B., *Inorg. Chem.* **2004**, *43* (1), 14-26.
2. Stiefel, E. I.; Matsumoto, K.; Editors, *Transition Metal Sulfur Chemistry: Biological and Industrial Significance. [In: ACS Symp. Ser., 1996; 653]*. 1996; p 358 pp.
3. Gaye, M.; Demerseman, B.; Dixneuf, P. H., *J. Organomet. Chem.* **1991**, *411* (1-2), 263-270.
4. Bennett, M. A.; Huang, T. N.; Matheson, T. W.; Smith, A. K., *Inorganic Syntheses* **1982**, *21*, 74-78.
5. Shin, R. Y. C.; Bennett, M. A.; Goh, L. Y.; Chen, W.; Hockless, D. C. R.; Leong, W. K.; Mashima, K.; Willis, A. C., *Inorg. Chem.* **2003**, *42* (1), 96-106.
6. Bennett, M. A.; Goh, L. Y.; Willis, A. C., *J. Am. Chem. Soc.* **1996**, *118* (21), 4984-4992.
7. Bailey, P. J.; Lorono-Gonzales, D. J.; McCormack, C.; Parsons, S.; Price, M., *Inorg. Chim. Acta* **2003**, *354*, 61-67.
8. Bhambri, S.; Tocher, D. A., *Polyhedron* **1996**, *15* (16), 2763-2770.
9. Kimblin, C.; Bridgewater, B. M.; Hascall, T.; Parkin, G., *Dalton Trans.* **2000**, (6), 891-897.
10. Alvarez, H. M.; Tran, T. B.; Richter, M. A.; Alyounes, D. M.; Rabinovich, D.; Tanski, J. M.; Krawiec, M., *Inorg. Chem.* **2003**, *42* (6), 2149-2156.
11. Maria, L.; Domingos, A.; Santos, I., *Inorg. Chem.* **2003**, *42* (10), 3323-3330.
12. Garcia, R.; Paulo, A.; Domingos, A.; Santos, I.; Ortner, K.; Alberto, R., *J. Am. Chem. Soc.* **2000**, *122* (45), 11240-11241.
13. Garcia, R.; Domingos, A.; Paulo, A.; Santos, I.; Alberto, R., *Inorg. Chem.* **2002**, *41* (9), 2422-2428.
14. Garcia, R.; Paulo, A.; Domingos, A.; Santos, I., *J. Organomet. Chem.* **2001**, *632* (1-2), 41-48.
15. Patel, D. V.; Mihalcik, D. J.; Kreisel, K. A.; Yap, G. P. A.; Zakharov, L. N.; Kassel, W. S.; Rheingold, A. L.; Rabinovich, D., *Dalton Trans.* **2005**, (14), 2410-2416.
16. Alvarez, H. M.; Tanski, J. M.; Rabinovich, D., *Polyhedron* **2004**, *23* (2-3), 395-403.
17. Foreman, M. R. S. J.; Hill, A. F.; Owen, G. R.; White, A. J. P.; Williams, D. J., *Organometallics* **2003**, *22* (22), 4446-4450.
18. Pauling, L. in *The Nature Of The Chemical Bond*. 3rd ed.; Cornell University Press: Oxford, **1960**.
19. Foreman, M. R. S. J.; Hill, A. F.; White, A. J. P.; Williams, D. J., *Organometallics* **2004**, *23* (4), 913-916.
20. Graham, L. A.; Fout, A. R.; Kuehne, K. R.; White, J. L.; Mookherji, B.; Marks, F. M.; Yap, G. P. A.; Zakharov, L. N.; Rheingold, A. L.; Rabinovich, D., *Dalton Trans.* **2005**, (1), 171-180.
21. Hill, A. F.; Owen, G. R.; White, A. J. P.; Williams, D. J., *Angew. Chem. Int. Ed.* **1999**, *38* (18), 2759-2761.
22. Goh, L. Y.; Teo, M. E.; Khoo, S. B.; Leong, W. K.; Vittal, J. J., *J. Organomet. Chem.* **2002**, *664* (1-2), 161-169.
23. Shin, R. Y. C.; Ng, S. Y.; Tan, G. K.; Koh, L. L.; Khoo, S. B.; Goh, L. Y.; Webster, R. D., *Organometallics* **2004**, *23* (3), 547-558.



## Chapter 4. Syntheses of mixed-sandwich Cp\*Ru complexes containing poly(methimazoly)borates (Cp\* = C<sub>5</sub>Me<sub>5</sub>)

Studies described in Chapter 3 showed that [(HMB)Ru<sup>II</sup>{HB(mt)<sub>2</sub>(pz)}] PF<sub>6</sub> (**11**) existed in the  $\kappa^3$ -*N,S'S''* and  $\kappa^3$ -*H,S,S'* isomeric forms in solution (Chart 4.1). However, the isomerisation process is too slow on the NMR timescale for us to obtain kinetics information on the system. Bailey had postulated that the ligand in CpRu<sup>II</sup>{HB(mt)<sub>3</sub>} complex (**U**) adopted a  $\kappa^2$ -*S,S'* coordination on the basis of the <sup>1</sup>H NMR spectral analysis, while the ligand prefers a  $\kappa^3$ -*S,S',S''* coordination in [(*p*-cymene)Ru<sup>II</sup>{HB(mt)<sub>3</sub>}]Cl (**T**).<sup>1</sup> It is possible that such fluxional behavior in the poly(methimazoly)borates is more likely to occur in the mixed sandwich complexes

**Chart 4.1.** Half-sandwich ruthenium complexes with poly(methimazoly)borates.



of  $\eta^5$ -(Cp/Cp\*)Ru than in  $\eta^6$ -arene Ru. Thus, it is hoped that the synthesis of Cp\*Ru<sup>II</sup> complexes with poly(methimazolyl)borates may give us more kinetics information on the isomerisation process.

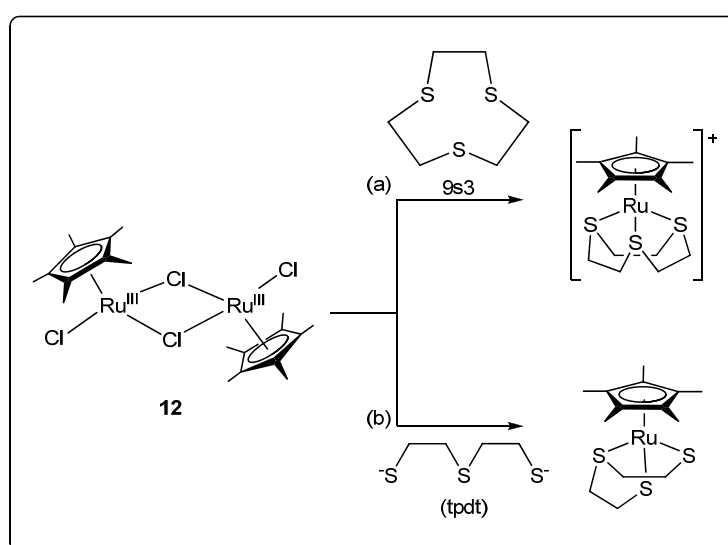
In addition, the cyclic voltammetric studies in the previous chapter on the [(HMB)Ru<sup>II</sup>{HB(mt)<sub>3</sub>}] (**9**) have shown that the oxidized species is unstable and hence we were unable to obtain supporting evidence for the occurrence of an isomerization reaction involving  $\kappa^3$ -H,S,S'- and  $\kappa^3$ -S,S',S''-coordination of the [HB(mt)<sub>3</sub>] ligand. The  $\eta^5$ -cyclopentadienyl Ru<sup>II</sup> system may provide us an alternative for such studies. Moreover, there exist a suitable Ru<sup>III</sup> precursor, *viz.* [Cp\*Ru<sup>III</sup>Cl<sub>2</sub>]<sub>2</sub> (**12**) that can serve as an entry to mixed sandwich ruthenium<sup>III</sup> complexes with poly(methimazolyl)borates, which will allow us to study the electrochemistry of Ru<sup>III</sup> poly(methimazolyl)borate complexes directly.

Compared to (Cp/Cp\*)Ru<sup>II</sup> complexes, studies on the analogous Ru<sup>III</sup> compounds are rare despite the availability of a convenient Ru<sup>III</sup> source-[Cp\*RuCl<sub>2</sub>]<sub>2</sub> (**12**) since 1984.<sup>2,3</sup> Koelle and Hidai demonstrated that the +3 metal oxidation state in **12** was maintained in their dichloro<sup>4</sup> and alkyl/arylthiolate-bridged<sup>5</sup> derivatives only in the presence of two uninegative ligands at each Ru center. In an investigation of the reactivity of **12** with tripodal sulfur ligands, Goh and coworkers had synthesized the monocationic complex, [Cp\*Ru<sup>II</sup>(9S3)]<sup>+</sup> and the neutral [Cp\*Ru<sup>III</sup>(tpdt)] (Scheme 4.1), which present to us a methodology that can be used for the synthesis of Cp\*Ru<sup>III</sup> complexes of poly(methimazolyl)borates.

On the other hand, this implies that **12** cannot be used as a precursor to the syntheses of the mixed sandwich Cp\*Ru<sup>II</sup> complexes of poly(methimazolyl)borates. Hence, an alternative methodology is proposed, different from that employed earlier for the (HMB)Ru<sup>II</sup> complexes, which uses the 16-electron Ru<sup>II</sup> species, [Cp\*RuOMe]<sub>2</sub>

(**13**) as a precursor. Even though the chemistry of **13** with sulfur-containing ligand is limited to the alkyl/arylthiolates, it is expected that this coordinatively and electronically unsaturated organometallic complex, will be highly reactive. Indeed we were able to synthesise the Cp\*Ru<sup>II</sup> complexes of poly(methimazolyl)borates via the elimination of an OMe salt from the reaction of the poly(methimazolyl)borate salts with **13**, and the results are described below.

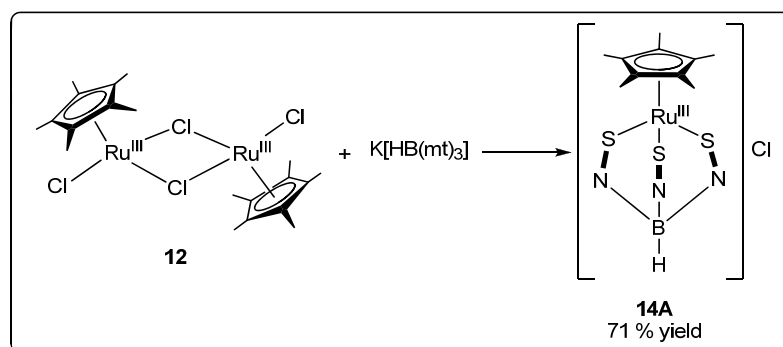
**Scheme 4.1.** Reaction of [Cp\*RuCl<sub>2</sub>]<sub>2</sub> with (a)9s3 and (b)tpdt.



#### 4.1. Syntheses of [Cp\*Ru] complexes containing poly(methimazoly)borate ligands

The Cp\*Ru[HB(mt)<sub>2</sub>]Cl (**14A**) was isolated as a brown solid, in 71 % yield from the reaction of the 17-electron species, [Cp\*RuCl<sub>2</sub>]<sub>2</sub> (**12**), with K[HB(mt)<sub>3</sub>] at RT (Scheme 4.2).

**Scheme 4.2.** Reaction of [Cp\*RuCl<sub>2</sub>]<sub>2</sub> with K[HB(mt)<sub>3</sub>].



The presence of a paramagnetic a d<sup>5</sup>-Ru(III) centre is substantiated by both the low temperature EPR spectrum of **14A** which displays a broad signal (Figure 4.1) and the <sup>1</sup>H NMR spectra of broad peaks in CD<sub>3</sub>CN.

The EPR signal was very broad and was not detectable above liquid nitrogen temperatures indicating that the unpaired electron was metal rather than ligand centered. The spectrum showed features similar to that expected for species with axial symmetry albeit with a degree of distortion that was difficult to accurately simulate. It is possible that the experimental spectrum represents several species with slightly differing geometries [due to twisting of the HB(mt)<sub>3</sub> ligand], which could also account for the surprisingly large line width that is not typical in Ru(III) compounds. Similar  $S = 1/2$  anisotropic spectra have been observed in complexes containing the dithiocarbamate ligand and for octahedral complexes containing bidentate sulfur ligands that have a high degree of covalency and a distorted structure.<sup>6-9</sup>

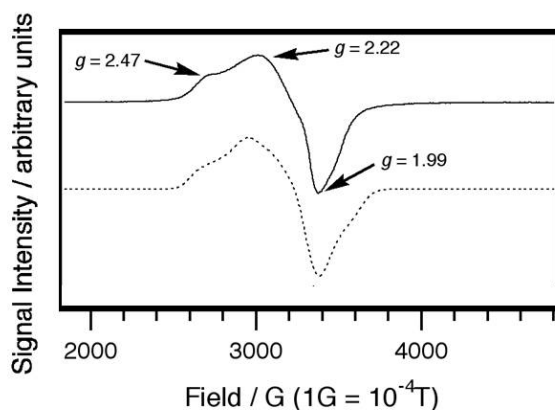


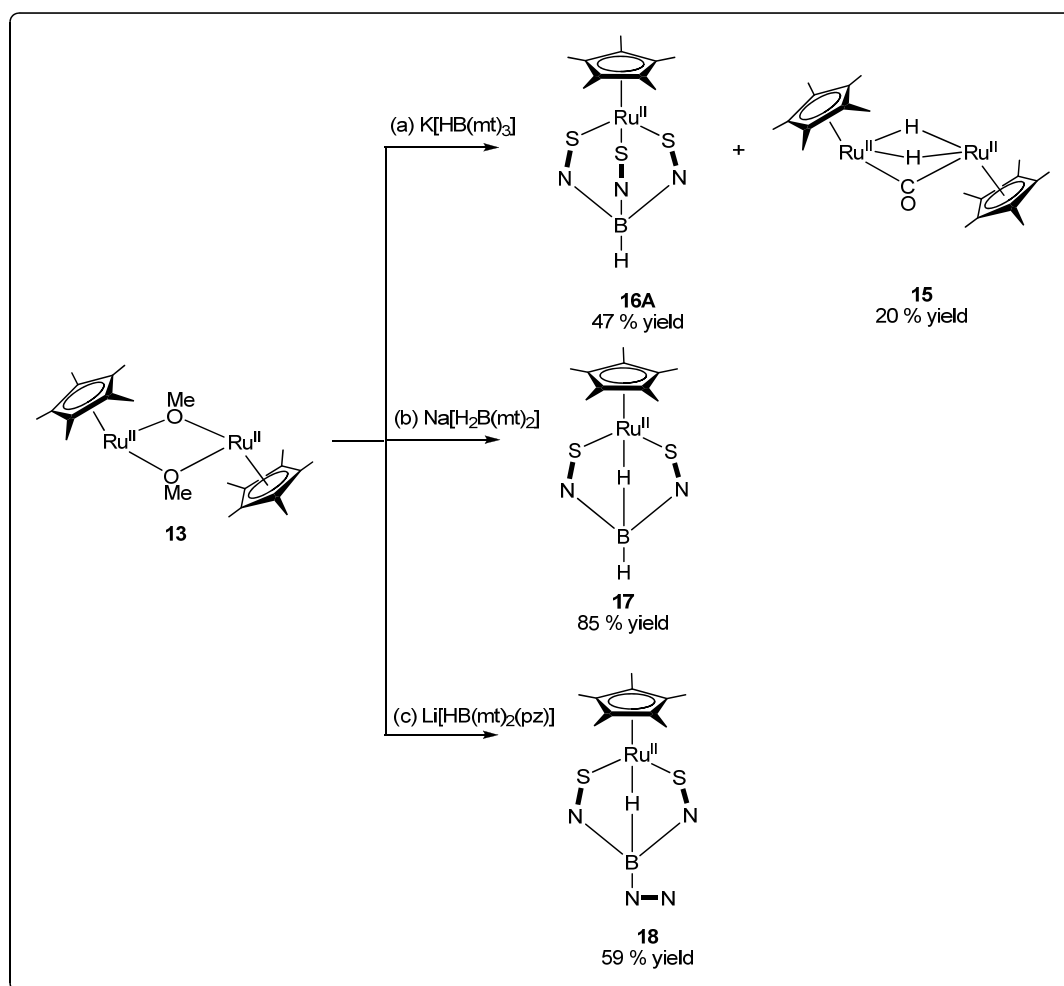
**Figure 4.1.** Continuous wave X-band EPR spectra for (—) **14A**. (----) Simulated spectrum.

The mixed-sandwich pentamethylcyclopentadienylruthenium (II) complexes consisting of the poly(methimazolyl)borate ligands,  $\text{Cp}^*\text{Ru}[\text{HB}(\text{mt})_3]$  (**16A**),  $\text{Cp}^*\text{Ru}[\text{H}_2\text{B}(\text{mt})_2]$  (**17**) and  $\text{Cp}^*\text{Ru}[\text{HB}(\text{mt})_2(\text{pz})]$  (**18**) were obtained from the reaction of the coordinatively unsaturated 16-electron species  $[\text{Cp}^*\text{RuOMe}]_2$  (**13**) with the corresponding poly(methimazolyl)borate salts in moderate yields (Scheme 4.3). Our synthetic method provides an alternative route to that reported in the literature where the  $\text{CpRu}[\text{HB}(\text{mt})_3]$  complex was isolated from the reaction of  $[\text{CpRu}(\text{NCMe})_3]\text{PF}_6$  with  $\text{Na}[\text{HB}(\text{mt})_3]$ .

In the synthesis of  $\text{Cp}^*\text{Ru}[(\kappa^3\text{-}S,S'S'')\text{-}\{\text{HB}(\text{mt})_3\}]$  (**16A**), a side product,  $\text{Cp}^*\text{Ru}(\mu\text{-H})_2(\mu\text{-CO})\text{RuCp}^*$  (**15**) was isolated in 20 % yield when the reaction was carried out at elevated temperature (Scheme 4.3a). Its NMR spectrum showed two singlets at  $\delta$  1.79 and -12.89 indicative of the presence of  $\text{Cp}^*$  and bridging hydride, respectively. The IR spectrum showed a strong absorption stretch at  $1793\text{ cm}^{-1}$ , indicating the presence of a bridging  $\text{C}\equiv\text{O}$ . The spectroscopic data is in agreement with that reported in the literature by Koelle and coworkers, where they isolated  $\text{Cp}^*\text{Ru}(\mu\text{-H})_2(\mu\text{-CO})\text{RuCp}^*$  via (i) the nucleophilic reaction of  $[\text{Cp}^*\text{RuOMe}]_2$  with  $(\text{Me}_3\text{Si})_2\text{NH}$  or (ii) the thermal degradation of  $[\text{Cp}^*\text{RuOMe}]_2$ .<sup>10</sup> Thus, when the

reaction of  $[\text{Cp}^*\text{RuOMe}]_2$  with  $\text{K}[\text{HB}(\text{mt})_3]$  was repeated at RT in toluene/MeOH, complex **16A** can be isolated in *ca.* 54% yield, without the formation of  $\text{Cp}^*\text{Ru}(\mu\text{-H})_2(\mu\text{-CO})\text{RuCp}^*$ .

**Scheme 4.3.** Reaction of  $[\text{Cp}^*\text{RuOMe}]_2$  with (a)  $\text{K}[\text{HB}(\text{mt})_3]$ , (b)  $\text{Na}[\text{H}_2\text{B}(\text{mt})_2]$  and (c)  $\text{Li}[\text{HB}(\text{mt})_2(\text{pz})]$ .



The  $^1\text{H}$  NMR spectrum of **16A** varies with the solvent. The spectrum in  $\text{C}_6\text{D}_6$  at 293 K shows six doublets for methimazolyl ring protons and three singlets for the NMe protons, which is more complex than that expected for a  $\kappa^3\text{-S,S',S''}$  coordination mode of the  $[\text{HB}(\text{mt})_3]$  ligand as determined by X-ray crystallography (Figure 4.3b).

In  $\text{CD}_2\text{Cl}_2$  or  $\text{CD}_3\text{CN}$ , the spectrum shows clearly the presence of only one species containing two types of ‘mt’ moieties in relative proportion 2:1, indicative of bidentate coordination of the ligand. The  $\kappa^3\text{-H,S,S'}$  coordination of the ligand in

species **16B** was confirmed by the presence of a quartet of equal intensity, due to quadrupolar coupling of the proton to the B atom, centered at  $\delta$  -7.67 in  $C_6D_6$ , a characteristic region due to the resonance of  $M \cdots H-B$ .  $^1H$  NMR spectra in different  $C_6D_6/CD_2Cl_2$  compositions showed that the **16A:16B** ratio varied with solvent composition (Table 4.1), indicative of a solvent dependent equilibrium between **16A** and **16B** (Scheme 4.4).

**Scheme 4.4.** Isomeric equilibrium of **16A/16B**.

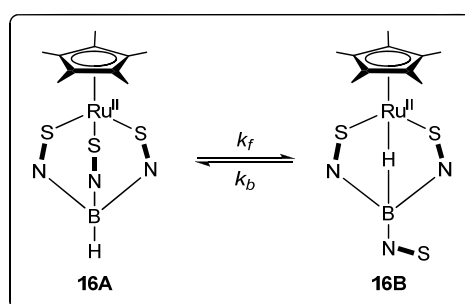


**Table 4.1** Variation of **16A: 16B**<sup>a</sup> with solvent composition.

$C_6D_6:CD_2Cl_2$	1:0	0.8:0.2	0.4:0.15	0:1
<b>16A:16B</b>	1:3	1:5	1:19	0:1

<sup>a</sup>Obtained from integral ratios of  $^1H$  NMR spectra.

This is further supported by 2D EXSY NMR experiment which showed that there is an exchange process between the 2 isomers (Figure 4.2). However, only form **16A** was obtained in the crystalline state, even when crystallized from acetonitrile/ether. The  $^1H$  NMR spectrum was completely assigned for the two species from  $^1H$  COSY and NOESY spectra (Figure A1 and A2 in appendix).

The  $^1H$  NMR spectra of **17** (in  $C_6D_6$ ) show a pair of doublets for the CH's of the methimazolyl rings in the region  $\delta$  5.75 – 6.96, and a quartet of equal intensity at  $\delta$  -7.83 for the agostic-like H's - consistent with  $\kappa^3-H,S,S'$  coordination of the Bm ligand. In  $CD_2Cl_2$  at 300 K, the  $\mu$ -HB resonance is observed as two very broad overlapping 'humps' (each possessing  $v_{1/2}$  ca. 100 Hz), the resolution of which

decreases further with lowering of temperature, until at 183 K, the ‘humps’ merged to give broad singlets ( $v_{1/2}$  ca.36 Hz), due to precipitation at low temperature. The  $^1\text{H}$  NMR spectrum is consistent with the solid state structure determined by x-ray crystallography (Figure 4.3c).

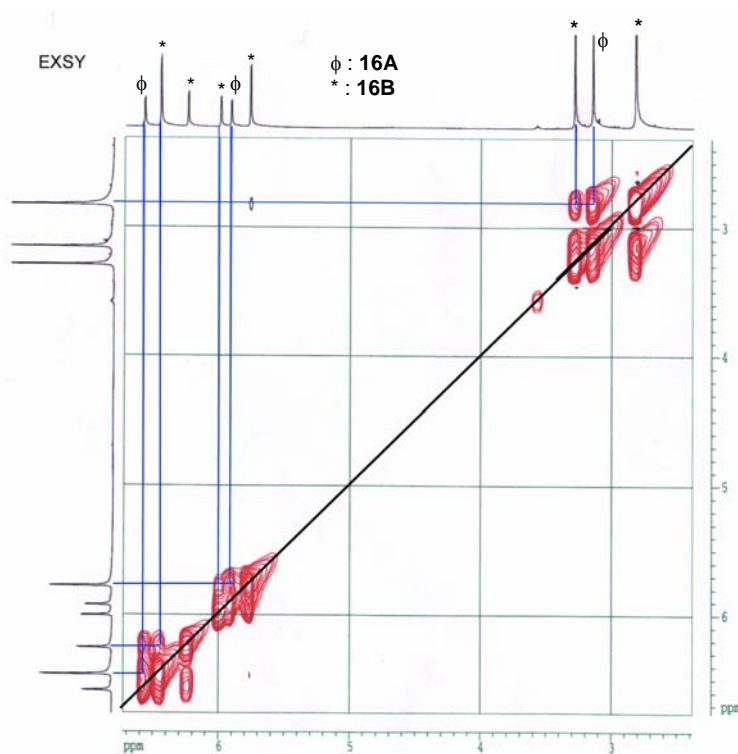


**Figure 4.2.** 2D  $^1\text{H}$  NMR EXSY spectrum for complex **16A/16B** in  $\text{C}_6\text{D}_6$ .

The  $^1\text{H}$  NMR spectra of **18** (in  $\text{C}_6\text{D}_6$ ) shows two doublets and a set of triplet (two overlapping doublets) for the pyrazole ring protons, two doublets for the methimazolyl ring protons and a singlet for the NMe protons. Both the methimazolyl ring protons are in the same chemical environment and a quartet of equal intensity at  $\delta$  -7.20 for the agostic-like B-H, in agreement with a  $\text{Cp}^*\text{Ru}[(\kappa^3\text{-}H,S,S')\text{[HB(mt)}_2(\text{pz})]$  formulation. The  $^1\text{H}$  NMR spectrum is consistent with the solid state structure determined by x-ray crystallography (Figure 4.3d). There was no sign of the occurrence of fluxional processes of a solution of **18** in  $\text{d}_8$ -toluene, down to 253K.



Comparing complexes **16** and **18** with the (HMB)Ru analogues, **9** and **11**, it is apparent that the [HB(mt)<sub>3</sub>] and [H(mt)<sub>2</sub>(pz)] ligands has a preference for the agostic-like M...H-B interactions in the Cp\*Ru system. This can be attributed to the positive charge on the [(HMB)Ru<sup>II</sup>] complex. The molecular structures of the monocationic Ru(III) complex **14A** and the neutral Ru(II) complex **16A**, **17** and **18** have been determined by x-ray crystallography and the structures are markedly similar, each containing a ruthenium centre sandwiched between a Cp\* ring and a tripodal poly(methimazolyl)borate ligand. The molecular structures are depicted in Figures 4.3a-d.

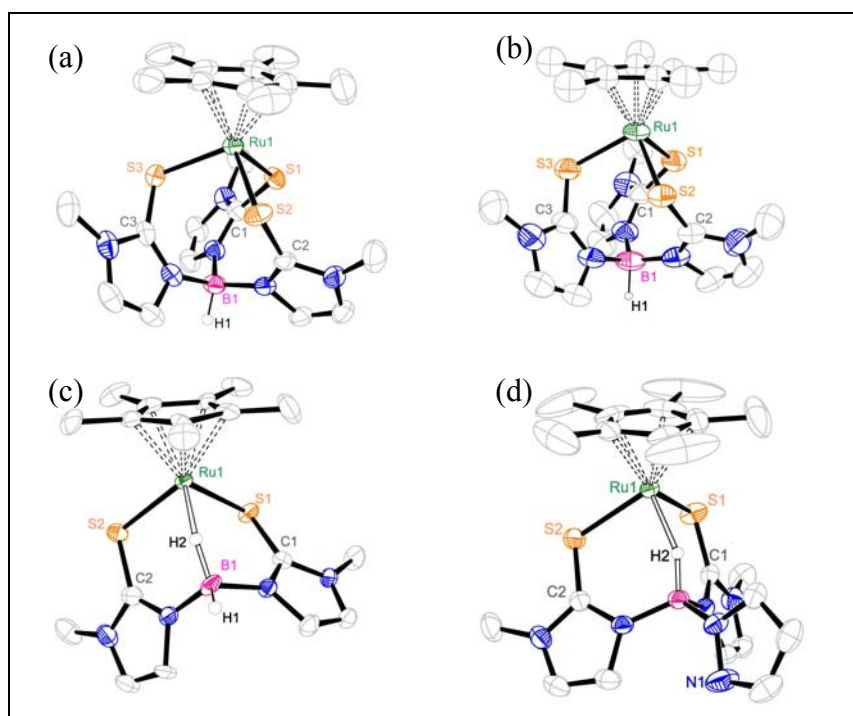


**Figure 4.3.** ORTEP plots for the molecular structures of (a) **14A** monocation, (b) **16A** (c) **17** and (d) **18**. The disordered parts of the Cp\* in **16A** has been omitted. All hydrogen atoms except those on the boron are omitted for clarity. Thermal ellipsoids are drawn at the 50% probability level for **14A**, **17** and **18** and 30% probability level for **16A**.

Complex **14A** is the first example of a Ru<sup>III</sup>[HB(mt)<sub>3</sub>] species reported to date. Bailey and co-workers had prepared an arene Ru(II) analogue of **14A**, [(*p*-cymene)Ru<sup>II</sup>{HB(mt)<sub>3</sub>}]Cl, and the Cp analogue of **16A** from the reaction of

Na[HB(mt)<sub>3</sub>] with [(*p*-cymene)RuCl<sub>2</sub>]<sub>2</sub> and [CpRu(MeCN)<sub>3</sub>]PF<sub>6</sub>, respectively.<sup>1</sup> The [HB(mt)<sub>3</sub>] ligand in **14A** and **16A** adopts a  $\kappa^3$ -*S,S',S''* coordination, similar to [Cp\*Cr{HB(mt)<sub>3</sub>}]Br (**2**) and [(HMB)Ru{HB(mt)<sub>3</sub>}] (**9**) reported in the previous chapters. The  $\kappa^3$ -*H,S,S'* coordination mode adopted by the [H<sub>2</sub>B(mt)<sub>2</sub>] ligand in **17** is similar to that reported for the Cp\*Cr and (HMB)Ru analogues reported earlier. Complex **18** possesses solid state structure similar to the [(HMB)Ru{HB(mt)<sub>2</sub>(pz)}] cation, where the [HB(mt)<sub>2</sub>(pz)] ligand adopts a  $\kappa^3$ -*H,S,S'* coordination mode. The bond parameters of **14A**, **16A**, **17** and **18** are given in Table 4.2.

**Table 4.2.** Selected bond lengths (Å) and bond angles (°).

	<b>14A.PF<sub>6</sub></b>	<b>16A</b>	<b>17</b>	<b>18</b>
Bond Distances (Å)				
Ru(1)-S(1)	2.3956(8)	2.440(2)	2.416(2)	2.3964(10)
Ru(1)-S(2)	2.4100(8)	-	2.392(2)	2.3809(9)
Ru(1)-S(3)	2.3213(8)	-	-	-
C(1)-S(1)	1.724(3)	1.72(1)	1.701(9)	1.688(4)
C(2)-S(2)	1.722(3)	-	1.698(9)	1.694(4)
C(3)-S(3)	1.724(3)	-	-	-
B(1)-H(1)	1.076(10)	1.172 (10)	1.18(1)	-
B(2)-H(2)	-	-	1.17(1)	1.163 (1)
Ru(1)-H(2)	-	-	1.813(10)	1.899 (10)
Bond Angles (°)				
S(1)-Ru(1)-S(2)	92.98(3)	92.6(1)	93.22(8)	93.14(4)
S(2)-Ru(1)-S(3)	92.58(3)	-	-	-
S(1)-Ru(1)-S(3)	100.62(3)	-	-	-
Ru(1)...H(2)-B(1)	-	-	140(1)	141.86 (10)

The C-S bonds of both molecules fall in the range of 1.688(4) - 1.724(3) Å, intermediate between values of a single bond (*ca.* 1.81 Å) and a double bond (*ca.* 1.56 Å),<sup>11</sup> as commonly found in metal complexes of Tm<sup>R</sup>.<sup>12-21</sup> The Ru-H<sub>agostic</sub> distance for complexes **17** and **18** were determined to be 1.813 (10) and 1.899 (10), respectively. These values are comparable to the B - H<sub>agostic</sub> bond distance in **10** (1.81(2) Å) and [RuH(CO)(PPh<sub>3</sub>)( $\kappa^3$ -*H,S',S''*(Tm))] (1.29(5) Å).<sup>22</sup>

## 4.2. Cyclic Voltammetry

The cyclic voltammograms of **14A**, **16-18** at 233 and 293 K are given in Figure 4.4. All the complexes except **14A** displayed a one-electron oxidation process between -0.86 to -0.65 V vs. Fc/Fc<sup>+</sup>, as shown in Table 4.3.

The  $E_{1/2}^r$ -values observed for the one electron oxidation of **16B**, **17** and **18** were lower than that observed for **16A**, implying that **16A** is easier to oxidize compared with the other three complexes, which is consistent with a more electron rich Ru centre in **16A** where the [HB(mt)<sub>3</sub>]<sup>-</sup> ligand adopt a  $\kappa^3$ -S,S',S'' coordination compared with the other three complexes where the poly(methimazolyl)borate ligands adopt a  $\kappa^3$ -S,S',H coordination.

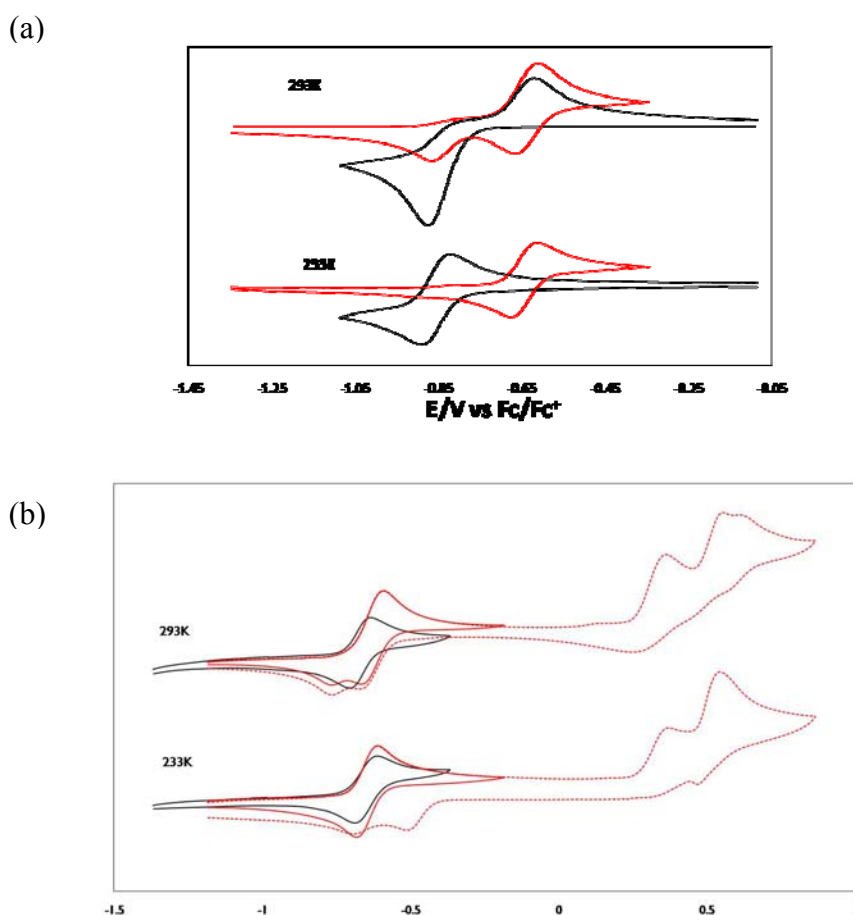


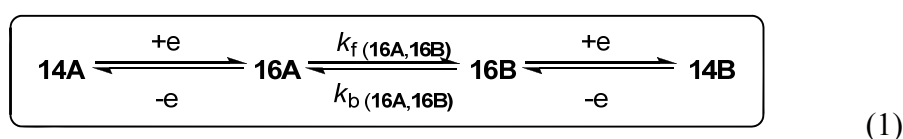
**Figure 4.4.** Cyclic voltammograms recorded at a scan rate of 100 mV s<sup>-1</sup> at a 1 mm GC electrode (a) 2.36 mM **14A.Cl** in CH<sub>2</sub>Cl<sub>2</sub> with 0.5 M *n*-Bu<sub>4</sub>NPF<sub>6</sub><sup>(-)</sup>; 2.61 mM **16A/16B** in CH<sub>2</sub>Cl<sub>2</sub> with 0.5 M *n*-Bu<sub>4</sub>NPF<sub>6</sub><sup>(-)</sup> (b) 0.5 mM **17** in CH<sub>2</sub>Cl<sub>2</sub> with 0.25 M *n*-Bu<sub>4</sub>NPF<sub>6</sub><sup>(-)</sup>; 1.0 mM **18** in CH<sub>2</sub>Cl<sub>2</sub> with 0.2 M *n*-Bu<sub>4</sub>NPF<sub>6</sub><sup>(-)</sup>.

**Table 4.3.** Oxidation potential of complexes **16-18** in CH<sub>2</sub>Cl<sub>2</sub> vs. Fc/Fc<sup>+</sup>.

Complex	<b>16A</b>	<b>16B</b>	<b>17</b>	<b>18</b>
Oxidation potential/V	-0.86	-0.65	-0.67	-0.65

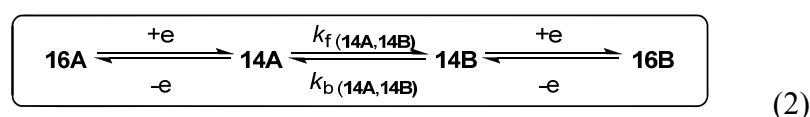
While the oxidation potential of **18** is close to those observed for complexes **16** and **17**, the reverse reduction process was split into two processes, Red<sub>A</sub> and Red<sub>B</sub> when the temperature was increased to 293K (Figure 4.4b). Red<sub>A</sub> is associated with reduction of **18**<sup>+</sup> back to **18**, while Red<sub>B</sub> is associated with the reduction of an additional product that forms *via* decomposition/reaction of **18**<sup>+</sup> (which appears to be semi-stable at 293 K on the voltametric time-scale). When the scan was extended in the positive direction, two chemically irreversible oxidation processes were detected at positive potentials, caused by chemical instability of more highly oxidised states of **18**<sup>+</sup>. Complex **18** was not able to be electrochemically reduced within the solvent/electrolyte potential window accessible in CH<sub>2</sub>Cl<sub>2</sub>.

More noteworthy is the CV of **14A** and **16A**. At 233 K, the CV of **14A** shows a chemically reversible one-electron reduction process at -0.855 V vs. Fc/Fc<sup>+</sup> involving Ru(III) converting to Ru(II) (Scheme 4.5, **14A** → **16A**). As the temperature was raised, the anodic peak current (*i*<sub>p</sub><sup>ox</sup>) associated with the reverse oxidation process (Scheme 4.5, **16A** → **14A**) diminished in size and an additional oxidation process became evident at a less negative potential (-0.645 V vs. Fc/Fc<sup>+</sup>). The new oxidation process at -0.645 V vs. Fc/Fc<sup>+</sup> was assigned to the oxidation of **16B** that forms *via* an intramolecular ligand exchange (Scheme 4.5, **16A** → **16B**). Therefore, the CV's in Figure 4.4a represent the series of reactions



Because **16A** is the one-electron reduced form of **14A**, it could be expected that solutions of **16A** would yield voltammetric processes at an identical potential to

**14A**, albeit with the current traces offset because **14A** can be electrochemically reduced whilst **16A** can be electrochemically oxidized. However, it was observed that solutions prepared from solid samples of crystallographically pure **16A** in  $\text{CH}_2\text{Cl}_2$  (with 0.5 M  $\text{Bu}_4\text{NPF}_6$ ) displayed a major oxidation process ( $E_{1/2}^{\text{r}}$ ) at  $\sim 0.2$  V more positive than that of **14A** (Figure 4.4a). Therefore, it was concluded that the main voltammetric process at  $-0.645$  V (vs.  $\text{Fc}/\text{Fc}^+$ ) was associated with oxidation of **16B** that predominantly forms in solution through the dissolution of **16A** (in agreement with the NMR data above). The CV's obtained for solutions of **16B** were analyzed in a similar manner to **14A**. At 233 K, solutions containing **16B** underwent a chemical reversible one-electron oxidation process involving the transformation of Ru(II) to Ru(III) (Scheme 4.5,  $\mathbf{16B} \rightarrow \mathbf{14B}$ ). The CV data at low temperatures (Figure 4.4a, 233 K) illustrates the stability of the  $k^3\text{-H,S,S'}$  form of  $[\text{Cp}^*\text{Ru}^{\text{III}}\text{HB}(\text{mt})_3]$  (**14B**) since the  $i_{\text{p}}^{\text{ox}}/i_{\text{p}}^{\text{red}}$ -value is close to unity. As the temperature was raised, the reverse reduction peak ( $i_{\text{p}}^{\text{red}}$ ) diminished in size and a new process associated with reduction of **14A** become evident at  $-0.855$  V vs.  $\text{Fc}/\text{Fc}^+$  (Figure 4.4a). Thus, the voltammograms of solutions of **16B** involve the mechanism

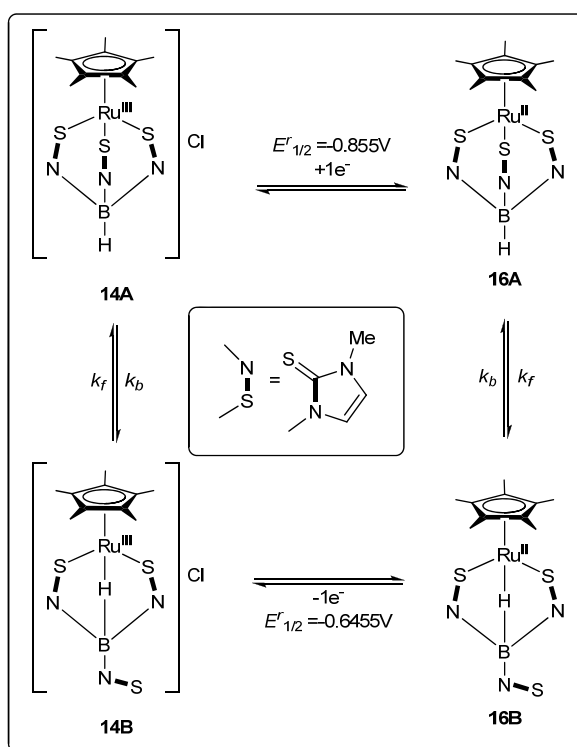


that was modeled over a range of voltammetric scan rates and temperatures analogously to **14A** (Appendix).

The one-electron oxidation of **16B** produced **14B** and the  $k_{\text{f}}$ -values given in Table 4.6 for the **14B** to **14A** isomerization indicate that the reaction occurs slowly at low temperatures, thus, it was thought probable that exhaustive electrolysis of **16B** at 233 K would produce solutions containing mainly **14B**. This hypothesis was tested and confirmed by the EPR spectrum (Figure 4.5) obtained of a frozen solution that

was prepared by exhaustive controlled potential (-0.5 V vs. Fc/Fc<sup>+</sup>) oxidation of **16B** at 233 K in CH<sub>2</sub>Cl<sub>2</sub>/0.5 M Bu<sub>4</sub>NPF<sub>6</sub> with the transfer of one-electron per molecule (measured by coulometry).

**Scheme 4.5.** Electrochemical square scheme depicting chemically reversible redox process for isomers involving Ru(III) converting to Ru(II)



The spectrum is substantially different from that of **14A** (Figure 4.1) and is dominated by a relatively narrow line width signal centered at  $g = 2.02$ , which can be explained by the presence of **14B**. Nevertheless, the spectrum is more complicated than expected for a single species (see the simulation in Figure 4.6) and could contain contamination from a lesser amount of another paramagnetic species. It is possible that **14B** is not indefinitely stable and decomposes or reacts to form an additional paramagnetic Ru<sup>III</sup> compound on the longer electrolysis time-scale. However, any slow decomposition/reaction of **14B** (to a species other than **14A**) is unlikely to have affected the DigiSim<sup>®</sup> modeling<sup>31</sup> of the CV data, since the CV experiments were performed over a much shorter time period.

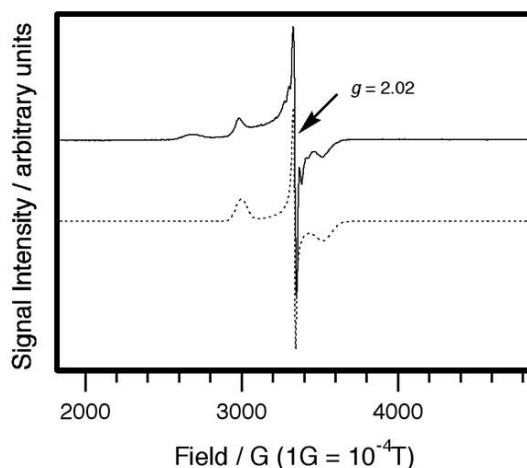


**Figure 4.5.** Continuous wave X-band EPR spectra for (—) **14B** and (----) Simulated spectrum.

The  $E_{1/2}^f$  values for  $[(\text{HMB})\text{Ru}\{\text{HB}(\text{mt})_3\}]\text{Cl}$  (**9**) and  $[(\text{HMB})\text{Ru}\{\text{HB}(\text{mt})_3\}]\text{Cl}$  (**10**) reported in Chapter 3 were determined to be +0.42 V and +0.56 V vs.  $\text{Fc}/\text{Fc}^+$  respectively. The narrow range observed for the oxidation potentials of the complexes **16-18** and for **9** and **10** suggest that the  $E_{1/2}^f$  values are very sensitive to the  $\text{Cp}^*$  and HMB ligands and are less sensitive to the difference in the  $[\text{HB}(\text{mt})_3]^-$ ,  $[\text{H}_2\text{B}(\text{mt})_2]^-$  and  $[\text{HB}(\text{mt})_3]^-$  ligands. The  $\sim 1$  V difference between the  $E_{1/2}^f$  values of the  $\text{Cp}^*$  and HMB coordinated compounds may be due to the positive charge on the  $[(\text{HMB})\text{Ru}\{\text{HB}(\text{mt})_3\}]\text{Cl}$  (**9**) and  $[(\text{HMB})\text{Ru}\{\text{HB}(\text{mt})_3\}]\text{Cl}$  (**10**) complexes, which makes the removal of an electron more difficult than from the neutral  $[(\text{Cp}^*)\text{Ru}^{\text{II}}\{\text{HB}(\text{mt})_3\}]$  (**16**),  $[(\text{Cp}^*)\text{Ru}^{\text{II}}\{\text{H}_2\text{B}(\text{mt})_2\}]$  (**17**) and  $[(\text{Cp}^*)\text{Ru}^{\text{II}}\{\text{HB}(\text{mt})_2(\text{pz})\}]$  (**18**) complexes.

### 4.3. Isomerisation

VT NMR spectral study of **16A/16B** (Figure 4.6) showed that at 253 K, there were 6 sets of doublets and 3 sets of singlets observed for the methimazolyl ring protons and the NMe protons, respectively. As the temperature was raised, the NMe signals converged and at 330 K, the NMe signal belonging to **16A** had coalesced with

that of the non-bonded methimazolyl ring, resulting in only two broad signals for both **16A** and **16B**. Finally, at 360 K, these broad singlets collapsed into a single broad ‘band’ ( $\nu_{1/2} = ca. 92$  Hz). Simultaneously, there also occurred the merging of resonances of the methimazolyl ring protons below 300 K, and at 360 K only two broad peaks ( $\nu_{1/2} = ca. 29$  Hz each) remained.

The thermodynamic parameters  $\Delta H^\circ$  [-6.38(13) kJ mol<sup>-1</sup>] and  $\Delta S^\circ$  [-13.4(5) J mol<sup>-1</sup> K<sup>-1</sup>] were obtained from the van't Hoff plot and the  $\Delta G^\circ$  value [-2.36(26) kJ mol<sup>-1</sup> for 300 K] was calculated from the Eyring equation. The negative  $\Delta G^\circ$  value is in agreement with the observed facile forward reaction leading to a high proportion of **16B** in solution. Thermochemical data for organometallic compounds are sparse but comparison of metal-hydride<sup>23</sup> with metal-sulphur<sup>24</sup> bond enthalpies for Cp<sub>2</sub>WX (where X = H or S) suggests that the latter are weaker.

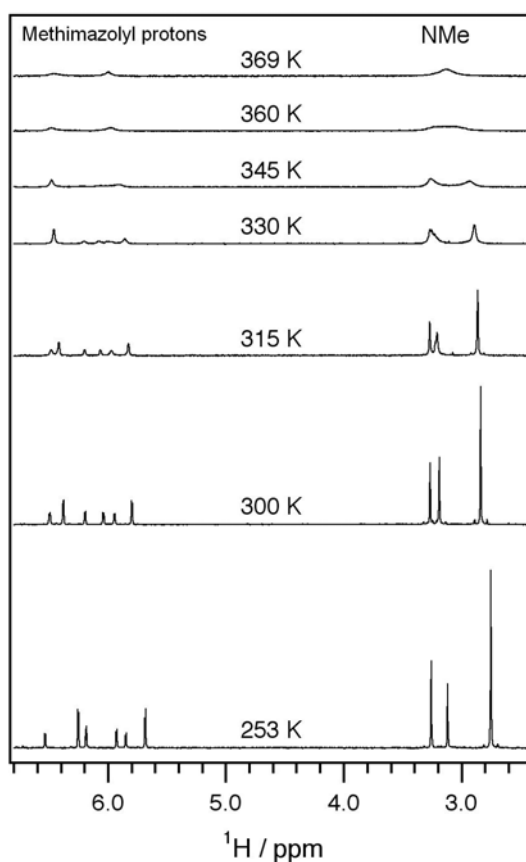


**Figure 4.6.** VT 300 MHz <sup>1</sup>H NMR spectra of **16A/16B** in *d*<sub>8</sub>-toluene.



Simulations of the VT  $^1\text{H}$  NMR spectra using the *g*NMR software<sup>25</sup> gave additional kinetic and thermodynamic parameters for the intramolecular exchange process (Scheme 4.4). The natural linewidths used were obtained from the spectrum at 253 K and there was essentially no exchange from temperatures below 273 K. The exchange rates were set and adjusted such that a reasonable fit was obtained between the calculated and experimental spectra (Figure 4.7). The rate constants,  $k_f$  and  $k_b$ , were then obtained from the equations,  $\text{rate} = k_f[\mathbf{16A}]$  and  $\text{rate} = k_b[\mathbf{16B}]$ , respectively (Table 4.4).

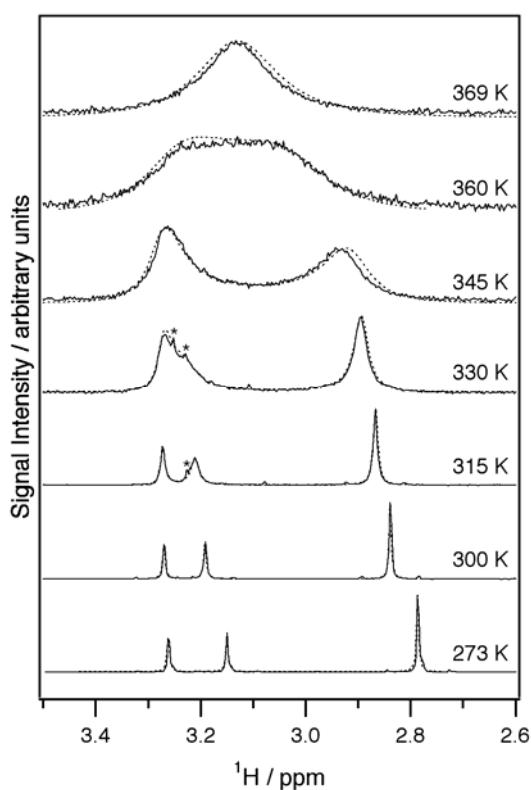


**Figure 4.7.** Experimental (solid line) and simulated (dashed line) VT 300 MHz  $^1\text{H}$  NMR spectra of **16A/16B** in  $d_8$ -toluene. The peaks denoted by \* are due to traces of impurities.

A linear fit using the least-squares method with variance  $r^2$  was obtained from an Eyring plot, to afford the thermodynamic parameters (Table 4.5). A similar Eyring plot was also applied to the CV data (see below). That these values are reasonable has

been checked by comparing the derived  $\Delta H^\circ$  and  $\Delta S^\circ$  values with those obtained from a van't Hoff plot discussed above.

**Table 4.4.** Kinetic data and equilibrium constants in  $d_8$ -toluene for Equilibrium II(Scheme 4.4).

T / K	<b>16A</b> $\rightleftharpoons$ <b>16B</b>				
	rate <sup>a</sup> ( <b>16A</b> $\rightarrow$ <b>16B</b> ) / mol L <sup>-1</sup> s <sup>-1</sup>	$k_f^a$ / s <sup>-1</sup>	$k_b^a$ / s <sup>-1</sup>	$K_{eq}^a$	$K_{eq}^b$
369	63	$1.0 \times 10^4$	$5.8 \times 10^3$	1.7(1)	1.6 (1)
360	38	$6.6 \times 10^3$	$3.3 \times 10^3$	2.0(1)	1.7(1)
345	12	$2.1 \times 10^3$	$1.0 \times 10^3$	2.1(1)	1.9(1)
330	3.0	$5.6 \times 10^2$	$2.6 \times 10^2$	2.2(1)	2.0(1)
315	$5.8 \times 10^{-1}$	$1.2 \times 10^2$	48	2.5(1)	2.2(1)
300	$7.5 \times 10^{-3}$	1.7	$6.0 \times 10^{-1}$	2.8(1)	2.6(1)
273	$1.0 \times 10^{-4}$	$2.3 \times 10^{-2}$	$8.0 \times 10^{-3}$	2.9(1)	3.3(1)
263	-	-	-	-	3.7(1)
253	-	-	-	-	4.2(1)

<sup>a</sup>Obtained by simulation of <sup>1</sup>H NMR data using gNMR (Version 4.1). <sup>b</sup>Obtained from integration ratios of <sup>1</sup>H NMR data.

**Table 4.5.** Thermodynamic parameters obtained from Eyring plots for Equilibrium II(Scheme 4.4).

	$\Delta H_f^\ddagger$ / kJ mol <sup>-1</sup>	$\Delta S_f^\ddagger$ / J mol <sup>-1</sup> K <sup>-1</sup>	$\Delta G_f^\ddagger$ / kJ mol <sup>-1</sup>	$\Delta H_b^\ddagger$ / kJ mol <sup>-1</sup>	$\Delta S_b^\ddagger$ / J mol <sup>-1</sup> K <sup>-1</sup>	$\Delta G_b^\ddagger$ / kJ mol <sup>-1</sup>	$\Delta G^\theta$ / kJ mol <sup>-1</sup>
$d_8$ -toluene <sup>a</sup>	114(9)	147(27)	70(9)	119(9)	154(27)	73(9)	-2(9)
CH <sub>2</sub> Cl <sub>2</sub> <sup>b</sup>	67(4)	0(13)	67(4)	78(3)	11(12)	74(3)	-7(5)

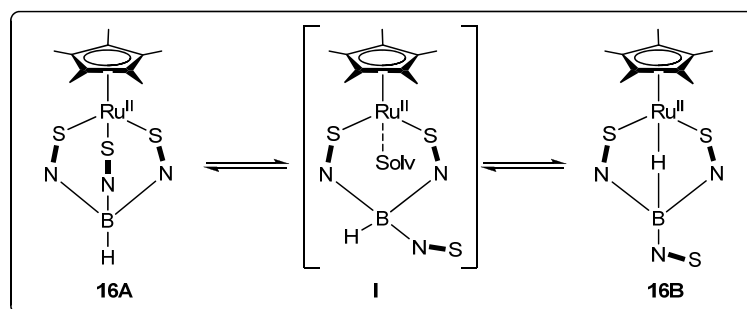
<sup>a</sup>Obtained by simulation of <sup>1</sup>H NMR data using gNMR (Version 4.1). <sup>b</sup>Obtained by simulation of CV data using DigiSim<sup>®</sup> (Version 3.03).

In comparison with the isomerisation process in [(HMB)Ru{HB(mt)<sub>2</sub>(pz)}]PF<sub>6</sub> between **11A** and **11B**, where the  $\Delta G^\circ$  value was found to 2.6(17) kJ mol<sup>-1</sup> at 300 K, the isomerisation process observed for the Cp\*Ru[HB(mt)<sub>2</sub>(pz)] between **16A** and **16B** is more spontaneous.

The thermodynamic values given in Table 4.5 are in agreement with the strong solvent dependence of the **16A/16B** equilibrium. The activation enthalpies in Table 4.5 are also revealing since they are positive in both solvents but very much more so in  $d_8$ -toluene. The implication is that an intermediate species exists between **16A** and **16B** that is more disordered than either **16A** or **16B**. Furthermore, the much smaller

$\Delta S^\ddagger$  value in  $\text{CH}_2\text{Cl}_2$  than in  $d_8$ -toluene suggests that there is a significant solvation effect in the intermediate, which is consistent with an exchange mechanism depicted in Scheme 4.6. It may be expected that the more polar solvent ( $\text{CH}_2\text{Cl}_2$ ) would interact more strongly with the Ru centre in the intermediate, while toluene (or benzene) does not favor such coordination. Examples of  $\text{CH}_2\text{Cl}_2$  acting as a ligand are known,<sup>43</sup> and such a picture of the intermediate is also consistent with the larger activation enthalpy in toluene compared to that in  $\text{CH}_2\text{Cl}_2$  as solvation in the latter would compensate for the cleavage of the Ru-S bond in the intermediate.

**Scheme 4.6.** Proposed exchange mechanism between **16A** ↔ **16B**.



In addition to the equilibrium between **16A** and **16B** that was identified by NMR spectroscopy, CV experiments enabled kinetic quantification of the complete thermodynamic square scheme involving ligand rearrangement about the central Ru atom following reduction of **14A** and oxidation of **16B** (Scheme 4.5). The electrochemical experiments were performed in  $\text{CH}_2\text{Cl}_2$  rather than  $\text{CH}_3\text{CN}$  in order to avoid complications to the square scheme mechanism that could arise through  $\text{CH}_3\text{CN}$  irreversibly coordinating to the ruthenium.

By varying the scan rate, the rate constants for the forward and reverse chemical steps (Scheme 4.5) were determined by digital simulation of the CV data over a range of temperatures. Representative data and simulations obtained at 293 K are given in Figure 4.7 and the equilibrium and rate constants listed in Table 4.6.

As discussed in the earlier section, the voltammograms of solutions of **16B** involve the mechanism that was modeled over a range of voltammetric scan rates and temperatures analogously to **14A** (Appendix Figure A3-4 and Table 4.6).

Digital simulations modeled on the CV data obtained during the reduction of solutions of **14A** and oxidation of solutions of **16A/16B** were performed using all four rate constants associated with the two homogenous chemical reactions given in Scheme 4.5.

**Table 4.6.** Equilibrium, rate constants<sup>a</sup> and electrochemical parameters obtained in CH<sub>2</sub>Cl<sub>2</sub> (with 0.5 M Bu<sub>4</sub>NPF<sub>6</sub>) for the reaction given in Scheme 7.

<i>T</i> / K	<i>D</i> × 10 <sup>-6</sup> /cm <sup>2</sup> s <sup>-1</sup>	<i>R</i> / ohms	<b>16A</b> ⇌ <b>16B</b>			<b>14A</b> ⇌ <b>14B</b>		
			<i>K</i> <sub>eq</sub>	<i>k</i> <sub>f</sub> / s <sup>-1</sup>	<i>k</i> <sub>b</sub> / s <sup>-1</sup>	<i>K</i> <sub>eq</sub>	<i>k</i> <sub>f</sub> / s <sup>-1</sup>	<i>k</i> <sub>b</sub> / s <sup>-1</sup>
293	3.25	800	20	6.00	0.30	205	0.25	1.2 × 10 <sup>-3</sup>
283	2.5	1000	25	3.25	0.13	220	0.10	4.6 × 10 <sup>-3</sup>
273	1.95	1200	30	1.00	3.3 × 10 <sup>-2</sup>	250	0.050	2.0 × 10 <sup>-4</sup>
263	1.65	1600	35	0.25	7.1 × 10 <sup>-3</sup>	300	0.025	8.3 × 10 <sup>-5</sup>
253	1.3	2000	40	0.080	2.0 × 10 <sup>-3</sup>	380	0.015	3.9 × 10 <sup>-5</sup>

<sup>a</sup>Obtained by digital simulation of cyclic voltammetry data.

Therefore, at any given temperature, the rate and equilibrium constants obtained by simulation were identical regardless of whether the CV's were conducted with solutions of **14A** or **16A/16B**. This self-consistency was necessary in order to confirm the correctness of the square-scheme mechanism. In actuality, digital simulations of the CV's obtained during the reduction of **14A** largely allowed the rate/equilibrium constants associated with the interconversion of species **16A** and **16B**, while simulations modeled on the oxidation of **16B** allowed the rate/equilibrium constants for the interconversion of **14B** and **14A**. One factor that helped to establish the equilibrium constant of the **14B** to **14A** conversion was the presence of a small amount of **16A** (that is oxidized at -0.855 V vs. Fc/Fc<sup>+</sup>) together in solution with **16B** at higher temperatures, (see Figure 4.4a, 293 K) which allowed a direct estimation of the *K*<sub>eq(14A,14B)</sub>-values. (Table 4.6) (The thermodynamic nature of the square scheme means that if one equilibrium constant [i.e. *K*<sub>eq(16A,16B)</sub>] and both reversible half-wave

potentials ( $E_{1/2}^f$ ) [that approximate the formal potential ( $E^0$ )] are known, then the second equilibrium constant [i.e.  $K_{\text{eq}(14\text{A},14\text{B})}$ ] can be automatically calculated.<sup>26, 27</sup>

The voltammetric data did not appear to be affected by slow rates of heterogeneous electron transfer over the scan rates used (that would also increase the  $\Delta E_{\text{pp}}$ -values and make extraction of the  $k_f$  and  $k_b$  values more difficult), thus the  $k_{\text{s}(14\text{A}/16\text{A})}$ - and  $k_{\text{s}(14\text{B}/16\text{B})}$ -values were set at their default values of  $10^4 \text{ cm s}^{-1}$ . In actuality, with the moderate scan rates used in this study, digital simulations indicate that the  $k_s$ -values could be as low as approximately  $0.05 \text{ cm s}^{-1}$ , before the effects of slow heterogeneous electron transfer have a dominating effect on  $\Delta E_{\text{pp}}$ -values above the effects of solution resistance. The  $\Delta E_{\text{pp}}$  values increased with increasing concentration (particularly noticeable at higher scan rates and lower temperatures), which supports the conclusion that the relatively high  $\Delta E_{\text{pp}}$  values observed under some conditions were due to uncompensated solution resistance. The diffusion coefficients of **14A** and **14B** were set equal and the diffusion coefficients of **16A** and **16B** were also set equal and decreased as the temperature was lowered (Table 4.6). The charge transfer coefficients ( $\alpha$ ) were left at their default values of 0.5 eV. The rates of the back homogeneous reactions in Table 4.6 were often too low to be estimated directly from the variable scan rate data and instead came from knowledge of the  $k_f$ - and  $K_{\text{eq}}$ -values derived from the simulations.

Varying the concentration between 0.5 - 5 mM led to no observable change in the kinetic values derived from the voltammetric data at a fixed temperature and scan rate, supporting the concept that the ligand exchange occurs *via* an intramolecular rather than intermolecular mechanism. Below 253 K, the voltammetric peaks associated with the species formed by homogeneous reaction were too small to enable accurate simulations. The variation in the  $K_{\text{eq}}$ -values with changing temperature

enabled the reaction enthalpies to be determined from van't Hoff plots, which, for both homogeneous reactions [ $K_{\text{eq}(16\text{A},16\text{B})}$  and  $K_{\text{eq}(14\text{B},14\text{A})}$ ] were calculated to be  $\sim -10$  kJ mol<sup>-1</sup>. CV experiments performed in mixed CH<sub>2</sub>Cl<sub>2</sub>/toluene (1:1) indicated a higher **16A/16B** ratio compared to that observed in pure CH<sub>2</sub>Cl<sub>2</sub>, in agreement with NMR data discussed above (and Table 4.4), which had indicated that Equilibrium II (Scheme 4.4) favors **16A** in low dielectric media.

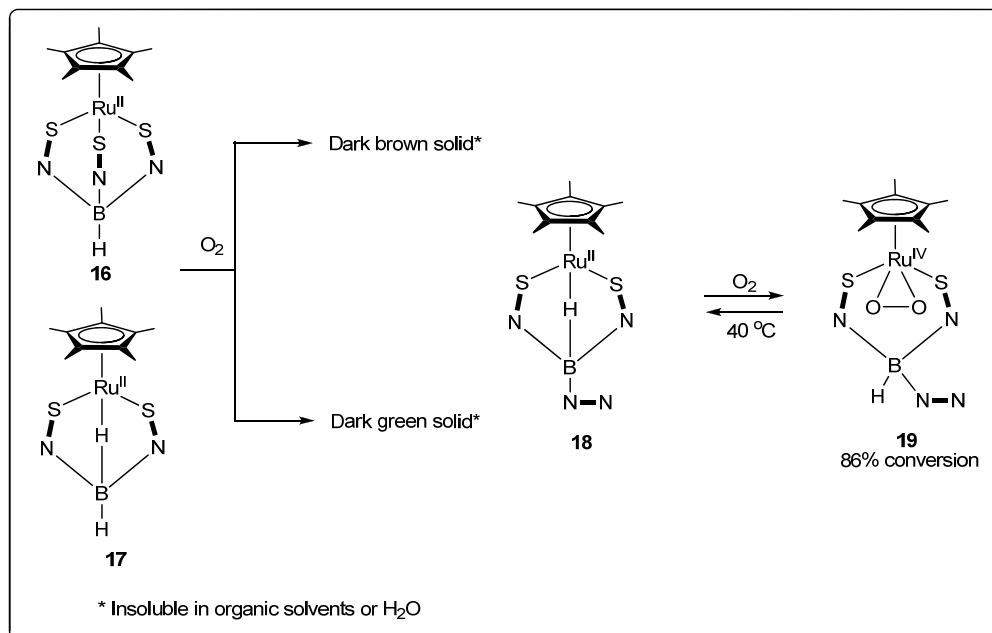
#### 4.4. Reactivity studies of Cp\*Ru[HB(mt)<sub>2</sub>(pz)] (**18**) towards O<sub>2</sub> and CO

Transition metal-O<sub>2</sub> adducts play crucial roles in a number of organic and biological transformations and in addition as O<sub>2</sub> transport in biological systems. One such class of complexes, the transition metal peroxo species are usually prepared by oxidative addition of an O<sub>2</sub> molecule to a low-valent precursor. For instance, Kirchner and coworkers reported the formation of a [ $(\eta^5\text{-C}_5\text{Me}_5)\text{Ru}(\eta^2\text{-O}_2)(\text{dppe})$ ] from the oxidation of [ $(\eta^5\text{-C}_5\text{Me}_5)\text{Ru}(\text{dppe})$ ]Cl. From the cyclic voltogram of complexes **16-18**, it was observed that the complexes exhibit an oxidation potential in the range of -0.65 to -0.86 V, suggesting that these complexes may undergo oxidation fairly easily. Hence, the reactivity of complexes **16-18** towards O<sub>2</sub> was investigated as they could be precursors for the synthesis of new transition peroxo complexes. The reactions of **16-18** with O<sub>2</sub> were carried out at RT by bubbling a stream of air into a THF solution of the respective complexes (Scheme 4.7).

In the reaction of **18** with O<sub>2</sub>, the Ru(IV)-peroxo complex, [ $\text{Cp}^*\text{Ru}\{\text{HB}(\text{mt})_2(\text{pz})\}(\eta^2\text{-O}_2)$ ] (**19**), was isolated as a green solid (86% conversion based on <sup>1</sup>H NMR integral) with unreacted **18**. Despite multiple recrystallisations or column purification, we were unable to achieve complete separation of the two complexes. This is possibly due to the reversibility of the reaction. Complex **19** can be

completely converted back to **18** by heating it overnight at 40 °C under Ar, as observed by  $^1\text{H}$  NMR spectroscopy.

**Scheme 4.7.** Reaction of **16-18** with  $\text{O}_2$ .



The  $^1\text{H}$  NMR spectrum of **19** shows 2 pairs of doublets at  $\delta$  8.45 and 5.91 due to the methimzoyl ring protons and a singlet at  $\delta$  3.28 due to the NMe group; 2 pairs of doublets at  $\delta$  7.98 and 7.91 and a triplet (overlapping doublets) at 6.19 corresponding to the pyrazolyl ring protons and a singlet at  $\delta$  1.30 corresponding to the Cp\* ligand. There was no proton signals observed in the  $\delta$  0 to -20 region, indicating the absence of the agostic-like B-H. The IR spectrum of **19** shows a stretch of medium intensity at  $896\text{ cm}^{-1}$ , which falls in the typical range for O-O stretch for metal peroxo complexes ( $800\text{-}900\text{ cm}^{-1}$ ).<sup>28</sup>

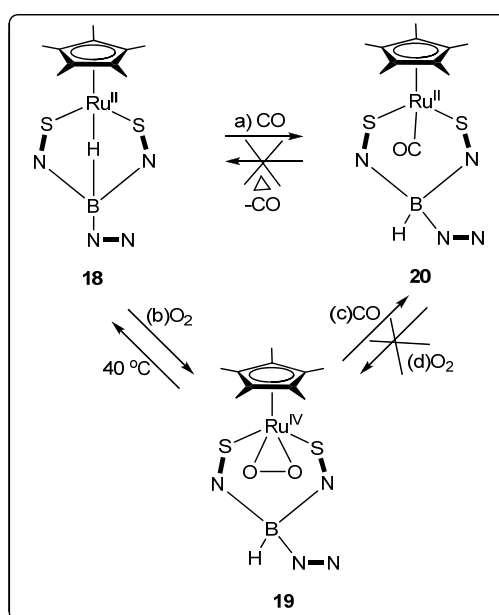
Based on the reversibility of the reaction of **18** with molecular oxygen, **18** and **19** were tested for catalytic activity in the epoxidation of cyclohexene but found to show no activity.

For the reactions of complexes **16** and **17** with  $\text{O}_2$ , solids precipitate out of the solution upon bubbling air immediately. Various attempts were made to characterize

the products by obtaining single crystals via slow diffusion of O<sub>2</sub> into a THF solution of **16** or **17** but proved to be unsuccessful.

The reactivity of **18** towards CO was investigated as well and it was found that the reaction of **18** with CO led to the formation [Cp\*Ru{HB(mt)<sub>2</sub>(pz)}(CO)] (**20**) (Scheme 4.8a). Unlike the product **19** formed from the reaction of **18** with O<sub>2</sub>, this reaction is irreversible, even with prolonged heating.

**Scheme 4.8.** Reactivity of [Cp\*Ru{HB(mt)<sub>2</sub>(pz)}] towards (a)CO and (b)O<sub>2</sub>.



The <sup>1</sup>H NMR spectrum of **20** shows 2 pairs of doublets at δ 7.47 and 5.34 due to the methimzoyl ring protons and a singlet at δ 3.00 due to the NMe group; 2 pairs of doublets at δ 7.02 and 7.01 and a triplet at 6.34 corresponding to the pyrazolyl ring protons and a singlet at δ 1.59 corresponding to the Cp\* ligand. There was no proton signals observed in the δ 0 to -20 region, indicating the absence of the agostic-like B-H. The IR spectrum of **20** shows a strong C≡O stretch at 1913 cm<sup>-1</sup>.

In addition, we also found that **19** can be completely converted to **20** by stirring a solution of **19** charged with 1 atm of CO at RT overnight. (Scheme 4.8c) However, the reverse reaction does not take place (Scheme 4.8d). As depicted in



Scheme 4.8, this implies that the  $[\text{Cp}^*\text{Ru}\{\text{HB}(\text{mt})_2(\text{pz})\}]$  complex (**18**) forms a stable adduct with CO but forms a peroxo complex, **19** with molecular oxygen that can be converted back to the precursor, **18**. The peroxo on **19** can be easily displaced by CO to give **20**. This is to be expected since M-CO bonds are typically stronger than M-(O<sub>2</sub>) bonds. The reactivity feature of complex **18** towards O<sub>2</sub> and CO is similar to hemoglobin. The molecular structures of **19** and **20** are depicted in Figures 4.7 and selected bond parameters are given in Table 4.7.

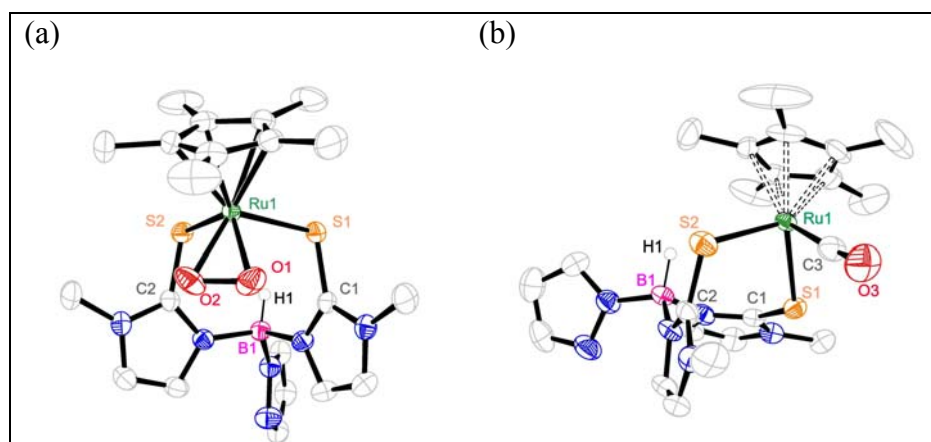


**Figure 4.8.** ORTEP plots for the molecular structures of (a) **19** and (b) **20**. Thermal ellipsoids are drawn at the 50% probability level. All hydrogen atoms except those on the boron are omitted for clarity.

**Table 4.7.** Selected bond lengths (Å) and bond angles (°).

	<b>19</b> *	<b>20</b>
Bond Distances (Å)		
Ru(1)-S(1)	2.4332(6)	2.4344(11)
Ru(1)-S(2)	-	2.4378(12)
C(1)-S(1)	1.724(3)	1.723(4)
C(2)-S(2)	-	1.715(5)
O(1)-O(1A)	1.405(5)	-
C(3)-O(3)	-	1.153(6)
Ru(1)-L(1)	2.0119(19)	1.842(5)
	(L(1) = O(1))	(L(1) = C(3))
B(1)-H(1)	1.032(10)	1.097(10)
Bond Angles (°)		
S(1)-Ru(1)-S(2)	87.05(3)	97.66(4)
O(1)-Ru(1)-O(1)	40.88(13)	-
O(1)-C(22)-Ru(1)	-	175.2(5)

\* Complex **19** possess crystallographic mirror plane

The Ru-S bond length in **19** is 2.4332(6) and that in **20** is 2.4344(11) Å, which are longer than the Ru-S bonds found in **18** (2.3809(9)-2.3964(10) Å). The

coordination of the CO bonded Ru presumably weaken the Ru-S leading to an increase in Ru-S bond length observed in **19**. The S-Ru-S angles in **19** ( $87.05(3)^\circ$ ) is smaller than that found for **18** ( $93.14(4)^\circ$ ) and **20** ( $97.66(4)^\circ$ ), presumably to accommodate the peroxo ( $O_2^{2-}$ ).

Cyclic voltammetry studies shown that complex **19** is more difficult to oxidise than **18** by approximately 0.8 V. The electrochemical oxidation of **19** occurs in a chemical irreversible process with  $E_p^{ox} = +0.115$  V vs. Fc/Fc<sup>+</sup> (Figure 4.9a). When the scan direction was reversed after the first oxidation process and applied in the negative direction, two reduction processes were detected (Red<sub>A</sub> and Red<sub>B</sub>) (Figure 4.9a) at identical potentials to those observed in the CVs of **18** at 293 K (Figure 4.4b). Therefore, it is likely that the chemically irreversible oxidation of **19** results in the formation of **18**<sup>+</sup> (*via* loss of O<sub>2</sub>), which then irreversible reacts to form a new compound. The notion that **19** is oxidised to form **18**<sup>+</sup> is supported by the observation that an additional oxidation peak (Ox<sub>A</sub>) is evident in the CVs of **19** at an identical potential to that observed for **18** (compare Figure 4.4b and 4.9a).

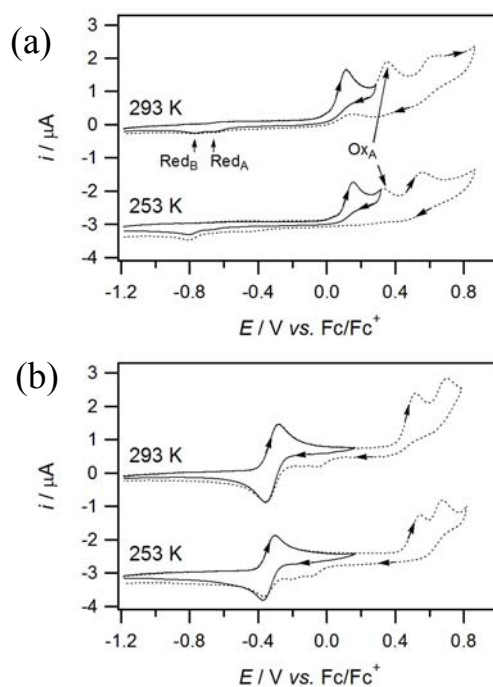


**Figure 4.9.** Cyclic voltammograms recorded at a scan rate of  $100 \text{ mV s}^{-1}$  at a 1 mm planar GC electrode in  $\text{CH}_2\text{Cl}_2$  solutions containing 0.2 M  $\text{Bu}_4\text{NPF}_6$  and 1 mM (a) **19**, and (b) **20**.

Complex **20** can be oxidised in a chemically reversible process at  $-0.340 \text{ V vs. Fc/Fc}^+$  (Figure 4.9b), with the CV data indicating that the oxidised compound ( $\mathbf{20}^+$ ) is stable on the voltametric time-scale at high and low temperatures. Complex **20** also displayed oxidation processes at more positive potentials ( $> +0.4 \text{ v}$ ), but these do not correlate with the additional processes observed for **18** and **19**.

#### 4.5. Conclusion

The 17 electron species  $[\text{Cp}^*\text{Ru}^{\text{III}}\text{Cl}_2]_2$  (**12**) or 16 electron species  $[\text{Cp}^*\text{Ru}^{\text{II}}\text{OMe}]_2$  (**13**) were found to be suitable precursors as an entry for the convenient syntheses of the mixed sandwich ruthenium complexes with poly(methimazolyl)borates, **14**, **16-18**.

A solvent dependent isomerisation was observed for complexes **14** and **16** in solution, where the  $[\text{HB}(\text{mt})_3]$  ligand at  $\text{Cp}^*\text{Ru}^{\text{II/III}}$  have demonstrated a facile  $\kappa^3\text{-S,S',S''}$  and  $\kappa^3\text{-H,S,S'}$  coordination exchange. The  $\kappa^3\text{-S,S',S''}$  form of  $[\text{Cp}^*\text{Ru}^{\text{III}}\{\text{HB}(\text{mt})_3\}]^+$  (**14A**) and the  $\kappa^3\text{-H,S,S'}$  form of  $[\text{Cp}^*\text{Ru}^{\text{II}}\{\text{HB}(\text{mt})_3\}]$  (**16B**) are the preferred isomers in solution (although there is a strong temperature and solvent dependence), while in the solid state, the  $\kappa^3\text{-S,S',S''}$  forms are preferred for both  $\text{Cp}^*\text{Ru}^{\text{III}}$  (**14A**) and  $\text{Cp}^*\text{Ru}^{\text{II}}$  (**16A**). For complex **18**, only one form of the two possible isomers was observed both in solution and in its solid state, indicating that the  $[\text{HB}(\text{mt})_2(\text{pz})]$  ligand preferred the  $\kappa^3\text{-H,S,S'}$  coordination over the  $\kappa^3\text{-S,S',N}$  coordination. It was found that the  $[\text{HB}(\text{mt})_3]$  and  $[\text{H}(\text{mt})_2(\text{pz})]$  ligands has a higher preference for the agostic-like  $\text{M}\cdots\text{H-B}$  interactions in the  $\text{Cp}^*\text{Ru}$  system than in the  $(\text{HMB})\text{Ru}$  system.

A comparison of **16-18** with **9** and **10** reported in Chapter 3 shows that the  $E_{1/2}^r$  values are very sensitive to the Cp\* and HMB ligands and are less sensitive to the difference in the [HB(mt)<sub>3</sub>]<sup>-</sup>, [H<sup>2</sup>B(mt)<sub>2</sub>]<sup>-</sup> and [HB(mt)<sub>3</sub>]<sup>-</sup> ligands. In addition, the redox processes involving the isomers gave raise to an electrochemical square scheme which provided information on the kinetics and thermodynamics, together with the NMR studies and simulation.

The reactions of [Cp\*Ru{HB(mt)<sub>2</sub>(pz)}] with O<sub>2</sub> and CO led to the isolation of a Ru(IV) peroxo complex, [Cp\*Ru{HB(mt)<sub>2</sub>(pz)}(η<sup>2</sup>-O<sub>2</sub>)] (**19**) and the CO adduct, [Cp\*Ru{HB(mt)<sub>2</sub>(pz)}(CO)] (**20**). We have found that the O<sub>2</sub> binds reversibly to the [Cp\*Ru{HB(mt)<sub>2</sub>(pz)}] moiety while the addition of CO to the [Cp\*Ru{HB(mt)<sub>2</sub>(pz)}] moiety was found to be reversible and **19** can be converted to **20** under CO atmosphere.

## 4.6. Experimental

General procedures are as described in Chapter 2. 2D  $^1\text{H}$  NMR spectra (COSY, NOESY and EXSY) of 2A/2B were obtained in  $\text{C}_6\text{D}_6$  on a Bruker DRX500MHz FT NMR spectrometer with a triple resonance cryoprobe head.  $[\text{Cp}^*\text{RuCl}_2]_2$  and  $[\text{Cp}^*\text{RuOMe}]_2$  were synthesized as reported in the literature.<sup>29, 30</sup> Conductivity measurements were conducted at 300 K on  $1 \times 10^{-5} - 5 \times 10^{-3}$  M solutions in acetonitrile, using a Kyoto Electronics CM-115 conductivity bridge.

**Cyclic voltammetric studies** are performed as described in Chapter 2. The background-subtracted curves were compared with cyclic voltammetry curves simulated using DigiSim<sup>®</sup> 3.03.<sup>27, 31</sup>

**EPR measurements.** Solutions of electrogenerated compounds for the EPR experiments were prepared at 233 K in a two compartment controlled potential electrolysis cell separated with a porosity no. 5 (1.0 - 1.7  $\mu\text{m}$ ) sintered glass frit. The working and auxiliary electrodes were identically sized Pt mesh plates symmetrically arranged with respect to each other with an Ag wire reference electrode (isolated by a salt bridge) positioned to within 2 mm of the surface of the working electrode. The electrolyzed solutions were transferred under vacuum into cylindrical 3 mm (id) EPR tubes that were immediately frozen in liquid  $\text{N}_2$ . EPR spectra were recorded on a Bruker ESP 300e spectrometer in a  $\text{TE}_{102}$  cavity at 10 K using liquid He cooling. EPR simulations were performed using the Bruker computer software, WINEPR SimFonia. Continuous wave X-band EPR spectra were recorded with microwave frequency = 9.44 GHz, microwave power = 0.2 mW, modulation amplitude = 0.5 mT, time constant = 164 ms, sweep width = 0.3 T and sweep time = 164 s.  $T = 10$  K. For complex **14A**, the spectrum was simulated with 100% Lorentzian line shape and  $g_x = 2.37$ ,  $g_y = 2.01$ ,  $g_z = 2.01$ ,  $(\Delta H_{\text{pp}})_x = 12$  mT,  $(\Delta H_{\text{pp}})_y = 13$  mT,  $(\Delta H_{\text{pp}})_z = 13$  mT and

$a_{\text{Ru}} = 4.0$  mT, and that for **14B** simulated with 100% Lorentzian line shape and  $g_x = 2.25$ ,  $g_y = 2.02$ ,  $g_z = 1.91$ ,  $(\Delta H_{\text{pp}})_x = 7$  mT,  $(\Delta H_{\text{pp}})_y = 1$  mT and  $(\Delta H_{\text{pp}})_z = 10$  mT.

**X-Ray structure determinations** are performed as described in Chapter 2. The structures of **14A**(PF<sub>6</sub>) and **16A** were solved by direct methods to locate the heavy atoms, followed by difference maps for the light non-hydrogen atoms. Compound **14A**(PF<sub>6</sub>) exhibited disorder of the [PF<sub>6</sub>]<sup>-</sup> anion. This was modeled as a disorder involving four of the F atoms lying in a square plane. These four F atoms were modeled as comprising of two sets, with occupancies of the two sets summed to unity. The F atoms in each set were restrained to be in a plane, and all nearest-neighbour F...F distances were restrained to be the same. Diagonally opposing F atoms were given equivalent anisotropic thermal parameters. There was disorder of the Cp\* ligand in **16A**. This was modeled with a complete Cp\* with 1/3 occupancy. Since the molecule sits on a 3-fold axis, this automatically generated three alternative sites which are symmetry-related, for the entire ligand. The C<sub>ring</sub>-C<sub>methyl</sub> bond lengths were all restrained to be the same. All the ring carbon atoms were given a common isotropic thermal parameter, as were all the methyl carbon atoms. The hydrogen atoms were placed and refined in a riding model. There was also half a water solvent molecule found; the hydrogen atoms for this were modeled as disordered over two alternative sites of equal occupancies. The crystal data collection and processing parameters are given in Table A3 (Appendix).

**Reaction of [Cp\*RuCl<sub>2</sub>]<sub>2</sub> (12) with K[HB(mt)<sub>3</sub>].** To a brown solution of **12** (31 mg, 0.05 mmol) in THF was added K[HB(mt)<sub>3</sub>] (39 mg, 0.10 mmol). The suspension was left to stir for 18 h. The resultant brown suspension was filtered through a glass sinter to give a dark brown solid product; it was found that some unreacted **12** remained in the mother liquor. The solid was extracted with CH<sub>3</sub>CN (4 x 5 mL) leaving behind the

KCl byproduct and some residual  $\text{K}[\text{HB}(\text{mt})_3]$ . The dark brown extract was concentrated to *ca.* 3 mL and ether added. After standing for 2 days at  $-30\text{ }^\circ\text{C}$ , the mixture yielded a dark brown solid of  $[\text{Cp}^*\text{Ru}^{\text{III}}\{\text{HB}(\text{mt})_3\}](1\text{A})\text{Cl}$  (44 mg, 0.71 mmol, 71 % yield). For anion exchange, a solution of **14A** (12 mg, 0.02 mmol) in  $\text{CH}_3\text{CN}$  was stirred with excess  $\text{NH}_4\text{PF}_6$  (7 mg, 0.04 mmol) at RT for 3 h. After removal of  $\text{NH}_4\text{Cl}$  by filtration on a glass sinter, the reddish brown filtrate was concentrated to *ca.* 2 mL and ether added. Dark brown rhombic crystals of **14A**( $\text{PF}_6$ ) were obtained after 2 days at  $-30\text{ }^\circ\text{C}$ . Diffraction-quality single crystals of **14A**( $\text{PF}_6$ ) were obtained at  $-30\text{ }^\circ\text{C}$  as dark brown rhombic crystals by slow diffusion of ether in an acetonitrile solution after 5 days.

**Data for 14A.** Anal. Found: C, 41.9; H, 5.0; N, 13.1; S, 15.0%. Calc. for  $\text{C}_{22}\text{H}_{31}\text{BCIN}_6\text{RuS}_3$ : C, 42.4; H, 5.0; N, 13.5; S, 15.4%.  $^1\text{H}$  NMR: 26.6 (s, br,  $\nu^{1/2}$  *ca.* 90 Hz, *ca.* 15H,  $\text{C}_5\text{Me}_5$ ); 11.2 (s,  $\nu^{1/2}$  *ca.* 5 Hz, *ca.* 6H, CH, imidazole); 9.8 (s,  $\nu^{1/2}$  *ca.* 6 Hz, *ca.* 9H, Me, imidazole);  $\text{BH}$  not observed. IR (KBr,  $\text{cm}^{-1}$ ):  $\nu(\text{BH})$  2428w.  $\nu(\text{other bands})$  1562m, 1461m, 1374m, 1210s, 1262s and 752s. MS  $\text{FAB}^+$  (m/z): 588  $[\text{M} = \text{C}_5\text{Me}_5\text{Ru}(\text{C}_4\text{H}_5\text{N}_2\text{S})_3\text{BH}]^+$ , 474  $[\text{M} - \text{C}_4\text{H}_5\text{N}_2\text{S} - \text{H}]^+$ , 350  $[\text{M} - (\text{C}_4\text{H}_5\text{N}_2\text{S})_2\text{BH}]^+$ . MS  $\text{FAB}^-$  (m/z): 351  $[\text{M} = (\text{C}_4\text{H}_5\text{N}_2\text{S})_3\text{BH}]^-$ . HR-MS  $\text{FAB}^+$  (m/z): for  $[\text{M}^+]$  588.0897 (found), 588.0909(calcd). The  $^1\text{H}$  NMR spectrum in  $\text{CD}_3\text{CN}$  shows peaks which are broad in agreement with a paramagnetic  $d^5$ -Ru(III) centre. The conductivity measurement of **1A**(Cl) in  $\text{CH}_3\text{CN}$  at 300 K gives the molar conductivity  $\Lambda_m$  ( $1 \times 10^{-3}\text{M}$ ) =  $145.9\ \Omega^{-1}\text{cm}^2\text{mol}^{-1}$ , which falls in the range ( $120$ - $160\ \Omega^{-1}\text{cm}^2\text{mol}^{-1}$ ) of a 1:1 electrolyte.<sup>33</sup> The slope of the Onsager plot of  $(\Lambda_o - \Lambda_m)$  vs.  $c^{1/2} = 133.61 \times 10^3$ , where  $\Lambda_m$  and  $\Lambda_o$  represents molar conductance at concentration  $M$  and infinite dilution, respectively.

**Reactions of [Cp\*Ru(OMe)]<sub>2</sub> (13)****(a) with K[HB(mt)<sub>3</sub>]**

**Method 1:** To a dark pink solution of **13** (54 mg, 0.10 mmol) in THF was added K[HB(mt)<sub>3</sub>] (78 mg, 0.20 mmol). The suspension was refluxed for 6 h, resulting in a brownish red suspension, which was filtered to remove the white KOMe byproduct. The brownish red filtrate was concentrated to *ca.* 2 mL and chromatographed on a silica gel column packed in hexane (1.5 cm x 8 cm). Elution gave 2 fractions, leaving behind an immovable brown band on the column: (i) a brownish yellow eluate (2:1 hexane-toluene, 20 mL), which on concentration gave a yellowish brown crystalline solid of Cp\*Ru(μ-H)<sub>2</sub>(μ-CO)RuCp\* (**15**) (10 mg, 0.02 mmol, 20 %), identified by a comparison of its <sup>1</sup>H NMR spectrum, its CO stretching frequency in the IR spectrum and the cell parameters of a single crystal with those of an identical compound obtained when [Cp\*RuOMe]<sub>2</sub> was heated at temperatures >90 °C in toluene for 4 h.<sup>10</sup> (Found for 3: Space group = *P*<sub>a</sub>, *a* = 10.027(5) Å, *b* = 8.511 (5) Å, *c* = 12.500 (6) Å, β = 108.64 (4)°. *V* = 1010.8 (7) Å<sup>3</sup>; <sup>1</sup>H NMR (C<sub>6</sub>D<sub>6</sub>): δ 1.79 (s, 30H), -12.89 (s, 2H); ν (CO, KBr): 1793 cm<sup>-1</sup>. [Lit.<sup>10, 32</sup>: Space group = *P*<sub>a</sub>, *a* = 12.621(3) Å, *b* = 8.574(2) Å, *c* = 10.089(2) Å, β = 108.56(3)°. *V* = 998.3(3) Å<sup>3</sup>. <sup>1</sup>H NMR (C<sub>6</sub>D<sub>6</sub>): δ 1.78 (s, 30H), -12.9 (s, 2H). ν(CO): 1794 cm<sup>-1</sup>]. (ii) a red eluate (1:2 toluene:THF, 50 mL), which upon concentration and addition of hexane gave reddish-orange microcrystalline solids, [Cp\*Ru<sup>II</sup>{HB(mt)<sub>3</sub>}] (**16A**) (55 mg, 0.09 mmol, 47 % yield), after a day at -30 °C. Diffraction-quality single crystals were obtained at -30 °C as **15** as purplish brown rhombic crystals from a THF-hexane solution after 3 days.

**Method 2:** To a dark pink solution of **13** (54 mg, 0.10 mmol) in toluene:MeOH (4:1, *ca* 15 mL) was added K[HB(mt)<sub>3</sub>] (798 mg, 0.20 mmol). The pink suspension was stirred for 10-20 mins to give an orange-brown suspension. The resultant suspension



was concentrated to *ca* 5 mL and filtered through a thin disc of Si gel to remove any unreacted starting material and the by-product, KOMe. The orange filtrate was concentrated to *ca.* 2 mL; multiple recrystallisations in toluene/hexane gave reddish-orange microcrystalline solids,  $[\text{Cp}^*\text{Ru}^{\text{II}}\{\text{HB}(\text{mt})_3\}]$  (**16A**) (63 mg, 0.11 mmol, 54 % yield). Diffraction-quality single crystals of **16A** were obtained at  $-30\text{ }^\circ\text{C}$  as pink hexagons from solution in THF-ether after 3 days.

**Data for 16.** Anal. Found: C, 46.2; H, 5.6; N, 13.5; S, 15.5%. Calc. for  $\text{C}_{22}\text{H}_{31}\text{B}_1\text{N}_6\text{Ru}_1\text{S}_3 \cdot 0.25\text{C}_6\text{H}_{12}$ : C, 46.5; H, 5.5; N, 13.8; S, 15.8%. IR (KBr,  $\text{cm}^{-1}$ ):  $\nu(\text{BH})$  2407w.  $\nu(\text{other bands})$  1560m, 1454m, 1412m, 1369s, 1317m, 1294m, 1204s, 730m and 720m. MS  $\text{FAB}^+$  ( $m/z$ ): 588 [ $\text{M}^+ = \text{C}_5\text{Me}_5\text{Ru}(\text{C}_4\text{H}_5\text{N}_2\text{S})_3\text{BH}$ ], 474 [ $\text{M}-\text{C}_4\text{H}_5\text{N}_2\text{S}-\text{H}$ ] $^+$ , 350 [ $\text{M}-(\text{C}_4\text{H}_5\text{N}_2\text{S})_2\text{BH}$ ] $^+$ .  $\text{FAB}^-$  ( $m/z$ ): 351 [ $\text{M} = (\text{C}_4\text{H}_5\text{N}_2\text{S})_3\text{BH}$ ] $^-$ .  $^1\text{H}$  NMR ( $\text{C}_6\text{D}_6$ ) (assignment of peaks was based on data from the 2D  $^1\text{H}$  NMR COSY and EXSY spectra (see appendix): *isomer 16A*:  $\delta$  6.58 (d, 3 x 2H,  $^3\text{J} = 2.5$  Hz,  $\text{SCN}_2\text{HC}=\text{CH}$ ), 5.93 (d, 3 x 2H,  $^3\text{J} = 2.5$  Hz,  $\text{SCN}_2\text{HC}=\text{CH}$ ), 3.16 (s, 3 x 3H, N- $\text{CH}_3$ ), 1.93 (s, Cp $\text{CH}_3$ ); *isomer 16B*:  $\delta$  6.47 (d, 2 x 2H,  $^3\text{J} = 1.6$  Hz,  $\text{SCN}_2\text{HC}=\text{CH}$ ), 6.25 (d, 2H,  $^3\text{J} = 1.6$  Hz,  $\text{SCN}_2\text{HC}=\text{CH}$ ), 6.01 (d, 2H,  $^3\text{J} = 1.6$  Hz,  $\text{SCN}_2\text{HC}=\text{CH}$ ), 5.78 (d, 2 x 2H,  $^3\text{J} = 1.6$  Hz,  $\text{SCN}_2\text{HC}=\text{CH}$ ), 3.29 (s, 3H, N $\text{CH}_3$ ), 2.83 (s, 2 x 3H, N $\text{CH}_3$ ), 1.93 (s, Cp $\text{CH}_3$ ), -7.67 (q of equal intensity, 1H, J 48 Hz,  $\mu$ -HB); approx. relative ratio of **16A:16B** = 1:3 from signal integrals.  $^1\text{H}$  NMR ( $\text{CD}_2\text{Cl}_2$ ) (indicative of **16B**): 6.70 (d, 1H,  $^3\text{J} = 2.5$  Hz, CH imidazole), 6.67 (d, 2H,  $^3\text{J} = 2.5$  Hz, CH imidazole), 6.58 (d, 2H,  $^3\text{J} = 1.7$  Hz, CH imidazole), 6.38 (d, 1H,  $^3\text{J} = 1.7$  Hz, CH imidazole), 3.53 (s, 6H, N $\text{CH}_3$ ), 3.50 (s, 3H, N $\text{CH}_3$ ), 1.63 (s, 15H, Cp $\text{CH}_3$ ), -8.16 (q of equal intensity, 1H, J 81 Hz,  $\mu$ -HB).  $^1\text{H}$  NMR ( $\text{CD}_3\text{CN}$ ) (indicative of **16B**): 6.84 (d, 1H,  $^3\text{J} = 1.7$  Hz, CH imidazole), 6.82 (d, 2H,  $^3\text{J} = 1.7$  Hz, CH imidazole), 6.69 (d, 2H,  $^3\text{J} = 1.7$  Hz, CH imidazole), 6.36 (d, 1H,  $^3\text{J} = 1.7$  Hz, CH imidazole), 3.49 (s, 6H, N $\text{CH}_3$ ), 3.46 (s, 3H,

NCH<sub>3</sub>), 1.92 (s, 15H, CpCH<sub>3</sub>), -8.27 (q of equal intensity, 1H, J 81 Hz,  $\mu$ -HB). <sup>13</sup>C NMR (C<sub>6</sub>D<sub>6</sub>): *isomer 16A*:  $\delta$  169.4 (s, SCN<sub>2</sub>HC=CH), 120.6 (s, C imidazole), 120.4 (s, C imidazole), 76.1 (s, C<sub>5</sub>(CH<sub>3</sub>)<sub>5</sub>), 34.9 (s, NCH<sub>3</sub>) 11.5 (s, C<sub>5</sub>(CH<sub>3</sub>)<sub>5</sub>); *isomer 16B*:  $\delta$  169.4 (s, SCN<sub>2</sub>HC=CH), 120.6 (s, C imidazole), 120.4 (s, C imidazole), 79.8 (s, C<sub>5</sub>(CH<sub>3</sub>)<sub>5</sub>), 35.0 (s, 2 x NCH<sub>3</sub>), 34.4 (s, NCH<sub>3</sub>), 11.7 (s, C<sub>5</sub>(CH<sub>3</sub>)<sub>5</sub>).

<sup>1</sup>H NMR spectral data of **16A/16B** in different solvent compositions of C<sub>6</sub>D<sub>6</sub>/CD<sub>2</sub>Cl<sub>2</sub>:

(i) <sup>1</sup>H NMR (0.40 mL C<sub>6</sub>D<sub>6</sub> + 0.10 mL CD<sub>2</sub>Cl<sub>2</sub>) (peaks referenced to residual solvent in C<sub>6</sub>D<sub>6</sub>): *isomer 16A*:  $\delta$  6.50 (d, unresolved, 3 x 2H, SCN<sub>2</sub>H $\underline{C}$ =CH), 6.07 (d, unresolved, 3 x 2H, SCN<sub>2</sub>HC= $\underline{C}$ H), 3.23 (s, 3 x 3H, N-CH<sub>3</sub>), 1.81 (s, CpCH<sub>3</sub>); *isomer 16B*:  $\delta$  6.38 (d, 2 x 2H, <sup>3</sup>J = 2.5 Hz, SCN<sub>2</sub>H $\underline{C}$ =CH), 6.18 (d, 2H, <sup>3</sup>J = 1.7 Hz, SCN<sub>2</sub>H $\underline{C}$ =CH), 6.11 (d, 2H, <sup>3</sup>J = 1.7 Hz, SCN<sub>2</sub>HC= $\underline{C}$ H), 5.95 (d, 2 x 2H, <sup>3</sup>J = 2.5 Hz, SCN<sub>2</sub>HC= $\underline{C}$ H), 3.28 (s, 3H, NCH<sub>3</sub>), 2.96 (s, 2 x 3H, NCH<sub>3</sub>), 1.81 (s, CpCH<sub>3</sub>), approx. relative ratio of **16A**: **16B** = 1:4.5 from signal integrals.

(ii) <sup>1</sup>H NMR (0.40 mL C<sub>6</sub>D<sub>6</sub> + 0.15 mL CD<sub>2</sub>Cl<sub>2</sub>) (peaks referenced to residual solvent in C<sub>6</sub>D<sub>6</sub>): *isomer 16A*:  $\delta$  6.36 (d, unresolved, 3 x 2H, SCN<sub>2</sub>H $\underline{C}$ =CH), 6.19 (d, <sup>3</sup>J = 2.5 Hz, 3 x 2H, SCN<sub>2</sub>HC= $\underline{C}$ H), 3.25 (s, 3 x 3H, N-CH<sub>3</sub>), 1.79 (s, CpCH<sub>3</sub>); *isomer 16B*:  $\delta$  6.36 (d, unresolved, 2 x 2H, SCN<sub>2</sub>H $\underline{C}$ =CH), 6.18 (d, 2H, <sup>3</sup>J = 2.5 Hz, 2H, SCN<sub>2</sub>H $\underline{C}$ =CH), 6.13 (d, 2H, <sup>3</sup>J = 2.5 Hz, SCN<sub>2</sub>HC= $\underline{C}$ H), 5.99 (d, 2 x 2H, <sup>3</sup>J = 1.7 Hz, SCN<sub>2</sub>HC= $\underline{C}$ H), 3.28 (s, 3H, NCH<sub>3</sub>), 3.00 (s, 2 x 3H, NCH<sub>3</sub>), 1.79 (s, CpCH<sub>3</sub>), approx. relative ratio of **16A**: **16B** = 1:19 from signal integrals.

(iii) <sup>1</sup>H NMR (0.25 mL C<sub>6</sub>D<sub>6</sub> + 0.25 mL CD<sub>2</sub>Cl<sub>2</sub>) (peaks referenced to residual solvent in C<sub>6</sub>D<sub>6</sub>, indicative of **16B**):  $\delta$  6.34 (d, unresolved, 2 x 2H, SCN<sub>2</sub>H $\underline{C}$ =CH), 6.25 (d, 2H, <sup>3</sup>J = 1.7 Hz, SCN<sub>2</sub>H $\underline{C}$ =CH), 6.16 (d, 2H, <sup>3</sup>J = 1.7 Hz, SCN<sub>2</sub>HC= $\underline{C}$ H), 6.14 (d, 2 x 2H, <sup>3</sup>J = 1.6 Hz, SCN<sub>2</sub>HC= $\underline{C}$ H), 3.29 (s, 3H, NCH<sub>3</sub>), 3.11 (s, 2 x 3H, NCH<sub>3</sub>), 1.68 (s, CpCH<sub>3</sub>).

## VT NMR

A VT NMR spectral study of **16A/16B** was conducted on a 0.0170 M solution in *d*<sub>8</sub>-toluene in the temperature range 253 – 369 K. Integrals of the NMe peaks of **16A** and **16B** gave relative concentration of each species in solution at each temperature, except at 360 and 369 K when the peaks merged. Hence the relative concentrations of species at these temperatures were obtained by extrapolation of the linear ( $R_2 = ca. 1$ ) conc. vs. temp. plot in the range 253-345 K.  $K_{eq}$  values listed in Table 4.4 were calculated directly from the  $[16B]/[16A]$  integral ratios. The thermodynamic parameters  $\Delta H^\circ$  [-6.38(13) kJ mol<sup>-1</sup>] and  $\Delta S^\circ$  [-13.4(5) J mol<sup>-1</sup> K<sup>-1</sup>] were obtained from a plot of  $\ln K_{eq}$  vs.  $(1/T)$  [ $\ln K_{eq} = -(\Delta H^\circ / RT) + (\Delta S^\circ / R)$ ] and the  $\Delta G^\circ$  value [-2.36(26) kJ mol<sup>-1</sup> for 300 K] was calculated from the equation  $\Delta G^\circ = \Delta H^\circ - T\Delta S^\circ$ .

### (b) with Na[H<sub>2</sub>B(mt)<sub>2</sub>].

To a dark pink solution of **13** (52 mg, 0.10 mmol) in toluene was added Na[H<sub>2</sub>B(mt)<sub>2</sub>] (54 mg, 0.20 mmol) and the suspension stirred for 2 h. The resultant suspension of a white precipitate of KOMe in a bright orange solution was then filtered through a thin disc of Celite on a glass sinter. The orange filtrate was evacuated to dryness and recrystallised in THF/hex at -30 °C. An air stable bright orange crystalline solid of [Cp\*Ru{H<sub>2</sub>B(mt)<sub>2</sub>}] (**17**) (81 mg, 0.17 mmol, 85 % yield) was obtained after 2 days. Diffraction-quality single crystals were obtained at -30 °C as red plates from THF-hexane solution after 3 days.

**Data for 17.** Anal. Found: C, 45.3; H, 5.5; N, 11.6; S, 13.4%. Calc. for C<sub>18</sub>H<sub>27</sub>BN<sub>4</sub>RuS<sub>2</sub>: C, 45.5; H, 5.7; N, 11.8; S, 13.5%. IR (KBr, cm<sup>-1</sup>):  $\nu$ (B-H) 2422w;  $\nu$ ( $\mu$ -B-H) 2073w. ESI<sup>+</sup>-MS:  $m/z$  476 [M<sup>+</sup>, C<sub>5</sub>Me<sub>5</sub>Ru(C<sub>4</sub>H<sub>5</sub>N<sub>2</sub>S)<sub>2</sub>BH<sub>2</sub>]. <sup>1</sup>H NMR ( $\delta$ , C<sub>6</sub>D<sub>6</sub>): 6.41 (d, 2 x 1H, <sup>3</sup>J = 1.7 Hz, CH imidazole), 5.75 (d, 2 x 1H, <sup>3</sup>J = 1.7 Hz, CH imidazole), 2.83 (s, 2 x 3H, N-CH<sub>3</sub>), 1.92 (s, 15H, Cp-CH<sub>3</sub>), -7.83 (q of equal

intensity, 1H,  $J_{\text{BH}} = 65$  Hz,  $\mu\text{-HB}$ ).  $^{13}\text{C}$  NMR ( $\delta$ ,  $\text{C}_6\text{D}_6$ ): 169.4 (s,  $\text{SCN}_2\text{HC}=\text{CH}$ ), 120.6 (s, C imidazole), 120.4 (s, C imidazole), 79.1 (s,  $\text{C}_5(\text{CH}_3)_5$ ), 34.4 (s,  $\text{N}-\text{CH}_3$ ) 11.6 (s,  $\text{C}_5(\text{CH}_3)_5$ ).  $^1\text{H}$  NMR ( $\delta$ ,  $\text{CD}_2\text{Cl}_2$ ,  $\mu\text{-HB}$ ): 300 K: -8.51 (center of two overlapping ‘humps’ at  $\delta$  -8.37 ( $v_{1/2}$  ca. 100 Hz) and  $\delta$  -8.65 ( $v_{1/2}$  ca. 125 Hz); 183 K: -8.90 br ( $v_{1/2}$  ca. 50 Hz).

(c) **with Li[HB(mt)<sub>2</sub>(pz)]**

To a dark pink solution of **13** (52 mg, 0.10 mmol) in hexane (*ca.* 8 mL) was added Li[HB(mt)<sub>2</sub>(pz)] (62 mg, 0.20 mmol) in DCM (*ca.* 2 mL) and the suspension was stirred for 1 h at RT. The resultant orange suspension was evacuated to dryness. The brownish orange was dissolved in *ca.* 1 mL DCM and chromatographed on a silica gel column packed in hexane (1.5 cm x 8 cm). Elution gave a red eluate (1:2, toluene:Et<sub>2</sub>O, 30 mL), which upon concentration and addition of hexane gave reddish-orange microcrystalline solids, [Cp\* $\text{Ru}^{\text{II}}$ {HB(mt)<sub>2</sub>(pz)}] (**18**) (64 mg, 0.11 mmol, 59 % yield), after a day at -30 °C, leaving behind an immovable brown band on the column. Diffraction-quality single crystals of **18** were obtained at -30 °C as red hexagons from THF-hexane solution after 3 days.

**Data for 18.** Anal. Found: C, 46.8; H, 5.8; N, 15.3; S, 11.6%. Calc. for  $\text{C}_{21}\text{H}_{29}\text{B}_1\text{N}_6\text{Ru}_1\text{S}_2$ : C, 46.6; H, 5.4; N, 15.5; S, 11.8%. IR (KBr,  $\text{cm}^{-1}$ ):  $\nu(\text{BH})$  2114mbr.  $\nu(\text{other bands})$  1565m, 1456s, 1420m, 1289m, 1191s, 1087m, 1039s and 728s. ESI<sup>+</sup>-MS ( $m/z$ ): 541 [ $\text{M}-\text{H}^+ = \text{C}_5\text{Me}_5\text{Ru}(\text{C}_4\text{H}_5\text{N}_2\text{S})_2(\text{C}_3\text{H}_3\text{N}_2)\text{BH}$ ].  $^1\text{H}$  NMR ( $\text{C}_6\text{D}_6$ ):  $\delta$  7.97 (d, 1H,  $^3J = 1.2$  Hz,  $\text{HC}=\text{CHNNCH}$ ), 7.91 (d, 1H,  $^3J = 2.3$  Hz,  $\text{HC}=\text{CHNNCH}$ ), 7.34 (d, 2 x 1H,  $^3J = 2.5$  Hz,  $\text{SCN}_2\text{HC}=\text{CH}$ ), 6.41 (t, 1H,  $^3J = \text{ca. } 1.9$  Hz,  $\text{HC}=\text{CHNNCH}$ ), 5.68 (d, 2 x 1H,  $^3J = 2.2$  Hz,  $\text{SCN}_2\text{HC}=\text{CH}$ ), 2.81 (s, 2 x 3H,  $\text{NCH}_3$ ), 1.81 (s, 15H,  $\text{CpCH}_3$ ), -7.20 (q of equal intensity, 1H,  $J = 79$  Hz,  $\mu\text{-HB}$ ).  $^{13}\text{C}$

NMR (C<sub>6</sub>D<sub>6</sub>):  $\delta$  161.2 (s, SCN<sub>2</sub>HC=CH), 141.9 (C<sub>pyrazole</sub>), 135.7 (C<sub>pyrazole</sub>), 120.2 (s, C imidazole), 119.2 (C<sub>imidazole</sub>), 106.1 (s, C<sub>pyrazole</sub>), 79.3 (s, C<sub>5</sub>(CH<sub>3</sub>)<sub>5</sub>), 34.3 (s, NCH<sub>3</sub>), 11.5(s, C<sub>5</sub>(CH<sub>3</sub>)<sub>5</sub>).

### Reactivity studies of Cp\*Ru[HB(mt)<sub>2</sub>(pz)](18)

(i) **Reaction of [Cp\*Ru{HB(mt)<sub>2</sub>(pz)}] with O<sub>2</sub>.** Air was bubbled into a bright red solution of **18** (20 mg, 0.04 mmol) in THF (*ca.* 10 mL) for 10 mins, upon which the solution turned green. The solution was concentrated to *ca.* 2 mL. Repeated recrystallisation yielded a mixture of Cp\*Ru[HB(mt)<sub>2</sub>(pz)](O<sub>2</sub>) (**19**) (0.03 mmol, 86% conversion) and **18** (14% unreacted) (Conversion calculated based on integration of NMe peak in <sup>1</sup>H NMR spectrum). Attempts to separate **18** and **19** by column chromatography were also unsuccessful. The reaction can be fully reversed by heating **19** at 40 °C overnight under Ar, as observed by <sup>1</sup>H NMR spectroscopy. **19** was tested as a catalyst for epoxidation of alkenes but showed no catalytic activity (see appendix). Diffraction-quality single crystals were obtained at -30 °C as dark green rhombus from solution in THF-ether after 3 days.

**Data for 19.** Anal. Found: C, 44.8; H, 5.2; N, 13.0; S, 10.1%. Calc. for C<sub>21</sub>H<sub>29</sub>B<sub>1</sub>N<sub>6</sub>O<sub>2</sub>Ru<sub>1</sub>S<sub>2</sub>: C, 44.0; H, 5.1; N, 14.7; S, 11.2%. IR (DCM, cm<sup>-1</sup>):  $\nu$ (O-O) 896m  $\nu$ (BH) 2412w, 2306m. ESI<sup>+</sup>-MS (m/z): 572 [M<sup>+</sup> = C<sub>5</sub>Me<sub>5</sub>Ru{(C<sub>4</sub>H<sub>5</sub>N<sub>2</sub>S)<sub>2</sub>(C<sub>3</sub>H<sub>3</sub>N<sub>2</sub>)BH}(O<sub>2</sub>)-2H], 556 [M<sup>+</sup>-O]. <sup>1</sup>H NMR (C<sub>6</sub>D<sub>6</sub>):  $\delta$  8.45 (d, 2 x 1H, <sup>3</sup>J = 2.0 Hz, SCN<sub>2</sub>HC=CH), 7.98 (d, 1H, <sup>3</sup>J = 1.4 Hz, HC=CHNNCH), 7.91 (d, 1H, <sup>3</sup>J = 2.2 Hz, HC=CHNNCH), 6.19 (t, 1H, <sup>3</sup>J = 2.0 Hz, HC=CHNNCH), 5.91 (d, 2 x 1H, <sup>3</sup>J = 2.1 Hz, SCN<sub>2</sub>HC=CH), 3.28 (s, 2 x 3H, NCH<sub>3</sub>), 1.30 (s, 15H, CpCH<sub>3</sub>). <sup>1</sup>H NMR (CD<sub>2</sub>Cl<sub>2</sub>):  $\delta$  8.04 (d, 2 x 1H, <sup>3</sup>J = 1.4 Hz, SCN<sub>2</sub>HC=CH), 7.71 (s, 1H, HC=CHNNCH), 7.65 (s, 1H, HC=CHNNCH), 6.85 (d, 2 x 1H, <sup>3</sup>J = 1.3 Hz,

SCN<sub>2</sub>HC=CH), 6.16 (d, 1H, <sup>3</sup>J = 1.6 Hz, HC=CHNNCH), 3.73 (s, 2 x 3H, NCH<sub>3</sub>), 1.44 (s, 15H, CpCH<sub>3</sub>). <sup>13</sup>C NMR (CD<sub>2</sub>Cl<sub>2</sub>): δ 156.5 (s, SCN<sub>2</sub>HC=CH), 140.9 (s, C<sub>pyrazole</sub>), 137.6 (s, C<sub>pyrazole</sub>), 122.7 (s, C imidazole), 120.8 (s, C<sub>imidazole</sub>), 104.0 (s, C<sub>pyrazole</sub>), 100.9 (s, C<sub>5</sub>(CH<sub>3</sub>)<sub>5</sub>), 36.1 (s, NCH<sub>3</sub>), 8.2 (s, C<sub>5</sub>(CH<sub>3</sub>)<sub>5</sub>).

The reaction of **16** and **17** with O<sub>2</sub> were carried out but lead to the formation of uncharacterisable, insoluble solids.

**(ii) Reaction of [Cp\**Ru*{HB(mt)<sub>2</sub>(pz)}] with CO.** 1 atm of CO was charged into a Carius tube containing **18** (55 mg, 0.11 mmol) in THF (*ca.* 10 mL). The solution turned from bright red to a deep red within 5 mins and was allowed to stir overnight at RT. The resultant red solution was evacuated to dryness. Repeated washing with Et<sub>2</sub>O:hex (1:2) yielded dark red solids of Cp\**Ru*[HB(mt)<sub>2</sub>(pz)](CO) (**20**) (30 mg, 53% yield). The reaction is irreversible and **20** cannot be converted to **18**, even with prolonged heating at 80 °C. Diffraction-quality single crystals were obtained at -30 °C as **20** as red plates from THF-hexane solutions after 3 days.

**Data for 20.** Anal. Found: C, 46.9; H, 5.2; N, 14.5; S, 11.2%. Calc. for C<sub>22</sub>H<sub>29</sub>B<sub>1</sub>N<sub>6</sub>ORu<sub>1</sub>S<sub>2</sub>: C, 46.4; H, 5.1; N, 14.8; S, 11.3%. IR (KBr, cm<sup>-1</sup>): ν(C-O) 1913s, ν(BH) 2369m, 2338m. ESI<sup>+</sup>-MS (m/z): 570 [MH<sup>+</sup> = C<sub>5</sub>Me<sub>5</sub>Ru{(C<sub>4</sub>H<sub>5</sub>N<sub>2</sub>S)<sub>2</sub>(C<sub>3</sub>H<sub>3</sub>N<sub>2</sub>)BH}(CO)H], 542 [MH<sup>+</sup>-CO]. <sup>1</sup>H NMR (C<sub>6</sub>D<sub>6</sub>): δ 8.02 (d, 1H, <sup>3</sup>J = 0.6 Hz, HC=CHNNCH), 8.01 (d, 1H, <sup>3</sup>J = 1.3 Hz, HC=CHNNCH), 7.47 (d, 2 x 1H, <sup>3</sup>J = 1.4 Hz, SCN<sub>2</sub>HC=CH), 6.34 (t, 1H, <sup>3</sup>J = 1.1 Hz, HC=CHNNCH), 5.74 (d, 2 x 1H, <sup>3</sup>J = 1.2 Hz, SCN<sub>2</sub>HC=CH), 3.00 (s, 2 x 3H, NCH<sub>3</sub>), 1.59 (s, 15H, CpCH<sub>3</sub>). <sup>13</sup>C NMR (C<sub>6</sub>D<sub>6</sub>): δ 206.2 (s, CO), 158.9 (s, SCN<sub>2</sub>HC=CH), 141.1 (C<sub>pyrazole</sub>), 136.5 (C<sub>pyrazole</sub>), 121.7 (s, C imidazole), 118.1, (C<sub>imidazole</sub>), 104.0 (s, C<sub>pyrazole</sub>), 92.5 (s, C<sub>5</sub>(CH<sub>3</sub>)<sub>5</sub>), 33.9 (s, NCH<sub>3</sub>), 9.3 (s, C<sub>5</sub>(CH<sub>3</sub>)<sub>5</sub>).

**Conversion of Cp\*Ru[HB(mt)<sub>2</sub>(pz)](O<sub>2</sub>) (**19**) to Cp\*Ru[HB(mt)<sub>2</sub>(pz)](CO) (**20**)**

A green THF solution (*ca.* 8 mL) of Cp\*Ru[HB(mt)<sub>2</sub>(pz)](O<sub>2</sub>) (**19**) (5 mg, 0.001 mmol) in a Carius tube was subjected to freeze-pump-thaw action three times and charged with CO. The dark green solution turned to a bright red, then to deep red after 20 minutes of stirring to give Cp\*Ru[HB(mt)<sub>2</sub>(pz)](CO) (**20**). The reaction mixture was left to stir overnight to allow the conversion to go to completion, as indicated by the complete disappearance of the Cp\* peak of **19** in the <sup>1</sup>H NMR spectrum. The conversion of **20** to **19** in a THF solution in a Schlenk flask cannot take place even with prolonged heating at elevated temperature.

## References

1. Bailey, P. J.; Lorono-Gonzales, D. J.; McCormack, C.; Parsons, S.; Price, M., *Inorg. Chim. Acta* **2003**, *354*, 61-67.
2. Tilley, T. D.; Grubbs, R. H.; Bercaw, J. E., *Organometallics* **1984**, *3* (2), 274-278.
3. Oshima, N.; Suzuki, H.; Morooka, Y., *Chem. Lett.* **1984**, (7), 1161-1164.
4. Koelle, U.; Kossakowski, J., *J. Organomet. Chem.* **1989**, *362* (3), 383-398.
5. Hidai, M.; Mizobe, Y., Toward novel organic synthesis on multimetallic centers: Synthesis and reactivities of polynuclear transition-metal-sulfur complexes. In *Transition Metal Sulfur Chemistry-Biological and Industrial Significance*, Stiefel, E., Matsumoto, K., Ed. American Chemical Society: Washington DC, 1996; pp 311-323.
6. Hall, G. R.; Hendrickson, D. N., *Inorg. Chem.* **1976**, *15* (3), 607-618.
7. DeSimone, R. E., *J. Am. Chem. Soc.* **1973**, *95* (19), 6238-6244.
8. Heath, G. A.; Martin, R. L., *Aust. J. Chem.* **1970**, *23* (9), 1721-1734.
9. Webster, R. D.; Heath, G. A.; Bond, A. M., *J. Chem. Soc., Dalton Trans.* **2001**, (21), 3189-3195.
10. Kang, B. S.; Koelle, U.; Thewalt, U., *Organometallics* **1991**, *10* (8), 2569-73.
11. Pauling, L. in *The Nature Of The Chemical Bond*. 3rd ed.; Cornell University Press: Oxford, **1960**.
12. Garner, M.; Reglinski, J.; Cassidy, I.; Spicer, M. D.; Kennedy, A. R., *Chem. Commun.* **1996**, (16), 1975-1976.
13. Reglinski, J.; Garner, M.; Cassidy, I. D.; Slavin, P. A.; Spicer, M. D.; Armstrong, D. R., *J. Chem. Soc., Dalton Trans.: Inorganic Chemistry* **1999**, (13), 2119-2126.
14. Slavin, P. A.; Reglinski, J.; Spicer, M. D.; Kennedy, A. R., *Dalton Trans.* **2000**, (3), 239-240.
15. Garner, M.; Lewinski, K.; Pattek-Janczyk, A.; Reglinski, J.; Sieklucka, B.; Spicer, M. D.; Szaleniec, M., *Dalton Trans.* **2003**, (6), 1181-1185.
16. Dodds, C. A.; Jagoda, M.; Reglinski, J.; Spicer, M. D., *Polyhedron* **2004**, *23* (2-3), 445-450.
17. Dodds, C. A.; Lehmann, M.-A.; Ojo, J. F.; Reglinski, J.; Spicer, M. D., *Inorg. Chem.* **2004**, *43* (16), 4927-4934.
18. Alvarez, H. M.; Tran, T. B.; Richter, M. A.; Alyounes, D. M.; Rabinovich, D.; Tanski, J. M.; Krawiec, M., *Inorg. Chem.* **2003**, *42* (6), 2149-2156.
19. Mihalcik, D. J.; White, J. L.; Tanski, J. M.; Zakharov, L. N.; Yap, G. P. A.; Incarvito, C. D.; Rheingold, A. L.; Rabinovich, D., *Dalton Trans.* **2004**, (10), 1626-1634.
20. Bridgewater, B. M.; Parkin, G., *Inorg. Chem. Comm.s* **2000**, *3* (10), 534-536.
21. Bridgewater, B. M.; Fillebeen, T.; Friesner, R. A.; Parkin, G., *Dalton Trans.* **2000**, (24), 4494-4496.
22. Foreman, M. R. S. J.; Hill, A. F.; Owen, G. R.; White, A. J. P.; Williams, D. J., *Organometallics* **2003**, *22* (22), 4446-4450.
23. Simoes, J. A. M.; Beauchamp, J. L., *Chem. Rev.* **1990**, *90* (4), 629-688.
24. Calhorda, M. J.; Carrondo, M. A. A. F. d. C. T.; Dias, A. R.; Domingos, A. M. T. S.; Simoes, J. A. M.; Teixeira, C., *Organometallics* **1986**, *5* (4), 660-7.
25. Budzelaar, P. H. M. "gNMR", version 4.1, **1995-1999**. Adept Scientific plc.: Amor Way, Letchworth, Herts, SG6 1ZA, UK.



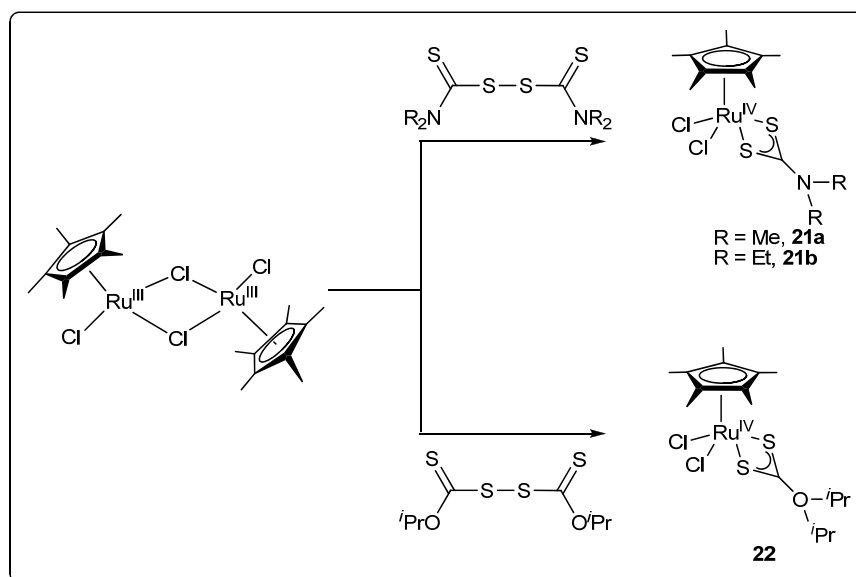
26. Hong, S. H.; Evans, D. H.; Nelsen, S. F.; Ismagilov, R. F., *J. Electroanal. Chem.* **2000**, 486 (1), 75-84.
27. Rudolph, M.; Reddy, D. P.; Feldberg, S. W., *Anal. Chem.* **1994**, 66 (10), 589A-600A.
28. Valentine, J., *Chem. Rev.* **1973**, 73, 235.
29. Koelle, U.; Kossakowski, J.; Grumbine, D.; Tilley, T. D., *Inorg. Synth.* **1992**, 29, 225-228.
30. Koelle, U.; Kossakowski, J., *J. Chem. Soc., Chem. Commun.* **1988**, (8), 549-551.
31. *DigiSim*<sup>®</sup> by Bioanalytical Systems, Inc. (BAS), 2701 Kent Avenue, West Lafayette, IN 47906, USA.
32. Forrow, N. J.; Knox, S. A. R., *J. Chem. Soc., Chem. Commun.* **1984**, (11), 679-681.

**Chapter 5. One-Electron Electrochemical Oxidation of Half Sandwich Ruthenium Complexes,  $[\text{Cp}^*\text{Ru}^{\text{IV}}\text{Cl}_2(\text{S}_2\text{CR})]$  ( $\text{Cp}^* = \text{C}_5\text{Me}_5$ ,  $\text{R} = \text{NMe}_2$ ,  $\text{NEt}_2$ ,  $\text{O}^i\text{Pr}$ )**

Transition metal complexes containing sulfur donor ligands command a continuing interest on account of their relevance to biological and industrial processes.<sup>1-9</sup> The dithiocarbamate (dtc) and xanthate ligands have attracted particular attention as a versatile ligand in both main group<sup>10</sup> and transition metal chemistry.<sup>11</sup> A notable feature of dithiocarbamate ligands is their ability to stabilize metal species in high or unusual oxidation states,<sup>12</sup> such as  $[\text{Co}^{\text{IV}}(\text{S}_2\text{CNR}_2)_3]^+$  ( $\text{R} = \text{alkyl}$  or cyclohexyl) which is stable in  $\text{CH}_2\text{Cl}_2$  at 233 K.<sup>13</sup>

Our group had previously reported the synthesis of the Ru(IV) complexes  $[\text{Cp}^*\text{RuCl}_2(\text{S}_2\text{CR})]$  (**21a**:  $\text{R} = \text{NMe}_2$ ; **21b**:  $\text{R} = \text{NEt}_2$  and **22**:  $\text{R} = \text{O}^i\text{Pr}$ ) in high yields from the reaction of  $[\text{Cp}^*\text{RuCl}_2]_2$  (**12**) with  $[\text{RC}(\text{S})\text{S}]_2$  (Scheme 5.1).<sup>14</sup>

**Scheme 5.1.** Syntheses of  $\text{Cp}^*\text{RuCl}_2(\text{S}_2\text{CR})$  complexes.



These dithiocarbamate complexes are one of the few examples of organoruthenium(IV) complexes. Ru containing dithiocarbamate compounds have recently been comprehensively reviewed,<sup>15</sup> and there exists a number of examples where the dithiocarbamate ligand has been coordinated to  $\eta^5$ -cyclopentadienyl organometallic complexes.<sup>11, 16-19</sup> The electrochemical behavior of dithiocarbamate complexes has also been extensively studied.<sup>12, 13</sup> One interesting case involves the oxidation of  $[\text{Ru}^{\text{III}}(\text{S}_2\text{CNR}_2)_3]$ , which was expected to form  $[\text{Ru}^{\text{IV}}(\text{S}_2\text{CNR}_2)_3]^+$  based on the observation that the related  $[\text{Fe}^{\text{IV}}(\text{S}_2\text{CNR}_2)_3]^+$  (and Mn(IV)) complexes were stable.<sup>20, 21</sup> Nevertheless, one-electron oxidation of  $[\text{Ru}^{\text{III}}(\text{S}_2\text{CNR}_2)_3]$  instead produced dimeric  $[\text{Ru}_2^{\text{III}}(\text{S}_2\text{CNR}_2)_5]^+$  complexes.<sup>22, 23</sup> Interestingly, the seven-coordinate  $[\text{Ru}^{\text{IV}}\text{Cl}(\text{S}_2\text{CNR}_2)_3]$  and  $[\text{Ru}^{\text{IV}}\text{Cl}(\text{S}_2\text{CNR}_2)_2(\eta^2\text{-SCNR}_2)]$  complexes were obtained by photolysis of  $[\text{Ru}^{\text{III}}(\text{S}_2\text{CNR}_2)_3]$ , suggesting that the presence of chloride aids in stabilizing the Ru(IV) state.<sup>23, 24</sup> Dithiocarbamate complexes of ruthenium invariably exist between the oxidation states of (II) to (IV)<sup>11, 16-18</sup>. Nevertheless, the observation of a one-electron oxidation of a formally Ru(IV) organometallic compound is an interesting and surprising result worthy of detailed investigation. On the other hand, the xanthate complexes of ruthenium has been less studied compared to their dithiocarbamate counterparts but nonetheless provide a comparison to the DTC in the current study.

In this chapter, we report the one-electron oxidation of  $(\eta^5\text{-C}_5\text{Me}_5)\text{Ru(IV)}$  complexes to form paramagnetic species, and discuss the distribution of the increased positive charge and spin density based on results from EPR spectroscopic experiments and DFT calculations.

## 5.1. Electrochemical oxidation and spectroscopic studies of [Cp\**Ru*<sup>IV/V</sup>Cl<sub>2</sub>(S<sub>2</sub>CR)] complexes

Cyclic voltammograms of CH<sub>2</sub>Cl<sub>2</sub> solutions containing [Cp\**Ru*Cl<sub>2</sub>(S<sub>2</sub>CR)] showed complicated reduction processes at negative potentials that varied depending on the electrode surface and temperature (Figure 5.1). The presence of electrochemical reduction responses is certainly the expected result considering the high oxidation state of Ru(IV) and the rich literature pertaining to low oxidation state  $\eta^5$ -(Cp/Cp\*)*Ru* compounds.<sup>25</sup> However, considerably more surprising was the observation of oxidation processes at  $E_{1/2}^r = + 0.65$  V vs. Fc/Fc<sup>+</sup> (Fc = ferrocene) for [Cp\**Ru*Cl<sub>2</sub>(S<sub>2</sub>CNMe<sub>2</sub>)] (**21a**) and [Cp\**Ru*Cl<sub>2</sub>(S<sub>2</sub>CNEt<sub>2</sub>)] (**21b**) and  $E_{1/2}^r = + 0.98$  V vs. Fc/Fc<sup>+</sup> for [Cp\**Ru*Cl<sub>2</sub>(S<sub>2</sub>CO<sup>*i*</sup>Pr)] (**22**), suggesting the formation of highly oxidized ruthenium organometallic compounds. In contrast to the reduction processes, the oxidation processes appeared fully chemically reversible at temperatures between 233-293 K with anodic ( $i_p^{ox}$ ) to cathodic ( $i_p^{red}$ ) peak-to-peak separations similar to those observed for Fc under identical conditions, and with  $i_p^{ox}$ -values proportional to  $\nu^{1/2}$  ( $\nu$  = scan rate). Furthermore, exhaustive bulk electrochemical oxidation at a potential 0.1 V more positive than the  $i_p^{ox}$ -values, resulted in the transfer of  $1.0 \pm 0.1$  electrons per molecule, with the oxidized compounds stable enough (at  $T = 233$  K) to be reduced back to the starting material when the applied potential was switched to  $\sim + 0.5$  V vs. Fc/Fc<sup>+</sup>. While compounds containing the dithiocarbamate ligand are known to undergo dimerization following oxidation (or other ligand-based reactions),<sup>12, 13</sup> the chemically reversible nature of the voltammetric process on the short (CV) and long (electrolysis) time-scales confirm the straightforward one-electron oxidation of [Cp\**Ru*Cl<sub>2</sub>(S<sub>2</sub>R)] to form [Cp\**Ru*Cl<sub>2</sub>(S<sub>2</sub>R)]<sup>+</sup> (the counter anion for all experiments was the supporting electrolyte anion, PF<sub>6</sub><sup>-</sup>).

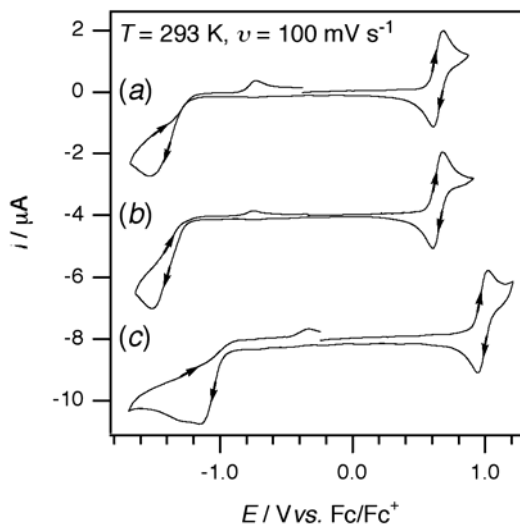


**Figure 5.1.** Cyclic voltammograms recorded in  $\text{CH}_2\text{Cl}_2$  with 0.5 M  $\text{Bu}_4\text{NPF}_6$  at a Pt electrode of 1.0 mM solutions of (a)  $[\text{Cp}^*\text{RuCl}_2(\text{S}_2\text{CNMe}_2)]$  (**21a**), (b)  $[\text{Cp}^*\text{RuCl}_2(\text{S}_2\text{CNEt}_2)]$  (**21b**) and (c)  $[\text{Cp}^*\text{RuCl}_2(\text{S}_2\text{CO}^i\text{Pr}_2)]$  (**22**). (b) and (c) are offset by  $-4 \mu\text{A}$  and  $-8 \mu\text{A}$  respectively. (The reversible half-wave potential,  $E_{1/2}^r = (E_p^{\text{ox}} + E_p^{\text{red}})/2$ , where  $E_p^{\text{ox}}$  and  $E_p^{\text{red}}$  are the anodic and cathodic peak potentials respectively)

There is little uncertainty that ruthenium is present as formally Ru(IV) in the neutral diamagnetic starting material (each ligand carries a charge of -1), but the formal oxidation state of Ru in the one-electron oxidized form is ambiguous when based solely on electrochemical experiments, especially considering that Ru(V) is unprecedented in organometallic chemistry and rarely observed in coordination chemistry.<sup>26</sup> However, the alternative possibility where the oxidation is entirely ligand-based is also unlikely since neither the dithiocarbamate or  $\text{Cp}^*$  ligands are strong candidates for a localized one-electron oxidation. Nevertheless, the strong dependence of  $E_{1/2}^r$  (that approximates the formal potential,  $E^0$ ), on the dithiocarbamate or carbonothiolate groups indicates that the bidentate sulfur ligands are critically involved in the oxidation process.

Samples of  $[\text{Cp}^*\text{RuCl}_2(\text{S}_2\text{R})]^+$  for EPR spectroscopic analysis were prepared by one-electron oxidation of the starting material in an electrolysis cell and then transferred under vacuum into silica EPR cells. The X-band EPR spectra of

$[\text{Cp}^*\text{RuCl}_2(\text{S}_2\text{CNMe}_2)]^+$  at 293 K showed an intense symmetrical ( $S = 1/2$ ) signal with a  $g$ -value of 2.035 and a peak-to-peak linewidth ( $\Delta H_{\text{pp}}$ ) of 15 G. The solution phase spectra also showed the presence of weaker satellite signals symmetrically arranged on either side of the main signal (Figure 5.2a). The presence of satellite signals of weaker intensity than the primary signal is an indication of hyperfine interactions with lower abundance isotopes. The intensity and pattern of the satellite signals are in excellent agreement with hyperfine coupling (of 25 G) to  $^{99}\text{Ru}$  ( $I = 5/2$ , 12.72% natural abundance) and  $^{101}\text{Ru}$  ( $I = 5/2$ , 17.07% natural abundance) (see simulation in Figure 5.2a) indicating an interaction of the unpaired electron with the metal ion.

The intensity of the  $^{99}\text{Ru}/^{101}\text{Ru}$  hyperfine coupling on either side of the main  $S = 1/2$  signal became increasingly less symmetrical as the temperature was lowered from 293 - 193 K, possibly due to an anisotropic tumbling effect (Figure 5.2b).<sup>27</sup> At temperatures below  $\sim 193$  K (when the solution began to freeze) the spectra were axial shaped ( $g_{\perp} = 2.050$ ,  $g_{\parallel} = 2.008$ ) and remained constant in appearance down to 6 K. The linewidth of the spectra also remained constant (15 G) over the entire temperature range (293 - 6 K) suggesting that the oxidized compound maintains the same geometric structure in solution and frozen solution states. The EPR signal began to diminish in intensity if the sample was left at 293 K for over 30 minutes, but at low temperatures ( $T < 233$  K) the compound appeared stable for at least 12 hours. Very similar EPR spectra were detected for  $[\text{Cp}^*\text{RuCl}_2(\text{S}_2\text{CNEt}_2)]^+$  (**21b**<sup>+</sup>) and  $[\text{Cp}^*\text{RuCl}_2(\text{S}_2\text{CO}^i\text{Pr})]^+$  (**22**<sup>+</sup>) (Figure 6.2c), with  $^{99}\text{Ru}/^{101}\text{Ru}$  hyperfine coupling values also equal to 25 G. Compound **22**<sup>+</sup> was not stable at temperatures above 233 K, possibly because its higher oxidation potential increased its reactivity.

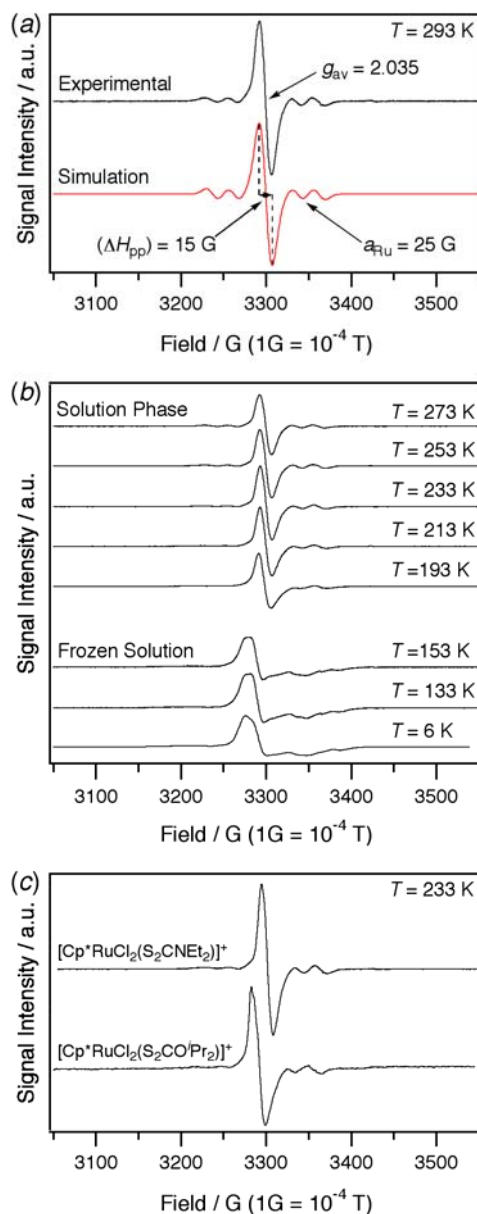


**Figure 5.2.** First derivative continuous wave X-band EPR spectra recorded in  $\text{CH}_2\text{Cl}_2$  with 0.5 M  $\text{Bu}_4\text{NPF}_6$ . (a)  $[\text{Cp}^*\text{RuCl}_2(\text{S}_2\text{CNMe}_2)]^+$  (**21a**<sup>+</sup>) at 293 K. (b)  $[\text{Cp}^*\text{RuCl}_2(\text{S}_2\text{CNMe}_2)]^+$  (**21a**<sup>+</sup>) between 273 - 6 K. (c)  $[\text{Cp}^*\text{RuCl}_2(\text{S}_2\text{CNEt}_2)]^+$  (**22b**<sup>+</sup>) and  $[\text{Cp}^*\text{RuCl}_2(\text{S}_2\text{CO}^i\text{Pr})]^+$  (**22**<sup>+</sup>) at 233 K.

Discussion on the EPR spectra of  $d^5$  Ru(III) coordination and organometallic compounds is usually restricted to  $g$  matrix components,<sup>28</sup> although Ru anisotropic hyperfine interactions are sometimes observed at low temperatures with hyperfine coupling of approximately 50 G.<sup>29, 30</sup> EPR spectra of complexes containing formally Ru(V) ions are scarce. A sharp single-line isotropic EPR signal (without any

hyperfine structure) was detected for  $(n\text{Pr}_4\text{N})[\text{Ru}^{\text{V}}(\text{O})(\text{O}_2\text{COCEt}_2)_2]$  at room temperature.<sup>31</sup> Most of the reports of hyperfine coupling in Ru compounds involve ligand-centered radicals coordinated to Ru(II) ions and with hyperfine coupling constants  $< 10$  G.<sup>32-39</sup> Therefore, the 25 G Ru hyperfine coupling found in this work is very large for a solely ligand centered radical, and suggests that the oxidized compounds contain Ru in the most highly oxidized state ever recorded in organometallic chemistry. Hyperfine coupling to other nuclei in the complexes such as Cl, N, or H is possible. However, because of the relatively narrow linewidth of the spectrum, any additional hyperfine coupling can be estimated to be very small ( $< 3$ -4 G) in order not to complicate the spectra in Figure 5.3. This indicates that most of the unpaired electron spin density must be located within the region of the Ru ion.

DFT calculations using the B3LYP functional were performed on  $[\text{Cp}^*\text{RuCl}_2(\text{S}_2\text{CMe}_2)]$  (**21a**) and its one-electron oxidized form to complement the experimental EPR studies, in order to locate the increased positive charge and unpaired electron spin density (Table 5.1). The calculations predict an increase of only 0.06 in the positive charge on the metal ion as a result of the oxidation, with the remaining increase in positive charge shared mainly between the Cp\* group (0.37), the chlorides (0.30) and the sulfurs (0.15). However, although the DFT calculations predict a relatively small increase in positive charge of the metal ion in the oxidized compound, they predict that the majority of the unpaired electron spin density (70%) is located on the metal ion, thereby leading to the important conclusion that the oxidized compound does have a metal-centered spin state. DFT calculations of the spin density at each nucleus in the oxidized compound reveal that this is an order of magnitude higher for Ru (-0.2) than for any other nucleus (Table 5.1), although there is also a significant contribution to spin density within the outer d-orbitals of the Ru.



Further evidence for the spin density on the metal in the one-electron oxidized compound came from UV-vis-NIR and EPR experiments. The spectrum of the starting material showed only two weak bands below  $25000\text{ cm}^{-1}$ , at  $16000$  and  $\sim 20000\text{ cm}^{-1}$  that are likely to be associated with d-d transitions due to their low intensity ( $\epsilon \approx 500\text{ L cm}^{-1}\text{ mol}^{-1}$ ).<sup>27</sup> The higher intensity ( $\epsilon \approx 10000\text{ L cm}^{-1}\text{ mol}^{-1}$ ) bands in the starting material at  $\sim 30000$  and  $35000\text{ cm}^{-1}$  are ligand-to-metal charge transfer (LMCT) excitations,<sup>40</sup> whilst the highest intensity band at  $\sim 40000\text{ cm}^{-1}$  ( $\epsilon \approx 35000\text{ L cm}^{-1}\text{ mol}^{-1}$ ) results from  $\pi\text{-}\pi^*$  transitions in the dithiocarbamate ligand.<sup>13</sup> The UV-vis-NIR spectra of  $[\text{Cp}^*\text{RuCl}_2(\text{S}_2\text{CNMe}_2)]^+$  (**21a**<sup>+</sup>) showed a series of bands at  $\nu = 12500$ ,  $18500$ ,  $20400$  and  $26500\text{ cm}^{-1}$  which, due to their intensity ( $\epsilon = 2000 - 4000\text{ L cm}^{-1}\text{ mol}^{-1}$ ), can be interpreted as LMCT excitations (and are likely to obscure any new d-d transitions).<sup>13, 40, 27</sup> The presence of new bands ( $\nu < 30000\text{ cm}^{-1}$ ) in the spectrum of the oxidized compound can be rationalized by a electronic state that facilitates low energy LMCT transitions to the partially filled metal orbital. A similar result was observed during the oxidation of  $[\text{Co}^{\text{III}}(\text{S}_2\text{CNET}_2)_3]$  to  $[\text{Co}^{\text{IV}}(\text{S}_2\text{CNET}_2)_3]^+$  (a  $d^6$  to  $d^5$  change).<sup>13</sup>

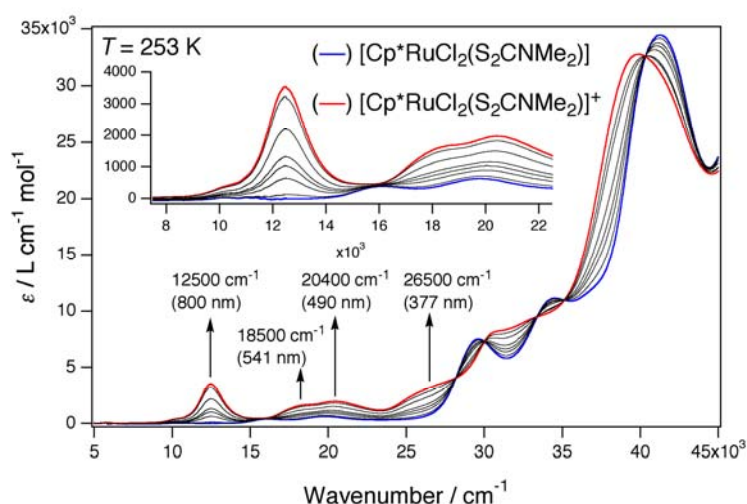


**Figure 5.3.** UV-vis-NIR spectra obtained during the one-electron *in situ* electrochemical oxidation of  $1.0\text{ mM}$   $[\text{Cp}^*\text{RuCl}_2(\text{S}_2\text{CNMe}_2)]$  (**21a**) in  $\text{CH}_2\text{Cl}_2$  with  $0.5\text{ M}$   $\text{Bu}_4\text{NPF}_6$  in an OTTE cell.

The *in situ* electrochemical-UV-vis-NIR spectra obtained during the one-electron oxidation of **21a** at 253 K were completely reversible, so that applying a potential sufficiently negative to cause the reduction of **21a**<sup>+</sup> resulted in the regeneration of the spectrum with the same appearance and signal intensity as the starting material (Figure 5.3). The stability of **21a**<sup>+</sup> on the time frame of the experiment (2-3 hours) was also supported by the occurrence of several isosbestic points at 15800, 28200, 30000, 33400, 35100 and 40300 cm<sup>-1</sup>.

Numbering system used for Table 5.1

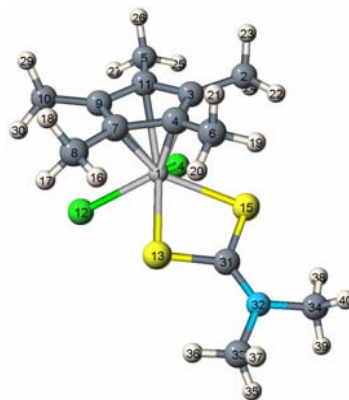


**Table 5.1.** Selected calculated<sup>a</sup> atomic charges, spin densities, and spin densities at the nuclei in the neutral and oxidized forms of [Cp\*RuCl<sub>2</sub>(S<sub>2</sub>CNMe<sub>2</sub>)] (**21a**) (Refer to Appendix Table A5 for full listing).

Atom Number	Atom Type	Charge			Spin Density	Spin Density At Nucleus
		[Cp*RuCl <sub>2</sub> (S <sub>2</sub> CR)]	[Cp*RuCl <sub>2</sub> (S <sub>2</sub> CR)] <sup>+</sup>	[Cp*RuCl <sub>2</sub> (S <sub>2</sub> CR)] <sup>+</sup> [Cp*RuCl <sub>2</sub> (S <sub>2</sub> CR)] <sup>-</sup>	[Cp*RuCl <sub>2</sub> (S <sub>2</sub> CR)] <sup>+</sup>	[Cp*RuCl <sub>2</sub> (S <sub>2</sub> CR)] <sup>+</sup>
1	Ru	0.377	0.43789	0.06089	0.69267	-0.2102290
3	C	-0.0254	0.0073	0.03270	0.00007	0.0041720
4	C	-0.02699	0.00698	0.03397	-0.00092	0.0046729
7	C	-0.02582	0.00728	0.03310	0.00076	0.0043677
9	C	0.00257	0.03965	0.03708	0.01266	0.0065492
11	C	0.00252	0.03952	0.03700	0.01299	0.0065688
12	Cl	-0.44907	-0.30116	0.14791	0.11556	0.0187709
13	S	0.03026	0.1075	0.07724	0.00154	0.0044718
14	Cl	-0.44995	-0.30105	0.14890	0.1177	0.0191466
15	S	0.03059	0.10728	0.07669	-0.00012	0.0039312

<sup>a</sup>Optimized structures and Natural Bond Orbital analysis using the B3LYP functional. See text for basis set and Rassolov-Chipman details.

## 5.2. Chemical oxidation of [Cp\*Ru<sup>IV</sup>Cl<sub>2</sub>(S<sub>2</sub>CNMe<sub>2</sub>)]

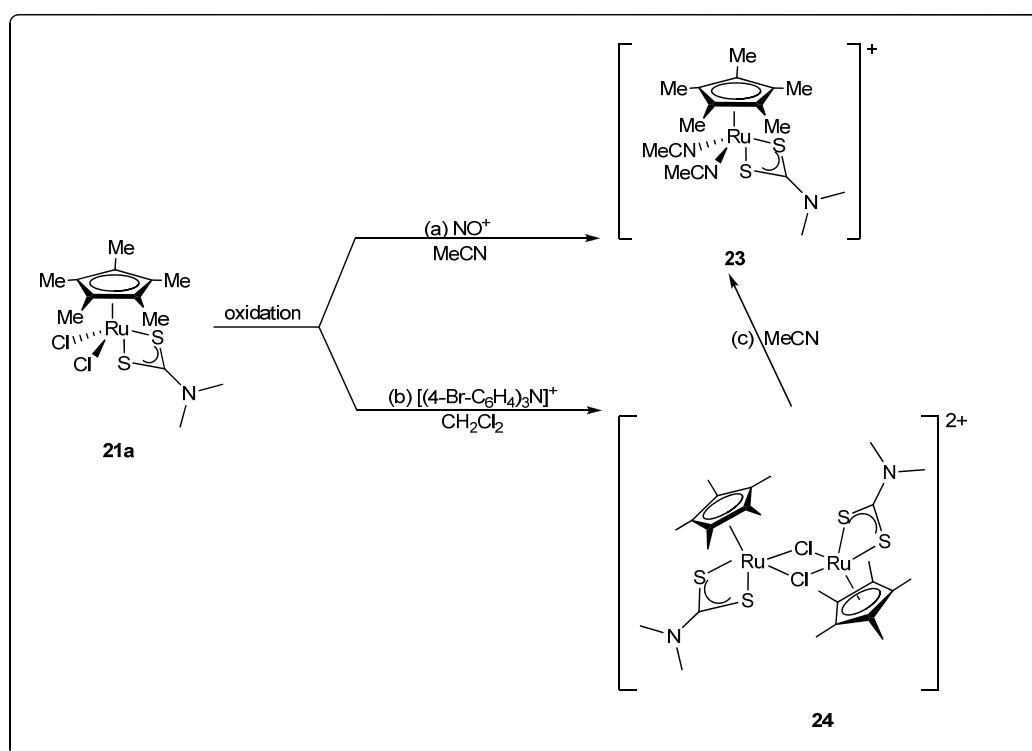
Attempts were made to isolate [Cp\*RuCl<sub>2</sub>(S<sub>2</sub>CNMe<sub>2</sub>)]<sup>+</sup> (**21a**<sup>+</sup>) detected in the electrochemical studies of complex **21a**, by performing a one-electron chemical oxidation. [Cp\*RuCl<sub>2</sub>(S<sub>2</sub>CNMe<sub>2</sub>)] (**21a**) is oxidized at  $E_{1/2}^r = + 0.65$  V vs. Fc/Fc<sup>+</sup> (Fc = ferrocene), hence NO(PF<sub>6</sub>), a known one-electron oxidant, with an  $E^0 = + 0.70$  V vs. Fc/Fc<sup>+</sup> (Fc = ferrocene) in acetonitrile<sup>41</sup> was chosen for this purpose. Upon addition of one equivalent of NO(PF<sub>6</sub>) to a purple solution of complex **21a**, the color of the solution turned red instantaneously. From this red solution, another Ru(IV) species, [Cp\*Ru(MeCN)<sub>2</sub>(S<sub>2</sub>CNMe)](PF<sub>6</sub>)<sub>2</sub> (**23**), was isolated, in which two of the chloro ligands have been substituted by acetonitrile molecules (Scheme 5.2a). Cyclic voltammetry experiments performed on **21a** in acetonitrile at  $\nu = 100$  mV s<sup>-1</sup> indicated that **21a** could be oxidized in a one-electron chemically reversible process (i.e. the same as in CH<sub>2</sub>Cl<sub>2</sub>). However, longer term CPE and *in situ* electrochemical UV-vis experiments in MeCN indicated that the one-electron oxidized compound, **21a**<sup>+</sup>, decomposed/reacted within one hour of its formation.

Chemical oxidation experiments were also performed with NO(PF<sub>6</sub>) in CH<sub>2</sub>Cl<sub>2</sub> but the one-electron oxidized product oxidant did not appear stable in this medium in the presence of NO<sup>+</sup> or NO<sub>(g)</sub>. Another attempt was made to synthesise the Ru(V) complex using the one-electron oxidant [(4-Br-C<sub>6</sub>H<sub>4</sub>)<sub>3</sub>N](SbCl<sub>6</sub>)<sup>41</sup>. The reaction in dichloromethane led to slow precipitation within 30 min of red solids, the x-ray structure of which showed a dichloro-bridged dimeric Ru(IV) species, [Cp\*Ru(S<sub>2</sub>CNMe<sub>2</sub>)<sub>2</sub>](SbCl<sub>6</sub>)<sub>2</sub> (**24**), in agreement with microanalytical data. (Scheme 5.2b)

The red solid of **24** was initially insoluble in CD<sub>3</sub>CN; however, ultrasonication for 20 min gave a light red solution. The <sup>1</sup>H NMR spectrum of this solution matched

that of complex **23**, (less the proton signals of coordinated MeCN) indicating that the polar coordinating acetonitrile has facilitated dissociation of the dimer, with concomitant or subsequent ligand displacement (Scheme 5.2c). It is likely that oxidation in acetonitrile also progresses through the dimeric compound **24** (such a process readily explains the charge balance), but MeCN quickly reacts to form the monomeric coordinated compound, **23**.

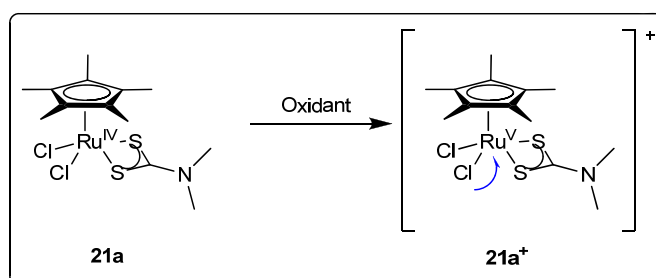
**Scheme 5.2.** Chemical oxidation of **21a**.



Electrochemical experiments proved that **21a** was indeed oxidized to **21a<sup>+</sup>** in both CH<sub>2</sub>Cl<sub>2</sub> and MeCN, thus the instability of **21a<sup>+</sup>** over synthetic timescales is likely to be due to the highly oxidizing nature of Ru(V). The consequence is secondary oxidation of the chloride ligands (Schemes 5.2 and 5.3), with concomitant reduction of the Ru(V) to Ru(IV), as found in **23** in a coordinating solvent and **24** in a non-coordinating solvent. This postulation is in agreement with DFT calculation on the Ru(V) species, **21a<sup>+</sup>**, which predicted that most of the increased positive charge is

located on the Cl atoms (although *not* the up spin density). Such reactions where the ligands are oxidized by the metal in high oxidation states are not unknown; for instance, Bond and co-workers had previously reported in their study of reactivity of  $\text{Ir}^{\text{IV}}$  dithiocarbamate (dtc) and diselenocarbamates (dsc) complexes in solution that  $[\text{Ir}(\text{Et}_2\text{dsc})_3]^+$  slowly dimerize during the course of bulk electrolysis experiments and subsequently undergoes an internal redox reaction to give  $[\text{Ir}_2(\text{Et}_2\text{dsc})_5]^+$  and oxidized ligand.<sup>42</sup> The authors also reported that the  $[\text{Ir}(\text{dtc})_3]^+$  cations are highly oxidizing in nature, as is demonstrated by their oxidation of free dithiocarbamate ion to give thiuram disulfide and by the oxidation with elemental mercury to give mixed-metal complexes  $[\text{HgIr}_2(\text{dtc})_6]^{2+}$ .

**Scheme 5.3.** One electron oxidation of **21**.



The molecular structures of the dication of **23** and **24** are shown in Figure 5.4b-c, with selected bond length and bond angles given in Table 5.2. The molecular structure of **21a** (Figure 5.4a) and its selected bond parameters are also given for comparison. In all three instances, the  $\text{Cp}^*\text{Ru}$  complexes adopt a four-legged piano stool configuration, with the dtc ligand occupying two coordination sites and the remaining two sites taken by chloride (in **21a** and **24**) or acetonitrile (in **23**). The structure of the dication **24** possesses a center of inversion in the  $\text{Ru}(1)\text{-Cl}(1)\text{-Ru}(1\text{A})\text{-Cl}(1\text{A})$  plane.

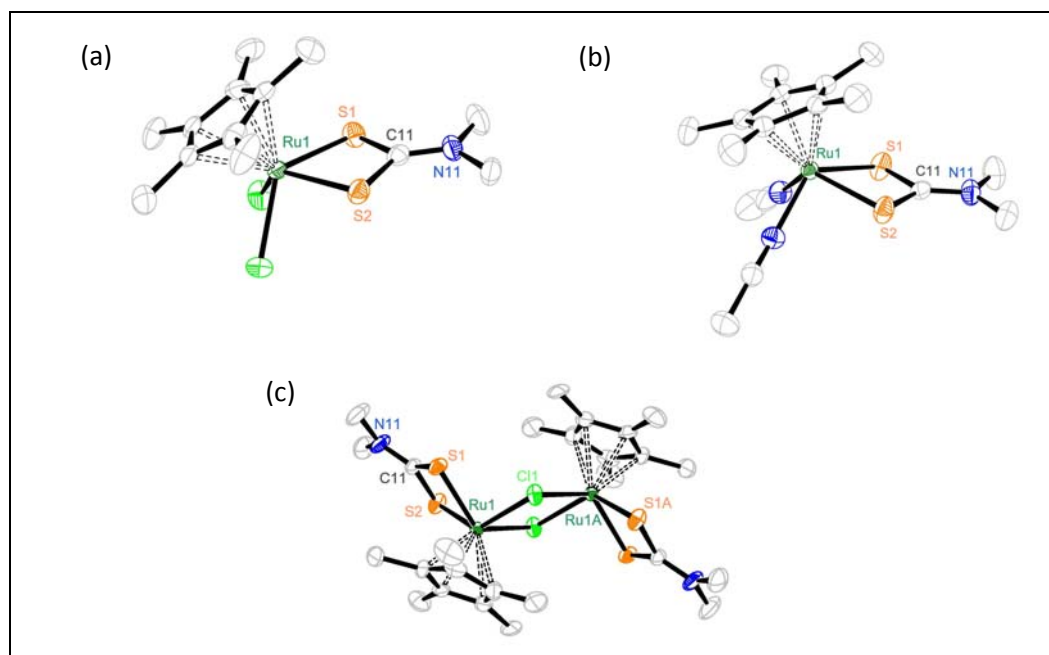


**Figure 5.4.** ORTEP plots for (a) the molecular structure of  $[\text{Cp}^*\text{RuCl}_2(\text{S}_2\text{CNMe}_2)]$  (**21a**) (a selected view which omits the disorder in Cp\*) (b) the molecular structure of  $[\text{Cp}^*\text{Ru}(\text{MeCN})_2(\text{S}_2\text{CNMe}_2)]^{2+}$  (**23**) and (c) the molecular structure of  $[\text{Cp}^*\text{RuCl}(\text{S}_2\text{CNMe}_2)]_2^{2+}$  (**24**). Thermal ellipsoids are drawn at the 50% probability level and hydrogen atoms are omitted for clarity.

**Table 5.2.** Selected bond parameters.

	<b>21a</b>	<b>23</b>	<b>24</b>
<b>Bond Distance (Å)</b>			
Ru(1)-S(1)	2.3706(12)	2.3906(13)	2.367(3)
Ru(1)-S(2)	2.3681(10)	2.3798 (14)	2.364(3)
S(1)-C(11)	1.712(5)	1.704(5)	1.712(10)
N(11)-C(11)	1.304(5)	1.715(5)	1.309(13)
Ru(1)-Cl(1)	-	-	2.424(3)
			2.447(2)
<b>Bond Angles (°)</b>			
S(2)-Ru(1)-S(1)	71.16(4)	70.64(5)	70.88(10)
S(1)-C(11)-S(2)	106.7(2)	107.5(3)	107.2 (5)
Ru(1)-Cl(1)-Ru(1A)	-	-	101.21 (9)

The Ru-S bond distances in complex **24** (2.364(3) and 2.367(3) Å) are comparable to that found in **21a** (2.3681(10) and 2.3706(12) Å) while that in **23** (2.3798(14) and 2.3906(13) Å) are longer, presumably due to the higher charge on the Ru center in **23**. The C-S bond distances in **23** and **24** falls in the range 1.697(10)-

1.715(5) Å, which are intermediate between values of a single bond (*ca.* 1.81 Å) and a double bond (*ca.* 1.56 Å).<sup>43</sup>

### 5.3. Conclusion

One-electron electrochemical oxidation of [Cp\*RuCl<sub>2</sub>(S<sub>2</sub>CR)] produce paramagnetic [Cp\*RuCl<sub>2</sub>(S<sub>2</sub>CR)]<sup>+</sup>, which are stable in CH<sub>2</sub>Cl<sub>2</sub> solution for at least several hours at 233 K. [Cp\*RuCl<sub>2</sub>(S<sub>2</sub>CNMe<sub>2</sub>)]<sup>+</sup> (**21a**<sup>+</sup>) contains Ru in the most highly oxidized state ever recorded in organometallic chemistry. Electrochemical, EPR and UV-vis spectroscopic studies indicate that in solution the oxidised compound (**21a**<sup>+</sup>) is stable for at least several hours at 233 K, but on preparative timescales reacts to form a dimeric compound (**24**) *via* loss of Cl<sup>-</sup>. **24** reacts readily with 4 equivalents of MeCN to form **23**, the monomeric analogue of **21a** containing 2 MeCN ligands. The assignment of a formally Ru(V) state in (**21a**<sup>+</sup>) is based on EPR experiments that detected hyperfine coupling to <sup>99/101</sup>Ru and from density-based calculations that predicted 70% unpaired electron spin density on the Ru. The high spin density on Ru is in contrast to the calculated small increase in positive charge on Ru (5%) following oxidation.



## 5.4. Experimental

General procedures are as described in Chapter 2. The tetraalkyldithiuram disulfides  $[\text{R}_2\text{NC}(\text{S})\text{S}]_2$  (R = Me, Et), isopropylxanthic disulfide  $[\text{iPrOC}(\text{S})\text{S}]_2$  and  $\text{RuCl}_3 \cdot n\text{H}_2\text{O}$  were purchased from Oxkem Ltd and used as supplied.  $[\text{Cp}^*\text{RuCl}_2(\text{S}_2\text{CR})]$  (**21a**: R = NMe<sub>2</sub>; **21b**: R = NEt<sub>2</sub> and **22**: R = O<sup>i</sup>Pr) were prepared according to published procedures.<sup>14</sup>

**Cyclic Voltammetry Studies** are performed as described in Chapter 2. *In situ* UV-vis-NIR spectra were obtained with a Varian Cary 5E spectrophotometer in an optically transparent thin layer electrochemical (OTTLE) cell (pathlength = 0.05 cm) at 253 K using a Pt mesh working electrode.<sup>13,44</sup> Typical exhaustive electrolysis time for the one-electron oxidation of 1 mM analyte in CH<sub>2</sub>Cl<sub>2</sub> (0.5 M Bu<sub>4</sub>NPF<sub>6</sub>) was 1.5 hours.

Solutions of  $[\text{Cp}^*\text{RuCl}_2(\text{S}_2\text{CR})]^+$  for the EPR experiments were prepared in a divided controlled potential electrolysis cell separated with a porosity no. 5 (1.0 - 1.7 μm) sintered glass frit.<sup>13,45-48</sup> The working and auxiliary electrodes were identically sized Pt mesh plates symmetrically arranged with respect to each other with an Ag wire reference electrode (isolated by a salt bridge) positioned to within 2 mm of the surface of the working electrode. The electrolysis cell was jacketed in a glass sleeve and cooled to 233 K using a Lauda RL6 variable temperature methanol-circulating bath. The volumes of both the working and auxiliary electrode compartments were approximately 10 mL each. The number of electrons transferred during the bulk oxidation process was calculated from

$$N = Q/nF \quad (1)$$

where  $N$  = no. of moles of starting compound,  $Q$  = charge (coulombs),  $n$  = no. of electrons and  $F$  is the Faraday constant (96485 C mol<sup>-1</sup>). The electrolyzed solutions

were transferred under vacuum into a cylindrical 3 mm (id) EPR tube that was immediately frozen in liquid N<sub>2</sub>, or to a silica flat cell that was cooled in dry ice/ethanol. EPR spectra were recorded on either a Bruker ER 200D (for  $T = 133 - 293$  K with liquid N<sub>2</sub> cooling) or Bruker ESP 300e (for  $T = 6$  K with liquid He cooling). Both spectrometers employed rectangular TE<sub>102</sub> cavities with the modulation frequency set at 50-100 kHz and microwave power between 20  $\mu$ W - 20 mW. EPR simulations were performed using the Bruker computer software, WINEPR SimFonia. Other general procedures were as previously described.<sup>46-50</sup>

**X-ray structural determinations** are as described in Chapter 2. The crystal data collection and processing parameters are given in Table A4 (Appendix).

**Theoretical Calculations.** Density functional (DFT) calculations were performed using the Q-Chem 3.0 software package<sup>51</sup> and molecular structures were optimized using the B3LYP functional.<sup>44</sup> The 3-21G basis set was used for all atoms except Ru, for which the SRSC basis and pseudopotential<sup>52</sup> were employed. The exchange-correlation quadrature used the SG-0 grid<sup>53</sup> on all atoms except Ru, for which the larger SG-1 grid<sup>54</sup> was used. Natural bond orbital (NBO) analysis of atomic charges and spin densities were obtained from orbitals computed using the B3LYP functional; for these calculations, a large, all-electron basis containing 90 basis functions<sup>55</sup> was used for Ru, the STO-3G basis for H atoms, and the 6-31G\* basis for all other atoms. To compute spin densities at the nuclei, it is common to sample the density using a delta function operator. However, because this can lead to inaccurate results when used with Gaussian basis sets, we have employed the Rassolov-Chipman operator and the range parameter  $r_0 = 0.25$  au.<sup>56, 57</sup>

**Oxidation of [Cp\*RuCl<sub>2</sub>(S<sub>2</sub>CNMe<sub>2</sub>)] (21a)**

**(i) With NO(PF<sub>6</sub>).** To a stirred purple solution of **21a** (25mg, 0.06 mmol) in *ca.* 5 mL of MeCN was added NO(PF<sub>6</sub>) (10 mg, 0.06 mmol, 1 mol equiv). The solution turned from purple to red instantly. After 5 min, the resultant solution was concentrated to *ca.* 2 mL and ether (3 mL) added. Subsequent cooling at -30 °C for 30 min gave a microcrystalline solid of **21a** (11 mg, 0.03 mmol, 44 % recovery). The mother liquor was concentrated to *ca.* 2 mL, followed by addition of ether (*ca.* 3 mL) and subsequent cooling at -30 °C for a day afforded a red microcrystalline solid of [Cp\*Ru(MeCN)<sub>2</sub>(S<sub>2</sub>CNMe<sub>2</sub>)](PF<sub>6</sub>)<sub>2</sub> (**23**) (7 mg, 0.01 mmol, 16 %), leaving a residual red oil, which showed the presence of only complex **23** in its <sup>1</sup>H NMR spectrum. Diffraction-quality single crystals were obtained at -30 °C as red plates from an acetonitrile solution layered with ether after a day.

Data for **23**. Anal. Found: C, 27.7; H, 3.9; N, 5.3; S, 8.9. Calcd. for C<sub>17</sub>H<sub>27</sub>F<sub>12</sub>N<sub>3</sub>P<sub>2</sub>Ru<sub>1</sub>S<sub>2</sub>: C, 28.0; H, 3.7; N, 5.8; S, 8.8 %. <sup>1</sup>H NMR (δ, CD<sub>3</sub>CN): 1.49 (s, 15H, Me<sub>5</sub>C<sub>5</sub>), 1.95 (s, CH<sub>3</sub>CN, overlapping with solvent peak), 3.29 (s, 6H, 2CH<sub>3</sub>). <sup>13</sup>C{<sup>1</sup>H} NMR (δ, CD<sub>3</sub>CN): 8.93 (Me<sub>5</sub>C<sub>5</sub>), 38.6 (CH<sub>3</sub>), 114.1 (Me<sub>5</sub>C<sub>5</sub>), 200.7 (CS). IR (KBr, cm<sup>-1</sup>): ν(C≡N) 2322w 2297w; ν(C-N) 1580m; ν(C-S) 1082w 1019m. FAB<sup>+</sup> MS: *m/z* 356 [M - 2MeCN]<sup>+</sup>; FAB<sup>-</sup> MS: *m/z* 145 [PF<sub>6</sub>]. ESI<sup>+</sup> MS: *m/z* 397 [M-MeCN]<sup>+</sup> 356 [M - 2MeCN]<sup>+</sup>, ESI<sup>+</sup> MS: *m/z* 145 [PF<sub>6</sub>].

A repeat of the reaction of **21a** (43 mg, 0.10 mmol), with two mol equiv of NO(PF<sub>6</sub>) (35 mg, 0.20 mmol), followed by a similar workup, gave a microcrystalline solid of **23** (36 mg, 0.05 mmol, 49.4 %), and a red mother liquor which showed the presence of only complex **23** in its <sup>1</sup>H NMR spectrum.

The reaction of **21a** (21 mg, 0.05 mmol), with two mol equiv of NO(PF<sub>6</sub>) (18 mg, 0.10 mmol) was repeated in 10 mL of dichloromethane at 0 °C. The purple color of the

solution gradually assumed a reddish tinge after 20 min, and then finally turned green after a further 10 min. Upon evacuation to dryness, a green oil was obtained. No attempt was made to characterize the green oil.

(ii) **With [(4-Br-C<sub>6</sub>H<sub>4</sub>)<sub>3</sub>N](SbCl<sub>6</sub>).** 10 mL of dichloromethane was added to a mixture of **21a** (21 mg, 0.05 mmol) and (4-Br-C<sub>6</sub>H<sub>4</sub>)<sub>3</sub>N](SbCl<sub>6</sub>) (41 mg, 0.05 mmol), with stirring. Red solids slowly precipitated out of the dark blue solution after ca. 30 min. The mixture was allowed to stir overnight; the supernatant was then light blue. The product mixture was filtered and the red solid of [Cp\**Ru*Cl(S<sub>2</sub>CNMe<sub>2</sub>)<sub>2</sub>](SbCl<sub>6</sub>)<sub>2</sub> (**24**) (20 mg, 0.03 mmol, 55.0%) was washed with diethyl ether (3 x 5 mL) and collected. Diffraction-quality single crystals were obtained at -30 °C as red plates by slow diffusion of layers of pre-cooled solutions of (4-Br-C<sub>6</sub>H<sub>4</sub>)<sub>3</sub>N](SbCl<sub>6</sub>) (10 mg in 2 mL in dichloroethane) over **21a** (5 mg in 1 mL in dichloromethane) over 2-3 days.

Data for **24**. Anal. Found: C, 21.1; H, 2.9; N, 1.9; S, 8.5. Calcd. for C<sub>26</sub>H<sub>42</sub>Cl<sub>14</sub>N<sub>2</sub>Ru<sub>2</sub>S<sub>4</sub>Sb<sub>2</sub>: C, 21.5; H, 2.9; N, 1.9; S, 8.8 %. IR (KBr, cm<sup>-1</sup>): 1561s 1543.2m (ν<sub>C-N</sub>); 1042w 1020m (ν<sub>C-S</sub>). Complex **24** was initially sparingly soluble in deuterated MeCN, but dissolved completely after ultrasonication for ca. 20 min to give a light red solution. The <sup>1</sup>H NMR spectrum of this solution indicated the presence of complex **23** while that of the blue supernatant indicated the presence of the starting material, **21a**, which was not recovered.

## References

1. DuBois, M. R., *Chem. Rev.* **1989**, 89 (1), 1-9.
2. Holm, R. H.; Ciurli, S.; Weigel, J. A., *Prog. Inorg. Chem.* **1990**, 38, 1-74.
3. Shibahara, T., *Coord. Chem. Rev.* **1993**, 123 (1-2), 73-147.
4. Sanchez-Delgado, R. A., *J. Mol. Catal.* **1994**, 86 (1-3), 287-307.
5. Stiefel, E. I.; Matsumoto, K.; Editors, *Transition Metal Sulfur Chemistry: Biological and Industrial Significance [In: ACS Symp. Ser., 1996; 653]*. **1996**; p 358 pp.
6. Burgess, B. K.; Lowe, D. J., *Chem. Rev.* **1996**, 96 (7), 2983-3011.
7. Sellmann, D.; Sutter, J., *Acc. Chem. Res.* **1997**, 30 (11), 460-469.
8. Mathur, P., *Adv. in Organomet. Chem.* **1997**, 41, 243-314.
9. Bianchini, C.; Meli, A., *Acc. Chem. Res.* **1998**, 31 (3), 109-116.
10. Heard, P. J., *Prog. Inorg. Chem.* **2005**, 53, 1-69.
11. Hogarth, G.; Faulkner, S., *Inorg. Chim. Acta* **2006**, 359 (3), 1018-1022.
12. Bond, A. M.; Martin, R. L., *Coord. Chem. Rev.* **1984**, 54, 23-98.
13. Webster, R. D.; Heath, G. A.; Bond, A. M., *J. Chem. Soc., Dalton Trans.* **2001**, (21), 3189-3195.
14. Tay, E. P. L.; Kuan, S. L.; Leong, W. K.; Goh, L. Y., *Inorg. Chem.* **2007**, 46 (4), 1440-1450.
15. Hogarth, G., *Prog. Inorg. Chem.* **2005**, 53, 71-561.
16. Wilczewski, T.; Bochenska, M.; Biernat, J. F., *J. Organomet. Chem.* **1981**, 215 (1), 87-96.
17. Rao, K. M.; Mishra, L.; Agarwala, U. C., *Polyhedron* **1987**, 6 (6), 1383-90.
18. McCubbin, Q. J.; Stoddart, F. J.; Welton, T.; White, A. J. P.; Williams, D. J., *Inorg. Chem.* **1998**, 37 (15), 3753-3758.
19. Kovacs, I.; Lebuis, A.-M.; Shaver, A., *Organometallics* **2001**, 20 (1), 35-41.
20. Pasek, E. A.; Straub, D. K., *Inorg. Chem.* **1972**, 11 (2), 259-63.
21. Golding, R. M.; Harris, C. M.; Jessop, K. J.; Tennat, W. C., *Aust. J. Chem.* **1972**, 25 (12), 2567-2576.
22. Given, K. W.; Mattson, B. M.; Pignolet, L. H., *Inorg. Chem.* **1976**, 15 (12), 3152-6.
23. Mattson, B. M.; Heiman, J. R.; Pignolet, L. H., *Inorg. Chem.* **1976**, 15 (3), 564-71.
24. Miessler, G. L.; Pignolet, L. H., *Inorg. Chem.* **1979**, 18 (1), 210-13.
25. Bennett, M. A.; Khan, K.; Wenger, E., In *Comprehensive Organometallic Chemistry II*, Abel, E. W.; Stone, F. G. A.; Wilkinson, G.; Shriver, D. F.; Bruce, M. I., Eds. Pergamon: Oxford, **1995**; Vol. 7.
26. Che, C.-M.; Lau, T.-C., In *Comprehensive Coordination Chemistry II*, McCleverty, J. A.; Meyer, T. J.; Constable, E. C.; Dilworth, J. R., Eds. Elsevier: Oxford, **2004**; Vol. 5, pp 800-809.
27. Weil, J. A.; Bolton, J. R.; Wertz, J. E., In *Electron Paramagnetic Resonance: Elementary Theory and Practical Applications*, Wiley: **1994**; Vol. New York, pp 320-327.
28. Rieger, P. H., *Coord. Chem. Rev.* **1994**, 135/136, 203-86.
29. Pruchnik, F. P.; Galdecka, E.; Galdecki, Z.; Kowalski, A., *Polyhedron* **1999**, 18 (15), 2091-2097.
30. Gugger, P. A.; Willis, A. C.; Wild, S. B.; Heath, G. A.; Webster, R. D.; Nelson, J. H., *J. Organomet. Chem.* **2002**, 643-644, 136-153.
31. Dengel, A. C.; Griffith, W. P., *Inorg. Chem.* **1991**, 30 (4), 869-871.

32. Kaim, W.; Ernst, S.; Kohlmann, S.; Welkerling, P., *Chem. Phys. Lett.* **1985**, *118* (4), 431-434.
33. Krejčík, M.; Zalis, S.; Klima, J.; Sykora, D.; Matheis, W.; Klein, A.; Kaim, W., *Inorg. Chem.* **1993**, *32* (15), 3362-3368.
34. Poppe, J.; Moscherosch, M.; Kaim, W., *Inorg. Chem.* **1993**, *32* (12), 2640-2643.
35. Ye, S.; Sarkar, B.; Duboc, C.; Fiedler, J.; Kaim, W., *Inorg. Chem.* **2005**, *44* (8), 2843-2847.
36. Sun, Y.; DeArmond, M. K., *Inorg. Chem.* **1994**, *33* (9), 2004-8.
37. Samuels, A. C.; DeArmond, M. K., *Inorg. Chem.* **1995**, *34* (22), 5548-51.
38. Araujo, C. S.; Drew, M. G. B.; Felix, V.; Jack, L.; Madureira, J.; Newell, M.; Roche, S.; Santos, T. M.; Thomas, J. A.; Yellowlees, L., *Inorg. Chem.* **2002**, *41* (8), 2250-2259.
39. Chanda, N.; Paul, D.; Kar, S.; Mobin, S. M.; Datta, A.; Puranik, V. G.; Rao, K. K.; Lahiri, G. K., *Inorg. Chem.* **2005**, *44* (10), 3499-3511.
40. Lever, A. B. P., In *Inorganic Electronic Spectroscopy*, Second ed.; Elsevier: Amsterdam, **1984**.
41. Connelly, N. G.; Geiger, W. E., *Chem. Rev. (Washington, D. C.)* **1996**, *96* (2), 877-910.
42. Bond, A. M.; Colton, R.; Mann, D. R., *Inorg. Chem.* **1990**, *29* (23), 4665-4671.
43. Pauling, L. in *The Nature Of The Chemical Bond*. 3rd ed.; Cornell University Press: Oxford, **1960**.
44. Stephens, P. J.; Devlin, F. J.; Chabalowski, C. F.; Frisch, M. J., *J. Phys. Chem.* **1994**, *98* (45), 11623-7.
45. Webster, R. D., *Magn. Reson. Chem.* **2000**, *38* (11), 897-906.
46. Shin, R. Y. C.; Tan, G. K.; Koh, L. L.; Goh, L. Y.; Webster, R. D., *Organometallics* **2004**, *23* (26), 6108-6115.
47. Shin, R. Y. C.; Tan, G. K.; Koh, L. L.; Vittal, J. J.; Goh, L. Y.; Webster, R. D., *Organometallics* **2005**, *24* (4), 539-551.
48. Shin, R. Y. C.; Teo, M. E.; Leong, W. K.; Vittal, J. J.; Yip, J. H. K.; Goh, L. Y.; Webster, R. D., *Organometallics* **2005**, *24* (7), 1483-1494.
49. Shin, R. Y. C.; Ng, S. Y.; Tan, G. K.; Koh, L. L.; Khoo, S. B.; Goh, L. Y.; Webster, R. D., *Organometallics* **2004**, *23* (3), 547-558.
50. Kuan, S. L.; Leong, W. K.; Goh, L. Y.; Webster, R. D., *Organometallics* **2005**, *24* (19), 4639-4648.
51. Shao, Y.; Molnar, L. F.; Jung, Y.; Kussmann, J.; Ochsenfeld, C.; Brown, S. T.; Gilbert, A. T. B.; Slipchenko, L. V.; Levchenko, S. V.; O'Neill, D. P.; DiStasio, R. A., Jr.; Lochan, R. C.; Wang, T.; Beran, G. J. O.; Besley, N. A.; Herbert, J. M.; Lin, C. Y.; Van Voorhis, T.; Chien, S. H.; Sodt, A.; Steele, R. P.; Rassolov, V. A.; Maslen, P. E.; Korambath, P. P.; Adamson, R. D.; Austin, B.; Baker, J.; Byrd, E. F. C.; Dachsel, H.; Doerksen, R. J.; Dreuw, A.; Dunietz, B. D.; Dutoi, A. D.; Furlani, T. R.; Gwaltney, S. R.; Heyden, A.; Hirata, S.; Hsu, C.-P.; Kedziora, G.; Khalliulin, R. Z.; Klunzinger, P.; Lee, A. M.; Lee, M. S.; Liang, W.; Lotan, I.; Nair, N.; Peters, B.; Proynov, E. I.; Pieniazek, P. A.; Rhee, Y. M.; Ritchie, J.; Rosta, E.; Sherrill, C. D.; Simmonett, A. C.; Subotnik, J. E.; Woodcock, H. L., III; Zhang, W.; Bell, A. T.; Chakraborty, A. K.; Chipman, D. M.; Keil, F. J.; Warshel, A.; Hehre, W. J.; Schaefer, H. F., III; Kong, J.; Krylov, A. I.; Gill, P. M. W.; Head-Gordon, M., *Phys. Chem. Chem. Phys.* **2006**, *8* (27), 3172-3191.

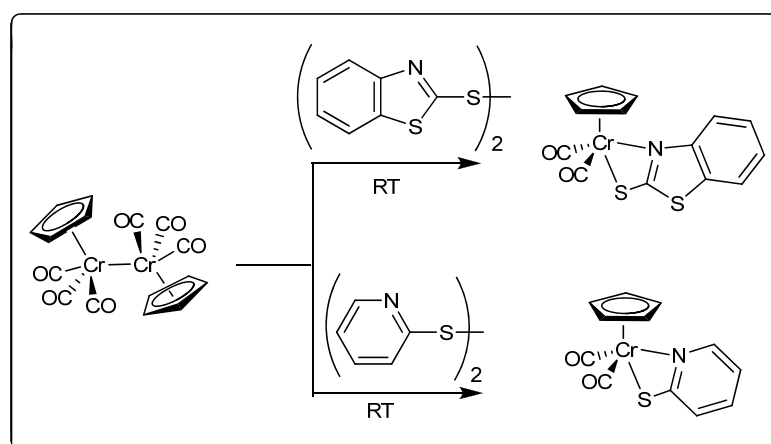
52. Andrae, D.; Haeussermann, U.; Dolg, M.; Stoll, H.; Preuss, H., *Theor. Chim. Acta* **1990**, 77 (2), 123-141.
53. Chien, S.-H.; Gill, P. M. W., *J. Comput. Chem.* **2006**, 27 (6), 730-739.
54. Gill, P. M. W.; Johnson, B. G.; Pople, J. A., *Chem. Phys. Lett.* **1993**, 209 (5-6), 506-512.
55. Poirier, R.; Kari, R.; Csizmadia, I. G., *Handbook of Gaussian basis sets*. Elsevier: New York, **1995**.
56. Rassolov, V. A.; Chipman, D. M., *J. Chem. Phys.* **1996**, 105 (4), 1470-1478.
57. Rassolov, V. A.; Chipman, D. M., *J. Chem. Phys.* **1996**, 105 (4), 1479-1491.

## Chapter 6. Reactivity of $[\text{Cp}'\text{Ru}(\text{CO})_2]_2$ ( $\text{Cp}' = \text{C}_5\text{H}_5$ or $\text{C}_5\text{Me}_5$ ) towards disulfide ligands

There have been many reports in the literature which showed that organotransition complexes, particularly the cyclopentadienyl carbonyl complexes of Group 6 metals, are capable of cleaving S-S bonds in various organic disulfides.

Goh and coworkers have studied extensively the role of  $[\text{CpCr}(\text{CO})_3]_2$  in the homolytic cleavage of non-metal-non-metal bond of Group 15 and 16 elements.<sup>1</sup> Continued work with this group has shown that the  $[\text{CpCr}(\text{CO})_3]_2$  is also effective in cleaving S-S bonds in a variety of acyclic organic complexes, such as dithiocarbamates and also heterocyclic disulfides. For instance, the  $[\text{CpCr}(\text{CO})_2((\kappa^2\text{-S,N})\text{-SR})]$  containing heterocyclic thiolates can be readily obtained from the reaction of  $[\text{CpCr}(\text{CO})_3]_2$  and the corresponding disulfides at room temperature, with no observation of the formation of the  $[\text{CpCr}(\text{CO})_3((\kappa^1\text{-S})\text{-SR})]$  complexes (Scheme 6.1).<sup>2</sup>

**Scheme 6.1.** Syntheses of  $[\text{CpCr}(\text{CO})_2((\kappa^2\text{-S, N-SR})]$ .

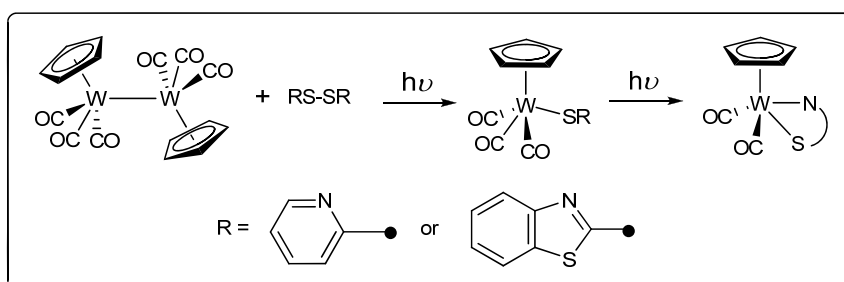


Abrahamson and coworkers reported in 1987, the photolytic and thermal reactions of  $[\text{CpW}(\text{CO})_3]_2$  ( $\text{Cp}=\text{C}_5\text{H}_5$ ) with the 2, 2'-dithiodipyridine and 2,2'-dibenzothiazolyl disulfide to yield the corresponding  $[\text{CpW}(\text{CO})_3((\kappa^1\text{-S})\text{SR})]$



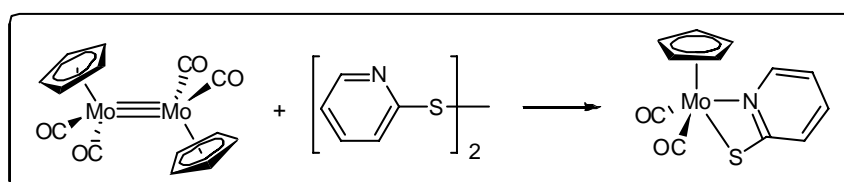
complexes (Scheme 6.2).<sup>3</sup> The  $[\text{CpW}(\text{CO})_3((\kappa^1\text{-S})\text{SR})]$  complexes will undergo decarbonylation to give the S, N-chelated products,  $[\text{CpW}(\text{CO})_2((\kappa^2\text{-S,N})\text{SR})]$  complexes (Scheme 6.2).<sup>20</sup>

**Scheme 6.2.** CpW carbonyl complexes of thiopyridine and thiobenzothiazole.



The  $[\text{CpMo}(\text{CO})_2((\kappa^2\text{-S,N})\text{-SNC}_5\text{H}_4)]$  complex was isolated by Hu and co-workers, from the reaction of  $[\text{CpMo}(\text{CO})_2]_2$  with 2,2'-dithiodipyridine in toluene at room temperature, where the Mo-Mo triple bond was cleaved (Scheme 6.3).<sup>4</sup> The  $[\text{CpMo}(\text{CO})_2((\kappa^2\text{-S,N})\text{-S}_2\text{NC}_7\text{H}_4)]$  complex is also known.<sup>5</sup>

**Scheme 6.3.** Synthesis of  $[\text{CpMo}(\text{CO})_2(\kappa^2\text{-SNC}_5\text{H}_4)]$ .

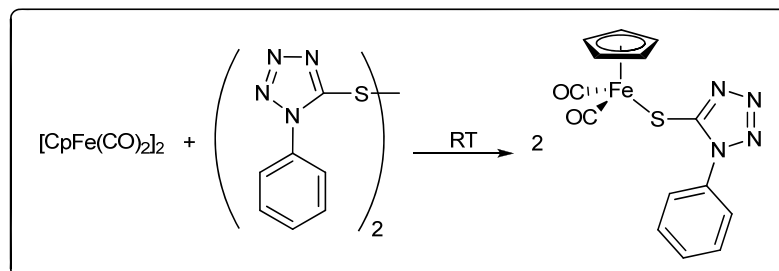


In these examples, the reactions of the  $[\text{CpM}(\text{CO})_3]_2$  (M=Cr or W) towards disulfide proceeded via the attack of the radical,  $[\text{CpM}(\text{CO})]$ , on the organic disulfides to give the products.

Recently, our group has shown that the cyclopentadienyliron carbonyl complex,  $[\text{CpFe}(\text{CO})_2]_2$  can react with 5,5'-dithiobis(1-phenyl-1H-tetrazole), (STz)<sub>2</sub>, at ambient temperature to give  $\text{CpFe}(\text{CO})_2[(\kappa^1\text{-S})(\text{STz})]$  in high yield (Scheme 6.4).<sup>6</sup> The  $[\text{CpFe}(\text{CO})_2]_2$  complex is known to form radical in solution, similar to the group

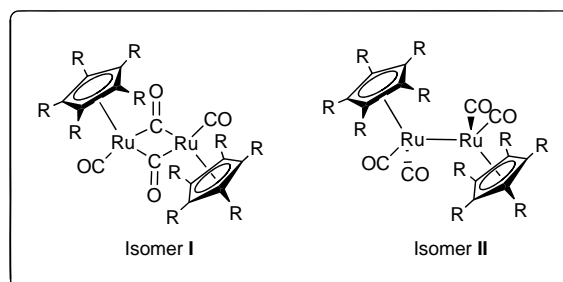
6  $[\text{CpM}(\text{CO})_3]_2$  complexes, though at a slower rate. Hence, the reactivity of the  $[\text{CpFe}(\text{CO})_2]_2$  complex towards disulfides could possibly proceed via a radical attack on the disulfide bonds.

**Scheme 6.4.** Reaction of  $[\text{CpFe}(\text{CO})_2]_2$  with  $(\text{STz})_2$ .



Similarly, the reported observation of the formation of radicals upon photolysis of a toluene solution of the nonbridged form of **25a** as the primary process<sup>7</sup> suggests that such species could exhibit similar reactivity to disulfides as for group 6 cyclopentadienyl metal carbonyl complexes,  $[\text{CpM}(\text{CO})_3]_2$  ( $\text{M} = \text{Cr}, \text{Mo}$  and  $\text{W}$ ).

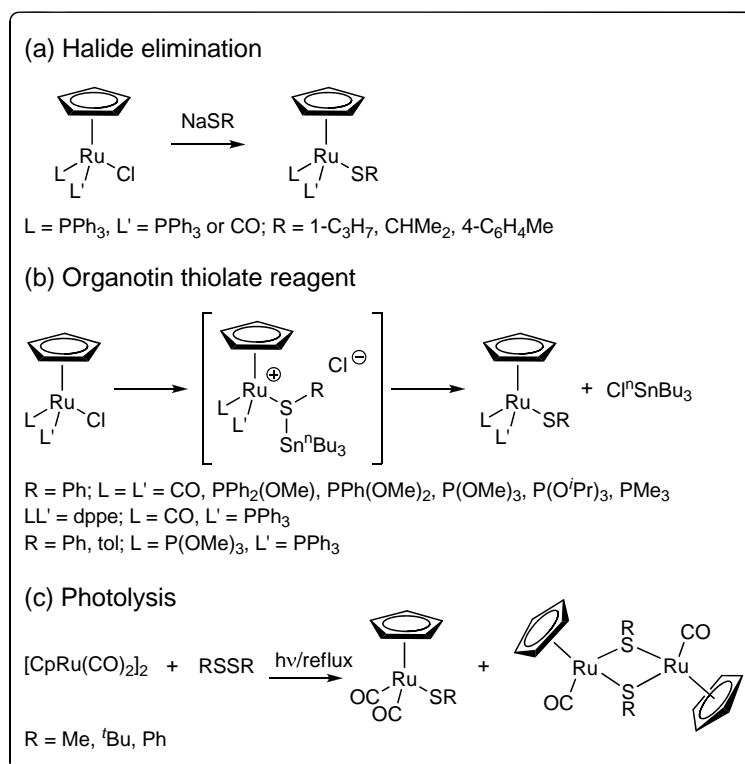
**Chart 6.1.** Isomeric forms of **25** in solution



The last decade has witnessed the development of half-sandwich ruthenium complexes as anticancer drugs. These are mainly (arene)ruthenium or cyclopentadienylruthenium complexes with amines or water soluble phosphines as co-ligands.<sup>8-19</sup> So far, there has been no report on the anticancer activity of half-sandwich ruthenium complexes with carbonyl or heterocyclic thiolates as co-ligands, probably due to a lack of a high yield synthetic preparation of these complexes.

Despite the discovery of CpRu-thiolate carbonyl complexes since more than 20 years ago, such complexes remained relatively scarce. Only a few ruthenium carbonyl complexes containing heterocyclic thiolates have been reported<sup>20</sup> Among the different classes of Ru-thiolate complexes, cyclopentadienyl ( $\eta^5\text{-C}_5\text{H}_5$ , Cp) complexes have been extensively studied with phosphines as co-ligands. In most cases, the organoruthenium thiolate complexes are prepared via halide elimination of the halogeno complexes using thiolate salts, to give  $\text{Cp}^*\text{Ru}(\text{L})(\text{L}')\text{SR}$  complexes. (Scheme 6.5(a)).<sup>21, 22</sup>

**Scheme 6.5.** Preparation of Cp<sup>\*</sup>Ru-thiolate complexes.



Some pentamethylcyclopentadienyl ( $\eta^5\text{-C}_5\text{Me}_5$ , Cp<sup>\*</sup>) analogues have also been synthesized using the same synthetic methodology.<sup>23,24</sup> Organotin thiolate reagents have also been employed in the synthesis of ruthenium thiolate complexes (Scheme 6.5(b)).<sup>25</sup> In contrast, there are few examples of half-sandwich Ru-thiolate complexes

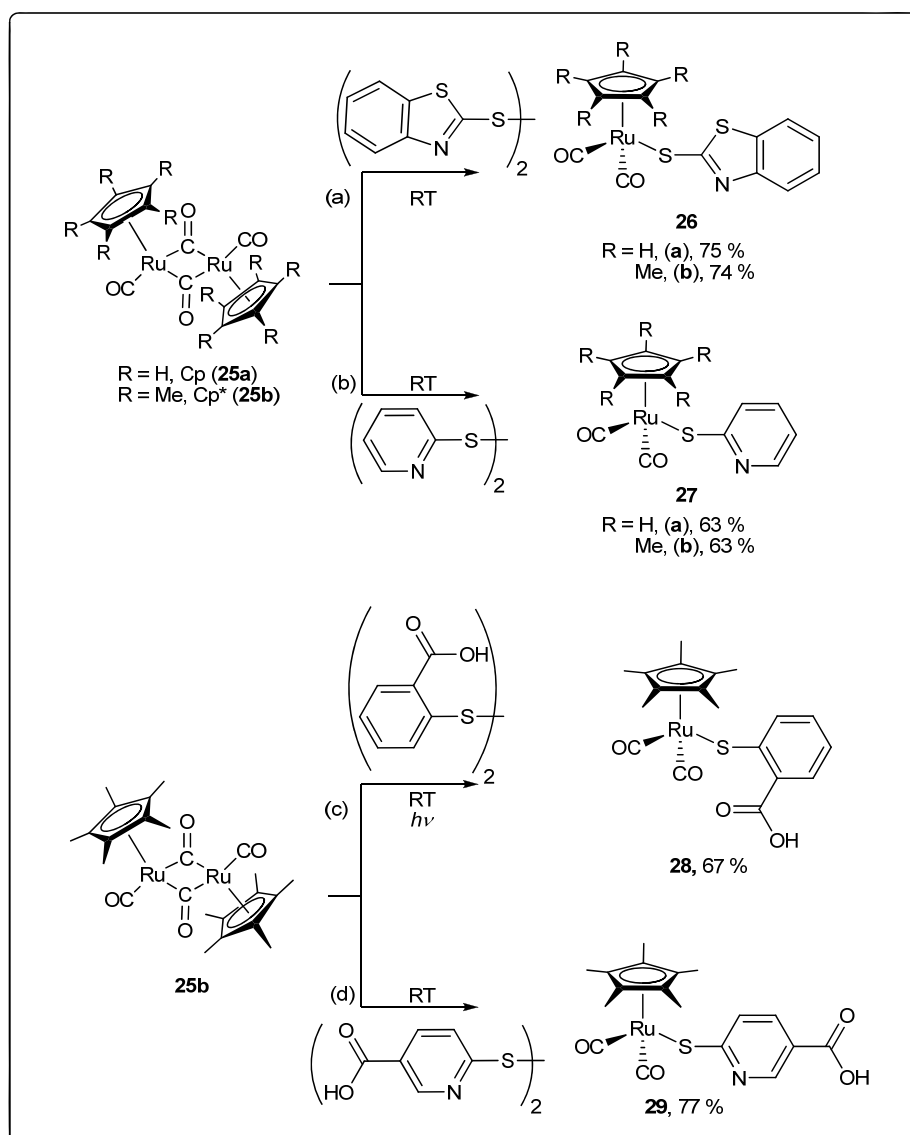
consisting only of CO as co-ligands. These include a series of CpRu carbonyl thiolate complexes,  $\text{CpRu}(\text{CO})_2(\text{SR})$  and  $[\text{CpRu}(\text{CO})(\mu_2\text{-SR})]_2$ , via photolysis or thermal reaction of  $[\text{CpRu}(\text{CO})_2]_2$  and a corresponding disulfide,  $\text{S}_2\text{R}_2$  (Scheme 6.5(c)),<sup>26</sup> and  $\text{CpRu}(\text{CO})_2(\text{SPh})$  via a salt elimination reaction.<sup>25</sup> The synthetic routes represented by scheme 6.5c is atom economical and is appealing for the synthesis of  $\text{Cp}'\text{Ru}(\text{CO})_2(\text{SR})$  complexes.

Since the  $[\text{Cp}'\text{Ru}(\text{CO})_2]_2$  ( $\text{Cp}' = \text{C}_5\text{H}_5$ , **25a**;  $\text{C}_5\text{Me}_5$ , **25b**) complexes and their metal complexes are known to form radicals in solution and may exhibit similar activity to the group 6 cyclopentadienyl metal carbonyl complexes,  $[\text{CpM}(\text{CO})_3]_2$  ( $\text{M} = \text{Cr}, \text{Mo}$  and  $\text{W}$ ) and at the same time, heterocyclic thiolates and their metal complexes are known to exhibit antitumour and antimicrobial properties,<sup>27-33</sup> it occurred to us that it is possible to develop a synthetic method to yield complexes of the type,  $[\text{Cp}'\text{Ru}(\text{CO})_2(\text{SR})]$  ( $\text{Cp}' = \text{C}_5\text{H}_5$  or  $\text{C}_5\text{Me}_5$ ,  $\text{SR} = \text{heterocyclic thiolate}$ ) and evaluate these complexes for their anticancer properties. In addition, an investigation of S-S bond cleavage in a protein, specifically lysozyme, using  $[\text{CpRu}(\text{CO})_2]_2$  (**25a**) will also be investigated.

### 6.1. Reaction of $[\text{Cp}'\text{Ru}(\text{CO})_2]_2$ ( $\text{Cp}' = \text{C}_5\text{H}_5$ or $\text{C}_5\text{Me}_5$ ) with heterocyclic disulfides

The ambient temperature reaction of  $[\text{Cp}'\text{Ru}(\text{CO})_2]_2$  ( $\text{Cp}' = \text{Cp}$  (**25a**),  $\text{Cp}^*$  (**25b**)) with one molar equivalent of disulfide  $(\text{SR})_2$  (2,2'-dithiobis(benzothiazole) ( $\text{SBzt}$ )<sub>2</sub>; 2,2'-dithiodipyridine ( $\text{SPy}$ )<sub>2</sub>) led to the compounds **26** and **27**, respectively, in moderate to high yields (Scheme 6.6).

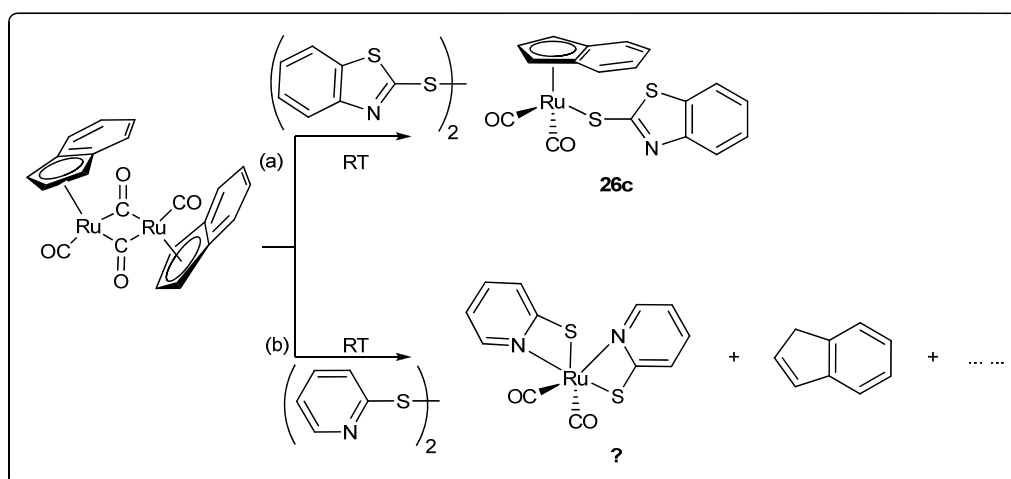
**Scheme 6.6.** Reaction of  $[\text{Cp}'\text{Ru}(\text{CO})_2]_2$  with (a)  $(\text{SBzt})_2$ , (b)  $(\text{SPy})_2$ , (c)  $(\text{SBzCOOH})_2$  and (d)  $(\text{SPyCOOH})_2$ .



The reaction of **25** with heterocyclic disulfides was found to give single product, and there are no side product observed. The reactions are cleaner and occurred at milder condition than those reported by Knox and coworkers, in which 5-15 fold excess of the disulfides  $S_2R_2$  ( $R=Me, Bu^t, CH_2Ph$  or  $Ph$ ) was needed, giving a mixture of products. On the other hand, the reaction of  $[Cp^*Ru(CO)_2]_2$  (**25b**) with 2,2'-dithiobenzoic acid  $(SBzCOOH)_2$  and 6,6'-dithiodinicotinic acid,  $(SPyCOOH)_2$ , required photoactivation, giving  $Cp^*Ru(CO)_2(SBzCOOH)$  (**28**) and  $Cp^*Ru(CO)_2(SPycOOH)$  (**29**) in moderate yield (Scheme 6.6).

The reactivity of **25a** and **25b** towards to  $(SBzt)_2$  is similar to that of  $[(Ind)Ru(CO)_2]_2$  which afforded the indenyl analogue, **26c** (Scheme 6.7a) but differ from their reaction with  $(SPy)_2$  where  $[(Ind)Ru(CO)_2]_2$  failed to react under similar conditions (Scheme 6.8b).<sup>34</sup> Instead, under photoactivation the reaction afforded a mixture of products, the major component of which was the complex  $[Ru(CO)_2(Spy)_2]$ ,<sup>35</sup> in which the indenyl ligand has been displaced (Scheme 6.7b).

**Scheme 6.7.** Reaction of  $[(Ind)Ru(CO)_2]_2$  with (a)  $(SBzt)_2$  and (b)  $(SPy)_2$ .



The difference between the  $Cp^*Ru$  system and the  $IndRu$  system can be attributed to the lability of the indenyl ligand, resulting in its slippage in the presence of strongly

chelating ligands. In comparison, we have found that  $[\text{TpRu}(\text{CO})_2]_2$  failed to react with both  $(\text{SBzt})_2$  and  $(\text{SPy})_2$  at RT after 2 days or photolysis at 365nm over a period of 2 days (Appendix).

All the complexes, **26-29**, showed two terminal CO stretches in the region 2045-1957  $\text{cm}^{-1}$ , consistent with those reported for the  $\text{CpRu}(\text{CO})_2(\kappa^1\text{-SR})$  complexes prepared by Knox and coworkers. Both complexes **28** and **29** show two strong signals at 1707-1675  $\text{cm}^{-1}$  for the free carboxylic groups. The  $\kappa^1\text{-S}$  coordination mode has been confirmed by single x-ray structure studies for **26b**, **27a**, **27b**, **28** and **29**. A comparison of the  $\nu_{\text{C=O}}$  of these complexes show that the electron donating ability of  $\text{SPy} > \text{SBzt} > \text{SPyCOOH} > \text{SBzCOOH}$  (Table 6.1). The order of electron donating ability for the dienyls is in the order  $\text{Cp}^* > \text{Cp} > \text{Ind}$ .

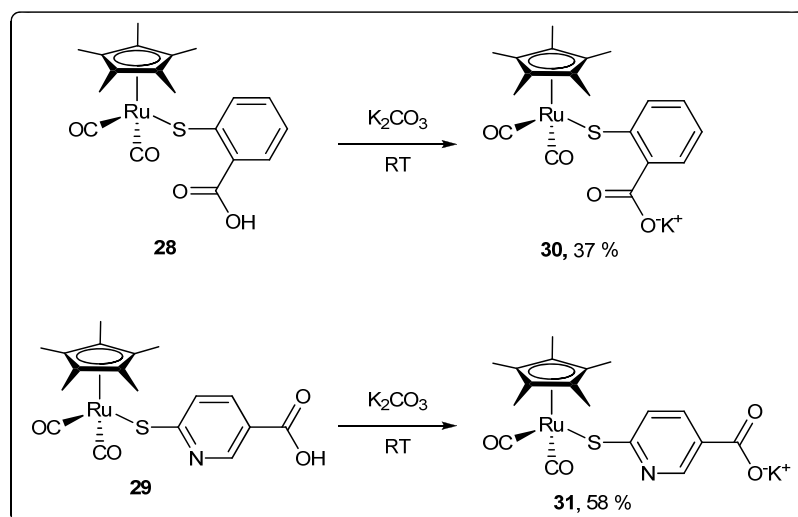
**Table 6.1.**  $\nu_{\text{C=O}}$  for complexes **26** and **27**.

	<b>26a</b>	<b>26b</b>	<b>26c</b>	<b>27a</b>
$\nu_{\text{CO}} (\text{cm}^{-1})$	2045, 1996	2020, 1965	2045, 1993	2029, 1985
	<b>27b</b>	<b>28</b>	<b>29</b>	
$\nu_{\text{CO}} (\text{cm}^{-1})$	2010, 1957	2024, 1981	2021, 1976	

The carboxylic acid groups in **28** and **29** can be deprotonated with  $\text{K}_2\text{CO}_3$  to form the respective potassium salts,  $\text{K}[\text{Cp}^*\text{Ru}(\text{CO})_2(\text{SBzCOO})]$  (**30**) and  $\text{K}[\text{Cp}^*\text{Ru}(\text{CO})_2(\text{SPyCOO})]$  (**31**), in 37 % and 58 % yields, respectively (Scheme 6.8). The IR spectrum of the two complexes showed two strong signals in the range 2025-1941  $\text{cm}^{-1}$  for the terminal carbonyls, and stretches in the range 1584-1562  $\text{cm}^{-1}$ , confirming the conversion of the free carboxylic acids to the carboxylates. We had previously reported the stabilization of Ag nanoparticles by triosmium clusters with a ligand containing a free carboxylic acid. Hence, complexes **28** and **29** were used in a study to stabilize Ag nanoparticles formed from reduction of  $\text{AgNO}_3$ . However, a silver mirror was formed and complexes **28** and **29** decomposed to brown solids with

no M-C≡O stretch (Appendix). As expected, complexes **30** and **31** were found to be water-soluble.

**Scheme 6.8.** Conversion of Cp\*Ru(CO)<sub>2</sub>(SRCOOH) complexes to water-soluble species.



All four complexes **28-31** were tested for catalytic activity in the hydration of terminal alkynes, specifically phenylacetylene and monitored by <sup>1</sup>H NMR. However, none of the complexes exhibit any catalytic activity (Appendix).

The molecular structure of **26b**, together with the general numbering scheme for complexes **27a**, **27b**, **28** and **29** are shown in Figure 6.1. These complexes are the first examples of [Cp'Ru(CO)<sub>2</sub>(SR)] to be structurally characterized. Attempts to obtain X-ray diffraction-quality crystals of **26a**, **30** and **31** were unsuccessful, as fine powders were formed in all cases. The structures of the five complexes are markedly similar, possessing three-legged piano-stool coordination at Ru, which is coordinated to a monodentate heterocyclic thiolate and two terminal CO ligands. Selected bond parameters are given in Table 6.2.

The C-O bond distances (1.118(7)-1.150(7) Å) in all the five complexes are intermediate between that of C≡O (1.07 Å) and C=O (1.21 Å). The longer C-O



distance of **27b** versus that of **27a**, is consistent with the greater electron-donating capability of Cp, as also evident in the trend of  $\nu_{\text{CO}}$  in the IR spectrum. Similarly, the order of the bond distances of **27b**>**26b**>**29**>**28**, implies that the electron donating strength of the heterocyclic ligands increases in the order: SPy>SBzt>SPyCOOH>SBzCOOH, as indicated by IR data.

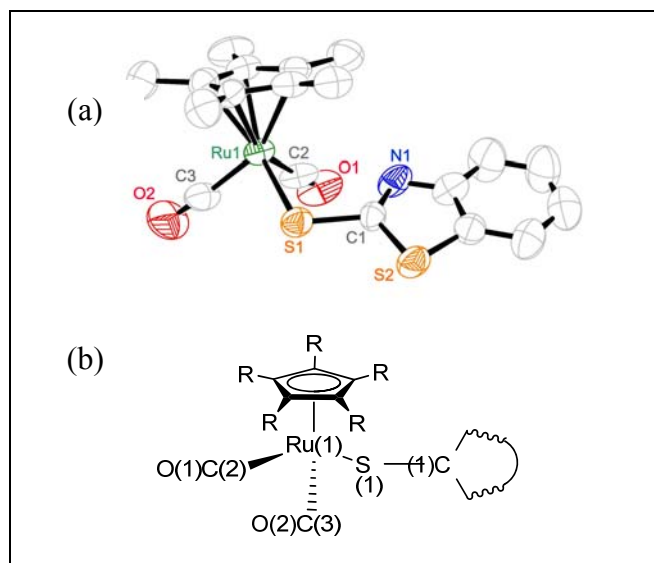


**Figure 6.1.** (a) ORTEP plot of **26b** (Selected view which omits the disorder in the complex). Thermal ellipsoids are drawn at the 50% probability level and all hydrogen atoms are omitted for clarity. (b) General numbering scheme for Cp'Ru(CO)<sub>2</sub>(SR) complexes.

**Table 6.2.** Selected bond lengths (Å) and bond angles (°).

	<b>26b</b>	<b>27a</b>	<b>27b</b>	<b>28</b>	<b>29</b>
<b>Bond Distance (Å)</b>					
Ru(1)-S(1)	2.3953(18)	2.368(5)	2.3973(17)	2.4207(14)	2.3877(10)
S(1)-C(1)	1.832(19)	1.749(2)	1.755(6)	1.788(6)	1.741(3)
C(2)-O(1)	1.143(7)	1.137(4)	1.150(7)	1.118(7)	1.145(5)
C(3)-O(2)	1.143(7)	1.129(4)	1.145(7)	1.148(7)	1.136(5)
<b>Bond Angles (°)</b>					
C(2)-Ru(1)-C(3)	91.0(3)	90.15(16)	91.5(3)	92.8(3)	92.15(17)
C(2)-Ru(1)-S(1)	91.68(19)	91.57(20)	88.8(2)	91.07(18)	91.81(12)
C(3)-Ru(1)-S(1)	91.12(19)	91.76(20)	91.6(3)	92.74(19)	92.64(12)
O(1)-C(2)-Ru(1)	175.8(6)	175.9(3)	174.6(9)	174.9(7)	175.0(4)
O(2)-C(3)-Ru(1)	176.6(6)	175.9(3)	176.8(6)	175.8(5)	175.2(3)
C(1)-S(1)-Ru(1)	106.2(5)	111.33(10)	108.7(2)	105.70(17)	108.65(12)

### 6.1.1. Electrochemical Studies

The cyclic voltammograms obtained of  $\text{CH}_2\text{Cl}_2$  solutions containing complexes **26a**, **26b** and **27b** at two different temperatures are displayed in Figure 6.2, with all compounds undergoing an oxidation process at positive potentials.

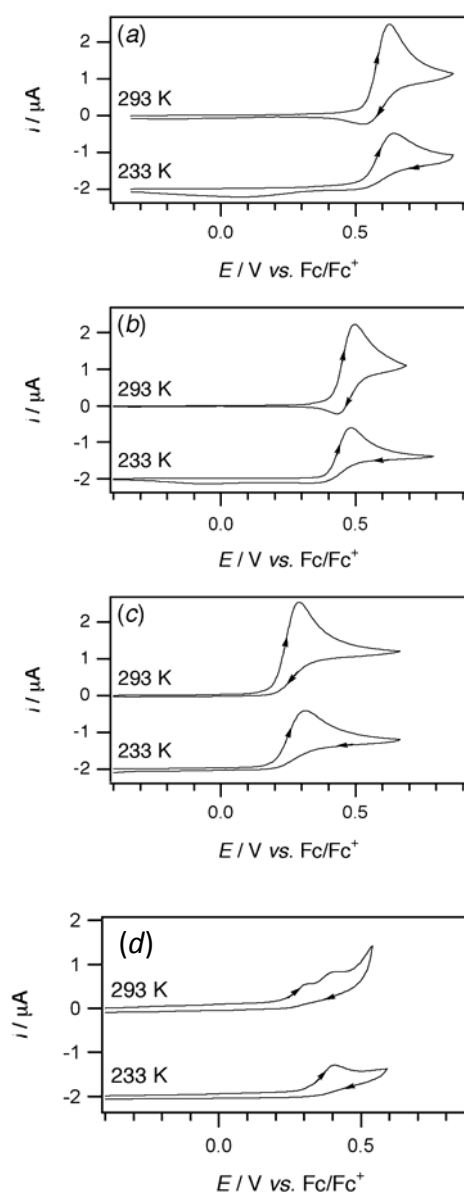


**Figure 6.2.** Cyclic voltammograms of 1.0 mM analytes recorded at a scan rate of  $100 \text{ mV s}^{-1}$  in  $\text{CH}_2\text{Cl}_2$  solutions containing 0.25 M  $\text{Bu}_4\text{NPF}_6$  at a 1 mm diameter planar Pt electrode. (a) **26a**. (b) **26b**. (c) **27b** and (d) **26c**. Voltammograms at 233 K are offset by  $-2 \mu\text{A}$ .

The process most likely involves one-electron oxidation of Ru(II) to Ru(III), although some delocalisation is expected to occur based on the observation that the oxidation potential varies as substituents on the Ru ion are changed (Figure 6.2). **26a** containing the Cp group is the most difficult to oxidize ( $E_p^{\text{ox}} = +0.626 \text{ V vs. Fc/Fc}^+$ , where  $E_p^{\text{ox}}$  is the oxidative peak potential) (Figure 6.2a). **26b** which contains the Cp\* group is easier to oxidize ( $E_p^{\text{ox}} = +0.498 \text{ V vs. Fc/Fc}^+$ ) than **26a** by  $\sim 130 \text{ mV}$ , due to the electron donating methyl groups on the cyclopentadienyl ring lowering the oxidation potential (Figure 6.2b). **27b** is easier to oxidize ( $E_p^{\text{ox}} = +0.288 \text{ V vs. Fc/Fc}^+$ ) than **26b** by  $\sim 200 \text{ mV}$ , indicating that the pyridine group is more electron donating than the benzo[*d*]thiazole group (Figure 6.2c), which is consistent with the observed Ru-C $\equiv$ O stretch in their IR spectrum.

The oxidation of **26a** and **26b** at 293 K shows evidence of chemical reversibility because reverse peaks can be detected in the cyclic voltammograms when the scan direction is reversed (Figure 6.2a and 6.2b). The expression "chemical reversibility" when used in connection with cyclic voltammetry experiments relates to the ratio of the oxidative ( $i_p^{\text{ox}}$ ) to reductive ( $i_p^{\text{red}}$ ) peak currents ( $i_p^{\text{ox}}/i_p^{\text{red}}$ ). (For a fully chemically reversible process at a particular scan rate, the  $i_p^{\text{ox}}/i_p^{\text{red}}$ -ratio approaches unity.) However, when the temperature is lowered to 233 K, the oxidation processes appears to become less chemically reversible ( $i_p^{\text{ox}}/i_p^{\text{red}} \gg 1$ ), suggesting decreasing stability of the oxidised state at low temperatures. A decrease in apparent chemical reversibility at low temperature is unusual, since lowering the temperature normally increases the stability of the oxidised form. Therefore, it is more likely that the oxidation process involves a follow-up homogeneous chemical equilibrium process, so that varying the temperature changes the equilibrium constants and thereby makes the processes *appear* less chemically reversible. Additional processes were evident at

233 K at  $\sim 0$  V vs. Fc/Fc<sup>+</sup> for **26a** and **26b** when the scan direction was reversed, which supports the assignment of an equilibrium reaction, where the equilibrium product is more evident at lower temperatures.

The voltammetric behaviour of **26c** remained chemically irreversible at high and low temperatures (Figure 6.2). While two closely spaced oxidation processes were detected at 293 K, only one process was detected at 233 K, but at both temperatures there was no evidence of stability of the oxidized compound. Interestingly, the voltammograms in Figure 6.2 were only clearly evident on GC surfaces; on identically sized Pt electrodes, the  $i_p^{\text{ox}}$ -values were an order of magnitude smaller. Also, the  $i_p^{\text{ox}}$ -values were significantly less than observed for equivalent concentrations of **26a**, **26b** and **27b**, which cannot readily be explained by differences in relatively diffusion coefficients.

### 6.1.2. Screening against cell lines

The MTT test was carried out on complexes **26-31** using the hormone independent MDA-MB231 breast cancer cell lines. MTT test was also carried out on complexes **26** and **27** using hormone dependent MCF7 breast cancer and a normal epithelial cell line, MCF-10A. The growth of these cells was evaluated after 24 h and 48 h treatment and some of the results are presented in Figure 6.3. Complexes **26-27** exhibit moderate to high anti-proliferative activity towards both the MDA-MB231 and MCF7 breast cancer cell lines at 1 or 2  $\mu\text{M}$ , with complex **26c**, having the highest activity (Figure 6.3a and c).

Generally, it was observed that the toxicity increased according to the electron donating ability of the ligands, from Cp to Cp\* (**26a** vs. **26b**; **27a** vs. **27b**) and from SBzt to SPy (**26** vs. **27**). In order to investigate whether complexes **26** and **27** are selective towards cancer cell lines, they were also tested against the normal epithelial

cell line, MCF10A. However, all of the five complexes were found to exhibit higher anti-proliferative activity towards MCF10A than to the cancer cell lines. For complexes **28-31**, which have an additional carboxylic/carboxylate functional group on the phenyl ring, they were found to exhibit little or no anti-proliferative activity towards the MDA-MB231 cell lines. In addition, there is no significant difference between the complexes with the free acid functional group, **28** and **29** and the water soluble species, **30** and **31** (Appendix Figure A4).

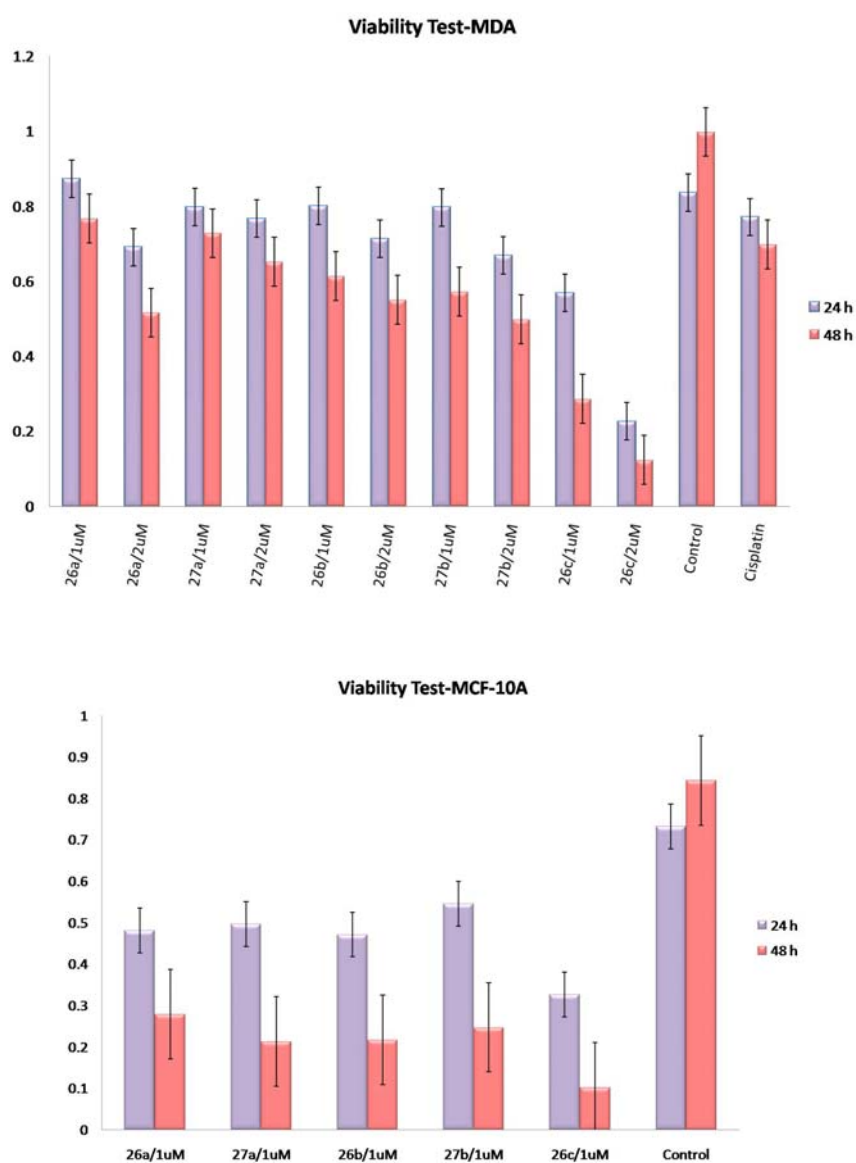


**Figure 6.3.** MTT assay for (a) **26-27** against MDA-MB231 and (b) **26-27** against MCF10A.

## 6.2. S-S bond cleavage reaction of $[\text{Cp}'\text{Ru}(\text{CO})_2]_2$ ( $\text{Cp}' = \text{C}_5\text{H}_5$ or $\text{C}_5\text{Me}_5$ ) with lysozyme

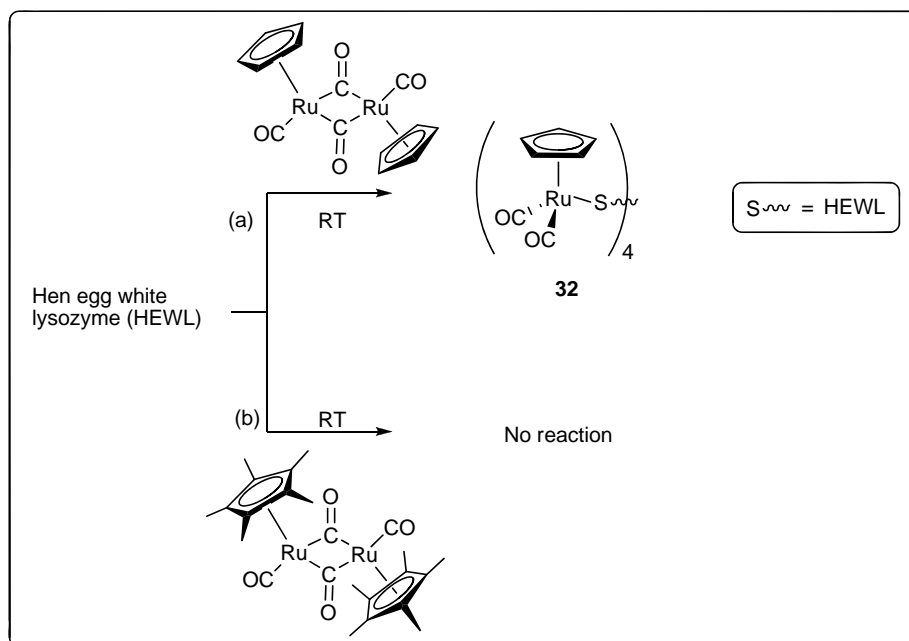
The study of cleavage of disulfide bond by organotransition metal complexes is of biological importance as disulfide bonds represent a significant structural motif in many peptides and proteins<sup>36, 37</sup> and it is known that the reaction of a metal ion with a disulfide bond usually results in S-S bond cleavage and a conformational change of the biomolecules.<sup>38-41</sup>

Reactions of organometallic complexes with biomolecules are known. In fact, the field of bioorganometallic is fast emerging and there are various groups which investigate the reactivity of various organometallic complexes towards biomolecules, one of which is focused on interactions of organometallic complexes with amino acids or proteins. For instance, there are recent reports of disulfide bond cleavage of the oxidized form of glutathione (GSSG) by Pd(II) ammine<sup>41</sup> and Pt(II) methionine<sup>42</sup> complexes. There is also a recent study by Sadler and co-workers, where they showed that  $[(p\text{-cymene})\text{RuCl}_2]_2$  binds selectively to N of the imidazole ring of His15 in lysozyme, a single polypeptide chain of 129 amino acids consisting of four pairs of cysteines that form disulfide bridges between positions.<sup>43</sup> Various groups have also attempted and successfully tagged metal carbonyl complexes onto lysozyme. For instance, Jaouen and co workers have made use of organotungsten reagents with a *N*-succinimidyl and *N*-sulfosuccinimidyl ester function to couple specifically with amino acids and proteins, namely lysozyme and bovine serum albumin (BSA) for X-ray structural analysis of biological systems.<sup>44</sup>

We have demonstrated that the  $[\text{Cp}'\text{Ru}(\text{CO})_2]_2$  complexes **25a** and **25b** can cleave the S-S bond in various organic disulfides under ambient conditions. Hence, it is of interest to us to extend the investigation to the cleavage of disulfide linkages in

proteins by the  $[\text{Cp}^*\text{Ru}(\text{CO})_2]_2$  complexes, which could be potentially used as IR probes for quantifying the disulfide linkages in proteins. For this purpose, we have carried out the reaction of  $[\text{Cp}^*\text{Ru}(\text{CO})_2]_2$  with hen egg white lysozyme (HEWL), which is made up of 129 amino acid residues and contains four disulfide bonds.

**Scheme 6.9.** Reaction of  $[\text{Cp}^*\text{Ru}(\text{CO})_2]_2$  towards HEWL.



The reactions of a THF solution of **25a** with an aqueous solution of HEWL at RT gave a bright yellow solution, from which a deep yellow microcrystalline solid,  $[\text{Cp}^*\text{Ru}(\text{CO})_2]_4(\kappa^1\text{-S-HEWL})$  (**32**) was isolated in high yield (Scheme 6.9). The analogous reaction with **25b** failed as **25b** precipitated out upon mixing the two solutions.

The UV/Vis spectrometry of **32** is shown in Figure 6.4, together with that for lysozyme (HEWL). The lysozyme showed an absorption maximum at 280 nm, typical of the aromatic amino acids and a shoulder at 221 nm. On the other hand, **32** displayed one extra maximum at 380 nm. In comparison, the UV/Vis spectrum of **25a** in acetonitrile display two maxima at 359 and 293 nm.

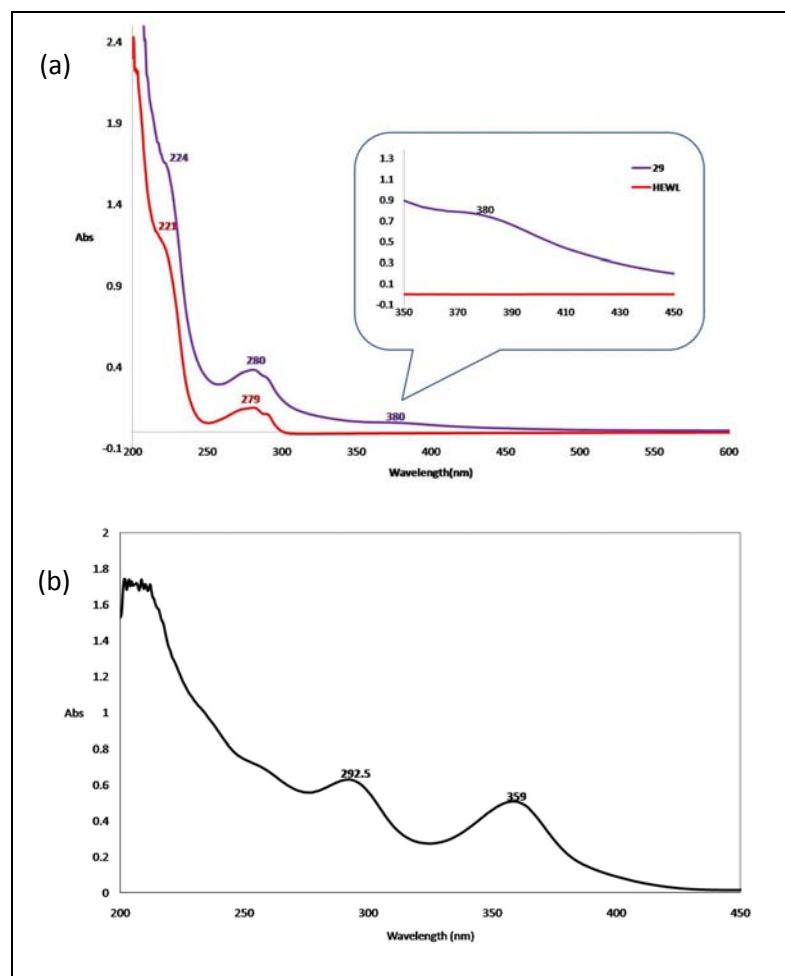


**Figure 6.4.** UV/Vis spectra of (a) HEWL ( $5 \mu\text{M}$ , -) and  $[\text{CpRu}(\text{CO})_2]_4$ -HEWL ( $5 \mu\text{M}$ , -) in water. Inset shows the expanded spectra at higher concentration ( $0.10 \text{ mM}$ ) and (b)  $[\text{CpRu}(\text{CO})_2]_2$  (**25a**) in MeCN.

The IR spectrum of **32** shows two  $\nu_{\text{C}\equiv\text{O}}$  bands of medium intensity at  $2032$  and  $1987 \text{ cm}^{-1}$ , typical of  $\text{CpRu}(\text{CO})_2(\kappa^1\text{-SR})$  complexes and strong, broad  $\nu_{\text{C}=\text{O}}$  and  $\nu_{\text{C}-\text{O}}$  stretches were also observed at  $1657$  and  $1238 \text{ cm}^{-1}$ , respectively, for the carboxylic acids (Figure 6.5).

The MALDI-ToF spectra (linear mode) for complex **32** and HEWL are given in Figure 6.6; an attempt to acquire the MALDI-ToF spectrum of **32** in the reflectance mode was unsatisfactory. Molecular fragments appear as broad envelopes at  $15.7 \text{ kDa}$  and  $14.1 \text{ kDa}$ , respectively. Peaks at higher molecular mass observed for HEWL and **32** are presumably due to oligomerisation of the complexes. The shift in the position of the  $14.1 \text{ kDa}$  envelope to  $15.7 \text{ kDa}$  in **32** is an indication that four



[CpRu(CO)<sub>2</sub>] has bound to the HEWL protein. This is also corroborated by elemental analysis which showed 2.75 % S and 4.57 % Ru, pointing to a 2:1 ratio of S:Ru.

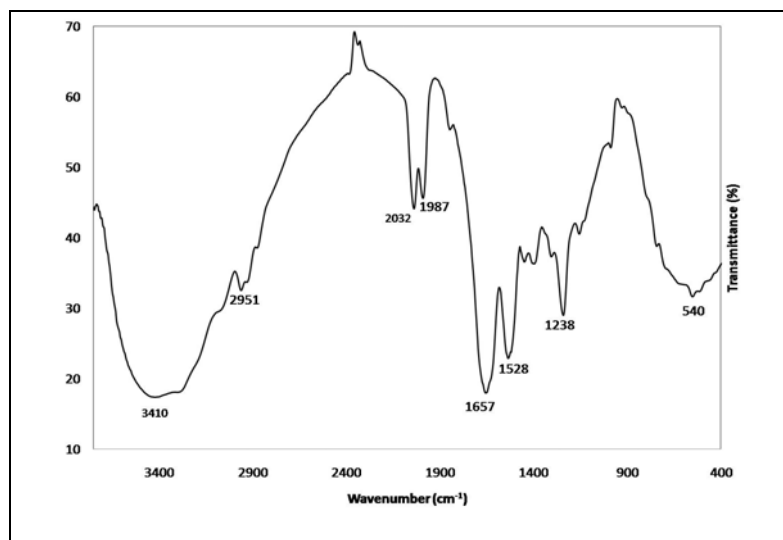


Figure 6.5. IR spectrum of [CpRu(CO)<sub>2</sub>]<sub>4</sub>-HEWL adduct (**32**).

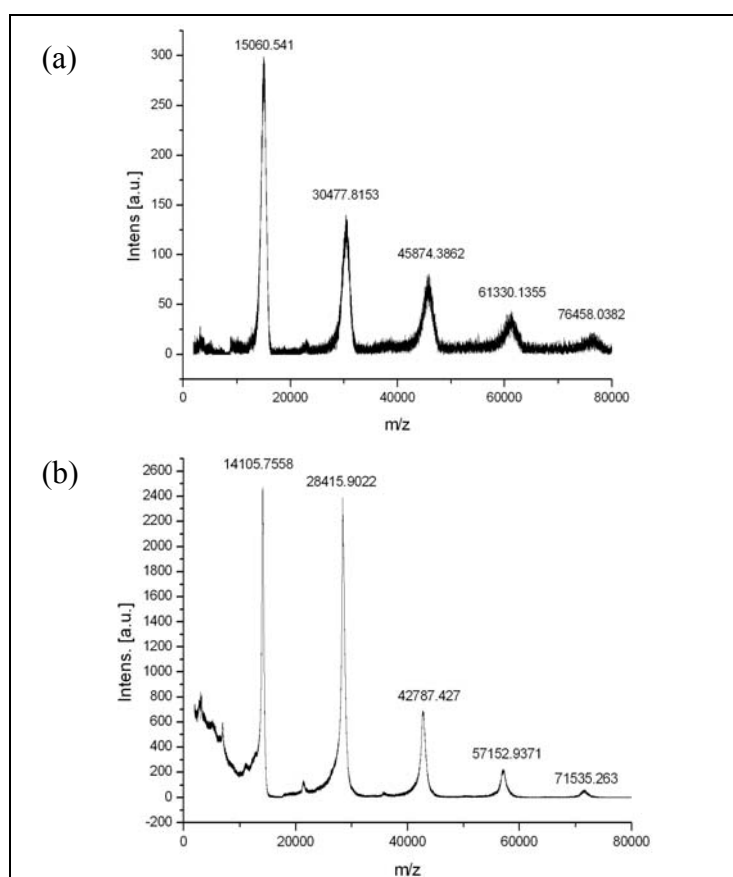


Figure 6.6. MALDI-ToF spectrum of (a) complex **32** and (b) HEWL.

### 6.3. Conclusion

We have shown that  $[\text{Cp}^*\text{Ru}(\text{CO})_2]_2$  can react with disulfides,  $\text{R}'\text{SSR}'$ , led to S-S bond cleavage to afford  $[\text{Cp}^*\text{Ru}(\text{CO})_2(\kappa^1\text{-SR}')]_2$  complexes in moderate to high yield. In view of the current interest in the development of ruthenium complexes as anticancer drugs and in catalytic applications, our results present a convenient synthetic route to a new class of cyclopentadienyl ruthenium carbonyl complexes containing heterocyclic thiolates. Two water-soluble, organometallic complexes, **30** and **31** were synthesised from the reaction of the free acid complexes, **28** and **29** with aqueous  $\text{K}_2\text{CO}_3$ . The S-S bond cleavage was also investigated for **25** with *hen's egg white lysozyme* (HEWL) using  $[\text{CpRu}(\text{CO})_2]_2$ , giving an organometallic adduct,  $[\text{CpRu}(\text{CO})_2]_4\text{-(HEWL)}$ , based on spectroscopic evidence and elemental analysis.

From the IR spectra of these complexes, the electron-donating ability were determined to decrease in the order:  $\text{SPy} > \text{SBzt} > \text{SPyCOOH} > \text{SBzCOOH}$  and  $\text{Cp}^* > \text{Cp} > \text{Ind}$ , in agreement with electrochemical and x-ray studies.

We have also shown that complexes **26** and **27** exhibit antiproliferative activity against MDA-MB231 and MCF-7 breast cancer cell lines and it was observed that the toxicity increased from Cp to Cp\* (**26a** vs. **26b** and **26c**; **27a** vs. **27b**) and from SBzt to SPy (**26** vs. **27**), in order of increasing electron-donating ability of the ligands. Complexes **28-31** were also screened against MDA-MB231 breast cancer cell lines and it was found that they do not exhibit any antiproliferative activity.

In addition, the reactivity of **25** towards *hen's egg white lysozyme* (HEWL) was investigated and **25a** was found to cleave two out of the four disulfide bonds present in HEWL. This result has implications in the field of bioorganometallic chemistry, where metal carbonyl complexes such as complex **25** can be used in metalloimmuno-assay to probe the presence of disulfide bonds present in proteins.

## 6.4. Experimental

General procedures, cyclic voltammetry studies and x-ray structure determination are as described in Chapter 2.  $[\text{Cp}^*\text{Ru}(\text{CO})_2]_2$  was synthesized as reported in the literature.<sup>45</sup>  $[\text{CpRu}(\text{CO})_2]_2$  was purchased from Strem;  $(\text{SBzt})_2$ ,  $(\text{SPy})_2$  and  $(\text{SPyCOOH})_2$  from Sigma Aldrich and  $(\text{SBzCOOH})$  from TCI and used without further purification. The ORTEP plots of **27-29** are given in Figure A6 and the crystal data collection and processing parameters are given in Table A6 (Appendix).

**Cell culture and viability assay.** Experimental cultures of the cell lines MDA-MB-231 and MCF7 were obtained from the American Type Culture Collection (ATCC) and cultured in tissue culture dishes (Nunc Inc., Naperville, IL, USA). The cells were maintained in DMEM (Grand Island, NY, USA) supplemented with 10% fetal bovine serum (FBS), 1% L-glutamate (GIBCO Laboratories) and 1% penicillin-streptomycin (GIBCO Laboratories) at 37 °C in a 5% CO<sub>2</sub> atmosphere. Cell cultures were maintained in an antibiotic-free condition during cell growing and experiments. Phosphate buffer saline (PBS) was obtained from 1<sup>st</sup> BASE.

Cell culture medium, L-glutamine, and trypsin were purchased from Sigma-Aldrich. Phosphate buffered saline (DPBS) was purchased from Fisher Scientific. The testing compounds were dissolved in dimethylsulfoxide (DMSO) with final concentration used for treatment being 0.1%. Cell viability under experimental conditions was assessed by the mitochondria-dependent reduction of 3-(4,5-Dimethylthiazol-2-yl)-2,5-diphenyltetrazolium-bromide (MTT) to formazan. The cells were treated with an equal amount of freshly prepared MTT solution (3 mg MTT reagent dissolved in plain media) per sample in triplicate in a 96-well plate. The plate was incubated for 2 h at 37 °C in the dark. After incubation, the plate was spun at 2,000 rpm for 5 min. The supernatant was removed and the crystals were dissolved in 200 µl of DMSO plus 10

$\mu\text{l}$  of Sorenson's glycine buffer. The plate was then read at 570 nm using an Biorad UV plate reader. Results of the MTT assays are given in Figure A7 (Appendix).

### Reaction [CpRu(CO)<sub>2</sub>]<sub>2</sub> (**25a**) with

(i) *2,2'-dithiobis(benzothiazole)*, (*SBzt*)<sub>2</sub>: To a brownish yellow solution of **25a** (44 mg, 0.10 mmol) in toluene (8 mL) was added (C<sub>7</sub>H<sub>4</sub>NS<sub>2</sub>)<sub>2</sub> (34 mg, 0.10 mmol) and the mixture was stirred at room temperature for 6 h. The resulting bright yellow solution was filtered through a thin disc of celite on a glass sinter, porosity No. 3 to remove any excess (C<sub>7</sub>H<sub>4</sub>NS<sub>2</sub>)<sub>2</sub>. The bright yellow filtrate was concentrated to *ca.* 2 mL and recrystallised in toluene/hexane at -30°C. Air stable, fine yellow needles of CpRu(CO)<sub>2</sub>(C<sub>7</sub>H<sub>4</sub>NS<sub>2</sub>) (**26a**) (58 mg, 0.07 mmol, 74.6 % yield) were obtained after a day.

Data for **26a**. Anal. Found: C, 43.5; H, 2.1; N, 3.6; S, 17.1%. Calc. for C<sub>14</sub>H<sub>9</sub>N<sub>1</sub>O<sub>2</sub>Ru<sub>1</sub>S<sub>2</sub>: C, 43.3; H, 2.3; N, 3.6; S, 16.5%. IR (KBr, cm<sup>-1</sup>): 2045s, 1996s ( $\nu_{\text{CO}}$ ) cm<sup>-1</sup>. ESI<sup>+</sup>-MS: m/z 390 [MH<sup>+</sup>]. <sup>1</sup>H NMR ( $\delta$ , C<sub>6</sub>D<sub>6</sub>): 7.87 (d, 1H, <sup>3</sup>J = 7.7 Hz, H<sub>benzothiazole</sub>), 7.26 (d, 1H, <sup>3</sup>J = 8.2 Hz, H<sub>benzothiazole</sub>), 7.14(1H, H<sub>benzothiazole</sub>, partially obscured by residual peaks of C<sub>6</sub>D<sub>6</sub>), 6.92 (t, 1H, <sup>3</sup>J = 7.1 Hz, H<sub>benzothiazole</sub>), 4.50 (s, 5H, Cp-CH<sub>3</sub>). <sup>13</sup>C NMR ( $\delta$ , C<sub>6</sub>D<sub>6</sub>): 198.5 (s, 2 x CO), 177.1 (s, NCS), 155.5, 139.1, 126.2, 123.9, 121.4, 120.9 (C<sub>benzothiazole</sub>), 88.8(s, C<sub>5</sub>H<sub>5</sub>).

(ii) *2,2'-dithiodipyridine*, (*SPy*)<sub>2</sub>: The reaction of **25a** (22 mg, 0.05 mmol) in toluene (8 mL) was added (C<sub>5</sub>H<sub>4</sub>NS)<sub>2</sub> (22 mg, 0.10 mmol) was carried out as above to give air stable, orange-yellow microcrystalline solids of CpRu(CO)<sub>2</sub>(C<sub>5</sub>H<sub>4</sub>NS) (**27a**) (51 mg, 0.13 mmol, 63.4 % yield) after recrystallisation from toluene/hexane at -30°C. Diffraction-quality single crystals were obtained at -30 °C as orange blocks from a toluene solution layered with hexane after a day.

Data for **27a**. Anal. Found: C, 43.2; H, 2.9; N, 4.4; S, 10.0%. Calc. for  $C_{12}H_9N_1O_2Ru_1S_1$ : C, 43.4; H, 2.7; N, 4.2; S, 9.7 %. IR (KBr,  $cm^{-1}$ ): 2029s, 1985s ( $\nu_{CO}$ )  $cm^{-1}$ . FAB<sup>+</sup>-MS: m/z 332.9 (MH<sup>+</sup>), 276.9 (M<sup>+</sup>-2CO). <sup>1</sup>H NMR ( $\delta$ ,  $C_6D_6$ ): 8.30 (m, 1H, H<sub>pyridine</sub>), 7.69 (m, 1H, H<sub>pyridine</sub>), 6.76 (m, 1H, H<sub>pyridine</sub>), 6.43 (m, 1H, H<sub>pyridine</sub>), 4.57 (s, 5H, Cp). <sup>13</sup>C NMR ( $\delta$ ,  $C_6D_6$ ): 199.7 (s, 2 x  $\underline{CO}$ ), 169.1 (s,  $\underline{NCS}$ ), 149.0, 134.1, 125.6, 117.3 (C<sub>pyridine</sub>), 88.7 (s,  $\underline{C_5H_5}$ ).

(iii) *hen's egg white lysozyme*, (**HEWL**): To a brownish yellow solution **25a** (33 mg, 0.08 mmol) in THF (20 mL) was added a degassed, aqueous solution (10 mL) of HEWL (0.73 g, 0.05 mmol) and the mixture was stirred at room temperature for 48 h. The resultant bright yellow solution was concentrated to *ca.* 10 mL and filtered to remove unreacted **24** (*ca.* 10 mg, 28 % recovery). The yellow filtrate was freeze dried overnight to give fine yellow solids, [CpRu(CO)<sub>2</sub>]<sub>4</sub>-(HEWL) (**32**) (0.70 g, 0.045 mmol, 90.4 % yield). A comparison of the <sup>1</sup>H NMR spectrum of the native HEWL and the resultant yellow solid in D<sub>2</sub>O indicated that there is a change in the protein structure. Anal. Found: C, 44.3; H, 5.6; N, 13.6; S, 2.8; Ru, 4.6 %. IR (KBr,  $cm^{-1}$ ): 3410sbr ( $\nu_{OH}$ ); 2032m, 1987m ( $\nu_{CO}$ ); 1657s ( $\nu_{C=O}$ ); 1238s ( $\nu_{C-O}$ )  $cm^{-1}$ . MALDI-ToF<sup>+</sup>-MS: m/z 15.1 kDa (~ 4 x CpRu(CO)<sub>2</sub> and HEWL).

#### Reaction [Cp\***Ru**(CO)<sub>2</sub>]<sub>2</sub> (**25b**) with

(i) *2,2'-dithiobis(benzothiazole)*, (**SBzt**)<sub>2</sub>: To a bright orange solution of **25b** (29 mg, 0.05 mmol) in toluene (8 mL) was added (C<sub>7</sub>H<sub>4</sub>NS<sub>2</sub>)<sub>2</sub> (17 mg, 0.05 mmol) and the mixture was stirred at room temperature for 6 h. The resulting bright yellow solution was filtered through a thin disc of celite on a glass sinter, porosity No. 3 to remove any excess (C<sub>7</sub>H<sub>4</sub>NS<sub>2</sub>)<sub>2</sub>. The bright yellow filtrate was concentrated to *ca.* 2 mL and recrystallised in toluene/hexane at -30°C. Air stable, fine yellow needles of Cp\***Ru**(CO)<sub>2</sub>(C<sub>7</sub>H<sub>4</sub>NS<sub>2</sub>) (**26b**) (34mg, 0.07 mmol, 74.2 % yield) were obtained after a

day. Diffraction-quality single crystals were obtained at -30 °C as yellow plates from a toluene solution layered with hexane after a day.

Data for **26b**. Anal. Found: C, 49.6; H, 4.4; N, 3.1; S, 13.6%. Calc. for  $C_{19}H_{19}N_1O_2Ru_1S_2$ : C, 49.8; H, 4.2; N, 3.1; S, 14.0%. IR (KBr,  $cm^{-1}$ ):  $\nu_{CO}$  2020, 1965  $cm^{-1}$ . FAB<sup>+</sup>-MS: m/z 459.1 [M-CO]. <sup>1</sup>H NMR ( $\delta$ ,  $C_6D_6$ ): 7.81 (d, 1H, <sup>3</sup>J = 7.7 Hz,  $H_{benzothiazole}$ ), 7.27 (d, 1H, <sup>3</sup>J = 7.7 Hz,  $H_{benzothiazole}$ ), 7.12 ( $H_{benzothiazole}$ , partially obscured by residual peaks of  $C_6D_6$ ), 6.91 (t, 1H, <sup>3</sup>J = 7.1 Hz,  $H_{benzothiazole}$ ), 1.48 (s, 15H, Cp-CH<sub>3</sub>). <sup>13</sup>C NMR ( $\delta$ ,  $C_6D_6$ ): 201.3 (s, 2 x  $\underline{CO}$ ), 177.7 (s,  $\underline{NCS}$ ), 155.7, 139.5, 126.0, 123.6, 121.4, 120.7 ( $C_{benzothiazole}$ ), 101.0 (s,  $\underline{C_5(CH_3)_5}$ ) 10.2 (s,  $C_5(\underline{CH_3})_5$ ).

(ii) **2,2'-dithiodipyridine, (SPy)<sub>2</sub>**: The reaction of **25b** (58 mg, 0.10 mmol) in toluene (8 mL) was added  $(C_5H_4NS)_2$  (22 mg, 0.10 mmol) was carried out as above to yield air stable, dark yellow microcrystalline solids of  $Cp^*Ru(CO)_2(C_5H_4NS)$  (**27b**) (51 mg, 0.13 mmol, 63.4 % yield) after recrystallisation from toluene/hexane at -30°C. Diffraction-quality single crystals were obtained at -30 °C as yellow blocks from a toluene solution layered with hexane after a day; and **28** as orange blocks.

Data for **27b**. Anal. Found: C, 50.9; H, 4.5; N, 3.7; S, 8.0%. Calc. for  $C_{19}H_{19}N_1O_2Ru_1S_2$ : C, 50.7; H, 4.8; N, 3.5; S, 8.0%. IR (KBr,  $cm^{-1}$ ): 2010s, 1957s ( $\nu_{CO}$ )  $cm^{-1}$ . FAB<sup>+</sup>-MS: m/z 404.1 [M-CO]. <sup>1</sup>H NMR ( $\delta$ ,  $C_6D_6$ ): 8.28 (m, 1H,  $H_{pyridine}$ ), 7.71 (m, 1H,  $H_{pyridine}$ ), 6.78 (m, 1H,  $H_{pyridine}$ ), 6.42 (m, 1H,  $H_{pyridine}$ ), 1.55 (s, 15H, Cp-CH<sub>3</sub>). <sup>13</sup>C NMR ( $\delta$ ,  $C_6D_6$ ): 202.4 (s, 2 x  $\underline{CO}$ ), 169.1 (s,  $\underline{NCS}$ ), 149.0, 139.5, 134.0, 125.8, 117.0 ( $C_{pyridine}$ ), 100.6 (s,  $\underline{C_5(CH_3)_5}$ ) 10.3 (s,  $C_5(\underline{CH_3})_5$ ).

(iii) **2,2'-dithiodibenzoic acid, (SBzCOOH)<sub>2</sub>**: To a bright orange solution of **25b** (58 mg, 0.10 mmol) in THF (10 mL) was added  $[C_6H_4(COOH)S]_2$  (31 mg, 0.10 mmol) and the mixture was irradiated using tungsten lamp (60 W) for 2 h in a carius tube. The resulting dark yellow solution was evacuated to dryness and extracted with

toluene:Et<sub>2</sub>O (1:1, 5 x 2 mL). The dark yellow extract was evacuated to dryness and recrystallised in THF/hexane at -30°C. Air stable, dark yellow microcrystalline solids of Cp\*Ru(CO)<sub>2</sub>(SC<sub>6</sub>H<sub>4</sub>COOH) (**28**) (59 mg, 0.13 mmol, 66.7 % yield) were obtained after a day. Diffraction-quality single crystals were obtained at -30 °C **28** as orange blocks from a THF solution layered with hexane after two days.

Data for **28**. Anal. Found: C, 51.5; H, 4.3; S, 7.2 %. Calc. for C<sub>19</sub>H<sub>20</sub>O<sub>4</sub>RuS: C, 51.2; H, 4.5; S, 7.2%. IR (KBr, cm<sup>-1</sup>): 2024vs, 1981vs (ν<sub>CO</sub>); 1707s (ν<sub>C=O</sub>); 1270m (ν<sub>C-O</sub>) cm<sup>-1</sup>. FAB<sup>+</sup>-MS: m/z 446 [MH<sup>+</sup>, M = Cp\*Ru(CO)<sub>2</sub>(SC<sub>6</sub>H<sub>4</sub>COOH)], 390 [M-2CO]. <sup>1</sup>H NMR (δ, C<sub>6</sub>D<sub>6</sub>): 14.53 (s, br, 1H, H<sub>COOH</sub>), 8.78 (dd, <sup>3</sup>J = 1.7 Hz; 7.4 Hz, 1H, H<sub>benzene</sub>), 8.76 (dd, <sup>3</sup>J = 1.7 Hz; 7.4 Hz, 1H, H<sub>benzene</sub>), 6.93 (m, 2H, H<sub>benzene</sub>), 1.32 (s, 15H, Cp-CH<sub>3</sub>). <sup>13</sup>C NMR (δ, C<sub>6</sub>D<sub>6</sub>): 200.5 (s, 2 x CO), 168.0 (s, COOH), 145.6 (s, NCS), 139.0, 132.5, 127.2, (C<sub>benzene</sub>), 100.7(s, C<sub>5</sub>(CH<sub>3</sub>)<sub>5</sub>), 9.9 (s, C<sub>5</sub>(CH<sub>3</sub>)<sub>5</sub>).

*iv*)**6,6'**- dithiodinicotinic acid, (SPyCOOH)<sub>2</sub>: Using the reaction condition as above, air stable, dark yellow microcrystalline solids of Cp\*Ru(CO)<sub>2</sub>(SC<sub>5</sub>H<sub>3</sub>NCOOH) (**29**) (69 mg, 0.15 mmol, 77.2 % yield) were obtained after recrystallisation from THF/hex at -30 °C from the reaction of **25b** (58 mg, 0.10 mmol) with [SC<sub>5</sub>H<sub>3</sub>NCOOH]<sub>2</sub> (32 mg, 0.10 mmol). Diffraction-quality single crystals were obtained at -30 °C as yellow blocks from a THF solution layered with hexane after two days.

Data for **29**. Anal. Found: C, 48.6; H, 4.5; N, 3.3; S, 7.0%. Calc. for C<sub>18</sub>H<sub>19</sub>NO<sub>4</sub>RuS: C, 48.4; H, 4.3; N, 3.1; S, 7.2%. IR (KBr, cm<sup>-1</sup>): 2021vs, 1976vs (ν<sub>CO</sub>); 1675s (ν<sub>C=O</sub>); 1575s (ν<sub>C-O</sub>) cm<sup>-1</sup>. ESI<sup>+</sup>-MS: m/z 448[MH<sup>+</sup>, M = Cp\*Ru(CO)<sub>2</sub>(SC<sub>5</sub>H<sub>3</sub>NCOOH)]; ESI<sup>-</sup>MS: m/z 446 [M-H<sup>-</sup>]; 418 [M-H-CO<sup>-</sup>]. <sup>1</sup>H NMR (δ, CD<sub>3</sub>OD): 8.68 (d, J = 2.1 Hz, 1H, H<sub>ring</sub>), 7.82 (dd, J = 2.2, 8.5 Hz, 1H, H<sub>ring</sub>), 7.45 (d, J = 8.5 Hz, 1H, H<sub>pyridine</sub>), 1.95 (s, 15H, Cp-CH<sub>3</sub>). <sup>13</sup>C NMR (δ, CD<sub>3</sub>OD): 201.6 (s, 2 x CO), 169.0 (s, COOH), 148.7 (s, NCS), 149.9, 136.1, 126.1, (C<sub>ring</sub>), 102.1(s, C<sub>5</sub>(CH<sub>3</sub>)<sub>5</sub>), 9.9 (s, C<sub>5</sub>(CH<sub>3</sub>)<sub>5</sub>).

(v) *hen's egg white lysozyme*, (*HEWL*): To an orange solution **24** (29 mg, 0.10 mmol) in THF (20 mL) was added a degassed, aqueous solution (10 mL) of HEWL (0.73 g, 0.05 mmol). Upon addition of the THF solution to the aqueous solution, orange solids precipitated out of solution. The suspension was stirred at room temperature for up to 48 h and monitored by IR but there was no reaction.

#### Reaction of $K_2CO_3$ with

(i)  $Cp^*Ru(CO)_2(SC_6H_5COOH)$  (**28**). To a bright orange solution of **25b** (58 mg, 0.10 mmol) in THF (10 mL) was added  $[C_6H_4(COOH)S]_2$  (31 mg, 0.10 mmol) and the mixture was irradiated using tungsten lamp (60 W) for 2 h in a carius tube. A degassed aqueous solution of  $K_2CO_3$  (20 mg, 0.15 mmol) was added to the resulting dark yellow solution and the solution was allowed to stir at RT for 4h, upon which it turned to a brighter yellow. The resultant solution was concentrated to half the volume, *ca.* 10 mL and the yellow precipitate was filtered off. The resultant filtrate was evacuated to dryness and extracted with MeOH:Et<sub>2</sub>O (1:1, 5 x 3 mL). The bright yellow extract was evacuated to dryness and recrystallised in THF/Et<sub>2</sub>O at -30°C. Air stable, dark yellow microcrystalline solids of  $Cp^*Ru(CO)_2(SC_6H_5COOK)$  (**30**) (36 mg, 0.07 mmol, 37 % overall yield) were obtained after a day.

Data for **30**. Anal. Found: C, 45.6; H, 4.2; S, 6.1%. Calc. for  $C_{19}H_{19}KO_4RuS \cdot 1.1H_2O$ : C, 45.3; H, 4.2; S, 6.4%. (The H<sub>2</sub>O is presumably from the reaction where we used aqueous  $K_2CO_3$ ) IR (KBr,  $cm^{-1}$ ): 2005vs, 1941vs ( $\nu_{CO}$ ); 1584s, 1562s ( $\nu_{C=O}$ ); 1391s ( $\nu_{C-O}$ )  $cm^{-1}$ . ESI<sup>-</sup>MS: m/z 445 [M<sup>-</sup>]; 417 [M-CO<sup>-</sup>]. <sup>1</sup>H NMR ( $\delta$ , CD<sub>3</sub>OD): 7.20 (dd, J = 0.8, 8.0 Hz, 1H, H<sub>benzene</sub>), 7.06 (dd, J = 1.5, 7.4 Hz, 1H, H<sub>benzene</sub>), 6.94 (dt, J = 1.7, 7.6 Hz, 1H, H<sub>benzene</sub>), 6.83 (dt, J = 1.3, 7.3 Hz, 1H, H<sub>benzene</sub>), 1.94 (s, 15H, Cp-CH<sub>3</sub>). <sup>13</sup>C NMR ( $\delta$ , CD<sub>3</sub>OD): 202.4 (s, 2 x CO), 169.0 (s, COOH), 141.9 (s, NCS), 146.3, 135.0, 127.6, (C<sub>ring</sub>), 102.3(s, C<sub>5</sub>(CH<sub>3</sub>)<sub>5</sub>), 10.0 (s, C<sub>5</sub>(CH<sub>3</sub>)<sub>5</sub>).



(ii) **Cp\*Ru(CO)<sub>2</sub>(SC<sub>5</sub>H<sub>3</sub>NCOOH) (29)**. The reaction was carried out as for **28** to give air stable, dark yellow microcrystalline solids of Cp\*Ru(CO)<sub>2</sub>(SC<sub>5</sub>H<sub>3</sub>NCOOK) (**31**) (56 mg, 0.12 mmol, 57.8 % overall yield) after recrystallisation from MeOH/Et<sub>2</sub>O at -30 °C.

Data for **31**. IR (KBr, cm<sup>-1</sup>): 2025vs, 1958vs (ν<sub>CO</sub>); 1580sbr (ν<sub>C=O</sub>); 1388s (ν<sub>C-O</sub>) cm<sup>-1</sup>. ESI<sup>+</sup>-MS: m/z 486 [MHK<sup>+</sup>, M = Cp\*Ru(CO)<sub>2</sub>(SC<sub>5</sub>H<sub>3</sub>NCOO)]; 448[MH<sub>2</sub><sup>+</sup>, M = Cp\*Ru(CO)<sub>2</sub>(SC<sub>5</sub>H<sub>3</sub>NCOOH)]; ESI<sup>-</sup>-MS: m/z 892 [M<sub>2</sub>H<sup>-</sup>]; 446 [M<sup>-</sup>]; 418 [M-CO<sup>-</sup>]. HR ESI<sup>-</sup>MS: 446.0001 (found); 446.0032 (calc.). <sup>1</sup>H NMR (δ, CD<sub>3</sub>OD): 8.71 (d, J = 1.2 Hz, 1H, H<sub>ring</sub>), 7.77 (dd, J = 1.1, 5.0 Hz, 1H, H<sub>ring</sub>), 7.34 (d, J = 5.0 Hz, 1H, H<sub>ring</sub>), 1.95 (s, 15H, Cp-CH<sub>3</sub>). <sup>13</sup>C NMR (δ, CD<sub>3</sub>OD): 202.0 (s, 2 x CO), 174.2 (s, COOH), 171.5 (s, NCS), 150.6, 136.1, 125.3, (C<sub>ring</sub>), 102.1(s, C<sub>5</sub>(CH<sub>3</sub>)<sub>5</sub>), 10.0 (s, C<sub>5</sub>(CH<sub>3</sub>)<sub>5</sub>).

## References

1. Goh, L. Y., *Coord. Chem. Rev.* **1999**, *186*, 257-276.
2. Weng, Z.; Goh, L. Y., *Acc. Chem. Res.* **2004**, *37* (3), 187-199.
3. Brandenburg, K. L.; Heeg, M. J.; Abrahamson, H. B., *Inorg. Chem.* **1987**, *26* (7), 1064-1069.
4. Shi, Y. M.; Cheng, G. B.; Lu, S. W.; Guo, H. F.; Wu, Q. J.; Huang, X. Y.; Hu, N. H., *J. Organomet. Chem.* **1993**, *455* (1-2), 115-120.
5. Cheng, G.; Wu, Q.; Huang, X., *Jiegou Huaxue* **1995**, *14*, 47-50.
6. Ng, V. W. L., *Chemistry of Cyclopentadienylchromium Complexes Containing C-, N- and S-organic Ligands*, MSc Thesis, National University of Singapore, Singapore, **2002**.
7. Bitterwolf, T. E., **2000**, *206-207*, 419-450.
8. Dougan, S. J.; Melchart, M.; Habtemariam, A.; Parsons, S.; Sadler, P. J., *Inorg. Chem.* **2006**, *45* (26), 10882-10894.
9. Habtemariam, A.; Melchart, M.; Fernandez, R.; Parsons, S.; Oswald, I. D. H.; Parkin, A.; Fabbiani, F. P. A.; Davidson, J. E.; Dawson, A.; Aird, R. E.; Jodrell, D. I.; Sadler, P. J., *J. Med. Chem.* **2006**, *49* (23), 6858-6868.
10. Dougan, S. J.; Sadler, P. J., *Chimia* **2007**, *61* (11), 704-715.
11. Melchart, M.; Habtemariam, A.; Parsons, S.; Sadler, P. J., *J. Inorg. Biochem.* **2007**, *101* (11-12), 1903-1912.
12. Peacock, A. F. A.; Parsons, S.; Sadler, P. J., *J. Am. Chem. Soc.* **2007**, *129* (11), 3348-3357.
13. Wang, F. Y.; Weidt, S.; Xu, J. J.; Mackay, C. L.; Langridge-Smith, P. R. R.; Sadler, P. J., *J. Am. Soc. Mass. Spectr.* **2008**, *19* (4), 544-549.
14. Ang, W. H.; De Luca, A.; Chapuis-Bernasconi, C.; Juillerat-Jeanneret, L.; Lo Bello, M.; Dyson, P. J., *Chemmedchem* **2007**, *2* (12), 1799-1806.
15. Dyson, P. J., *Chimia* **2007**, *61* (11), 698-703.
16. Scolaro, C.; Chaplin, A. B.; Hartinger, C. G.; Bergamo, A.; Cocchietto, M.; Keppler, B. K.; Sava, G.; Dyson, P. J., *Dalton Trans.* **2007**, (43), 5065-5072.
17. Vock, C. A.; Ang, W. H.; Scolaro, C.; Phillips, A. D.; Lagopoulos, L.; Juillerat-Jeanneret, L.; Sava, G.; Scopelliti, R.; Dyson, P. J., *J. Med. Chem.* **2007**, *50* (9), 2166-2175.
18. Auzias, M.; Therrien, B.; Suss-Fink, G.; Stepnicka, P.; Ang, W. H.; Dyson, P. J., *Inorg. Chem.* **2008**, *47* (2), 578-583.
19. Dutta, B.; Scolaro, C.; Scopelliti, R.; Dyson, P. J.; Severin, K., *Organometallics* **2008**, *27* (7), 1355-1357.
20. El-khateeb, M., *Transit. Metal. Chem.* **2001**, *26*, 267.
21. Shaver, A.; Plouffe, P. Y.; Bird, P.; Livingstone, E., *Inorg. Chem.* **1990**, *29* (10), 1826-1832.
22. Sato, T.; Nishio, M.; Ishii, Y.; Yamazaki, H.; Hidai, M., *J. Organomet. Chem.* **1998**, *569* (1-2), 99-108.
23. Dev, S.; Imagawa, K.; Mizobe, Y.; Cheng, G.; Wakatsuki, Y.; Yamazaki, H.; Hidai, M., *Organometallics* **1989**, *8* (5), 1232-7.
24. Coto, A.; Tenorio, M. J.; Puerta, M. C.; Valerga, P., *Organometallics* **1998**, *17* (20), 4392-4399.
25. Treichel, P. M.; Schmidt, M. S.; Crane, R. A., *Inorg. Chem.* **1991**, *30* (3), 379-381.
26. Killop, S. D.; Knox, S. A. R., *J. Chem. Soc., Dalton Trans.* **1978**, 1260.
27. Anjaneyulu, Y.; Rao, R. P., *Syn. React. in Inorg. Met.* **1986**, *16* (2), 257-272.

28. Anjaneyulu, Y.; Rao, R. P., *Proceedings of the Indian National Science Academy, Part A: Physical Sciences* **1989**, *55* (3), 563-9.
29. Gupta, S. K.; Sharma, R. C.; Gupta, A. K., *Asian J. Chem.* **1992**, *4* (2), 234-8.
30. Dinger, M. B.; Henderson, W., *J. Organomet. Chem.* **1998**, *560* (1-2), 233-243.
31. Nomiya, K.; Kasuga, N. C.; Takamori, I.; Tsuda, K., *Polyhedron* **1998**, *17* (20), 3519-3530.
32. Nomiya, K.; Noguchi, R.; Shigeta, T.; Kondoh, Y.; Tsuda, K.; Ohsawa, K.; Chikaraishi-Kasuga, N.; Oda, M., *B. Chem. Soc. Jpn.* **2000**, *73* (5), 1143-1152.
33. Nomiya, K.; Yamamoto, S.; Noguchi, R.; Yokoyama, H.; Kasuga, N. C.; Ohshima, K.; Kato, C., *J. Inorg. Biochem.* **2003**, *95* (2-3), 208-220.
34. Ng, S. Y. *Synthetic, Structural and Reactivity Studies of Indenyl Ruthenium Complexes. PhD thesis*, National University of Singapore, Singapore, **2006**.
35. Deeming, A. J.; Karim, M., *Polyhedron* **1991**, *10* (8), 837-840.
36. Simpson, L. L.; Maksymowych, A. B.; Park, J. B.; Bora, R. S., *J. Pharmacol. Exp. Ther.* **2004**, *308* (3), 857-864.
37. Ritz, D.; Beckwith, J., *Annu. Rev. Microbiol.* **2001**, *55*, 21-48.
38. Ohta, N.; Chen, D.; Ito, S.; Futo, T.; Yotsuyanagi, T.; Ikeda, K., *Int. J. Pharm.* **1995**, *118* (1), 85-93.
39. Ohta, N.; Inagaki, K.; Muta, H.; Yotsuyanagi, T.; Matsuo, T., *Int. J. Pharm.* **1998**, *161* (1), 15-21.
40. Wang, D. R.; Behrens, A.; Farahbakhsh, M.; Gatjens, J.; Rehder, D., *Chem. Eur. J.* **2003**, *9* (8), 1805-1813.
41. Munk, V. P.; Sadler, P. J., *Chem. Commun.* **2004**, (16), 1788-1789.
42. Wei, H. Y.; Wang, X. Y.; Liu, Q.; Mei, Y. H.; Lu, Y.; Guo, Z. J., *Inorg. Chem.* **2005**, *44* (17), 6077-6081.
43. McNae, I. W.; Fishburne, K.; Habtemariam, A.; Hunter, T. M.; Melchart, M.; Wang, F. Y.; Walkinshaw, M. D.; Sadler, P. J., *Chem. Commun.* **2004**, (16), 1786-1787.
44. Salmain, M., Labeling of proteins with organometallic Complexes: Strategies and Applications. In *Bioorganometallics*, Jaouen, G., Ed. Wiley-VCH Verlag GmbH & Co.: **2006**; pp 181-213.
45. King, R. B.; Iqbal, M. Z.; King, A. D., Jr., *J. Organomet. Chem.* **1979**, *171*(1), 53-63.

### Concluding remarks

In this thesis, we have reported the synthesis of mixed-sandwich complexes of Cr<sup>III</sup> and Ru<sup>II/III</sup> containing poly(methimazolyl)borates from the reactions of [Cp\*Cr<sup>III</sup>Br<sub>2</sub>]<sub>2</sub> (**1**), [(HMB)RuCl<sub>2</sub>]<sub>2</sub> (**8**), [Cp\*RuCl<sub>2</sub>]<sub>2</sub> (**12**) and [Cp\*RuOMe]<sub>2</sub> (**13**) with the salts of the corresponding poly(methimazolyl)borate. Some of these mixed-sandwich complexes exhibited isomerisation equilibria in solution, which were studied via electrochemical and NMR spectroscopic methods. This isomerisation process is important towards an understanding of B-H activation in metal complexes comprising poly(methimazolyl)borates. In the case of the [Cp\*Ru<sup>II/III</sup>{HB(mt)<sub>3</sub>}] complexes, we were able to model the equilibrium process involving the isomerisation between the  $\kappa^3$ -S,S',S'' and  $\kappa^3$ -H,S,S' coordination modes about the Ru centre; the activation energy ( $\Delta G^\ddagger$ ) determined through simulations of the <sup>1</sup>H NMR spectroscopic and cyclic voltammetric data is -2(9) and -7(5) kJ mol<sup>-1</sup>, respectively. The simulations also revealed a significant solvation effect in the intermediate as suggested by the much smaller  $\Delta S^\ddagger$  value in CH<sub>2</sub>Cl<sub>2</sub> than in d<sub>8</sub>-toluene.

The complex [Cp\*Ru{HB(mt)<sub>2</sub>(pz)}] was found to bind to O<sub>2</sub> and CO, in a manner similar to hemoglobin. It may thus serve as a simple molecular model. Furthermore, the oxidative addition of O<sub>2</sub> to the Ru centre has important implications in catalytic applications.

The reaction of [Cp'Ru(CO)<sub>2</sub>] (Cp'=C<sub>5</sub>H<sub>5</sub>, **25a**; Cp'=C<sub>5</sub>Me<sub>5</sub>, **25b**) with the heterocyclic disulfides led to S-S bond cleavage to form complexes of the type, [Cp'Ru(CO)<sub>2</sub>( $\kappa^1$ -SR)] (**26-29**). Those carrying a carboxylic acid functionality on the thiolate ligand could be converted to water-soluble organometallic complexes, K[Cp'Ru(CO)<sub>2</sub>( $\kappa^1$ -SR'COO)] (**30-31**), via reaction with K<sub>2</sub>CO<sub>3</sub>. The antiproliferative activity of these complexes against the MDA-MB231 and MCF7 breast cancer cell

lines was investigated, but the results were not encouraging. Nevertheless, in view of the current interest in the development of ruthenium complexes as anticancer drugs, the synthetic methodology developed will allow access to a broader range of ruthenium complexes with sulfur-containing heterocyclic ligands to be tested for medicinal applications. The ability of **25** to selectively cleave the disulfide bond was also utilised to cleave two of the four disulfide bonds in hen's egg white lysozyme. This may be further exploited for probing disulfide bonds in proteins.

**Publications:**

- Tay, E. P. L.; Kuan, S. L.; Leong, W. K.; Goh, L. Y. **Synthetic and x-ray Structural and Reactivity Studies of Cp\*Ru<sup>IV</sup> Complexes Containing Bidentate Dithiocarbonate, Xanthate, Carbonate, and Phosphinate Ligands (Cp\* =  $\eta^5$ -C<sub>5</sub>Me<sub>5</sub>).** *Inorganic Chemistry* (2007), 46(4), 1440-1450.
- Kuan, S. L.; Tay, E. P. L.; Leong, W. K.; Goh, L. Y.; Lin, C. Y.; Gill, P. M. W.; Webster, R. D. **Highly Oxidized Ruthenium Organometallic Compounds. The Synthesis and One-Electron Electrochemical Oxidation of [Cp\*Ru<sup>IV</sup>Cl<sub>2</sub>(S<sub>2</sub>CR)] (Cp\* =  $\eta^5$ -C<sub>5</sub>Me<sub>5</sub>, R = NMe<sub>2</sub>, NEt<sub>2</sub>, O<sup>i</sup>Pr).** *Organometallics* (2006), 25(26), 6134-6141.
- Kuan, S. L.; Leong, W. K.; Goh, L. Y.; Webster, R. D. **HMB and Cp\* ruthenium(II) complexes containing bis- and tris-(mercaptomethimazolyl)borate ligands: Synthetic, x-ray structural and electrochemical studies (HMB =  $\eta^6$ -C<sub>6</sub>Me<sub>6</sub>, Cp\* =  $\eta^5$ -C<sub>5</sub>Me<sub>5</sub>).** *Journal of Organometallic Chemistry* (2006), 691(5), 907-915.
- Kuan, S. L.; Leong, W. K.; Goh, L. Y.; Webster, R. D. **Redox-Dependent Isomerization of Organometallic Ru<sup>II</sup>/Ru<sup>III</sup> Compounds Containing the Hydrotris(methimazolyl)borate Ligand: An Electrochemical Square Scheme Mechanism.** *Organometallics* (2005), 24(19), 4639-4648.

**Manuscripts in preparation:**

- *Mixed-sandwich Cp\* chromium(III) complexes containing the poly(methimazolyl)borate ligands: Synthetic, structural and electrochemical studies (Cp\* =  $\eta^5$ -C<sub>5</sub>Me<sub>5</sub>).*  
Kuan, S. L.; Leong, W. K.; Goh, L. Y.; Webster, R. D.
- *HMB and Cp\* ruthenium(II) complexes containing mixed S, N-scorpionate ligands: Synthetic, X-ray structural and electrochemical studies (HMB =  $\eta^6$ -C<sub>6</sub>Me<sub>6</sub>, Cp\* =  $\eta^5$ -C<sub>5</sub>Me<sub>5</sub>).*  
Kuan, S. L.; Leong, W. K.; Goh, L. Y.; Webster, R. D.
- *Convenient syntheses of Cp'Ru(CO)<sub>2</sub>(SR) complexes containing heterocyclic ligands and syntheses of water-soluble Cp'Ru(CO)<sub>2</sub>(SR) complexes.*  
Kuan, S. L.; Tan, J.; Ng, S. Y.; Kong, K.V.; Leong, W. K.; Goh, L. Y.; Webster, R. D.

---

## Appendices

Table A1: Crystallographic Table for **2-7**

Table A2: Crystallographic Table for **9-11**

Table A3: Crystallographic Table for **14-20**

Figure A1: 2D  $^1\text{H}$  NMR NOESY spectrum for complex **16A/16B** in  $\text{C}_6\text{D}_6$

Figure A2: 2D  $^1\text{H}$  NMR COSY spectrum for complex **16A/16B** in  $\text{C}_6\text{D}_6$

Description of *g*NMR software

Figure A3: Cyclic voltammograms (Experimental and simulated) of 2.36 mM **14A** in  $\text{CH}_2\text{Cl}_2$  with 0.5 M *n*- $\text{Bu}_4\text{NPF}_6$

Figure A4: Cyclic voltammograms (Experimental and simulated) of 2.61 mM **16A/16B** in  $\text{CH}_2\text{Cl}_2$  with 0.5 M *n*- $\text{Bu}_4\text{NPF}_6$

Figure A5: Cyclic voltammograms of 2.36 mM **14A** and 2.5 mM ferrocene (**Fc**) in  $\text{CH}_2\text{Cl}_2$  with 0.5 M *n*- $\text{Bu}_4\text{NPF}_6$  at 293 K at different scan rates

Table A4: Crystallographic Table for **23-24**

Table A5: Calculated atomic charges, spin densities, and spin densities at the nuclei in the neutral and oxidized forms of  $[\text{Cp}^*\text{RuCl}_2(\text{S}_2\text{CNMe}_2)]$  (**21**).

Table A6: Crystallographic Table for **26-29**

Figure A6: ORTEP plots of **26-29**

Figure A7: MTT assay for complexes **26-31**

Experimental for trial reactions

**Table A1:** Crystallographic table for complexes **2-7**

Complexes	<b>2</b>	<b>3(0.25C<sub>4</sub>H<sub>10</sub>O)</b>	<b>4</b>
formula	C <sub>22</sub> H <sub>31</sub> BF <sub>6</sub> N <sub>6</sub> PRuS <sub>3</sub>	C <sub>19</sub> H <sub>29.50</sub> BBrCr N <sub>4</sub> O <sub>0.25</sub> S <sub>2</sub>	C <sub>21</sub> H <sub>29</sub> BBrCrN <sub>6</sub> S <sub>2</sub>
<i>M<sub>r</sub></i>	732.56	524.81	572.34
temp, K	223(2)	223(2)	223(2)
cryst color and habit	Blue, plate	Blue, block	Blue, plate
cryst size, mm	0.24 x 0.12 x 0.06	0.20 x 0.18 x 0.06	0.23 x 0.16 x 0.06
cryst system	Triclinic	Monoclinic	Monoclinic
space group	P-1	C2/m	P2 <sub>1</sub> /n
<i>a</i> , Å	10.0768(6)	28.3957(16)	16.9441(5)
<i>b</i> , Å	14.6139(8)	11.6257(6)	10.8424(3)
<i>c</i> , Å	21.3322(12)	20.3920(11)	27.3449(8)
<i>α</i> , deg	76.467(2)	90	90
<i>β</i> , deg	76.7890(10)	131.628(2)	98.9030(10)
<i>γ</i> , deg	70.187(2)	90	90
<i>V</i> , Å <sup>3</sup>	2834.9(3)	5031.8(5)	4963.1(2)
<i>Z</i>	4	8	8
density, Mg m <sup>-3</sup>	1.449	1.386	1.532
abs. coeff, mm <sup>-1</sup>	2.056	2.222	2.261
<i>F</i> (000)	1268	2156	2344
<i>θ</i> range for data collection	2.18 to 26.37	2.00 to 26.37	2.02 to 29.63
	-12<= <i>h</i> <=12,	-35<= <i>h</i> <=26,	-23<= <i>h</i> <=23,
index ranges	-17<= <i>k</i> <=18,	0<= <i>k</i> <=14,	0<= <i>k</i> <=14,
	0<= <i>l</i> <=26	0<= <i>l</i> <=25	0<= <i>l</i> <=37
no. of reflns collected	39455	21548	42138
indep reflns	11605 [R(int) = 0.0949]	5417 [R(int) = 0.0725]	12637 [R(int) = 0.0655]
no. of data/restraints/parameters	11605 / 0 / 656	5417 / 2 / 365	12637 / 0 / 599
final <i>R</i> indices [ <i>I</i> > 2σ( <i>I</i> )] <sup>a, b</sup>	R1 = 0.0853, wR2 = 0.1871	R1 = 0.0899, wR2 = 0.2089	R1 = 0.1155, wR2 = 0.2262
<i>R</i> indices (all data)	R1 = 0.1428, wR2 = 0.2159	R1 = 0.1291, wR2 = 0.2329	R1 = 0.1305, wR2 = 0.2330
goodness-of-fit on <i>F</i> <sup>2 c</sup>	1.055	1.078	1.379
large diff peak and hole, e Å <sup>-3</sup>	1.787 and -0.683	1.663 and -1.496	1.032 and -0.987



Complexes	5(1.0CH <sub>3</sub> CN;1.0C <sub>4</sub> H <sub>10</sub> O)	6	7(1.0CH <sub>3</sub> CN)
formula	C <sub>26</sub> H <sub>43</sub> BCrF <sub>6</sub> N <sub>6</sub> OPS <sub>2</sub>	C <sub>18</sub> H <sub>27</sub> BCrF <sub>6</sub> N <sub>4</sub> PS <sub>2</sub>	C <sub>23</sub> H <sub>32</sub> BCrF <sub>6</sub> N <sub>7</sub> PS <sub>2</sub>
<i>M<sub>r</sub></i>	727.56	571.34	678.46
temp, K	223(2)	223(2)	223(2)
cryst color and habit	Dark, block	Green, block	Blue, block
cryst size, mm	0.40 x 0.30 x 0.06	0.34 x 0.28 x 0.14	0.40 x 0.34 x 0.20
cryst system	Monoclinic	Monoclinic	Monoclinic
space group	P2 <sub>1</sub> /c	C2/c	P2 <sub>1</sub> /c
<i>a</i> , Å	16.7803(8)	23.0271(11)	12.4508(6)
<i>b</i> , Å	15.3114(7)	18.2357(9)	8.9491(4)
<i>c</i> , Å	14.9394(7)	15.2357(7)	27.4984(13)
<i>α</i> , deg	90	90	90
<i>β</i> , deg	111.7480(10)	129.6980(10)	96.3050(10)
<i>γ</i> , deg	90	90	90
<i>V</i> , Å <sup>3</sup>	2834.9(3)	5031.8(5)	3045.4(2)
<i>Z</i>	4	8	4
density, Mg m <sup>-3</sup>	1.356	1.542	1.480
abs. coeff, mm <sup>-1</sup>	0.544	0.759	0.629
<i>F</i> (000)	1516	2344	1396
<i>θ</i> range for data collection	1.86 to 27.50	2.23 to 30.52	2.10 to 30.50
index ranges	-21 ≤ <i>h</i> ≤ 21,	-31 ≤ <i>h</i> ≤ 24,	-17 ≤ <i>h</i> ≤ 16,
	-19 ≤ <i>k</i> ≤ 19,	0 ≤ <i>k</i> ≤ 25,	0 ≤ <i>k</i> ≤ 12,
	-19 ≤ <i>l</i> ≤ 19	0 ≤ <i>l</i> ≤ 21	0 ≤ <i>l</i> ≤ 39
no. of reflns collected	46041	22430	27495
indep reflns	8195 [R(int) = 0.0353]	6996 [R(int) = 0.0378]	8736 [R(int) = 0.0299]
no. of data/restraints/parameters	8195 / 11 / 449	6996 / 150 / 333	8736 / 0 / 382
final <i>R</i> indices [ <i>I</i> > 2σ( <i>I</i> )] <sup>a, b</sup>	R1 = 0.0536, wR2 = 0.1276	R1 = 0.0668, wR2 = 0.1718	R1 = 0.0478, wR2 = 0.1172
<i>R</i> indices (all data)	R1 = 0.0610, wR2 = 0.1321	R1 = 0.0862, wR2 = 0.1854	R1 = 0.0575, wR2 = 0.1229
goodness-of-fit on F <sup>2</sup> <sup>c</sup>	1.138	1.029	1.072
large diff peak and hole, e Å <sup>-3</sup>	0.589 and -0.265	1.460 and -0.526	0.590 and -0.329

$$^a R = (\sum |F_o| - |F_c|) / \sum |F_o| \quad ^b wR_2 = [(\sum \omega |F_o| - |F_c|)^2 / \sum \omega |F_o|^2]^{1/2} \quad ^c \text{GoF} = [(\sum \omega |F_o| - |F_c|)^2 / (N_{\text{obs}} - N_{\text{param}})]^{1/2}$$

**Table A2:** Crystallographic table for complexes **9-11**

Complexes	<b>9</b>	<b>10(0.25CH<sub>2</sub>Cl<sub>2</sub>)</b>	<b>11(0.75CH<sub>3</sub>CN)</b>	<b>11'(1.0CH<sub>2</sub>Cl<sub>2</sub>)</b>
formula	C <sub>24</sub> H <sub>34</sub> BClN <sub>6</sub> RuS <sub>3</sub>	C <sub>20.50</sub> H <sub>31</sub> BCl <sub>2</sub> N <sub>4</sub> RuS <sub>2</sub>	C <sub>23.50</sub> H <sub>32.25</sub> BF <sub>6</sub> N <sub>6.75</sub> PRuS <sub>2</sub>	C <sub>24</sub> H <sub>34</sub> BCl <sub>3</sub> N <sub>6</sub> RuS <sub>2</sub>
<i>M<sub>r</sub></i>	650.08	580.39	730.28	688.92
temp, K	223(2)	223(2)	223(2)	223(2)
cryst color and habit	Red, block	Red, needle	Red, needle	Red, block
cryst size, mm	0.34 × 0.30 × 0.14	0.40 × 0.11 × 0.09	0.37 x 0.10 x 0.01	0.20 x 0.20 x 0.16
cryst system	Trigonal	Monoclinic	Monoclinic	Monoclinic
space group	P-3	C2/m	P2 <sub>1</sub> /m	P2 <sub>1</sub> /n
<i>a</i> , Å	13.2095(7)	19.637(7)	12.9471(13)	13.0005(7)
<i>b</i> , Å	13.2095(7)	1411.703(4)	12.1262(13)	17.7640(8)
<i>c</i> , Å	9.9220(11)	11.970(4)	21.102(2)	13.2947(6)
<i>α</i> , deg	90	90	90	90
<i>β</i> , deg	90	105.109(7)	93.458(3)	110.6150(10)
<i>γ</i> , deg	120	90	90	90
<i>V</i> , Å <sup>3</sup>	1499.3(2)	2655.6(17)	3307.0(6)	2873.7(2)
<i>Z</i>	2	4	4	4
density, Mg m <sup>-3</sup>	1.440	1.452	1.467	1.592
abs. coeff, mm <sup>-1</sup>	0.845	0.964	0.708	0.997
<i>F</i> (000)	668	1188	1482	1408
<i>θ</i> range for data collection	2.05 to 26.37	2.05 to 29.83	2.30 to 26.37	2.00 to 27.50
	-16<= <i>h</i> <=8,	-26<= <i>h</i> <=25,	-16<= <i>h</i> <=16,	-12<= <i>h</i> <=16,
index ranges	0<= <i>k</i> <=16, 0<= <i>l</i> <=12	0<= <i>k</i> <=16, 0<= <i>l</i> <=16	0<= <i>k</i> <=15, 0<= <i>l</i> <=26	-23<= <i>k</i> <=19, -17<= <i>l</i> <=17
no. of reflns collected	11422	15089	43337	20248
indep reflns	2065 [R(int) = 0.0516]	3684 [R(int) = 0.0828]	7086 [R(int) = 0.1606]	6561 [R(int) = 0.0430]
no. of data/restraints/parameters	2056 / 0 / 161	3684 / 1 / 177	7086 / 72 / 403	6561 / 2 / 338
final <i>R</i> indices [ <i>I</i> > 2σ( <i>I</i> )] <sup>a, b</sup>	R1 = 0.0679, wR2 = 0.1898	R1 = 0.1092, wR2 = 0.2553	R1 = 0.1632, wR2 = 0.3434	R1 = 0.0702, wR2 = 0.1768
<i>R</i> indices (all data)	R1 = 0.0778, wR2 = 0.1992	R1 = 0.1175, wR2 = 0.2603	R1 = 0.1798, wR2 = 0.3515	R1 = 0.0843, wR2 = 0.1861
goodness-of-fit on <i>F</i> <sup>2 c</sup>	1.178	1.281	1.257	1.091
large diff peak and hole, e Å <sup>-3</sup>	3.859 and -0.868	2.584 and -1.983	2.161 and -3.268	2.277 and -1.529

<sup>a</sup>  $R = (\sum |F_o| - |F_c|) / \sum |F_o|$ . <sup>b</sup>  $wR_2 = [(\sum w|F_o| - |F_c|)^2 / \sum w|F_o|^2]^{1/2}$ . <sup>c</sup>  $GoF = [(\sum w|F_o| - |F_c|)^2 / (N_{obs} - N_{param})]^{1/2}$

**Table A3:** Crystallographic Table for complexes **14-20**

Complexes	<b>14A.PF<sub>6</sub></b>	<b>16A(0.5H<sub>2</sub>O)</b>	<b>17(0.25C<sub>7</sub>H<sub>8</sub>)</b>	<b>18</b>
formula	C <sub>22</sub> H <sub>31</sub> BF <sub>6</sub> N <sub>6</sub> PRuS <sub>3</sub>	C <sub>22</sub> H <sub>32</sub> BN <sub>6</sub> O <sub>0.50</sub> RuS <sub>3</sub>	C <sub>19.75</sub> H <sub>29</sub> BN <sub>4</sub> RuS <sub>2</sub>	C <sub>21</sub> H <sub>29</sub> BN <sub>6</sub> RuS <sub>2</sub>
<i>M<sub>r</sub></i>	732.56	596.60	498.47	541.50
temp, K	223(2)	223(2)	223(2)	223(2)
cryst color and habit	Dark brown, rhombus	Pink, hexagon	Red, plate	Red, block
cryst size, mm	0.34 × 0.26 × 0.06	0.28 × 0.28 × 0.28	0.14 × 0.12 × 0.02	0.40 × 0.20 × 0.16
cryst system	Triclinic	Trigonal	Monoclinic	Monoclinic
space group	P-1	P-3	C2/c	P2 <sub>1</sub> /n
<i>a</i> , Å	10.2117(6)	14.7149(3)	14.2301(7)	11.2294(7)
<i>b</i> , Å	11.8399(7)	14.7149(3)	14.2921(7)	15.0839(10)
<i>c</i> , Å	14.4314(8)	10.1605(4)	24.8174(12)	14.5169(9)
<i>α</i> , deg	66.313(1)	90	90	90
<i>β</i> , deg	70.034(1)	90	106.524 (2)	107.9080(10)
<i>γ</i> , deg	86.069(1)	120	90	90
<i>V</i> , Å <sup>3</sup>	31497.02(15)	1905.29(9)	4838.9(4)	2339.8(3)
<i>Z</i>	2	2	8	4
density, Mg m <sup>-3</sup>	1.625	1.040	1.368	1.537
abs. coeff, mm <sup>-1</sup>	0.849	0.593	0.832	0.870
<i>F</i> (000)	742	614	2052	1112
<i>θ</i> range for data collection	2.13 to 30.00	2.56 to 26.36	2.06 to 26.37	2.00 to 27.49
index ranges	-13 ≤ <i>h</i> ≤ 14, -14 ≤ <i>k</i> ≤ 16, 0 ≤ <i>l</i> ≤ 20	-18 ≤ <i>h</i> ≤ 9, 0 ≤ <i>k</i> ≤ 18, 0 ≤ <i>l</i> ≤ 12	-17 ≤ <i>h</i> ≤ 17, 0 ≤ <i>k</i> ≤ 17, 0 ≤ <i>l</i> ≤ 30	-8 ≤ <i>h</i> ≤ 14, -19 ≤ <i>k</i> ≤ 19, -18 ≤ <i>l</i> ≤ 18
no. of reflns collected	22948	15804	34190	15908
indep reflns	8479 [R(int) = 0.0366]	2611 [R(int) = 0.0333]	4959 [R(int) = 0.1126]	5355 [R(int) = 0.0443]
no. of data/restraints/parameters	8479/30/374	2611/ 27 / 97	4959 / 2 / 260	5355 / 0 / 291
final <i>R</i> indices [ <i>I</i> > 2σ( <i>I</i> )] <sup>a, b</sup>	R1 = 0.0496, wR2 = 0.1183	R1 = 0.0761, wR2 = 0.231	R1 = 0.1025, wR2 = 0.2128	R1 = 0.0484, wR2 = 0.1287
<i>R</i> indices (all data)	R1 = 0.0593 wR2 = 0.1242	R1 = 0.1113, wR2 = 0.2661	R1 = 0.1136, wR2 = 0.2187	R1 = 0.0565, wR2 = 0.1344
goodness-of-fit on F <sup>2</sup> <sup>c</sup>	1.069	1.156	1.318	1.041
large diff peak and hole, e Å <sup>-3</sup>	1.008 and -0.617	0.779 and -0.286	1.487 and -1.988	0.833 and -0.489

Complexes	<b>19(1.0C<sub>4</sub>H<sub>8</sub>O)</b>	<b>20</b>
formula	C <sub>25</sub> H <sub>37</sub> BN <sub>6</sub> O <sub>3</sub> RuS <sub>2</sub>	C <sub>22</sub> H <sub>29</sub> BN <sub>6</sub> ORuS <sub>2</sub>
<i>M<sub>r</sub></i>	645.61	569.51
temp, K	223(2)	223(2)
cryst color and habit	Brown, plate	Red, plate
cryst size, mm	0.30 x 0.22 x 0.04	0.26 x 0.14 x 0.06
cryst system	Monoclinic	Monoclinic
space group	C2/m	C2/c
<i>a</i> , Å	18.3084(7)	40.061(2)
<i>b</i> , Å	12.0020(4)	13.1846(8)
<i>c</i> , Å	15.6542(6)	9.6673(6)
<i>α</i> , deg	90	90
<i>β</i> , deg	123.1980(10)	92.5340(10)
<i>γ</i> , deg	90	90
<i>V</i> , Å <sup>3</sup>	2878.38(18)	5101.2(5)
<i>Z</i>	4	8
density, Mg m <sup>-3</sup>	1.490	1.483
abs. coeff, mm <sup>-1</sup>	0.728	0.805
<i>F</i> (000)	1336	2336
<i>θ</i> range for data collection	2.16 to 30.00	1.02 to 27.50
index ranges	-25 ≤ <i>h</i> ≤ 20, 0 ≤ <i>k</i> ≤ 16, 0 ≤ <i>l</i> ≤ 21	-51 ≤ <i>h</i> ≤ 52, -17 ≤ <i>k</i> ≤ 17, -12 ≤ <i>l</i> ≤ 12
no. of reflns collected	20847	33112
indep reflns	4086 [R(int) = 0.0330]	5871 [R(int) = 0.0863]
no. of data/restraints/parameters	4086 / 13 / 212	5871 / 0 / 308
final <i>R</i> indices [ <i>I</i> > 2σ( <i>I</i> )] <sup>a, b</sup>	R1 = 0.0439, wR2 = 0.1054	R1 = 0.0617, wR2 = 0.1329
<i>R</i> indices (all data)	R1 = 0.0474, wR2 = 0.1079	R1 = 0.0740, wR2 = 0.1414
goodness-of-fit on F <sup>2</sup> <sup>c</sup>	1.173	1.147
large diff peak and hole, e Å <sup>-3</sup>	1.063 and -0.619	1.036 and -1.094

<sup>a</sup>  $R = (\sum |F_o| - |F_c|) / \sum |F_o|$ . <sup>b</sup>  $wR_2 = [(\sum w|F_o| - |F_c|)^2 / \sum w|F_o|^2]^{1/2}$ . <sup>c</sup>  $GoF = [(\sum w|F_o| - |F_c|)^2 / (N_{obs} - N_{param})]^{1/2}$

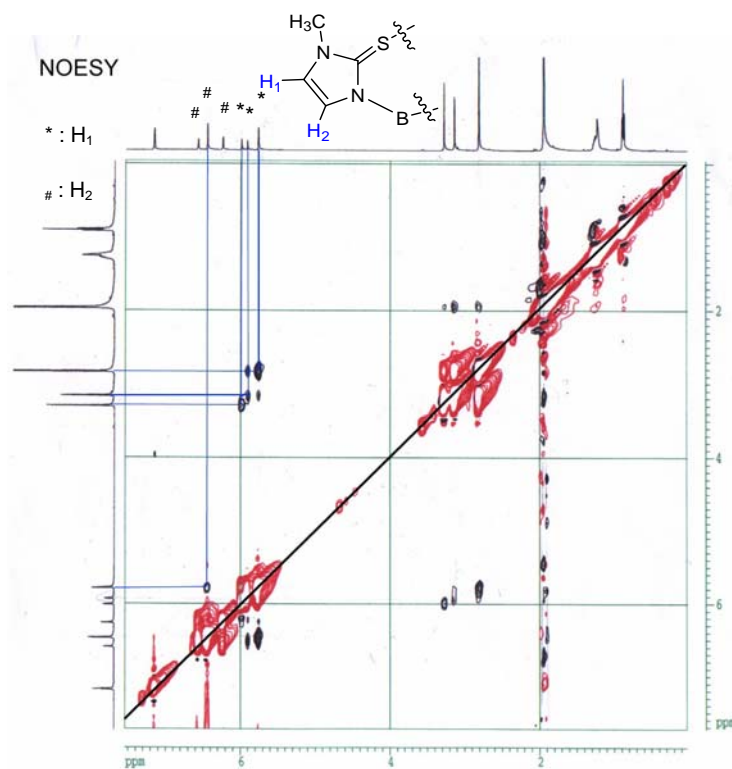


Figure A1. 2D <sup>1</sup>H NMR NOESY spectrum for complex **16A/16B** in C<sub>6</sub>D<sub>6</sub>.

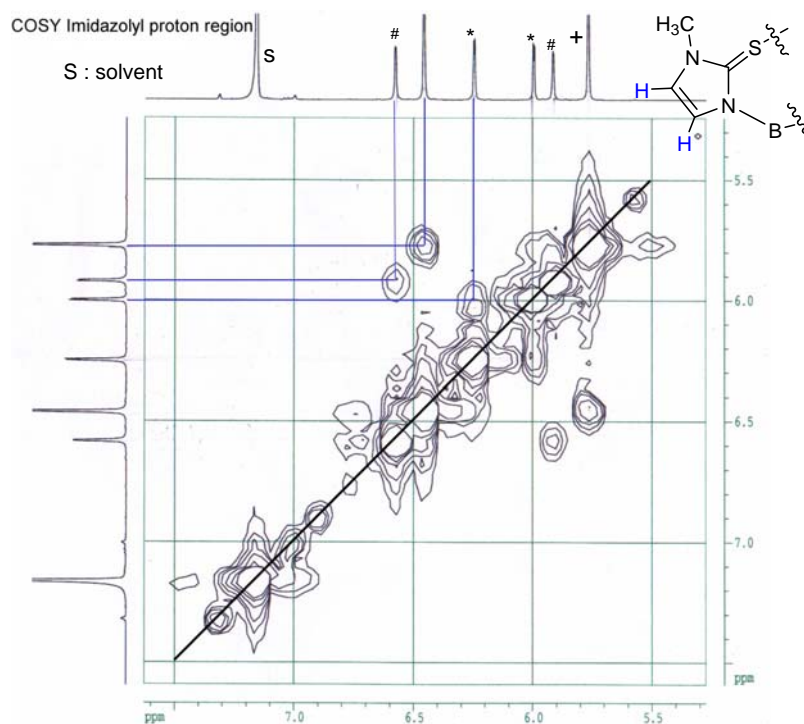
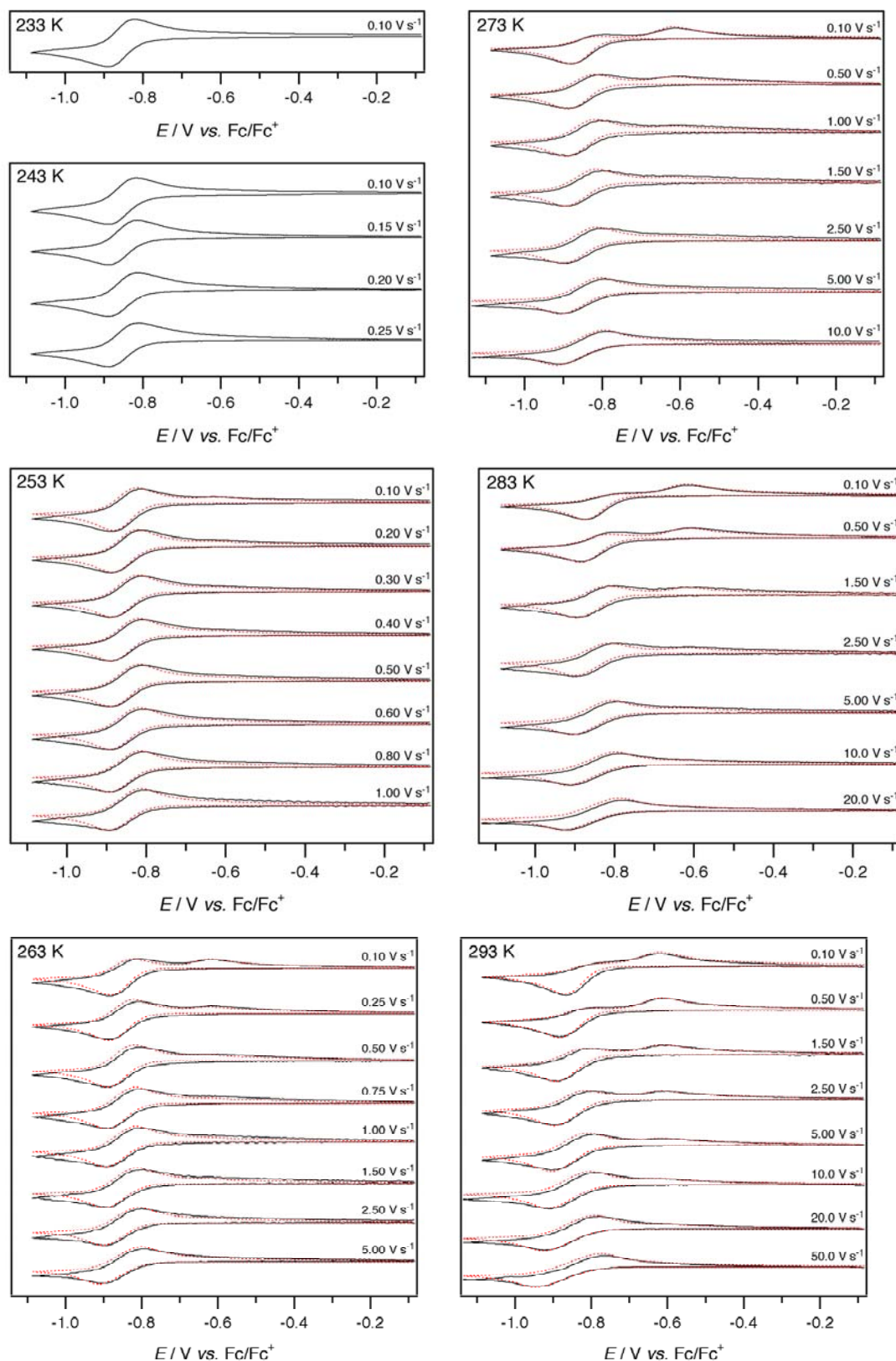
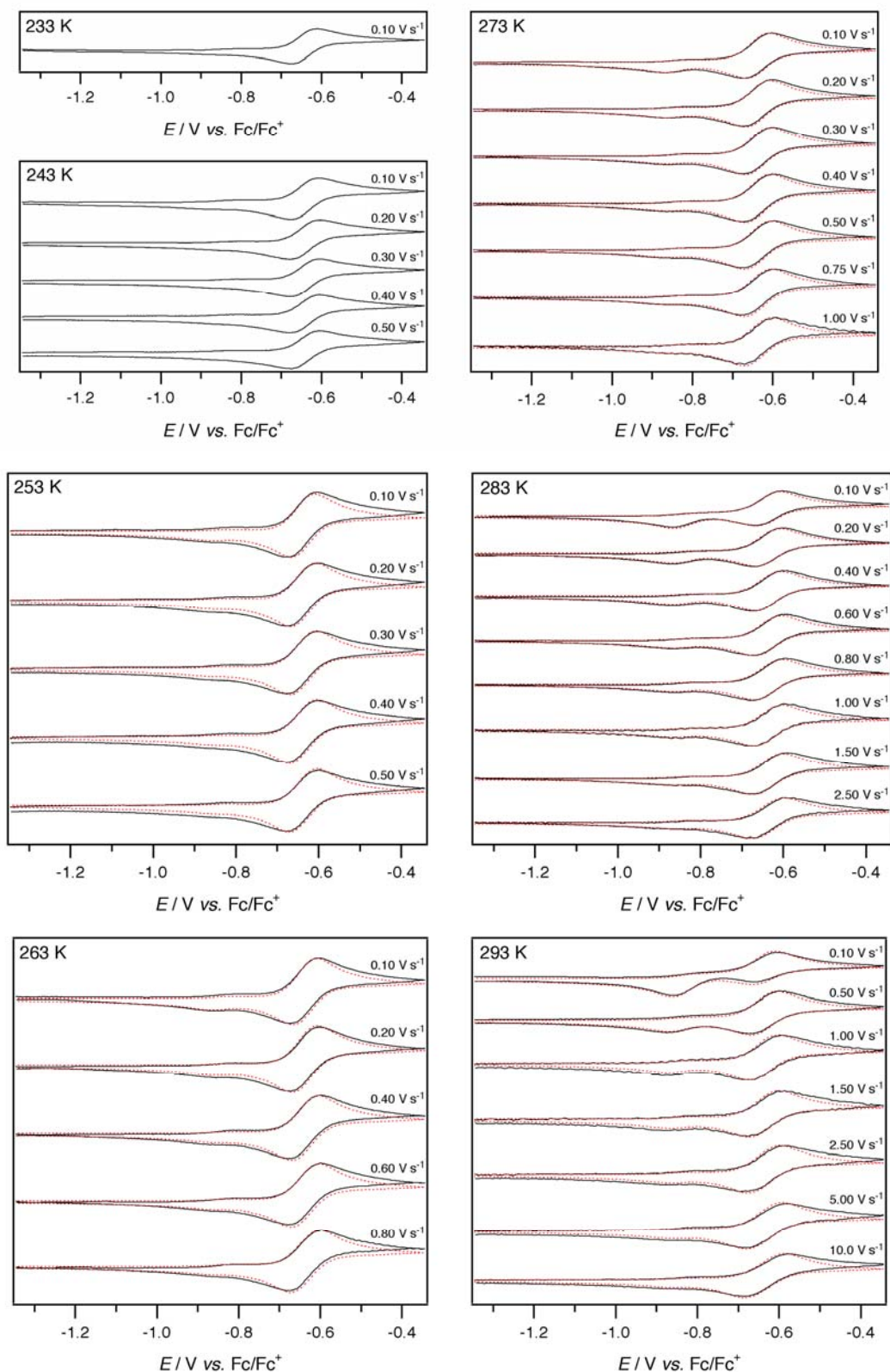


Figure A2. 2D <sup>1</sup>H NMR COSY spectrum for complex **16A/16B** in C<sub>6</sub>D<sub>6</sub>.

**gNMR** is a program for simulating one dimensional NMR spectra for any NMR-active nucleus, in single molecules or mixtures. Either direct input for chemical shifts and coupling constants, or prediction using chemical structures imported from drawing packages can be used for simulations. Information that can be obtained includes evaluation of second-order effects, isotope effects and identification and measurement of chemical exchange.



**Figure A3.** Cyclic voltammograms of 2.36 mM **14A** in  $\text{CH}_2\text{Cl}_2$  with 0.5 M  $n\text{-Bu}_4\text{NPF}_6$ . (a) Scan rate ( $\nu$ ) = 0.1  $\text{V s}^{-1}$ . (b)  $T = 293$  K. Current data were scaled by multiplying by  $\nu^{-0.5}$ . (—) Experimental data. (---) Voltammograms simulated using DigiSim<sup>®</sup>.



**Figure A4.** Cyclic voltammograms of 2.61 mM **16A/16B** in  $\text{CH}_2\text{Cl}_2$  with 0.5 M  $n\text{-Bu}_4\text{NPF}_6$ . (a) Scan rate ( $\nu$ ) =  $0.1 \text{ V s}^{-1}$ . (b)  $T = 293 \text{ K}$ . Current data were scaled by multiplying by  $\nu^{-0.5}$ . (—) Experimental data. (---) Voltammograms simulated using DigiSim<sup>®</sup>.



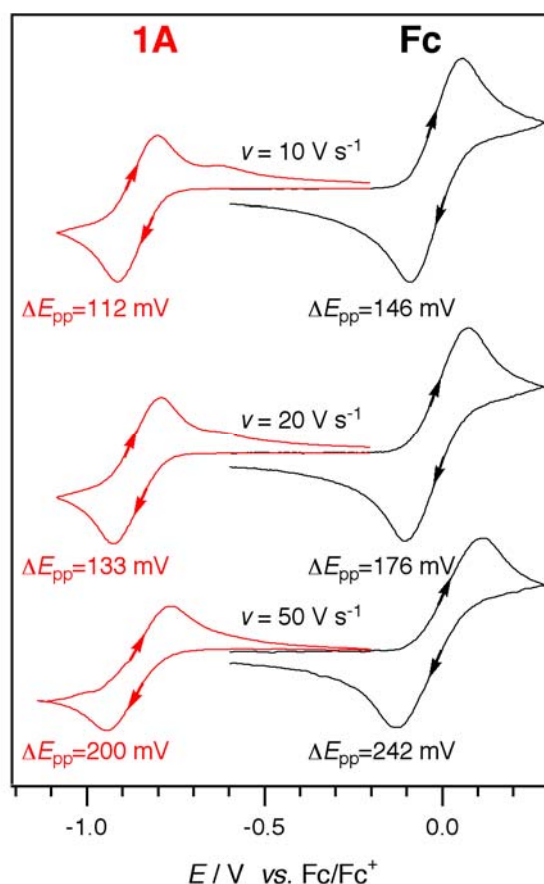


**Figure A5.** Cyclic voltammograms of 2.36 mM **1A** and 2.5 mM ferrocene (**Fc**) in  $\text{CH}_2\text{Cl}_2$  with 0.5 M  $n\text{-Bu}_4\text{NPF}_6$  at 293 K at different scan rates ( $v$ ). Current data were scaled by multiplying by  $v^{-0.5}$ . The voltammograms were background subtracted at each scan rate to remove the effects of capacitance.

The  $\Delta E_{\text{pp}}$ -values for **Fc** were greater than **1A** at each scan rate because the **Fc/Fc**<sup>+</sup> redox couple is completely chemically reversible, whilst **1A** undergoes a homogeneous reaction following electron transfer (thus the reverse peak is substantially smaller than the forward peak). **Fc** is considered to be a model compound that undergoes relatively fast heterogeneous electron transfer in organic solvents. The heterogeneous rate constant for **Fc** has been estimated to be between 1 - 4  $\text{cm s}^{-1}$  (in  $\text{CH}_3\text{CN}$ ).<sup>1</sup> Therefore, the large  $\Delta E_{\text{pp}}$ -values shown in Figure S6 for both **1A** and **Fc** at moderately fast scan rates are consistent with the effects of uncompensated solution resistance, rather than slow heterogeneous electron transfer.

#### Additional Reference

1. Clegg, A. D.; Rees, N. V.; Klymenko, O. V.; Coles, B. A.; Compton, R. G. *J. Electroanal. Chem.* **2005**, *580*, 78-86, and references within.

**Table A3:** Crystallographic Table for complexes **23** and **24**

Complexes	<b>23</b>	<b>24</b>
formula	C <sub>21</sub> H <sub>33</sub> F <sub>12</sub> N <sub>5</sub> P <sub>2</sub> RuS <sub>2</sub>	C <sub>13</sub> H <sub>21</sub> Cl <sub>7</sub> NRuS <sub>2</sub> Sb
<i>M<sub>r</sub></i>	810.65	726.40
temp, K	223(2)	223(2)
cryst color and habit	Red plate	Red plate
cryst size, mm	0.28 × 0.20 × 0.06	0.48 × 0.36 × 0.02
cryst system	Orthorhombic	Monoclinic
space group	P2 <sub>1</sub> 2 <sub>1</sub> 2 <sub>1</sub>	P2 <sub>1</sub> /n
<i>a</i> , Å	9.3012(4)	8.2628(5)
<i>b</i> , Å	12.2982(5)	11.0759(7)
<i>c</i> , Å	28.5968(13)	26.4815(16)
<i>α</i> , deg	90	90
<i>β</i> , deg	90	96.5860(10)
<i>γ</i> , deg	90	90
<i>V</i> , Å <sup>3</sup>	3271.1(2)	2407.5(3)
<i>Z</i>	4	4
density, Mg m <sup>-3</sup>	1.646	2.004
abs. coeff, mm <sup>-1</sup>	0.795	2.700
<i>F</i> (000)	1632	1408
<i>θ</i> range for data collection	1.80 to 27.49	2.40 to 26.37
index ranges	-12 ≤ <i>h</i> ≤ 9, 15 ≤ <i>k</i> ≤ 15, -37 ≤ <i>l</i> ≤ 36	-10 ≤ <i>h</i> ≤ 10, 0 ≤ <i>k</i> ≤ 13, 0 ≤ <i>l</i> ≤ 33
no. of reflns collected	23277	19829
indep reflns	7472 [R(int) = 0.0487]	4928 [R(int) = 0/0513]
no. of data/restraints/parameters	7472 / 0 / 399	4928/0/233
final <i>R</i> indices [ <i>I</i> > 2σ( <i>I</i> )] <sup>a, b</sup>	R1 = 0.0520, wR2 = 0.1153	R1 = 0.0893, wR2 = 0.1903
<i>R</i> indices (all data)	R1 = 0.0589, wR2 = 0.1186	R1 = 0.0969, wR2 = 0.1940
goodness-of-fit on F <sup>2 c</sup>	1.097	1.315
large diff peak and hole, e Å <sup>-3</sup>	1.044 and -0.734	2.483 and -1.844

$$^a R = (\sum |F_o| - |F_c|) / \sum |F_o| \quad ^b wR_2 = [(\sum w|F_o| - |F_c|)^2 / \sum w|F_o|^2]^{1/2} \quad ^c \text{GoF} = [(\sum w|F_o| - |F_c|)^2 / (N_{\text{obs}} - N_{\text{param}})]^{1/2}$$

**Table A5.** Calculated<sup>a</sup> atomic charges, spin densities, and spin densities at the nuclei in the neutral and oxidized forms of [Cp\*RuCl<sub>2</sub>(S<sub>2</sub>CNMe<sub>2</sub>)] (21).

Atom Number	Atom Type	Charge			Spin Density	Spin Density At Nucleus
		[Cp*RuCl <sub>2</sub> (S <sub>2</sub> CR)]	[Cp*RuCl <sub>2</sub> (S <sub>2</sub> CR)] <sup>+</sup>	[Cp*RuCl <sub>2</sub> (S <sub>2</sub> CR)] <sup>+</sup> [Cp*RuCl <sub>2</sub> (S <sub>2</sub> CR)] <sup>-</sup>	[Cp*RuCl <sub>2</sub> (S <sub>2</sub> CR)] <sup>+</sup>	[Cp*RuCl <sub>2</sub> (S <sub>2</sub> CR)] <sup>+</sup>
1	Ru	0.377	0.43789	0.06089	0.69267	-0.2102290
2	C	-0.69777	-0.6999	-0.00213	0.00141	0.0001311
3	C	-0.0254	0.0073	0.03270	0.00007	0.0041720
4	C	-0.02699	0.00698	0.03397	-0.00092	0.0046729
5	C	-0.69535	-0.69841	-0.00306	0.00031	-0.0005398
6	C	-0.69405	-0.69566	-0.00161	0.00231	0.0002290
7	C	-0.02582	0.00728	0.03310	0.00076	0.0043677
8	C	-0.69784	-0.69994	-0.00210	0.00136	0.0000658
9	C	0.00257	0.03965	0.03708	0.01266	0.0065492
10	C	-0.69527	-0.69827	-0.00300	0.00034	-0.0005421
11	C	0.00252	0.03952	0.03700	0.01299	0.0065688
12	Cl	-0.44907	-0.30116	0.14791	0.11556	0.0187709
13	S	0.03026	0.1075	0.07724	0.00154	0.0044718
14	Cl	-0.44995	-0.30105	0.14890	0.1177	0.0191466

15	S	0.03059	0.10728	0.07669	-0.00012	0.0039312
16	H	0.25753	0.26773	0.01020	-0.0001	-0.0000694
17	H	0.27204	0.27995	0.00791	-0.00031	-0.0002385
18	H	0.25883	0.28107	0.02224	-0.00017	-0.0001158
19	H	0.26005	0.26851	0.00846	-0.00028	-0.0001958
20	H	0.26017	0.26863	0.00846	-0.00028	-0.0001946
21	H	0.25902	0.2819	0.02288	-0.00053	-0.0003549
22	H	0.2577	0.26788	0.01018	-0.00011	-0.0000758
23	H	0.25891	0.28111	0.02220	-0.00022	-0.0001497
24	H	0.27159	0.2796	0.00801	-0.00033	-0.0002490
25	H	0.27177	0.28018	0.00841	-0.00017	-0.0001952
26	H	0.25741	0.28111	0.02370	-0.0005	-0.0003710
27	H	0.26899	0.27932	0.01033	-0.00016	-0.0001609
28	H	0.27015	0.28026	0.01011	-0.00017	-0.0001733
29	H	0.25738	0.28106	0.02368	-0.00049	-0.0003600
30	H	0.27075	0.27935	0.00860	-0.00016	-0.0001764
31	C	-0.06099	-0.05044	0.01055	0.003	0.0001432
32	N	-0.42084	-0.38085	0.03999	0.0403	0.0129684

33	C	-0.47577	-0.47265	0.00312	-0.00174	-0.0014372
34	C	-0.47587	-0.47279	0.00308	-0.00176	-0.0014459
35	H	0.24396	0.26088	0.01692	0.00079	0.0005066
36	H	0.26241	0.26159	-0.00082	0.00022	0.0000636
37	H	0.24148	0.25754	0.01606	0.00177	0.0012000
38	H	0.26245	0.26168	-0.00077	0.00024	0.0000687
39	H	0.24396	0.2609	0.01694	0.00078	0.0004998
40	H	0.24149	0.25748	0.01599	0.00177	0.0012024

<sup>a</sup> Optimized structures and Natural Bond Orbital analysis using the B3LYP functional. See text for basis set and Rassolov-Chipman details.

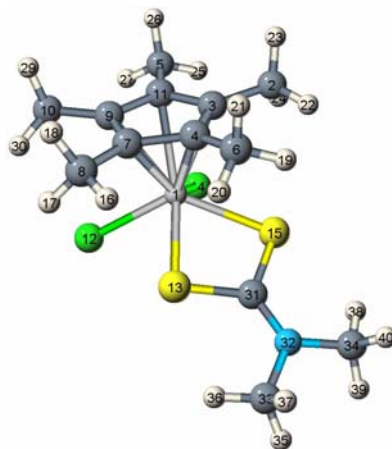


**Table A6:** Crystallographic table for complexes **26-29**

Complexes	<b>26b</b>	<b>27a</b>	<b>27b</b>	<b>28</b>	<b>29(0.5C<sub>6</sub>H<sub>14</sub>)</b>
formula	C <sub>19</sub> H <sub>19</sub> NO <sub>2</sub> RuS <sub>2</sub>	C <sub>12</sub> H <sub>9</sub> NO <sub>2</sub> RuS	C <sub>17</sub> H <sub>19</sub> NO <sub>2</sub> RuS	C <sub>19</sub> H <sub>20</sub> O <sub>4</sub> RuS	C <sub>19.50</sub> H <sub>22.50</sub> NO <sub>4</sub> RuS
<i>M<sub>r</sub></i>	458.54	332.33	402.46	445.48	468.02
temp, K	223(2)	223(2)	223(2)	223(2)	223(2)
cryst color and habit	Yellow, plate	Orange, block	Yellow, block	Orange, block	Yellow, block
cryst size, mm	0.14 x 0.12 x 0.08	0.28 x 0.10 x 0.08	0.28 x 0.24 x 0.24	0.30 x 0.16 x 0.10	0.50 x 0.40 x 0.24
cryst system	Monoclinic	Triclinic	Orthorhombic	Monoclinic	Monoclinic
space group	C2/c	P-1	Pna2 <sub>1</sub>	P2 <sub>1</sub> /n	P2 <sub>1</sub> /c
<i>a</i> , Å	32.6716(13)	7.4109(9)	13.9096(9)	8.8385(6)	19.393(5)
<i>b</i> , Å	8.7481(4)	7.5542(9)	14.2583(9)	14.4533(11)	8.2409(19)
<i>c</i> , Å	14.0204(6)	11.5075(13)	8.5584(5)	15.3005(12)	15.563(4)
<i>α</i> , deg	90	94.779(2)	90	90	90
<i>β</i> , deg	96.7180(10)	99.857(2)	90	90.886(2)	113.121(5)
<i>γ</i> , deg	90	101.763(2)	90	90	90
<i>V</i> , Å <sup>3</sup>	3979.7(3)	616.70(13)	1697.36(18)	1954.3(3)	2287.5(9)
<i>Z</i>	8	2	4	4	4
density, Mg m <sup>-3</sup>	1.531	1.790	1.575	1.514	1.359
abs. coeff, mm <sup>-1</sup>	1.009	1.427	1.052	0.928	0.797
<i>F</i> (000)	1856	328	816	904	954
<i>θ</i> range for data collection	2.41 to 27.50	1.81 to 27.50	2.05 to 27.50	1.94 to 25.00	2.28 to 27.50
index ranges	-42<= <i>h</i> <=42, -11<= <i>k</i> <=11, -18<= <i>l</i> <=18	-9<= <i>h</i> <=9, -9<= <i>k</i> <=9, -14<= <i>l</i> <=14	-18<= <i>h</i> <=18,- 18<= <i>k</i> <=18, -11<= <i>l</i> <=11	-7<= <i>h</i> <=10, -16<= <i>k</i> <=17, -18<= <i>l</i> <=17	-24<= <i>h</i> <=25, -10<= <i>k</i> <=9, -19<= <i>l</i> <=20
no. of reflns collected	25344	8151	21302	11381	15664
indep reflns	4573 [R(int) = 0.0486]	2824 [R(int) = 0.0322]	3884 [R(int) = 0.0302]	3443 [R(int) = 0.0438]	5249 [R(int) = 0.0355]
no. of data/restraints/parameters	4573 / 10 / 403	2824 / 0 / 170	3884 / 1 / 204	3443 / 0 / 235	5249 / 22 / 261
final <i>R</i> indices [ <i>I</i> > 2σ( <i>I</i> )] <sup>a, b</sup>	R1 = 0.0515, wR2 = 0.1070	R1 = 0.0364, wR2 = 0.0868	R1 = 0.0406, wR2 = 0.1093	R1 = 0.0530, wR2 = 0.1181	R1 = 0.0456, wR2 = 0.1322
<i>R</i> indices (all data)	R1 = 0.0722, wR2 = 0.1152	R1 = 0.0408, wR2 = 0.0886	R1 = 0.0406, wR2 = 0.1093	R1 = 0.0701, wR2 = 0.1261	R1 = 0.0541, wR2 = 0.1373
goodness-of-fit on F <sup>2</sup> <sup>c</sup>	1.113	1.096	1.233	1.075	1.073
large diff peak and hole, e Å <sup>-3</sup>	0.431 and -0.203	0.873 and -0.413	1.170 and -1.246	0.778 and -0.288	1.313 and -0.515

<sup>a</sup>  $R = (\sum |F_o| - |F_c|) / \sum |F_o|$ . <sup>b</sup>  $wR_2 = [(\sum w|F_o| - |F_c|)^2 / \sum w|F_o|^2]^{1/2}$ . <sup>c</sup>  $GoF = [(\sum w|F_o| - |F_c|)^2 / (N_{obs} - N_{param})]^{1/2}$

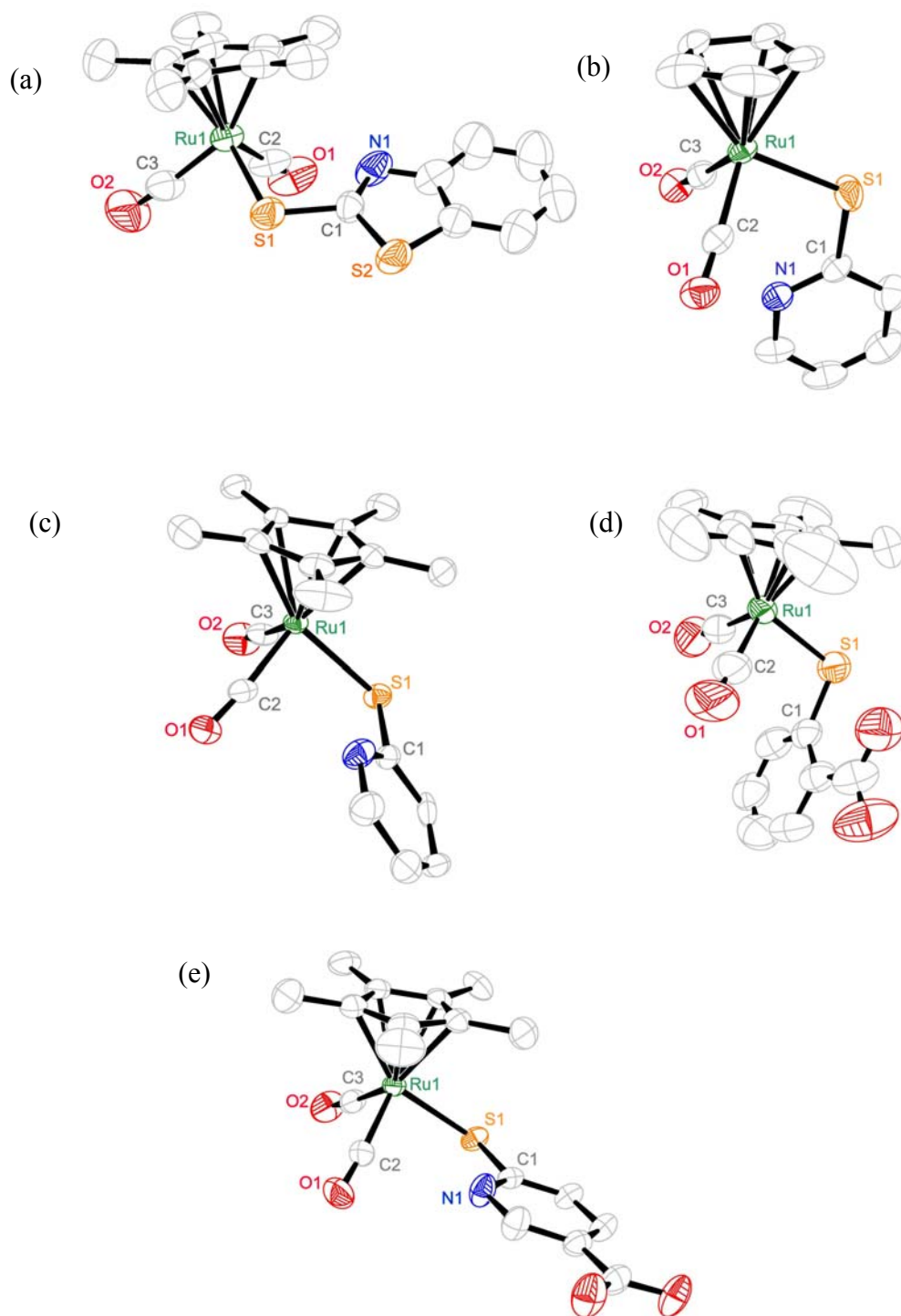
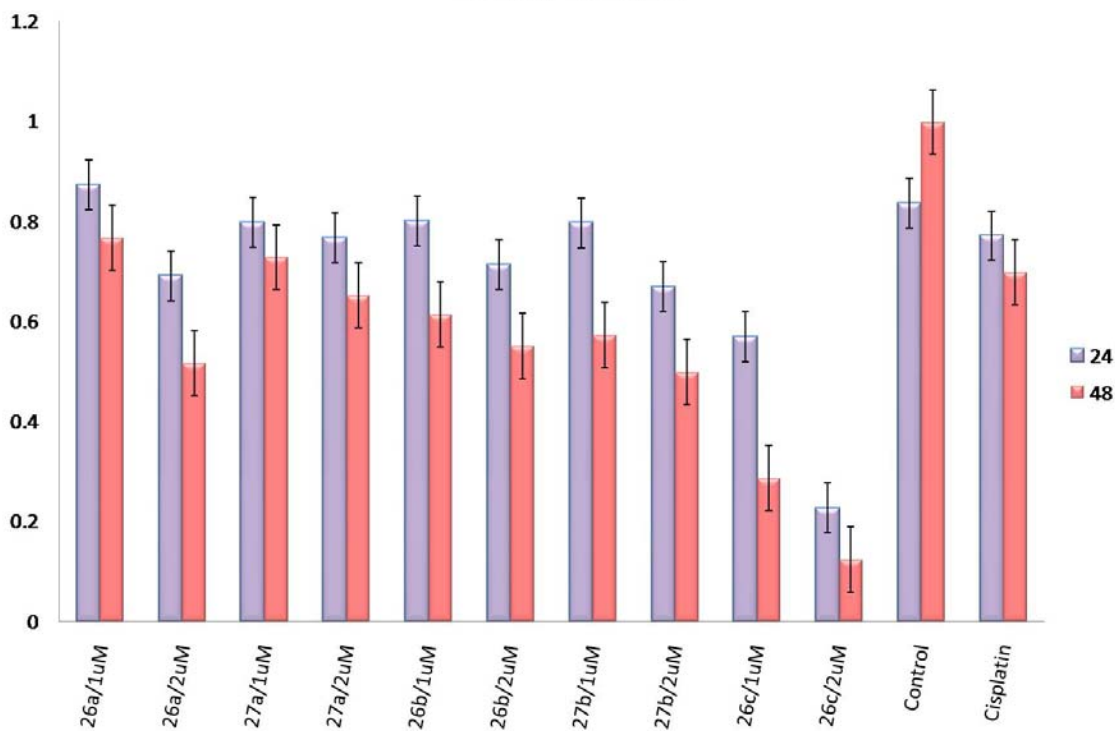
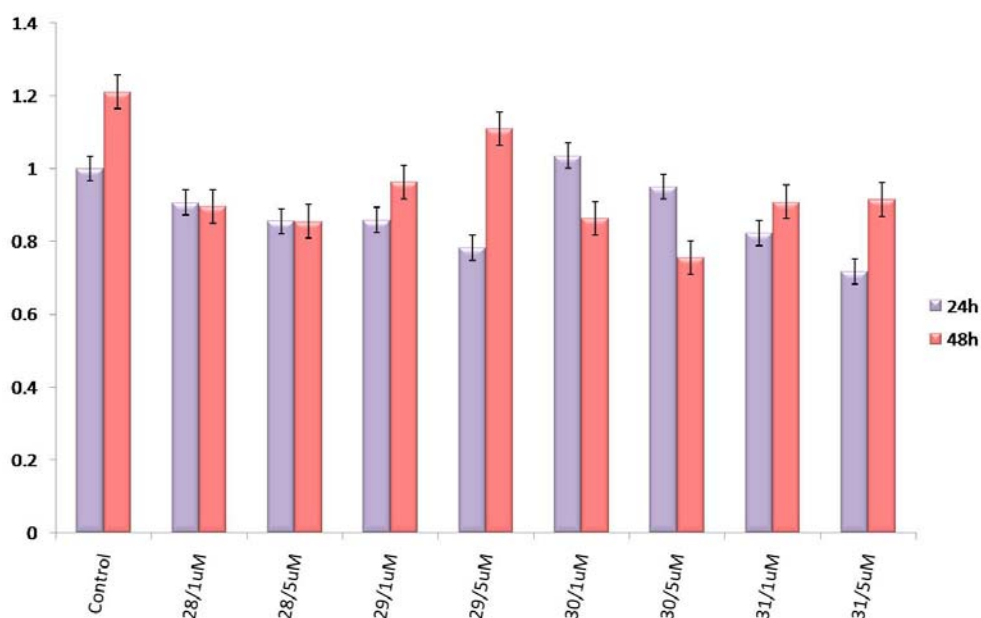


**Figure A6** Ortep plots of (a) **26b** (Selected view which omits the disorder in the complex) (b) **27a** (c) **27b** (d) **28** and (e) **29**. Thermal ellipsoids are drawn at the 50% probability level and all hydrogen atoms are omitted for clarity.

### Viability Test-MDA



### MDA-MB-231





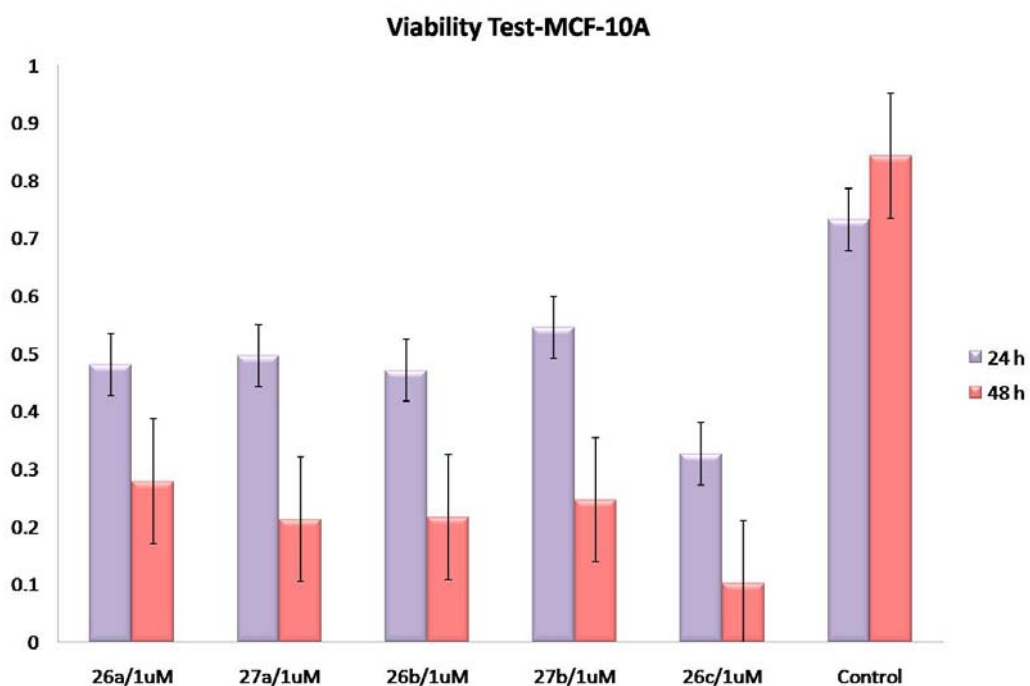
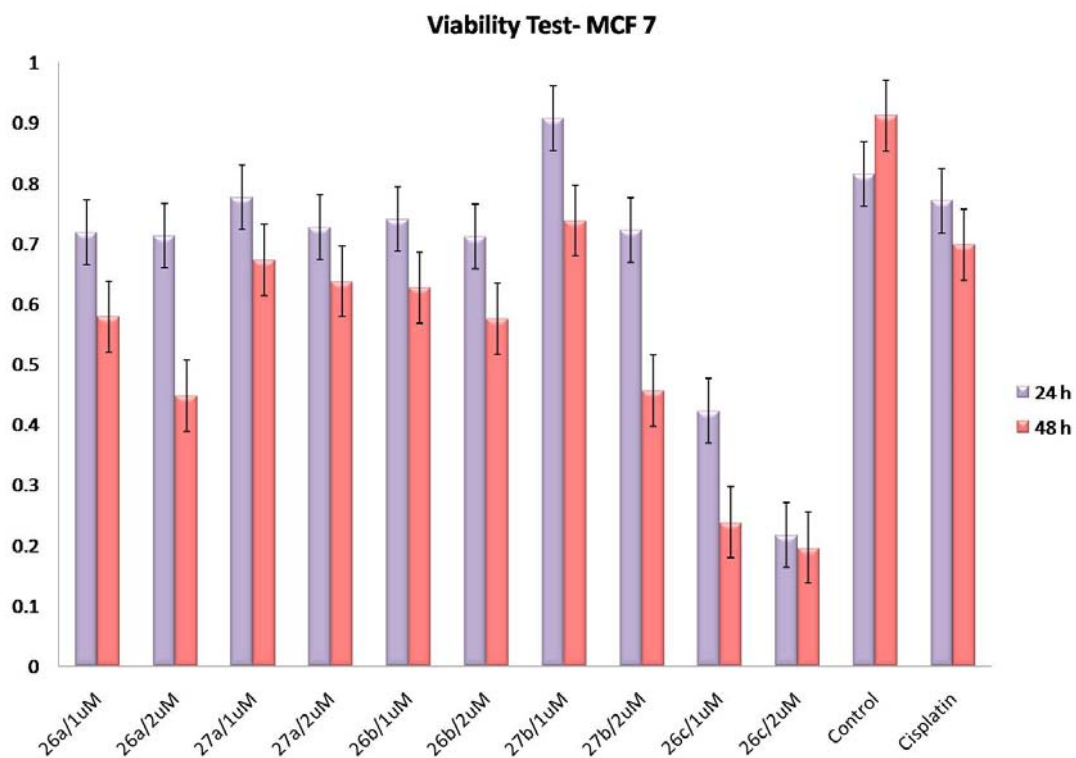


**Figure A4.** MTT assay for (a) **26-27** against MDA-MB231 (b) **28-31** against MDA-MB231 (c) **26-27** against MCF7 and (d) **26-27** against MCF10A.

### **Trial reactions $\text{Cp}^*\text{Ru}(\text{CO})_2(\text{SC}_6\text{H}_5\text{COOH})$ and $\text{Cp}^*\text{Ru}(\text{CO})_2(\text{SC}_5\text{H}_3\text{NCOOH})$ to stabilize Ag nanoparticles.**

We had previously reported the stabilization of Ag nanoparticles by triosmium clusters with a ligand containing a free carboxylic acid. Hence, complexes **28** and **29** were used in a study to stabilize Ag nanoparticles formed from reduction of  $\text{AgNO}_3$ . However, a silver mirror was formed and complexes **28** and **29** decomposed to brown solids with no  $\text{M-C}\equiv\text{O}$  stretch.

A typical trial reaction is as follows: To a solution of  $\text{AgNO}_3$  (17 mg, 0.10 mmol) in MeOH (*ca.* 10 mL) was added  $\text{Cp}^*\text{Ru}(\text{CO})_2(\text{SC}_6\text{H}_5\text{COOH})$  (**25b**) (22 mg, 0.05 mmol). After stirring for 2 h, a degassed, aqueous solution of  $\text{NaBH}_4$  (4 mg, 0.10 mmol) was added to the reaction mixture resulting in the precipitation of dark brown solids and the immediate formation of a silver mirror on the glass wall of the reaction flask. No  $\text{M-C}\equiv\text{O}$  stretch was observed in the IR spectrum for the brown solids, indicating decarbonylation and decomposition of the  $\text{Cp}^*\text{Ru}(\text{SR})$  complex.

### **Testing for Catalytic activity in the hydration of terminal alkynes.**

Complexes **28-31** were tested for catalytic activity in the hydration of terminal alkyne.

The organic substrate chosen was phenylacetylene and the typical setup is as follow:

$\text{PhC}\equiv\text{CH}$  (22  $\mu\text{L}$  mmol) was added to a solution of **29** (2.5 mg, 3 mol% catalyst loading) in  $\text{H}_2\text{O}:\text{MeOH}$  (1:1, 1 mL) in a 2 mL Wheaton vial. The mixture was heated at 50 °C and a 100  $\mu\text{L}$  aliquot was drawn at different interval and  $\text{CDCl}_3$  was used to extract any organic product/s formed and monitored by  $^1\text{H}$  NMR spectroscopy.

For all the four complexes above,  $^1\text{H}$  NMR spectrum indicated that there is no catalytic activity under the reaction conditions stated above.

### **Trial reactions of [TpRu(CO)<sub>2</sub>]<sub>2</sub> with disulfides**

A stoichiometric amount of the individual disulfides was added to [TpRu(CO)<sub>2</sub>]<sub>2</sub> (7 mg, 0.001 mmol) in 0.5 mL of C<sub>6</sub>D<sub>6</sub> and the reaction mixture was ultrasonicated over a period of 2 days. The reaction mixtures were monitored periodically by <sup>1</sup>H NMR spectroscopy and there was no reaction, even upon photolysis of the samples using a 365nm UV lamp. The solvent was changed to d<sub>6</sub>-acetone to solubilise the reactants. However, there was no reaction observed between [TpRu(CO)<sub>2</sub>]<sub>2</sub> and any of the disulfides. The reaction mixture was evacuated to dryness after 2 days and the IR spectrum of the reaction mixture in DCM was acquired, which indicated only the presence of the [TpRu(CO)<sub>2</sub>]<sub>2</sub> dimer.